Cyclo- and Polyphosphazenes Containing 2-oxypyridine Moieties Coordinated to Selected Transition Metals

A thesis presented in partial fulfilment of the requirements for the degree of Doctor of Philosophy in Chemistry at Massey University, Palmerston North.

Stephen Kirk

2008

Acknowledgements

To say that I owe a vast debt of gratitude to Professor Andrew Brodie and Associate Professor Eric Ainscough, possibly classifies as the greatest understatement of my professional career. My prior academic achievements have been undertaken (many years ago) on a part-time basis, whilst having been employed in completely different subject areas and in an industrial context. Notwithstanding this, Andrew and Eric saw fit to extend to me the privilege of a scholarship to undertake full-time research in chemistry. Their expertise, guidance, and often very entertaining and esoteric conversations will forever remain with me. One day I will write a book on Aincoughs' Laws.

Dr. Carl Otter deserves a mention, without his expertise and humour I would not have been able to complete the practical element of this work in the prescribed timescale. The incidents in Hobart and Sydney will go with me to my grave.

On a serious note, I must acknowledge the expertise and assistance of Professor Geoff Jameson and Dr, Jan Wikaira for their crystallographic efforts, Dr. Geoff Waterhouse for Raman spectroscopy, Dr. Steve Moratti for GPC work, Dr. Pat Edwards for invaluable NMR insights, Ross Davidson for DFT insights and Lee Steely for all his efforts in the laboratory facilities of Penn State University. To Professor Harry Allcock, I think a Nobel Prize is well overdue. I would also like to acknowledge the RSNZ Marsden Fund for financial support (MAU208).

I also have to acknowledge my wife, Glenda, who took the photographs in Chapter 5, supported me financially through this whole thing and feigned interest in my inane ramblings. Without her I would not have achieved anything.

Man's mind, once stretched by a new idea, never regains its original dimensions.
Oliver Wendell Holmes
US author & physician (1809 - 1894)
(http://www.quotationspage.com/quotes/Oliver_Wendell_Holmes/accessed 18 June 2008)

Abstract

The phosphazene ligands spiro(biph)tetrakis(2-oxypyridine)cyclotriphosphazene (**L**^{1}), spiro(biph)tetrakis(4-methyl-2-oxypyridine)cyclotriphosphazene (**L**^{2}), and spiro(biph)tetrakis(6-methyl-2-oxypyridine)cyclotriphosphazene (**L**^{3}) have been synthesised and characterised as small molecule templates for the polymeric analogues. Complexes of each ligand with selected transition metals have been synthesised and characterised. Where X-ray crystal structures have been obtained, the predominant geometry is a five-coordinate trigonal bipyramidal (TBP) form, though variations exist. In solution, [$CuL^{2}Cl_{2}$] retains the TBP form whereas [$CoL^{2}Cl_{2}$] rearranges to a tetrahedral geometry. In order to elucidate this behaviour, diamagnetic complexes were synthesised and variable temperature NMR (VTNMR) studies conducted.

The complexes [$ZnL^{2}Cl_{2}$], [$CdL^{2}Cl_{2}$] and [$HgL^{2}Cl_{2}$] exhibit fluxional behaviour as monitored by VTNMR studies. The X-ray structure of [$CdL^{2}Cl_{2}$] contains three molecules in the unit cell that demonstrate what is thought to be the first evidence for a fluxional mechanism in phosphazene compounds. The complex [$ZnL^{2}Cl_{2}$] exists at low temperature as discernable major and minor species.

Polyphosphazene analogues have been synthesised and complexed with selected transition metals. The polymer complexes display variations in solubility and stability which is postulated to be due to the ratio of side group substitution, position of the pyridyl methyl group and the nature of the complexing metal. A number of the polymers degrade prior to workup, possibly as a result of base-promoted attack on the backbone by the pyridyl nitrogen atoms. Electronic spectra reveal that where soluble, the Co(II) polymer complexes have a tetrahedral geometry, whereas the Cu(II) polymer complexes distort between TBP and square-based pyramidal dependent on the ratio of metal used. Polymer complexes with Zn(II) demonstrate fluxional behaviour.

Table of Contents

Chapter 2: Phosphazene Ligand Syntheses **Page**

List of Figures and Tables

Page

Chapter 1

Page

Chapter 2

Page

Chapter 3 **Page**

Page

Page

Chapter 4

Page

Page

Page

Chapter 5

Page

Page

Page

Appendix 1

List of Graphs

Chapter 4

For Glenda

Chapter 1: Introduction to Phosphazenes

1.0 Abbreviations used in Chapter 1

2OPy	2-oxypyridine
2O-4-MePy	2-oxy-4-methylpyridine
2O-6-MePy	2-oxy-6-methylpyridine
biph	2,2'-dioxybiphenyl

1.1 Introduction

This thesis has been arranged such that each chapter contains a specific introduction, providing examples that lead the reader into a logical context for each body of research. This primary introduction serves to give a more general overview of polymers and phosphazene research, including the history and some of the latest developments in the field.

1.1.1 The beauty of hindsight

In the 1920s, H. Wieland[1] gave the following advice to Hermann Staudinger:
"Dear colleague, drop the idea of large molecules; organic molecules with a molecular weight higher than 5000 do not exist. Purify your products, for example your rubber, then it will crystallize and prove to be a low molecular compound!"

In the 1960s, Allcock *et al*.[2] synthesised the first stable uncrosslinked polymers based on the inorganic phosphazene backbone, at a time when the conventional wisdom held that all the major polymer systems had been discovered. Indeed, inorganic polymers were deemed likely to be of little utility, brittle and insoluble.[3]

It is of historical record that Staudinger went on to win the 1953 Nobel Prize in Chemistry for his work on macromolecules and changed the established view of polymer chemistry. It is also somewhat prophetic that today, there exists a growing field of research into inorganic phosphazene high polymers with molecular weights of between two and ten million Daltons and that this work started at least 30 years before Staudinger's macromolecular hypothesis was accepted.

1.1.2 Polymers - an introduction

A principal aim of this research is to synthesise polyphosphazenes and their metallated derivatives. Therefore, this section will cover some of the basic nomenclature and structure of known polyphosphazene compounds. Methods of polymerisation are discussed in some depth in Chapter 5 and the laboratory synthesis is detailed in Appendix 1.

Allcock *et al.*[3] define three broad ranges to classify polymeric systems based on degree of polymerisation (or number of repeat units in the backbone).

(i) Oligomers comprise between 2 and 100 repeat units

(ii) Low to medium weight polymers comprise between 100 to 1000 repeat units

(iii) High polymers comprise 1000 to 15000 repeat units, which result in very high molecular weights (up to 10 million Daltons) dependent on the side groups.

Oligomers generally display little of the bulk properties of the high polymeric analogues, either in the solid or in solution. A primary reason for this is that end group density becomes a major factor in the characterisation and properties. Low to medium weight polymers display dramatic variation in properties, whereas above about 1000 repeat units i.e. for the high polymers, the bulk properties are stabilised and statistically averaged such that characterisation tends to be repeatable. These ranges are of course only approximate and the bulk properties of polymers are also highly dependent upon the nature of the side groups attached to the backbone as well as the particular polymer structure.

1.1.3 Polymer structure - an introduction

In this work, the ligand spiro(2,2'-biphenyl)tetrakis(2-oxypyridine)cyclotriphosphazene (Figure1) has been designed as a small molecule model platform, allowing the coordination mode to transition metals to be assessed.

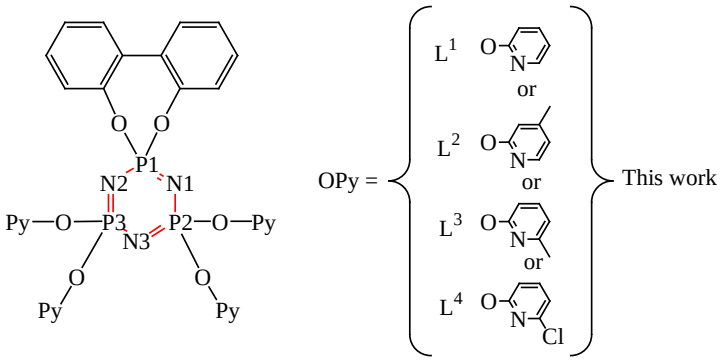

Figure 1 Generic ligand design

At the polymer level, although single- and mixed-substituent polymers have been synthesised in this work, only one of the moieties (i.e. the 2-oxypyridine derivative), in addition to the backbone nitrogen atoms has the potential to coordinate. In this respect, these polymers differ from those previously reported by Carriedo *et al*.[4] and by Diefenbach *et al*.,[5] where the backbone nitrogen atoms do not bind.

Polymers in general can sometimes be deliberately tailored to a range of structures. Open chain structures depicted in Figure 2, assume only one type of polymer is present, whereas copolymers with organic and inorganic substituents lead to the hybrid forms shown in Figure 3.

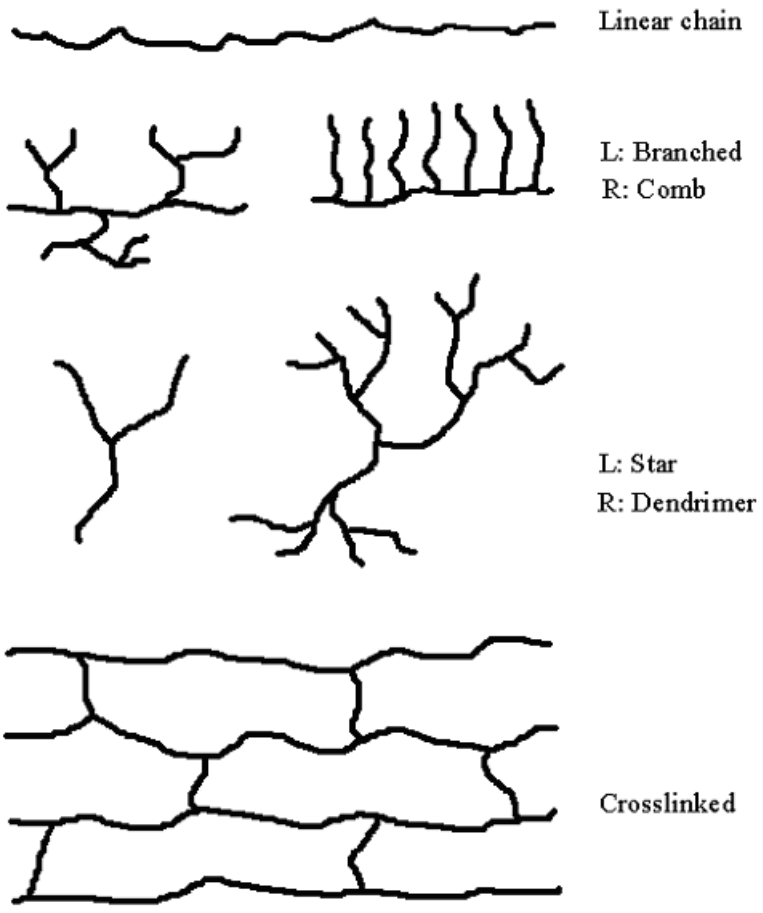

Figure 2 Examples of open chain polymer architectures

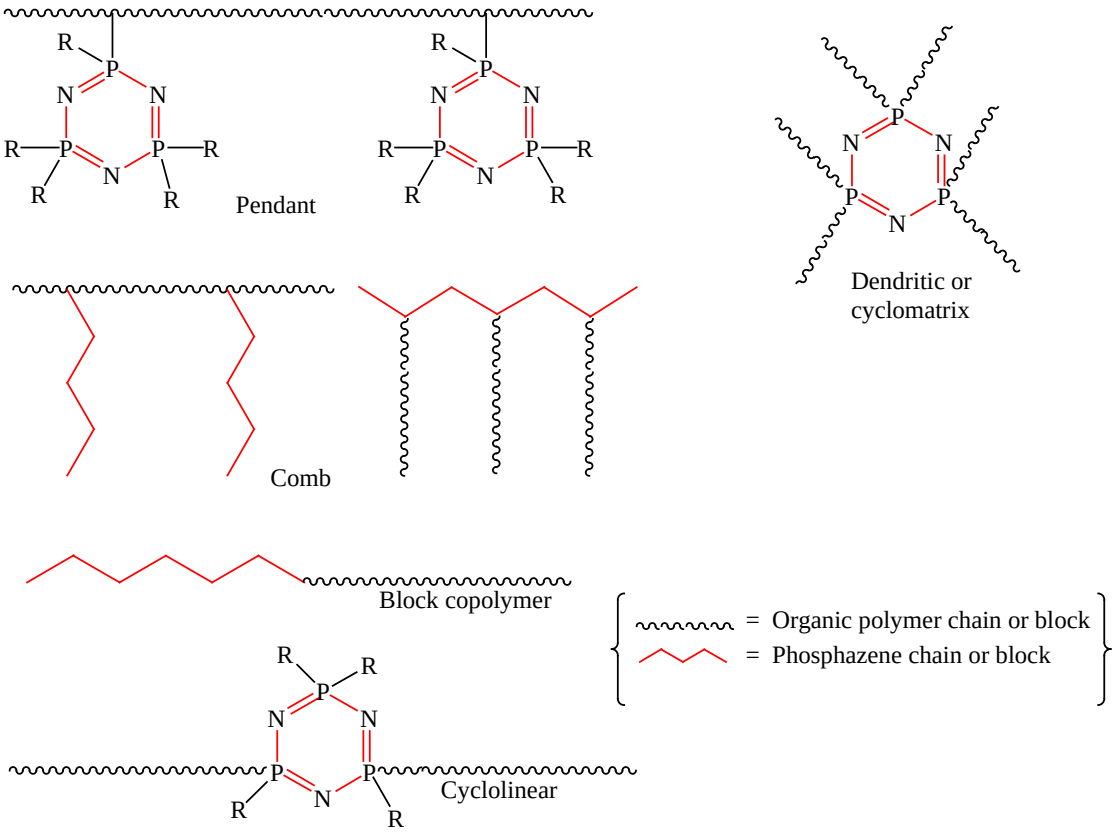

Figure 3 Examples of hybrid polymer architectures

In contrast to organic polymers, the inorganic backbone of phosphazenes confers several very important advantages including biomedical compatibility, fire resistance, high materials flexibility, near-ultraviolet transparency and gamma-radiation stability. These properties, and the ability to readily attach side groups and form metal complexes, have resulted in diverse applications for inorganic-organic macromolecular polymeric phosphazenes.

1.1.4 The history of phosphazenes

Phosphazenes are a remarkable class of inorganic molecules having the general formula $[NPX_2]_n$, where the phosphorus and nitrogen atoms are connected by formally unsaturated bonds and the repeat units can form cyclic compounds or polymeric chains. This representation is, however, somewhat misleading and the electronic nature of the bonding is now considered to be predominantly ionic as shown in Figure 4.[6]

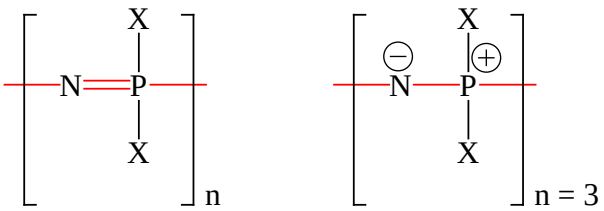

(a) π-bonded structure (b) ionic structure

Figure 4 Possible representations of the electronic structure of phosphazenes

First reports of phosphazenes date back to 1834 when work by Liebig *et al.*[7] and by Rose,[8] led to the isolation of an unexpected and stable product from attempts to prepare amides of phosphoric acid. This product could be steam distilled or boiled with acids and alkalis without significant decomposition and was analysed to have the formula $P_3N_2Cl_5$. In 1870, Wichelhaus[9] reported the compound to be a trimeric species with the formula $[PNCl_2]_3$. It was Stokes[10] however, in 1897, who first suggested that the compound was cyclic and that it was one of a homologous series of polymers. Stokes[10] also managed to thermally polymerise cyclophosphazene to give a cross-linked "inorganic rubber", though it was of little practical utility.

Research output has been steadily increasing since the mid 1960's when Allcock *et al.*[2] discovered a controlled thermal route to the uncrosslinked polymer $[NPCl_2]_n$. To date, more than six thousand papers, patents and reports have been published including more than 700 polymers, making polyphosphazenes the largest class of inorganic macromolecules.[11] Reports cover such diverse applications as biomedical, membranes, high performance elastomers, fire resistant materials, electro-optical and semi-conducting materials, energy generation and storage, hydraulic fluid additives and lubricants for magnetic recording applications.[12] It is perhaps partly due to legalities that phosphazenes have not yet had a major commercial impact, with companies such as the Ethyl Corporation retaining intellectual property rights through patents on some of the basic manufacturing aspects.[13]

It should be noted that the use of specific nomenclature to describe phosphazene systems was proposed by Shaw[14] in 1962, building on work by Audrieth *et al.*[15] This is now widely adopted in the scientific literature. As Allcock[16] points out, the official

IUPAC/Chemical Abstracts nomenclature for hexachlorocyclotriphosphazene ($[NPCl_2]_3$) is in fact, 2,2,4,4,6,6-hexachloro-1,3,5,2,4,6-triazotriphosphorine, hence the preference by researchers for the "phosphazene"- based nomenclature.

1.1.5 Cyclotriphosphazenes and model systems for polyphosphazenes

Although much current research is focussed on polymer synthesis and properties, the vast majority of knowledge has come from the synthesis and characterisation of small molecules, most notably the trimeric ring system, hexachlorocyclotriphosphazene and to a lesser extent, the tetrameric ring system, octachlorocyclotetraphosphazene (Figure 5) and higher homologues.

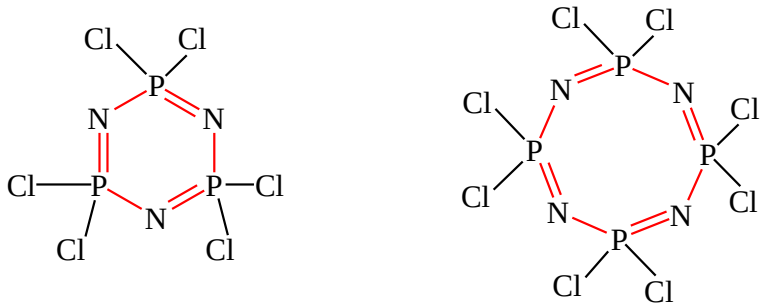

Hexachlorocyclotriphosphazene Octachlorocyclotetraphosphazene

Figure 5 Cyclic phosphazenes commonly used for synthesis

Allcock[17] describes the use of small ring templates as being crucial to the development of new polymers, citing the following reasons:

(i) They are employed as monomers for the ring opening route to high polymers,

(ii) They are crucial model systems for the halogen replacement reactions to be applied to the high polymer systems and for X-ray determination of structure,

(iii) The rings themselves can be incorporated into the polymers either as side groups or as components in the main chains of cyclolinear polymers.

The synthetic utility of the cyclophosphazenes lies in the reactivity of the halogens and their ease of nucleophilic substitution. Such systems can usually be fully characterised by a range of common analytical techniques leading to valuable insights regarding the chemistry and properties of the polymeric analogues, as well as having applications in their own right.

The bromo- and fluoro- homologues are known and have been shown by Allen[18] to react with primary and secondary amines, where reactivity follows the order P-Br > P-Cl > P-F. The synthesis of $[N_3P_3Br_6]$ is somewhat elaborate and the compound is moisture sensitive, whereas the strong P-F bond in $[N_3P_3F_6]$ and its subsequent poor leaving ability, probably explains why these halogenated phosphazenes have not, as yet, been more widely researched.[19] Cyclotriphosphazenes carrying the first P-I bond were reported by Allcock *et al*.[20] in 1981.

Hexachlorocyclotriphosphazene has a total of twelve possible regio- and stereoisomeric conformations (Figure 6) on replacement of the halogen atoms with mono-functional reagents. Thus from a small stable platform, many options exist for the synthetic chemist.

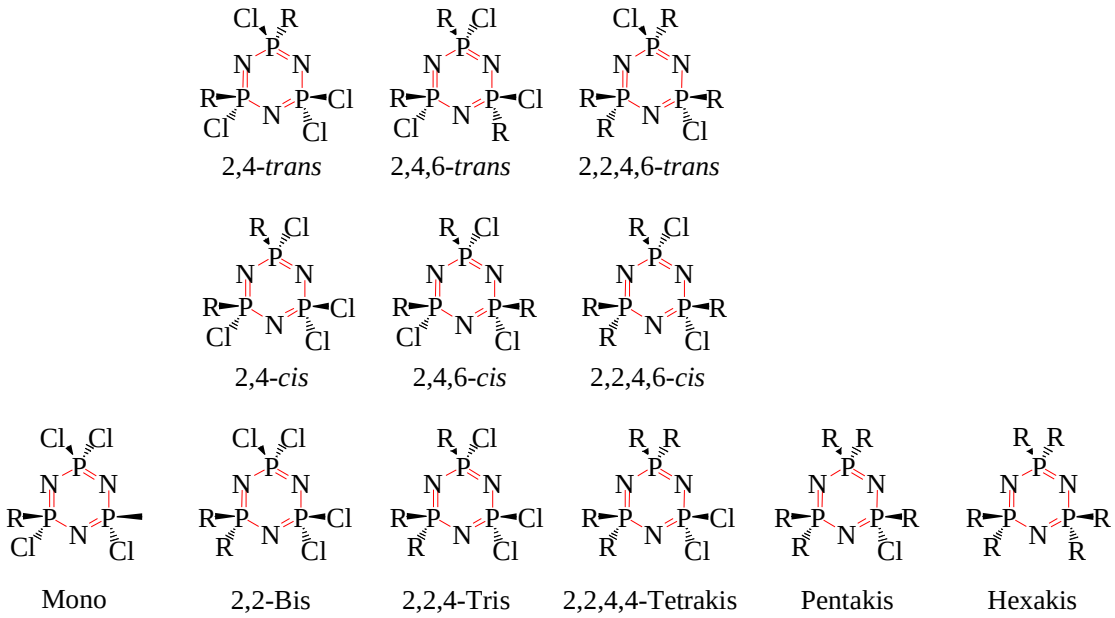

Figure 6 Isomers of hexachlorocyclotriphosphazene with mono-functional reagents

Le Chatelier's Principle applies as a general rule for driving the reaction equilibrium towards full halogen substitution. Ideally, a solvent should be chosen in which the halophosphazene and R groups are good solutes, and in which the side products (e.g. NaCl) are poor solutes such that precipitation from solution drives the reaction to completion.

The substitution pattern for halogen replacement relies on a complex interplay of steric, electronic and solvent parameters, which are not yet fully understood. Substitution patterns can be geminal, i.e. from side groups attached to the same phosphorus atom, or non-geminal, from side groups attached to different phosphorus atoms as illustrated in Figure 7.

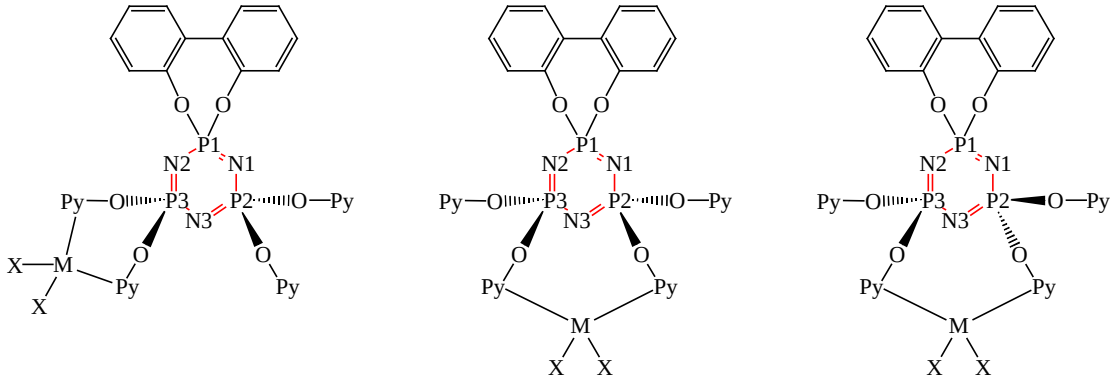

Figure 7 Substitution patterns for the ligands in this work
M=metal, X=halogen Py=2-oxypyridine

Primary amines, for example, display geminal and non-geminal pathways, dependent upon the parameters used, whereas secondary amines afford largely non-geminal products.[18, 21] However, for primary amines, different pathways have also been observed for the same reagents but dependent on whether it is the trimer or the tetramer that is undergoing nucleophilic substitution.[22-24] Thus it is unclear whether the substitution patterns are wholly applicable to the analogous high polymers.

The model compound approach is limited in its applicability to the high polymer but as Allcock[25] states, "...investigators who have had the most difficulty with the synthesis

and study of new polyphosphazenes are often those who have neglected to carry out the model compound work first".

1.1.6 Polyphosphazenes containing aryl, alkyl, aryloxy and alkoxy moieties

Whilst the parent compounds $[N_3P_3Cl_6]$ and $[NPCl_2]_n$ have little practical utility in their own right, being subject to hydrolysis[26, 27] with the concomitant loss of HCl, the appropriate selection of pendant side groups can confer a wide range of properties. The long organic side chains in $[NP(O(CH_2)_3CH_3)_2]_n$ results in an amorphous elastomeric polymer with a glass transition temperature (T_g) of -105°C, whereas [NP(NH-adamantyl) $(OCH_2CF_3)]_n$ is a glass with a T_g of +180°C.[3] T_g is the temperature below which the material is a glass and above which there is sufficient thermal energy for bond torsion to occur giving thermoplastic or elastomeric behaviour.

Relatively few polyphosphazenes are known where alkyl groups are attached directly to the backbone phosphorus atoms by P-C bonds. Poly(dimethylphosphazene), for example, was first prepared by Wisian-Neilson *et al.*[28] This flexible material is soluble in chlorinated solvents such as CH_2Cl_2 and $CHCl_3$, and in ethanol, but is insoluble in water, THF and acetone. Poly(diethylphosphazene)[29] and poly(di-n-propylphosphazene)[30] on the other hand are highly crystalline materials which are insoluble in common solvents (Figure 8).

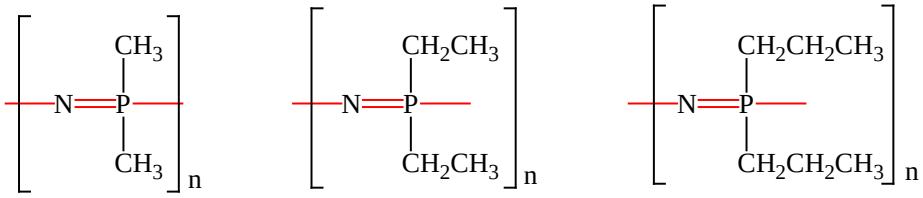

Figure 8 Poly(alkyl)phosphazenes reported by Wisian-Neilson *et al.*[28]

Alkyloxypolyphosphazenes are more common than the alkylphosphazenes, presumably due to the insolubility of the latter. Alkyloxypolyphosphazenes have greater flexibility through the P-O bonds which result in lower T_g values and often no crystallinity (although the presence of a terminal CF_3 group does confer some crystallinity).

Arylpolyphosphazenes suffer from steric crowding, for example, in poly(diphenylphosphazene) where the aryl moiety is attached directly to the backbone phosphorus atom. Far more widely reported is the use of an oxy or alkoxy spacer between the phosphazene backbone and the aryl moiety (Figure 9). Crystallinity can be conferred in alkyloxy-aryl polymers by transposing a biphenyl or napthyl group at the terminus of the alkyloxy chain.

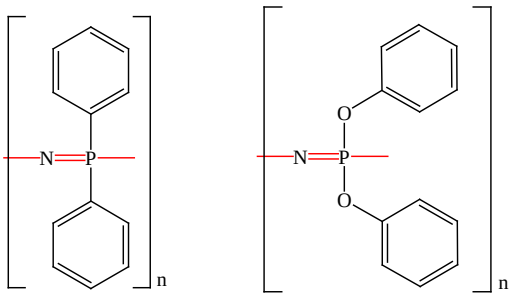

Figure 9 Poly(diphenyl)phosphazene with and without oxy spacer groups

Monofunctional aryloxy side groups, such as the phenoxy moiety, require a degree of forcing to achieve full substitution, e.g. six to eight hours at reflux depending on the base used.[31] Similarly, full substitution using the bifunctional moiety, 2,2'-dioxybiphenol, requires five hours at reflux.[32] It is not certain whether spiro difunctional moieties are more favoured than geminal monofunctional ones.

Non-fluorinated alkoxy groups, such as methoxy and ethoxy, tend to rearrange at elevated temperatures (>200°C),[33-36] whereas fluorinated alkoxy groups such as the trifluoroethoxy group, produce extremely hydrophobic materials that are stable as cyclo- and polyphosphazenes (Figure 10).[37, 38] The fluorinated polymers are also soluble in organic solvents such as acetone and THF.

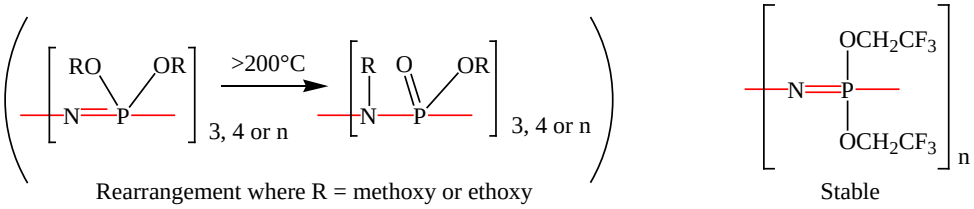

Figure 10 Thermal stability dependent on R group. Left: rearrangement by migration of alkoxy groups. Right: Poly(trifluoroethoxy)phosphazene

Small groups, such as CH_3, are not bulky enough to shield the backbone nitrogen atoms and so yield polymers that are hydrophilic but not water soluble,[3] whereas polyphosphazenes containing glyceryl substituents are water soluble and biodegradable.[39] The glyceryl group is trifunctional and as such requires protection of two of the hydroxyl groups prior to nucleophilic substitution onto a polyphosphazene backbone to prevent crosslinking (Figure 11). Following substitution, the hydroxyl groups can be deprotected and serve as sites for drug attachment. In vivo, the drug is released as the glyceryl component is hydrolysed to glycerol and the phosphazene backbone breaks down to ammonia and phosphate.

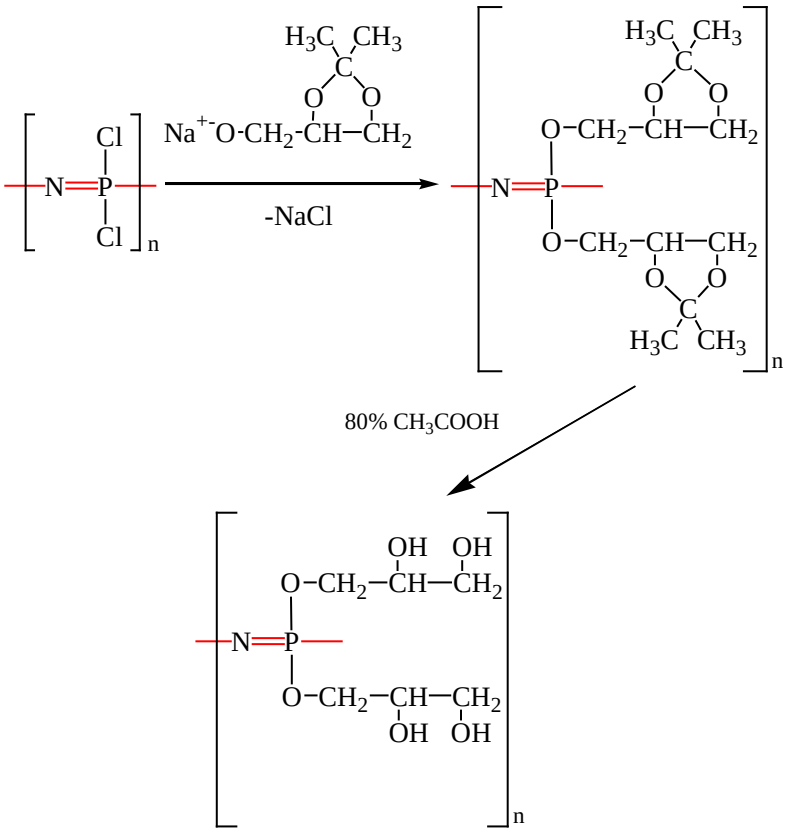

Figure 11 One method of synthesising poly(bis(glyceryl))phosphazene

Backbone flexibility is, in itself, an important factor in conferring macroscopic properties. Allcock *et al*.[40] describe the synthesis of cyclotri- and polyphosphazenes containing $(O\text{-}(CH_2CH_2O)_3C_6H_4C_6H_4R)_2$ groups i.e. biphenyl derivatives with an ethyleneoxy spacer, where R = OMe or OEt for example. The backbone flexibility of

the polyphosphazene allows the side groups to stack together conferring liquid crystalline properties whereas no such behaviour occurs for the trimeric compounds. With appropriate selection of phosphazene architecture and side groups, applications range from dentistry[41] to engine seals.[42]

1.1.7 Side groups in phosphazenes containing nitrogen donor atoms and their coordination behaviour

Of particular interest in recent years has been the development of phosphazene ligands capable of metal coordination.[43] The mode of coordination, discussed in greater detail in Chapter 3, can take on several forms:

(i) Ionic salts as shown in Figure 12

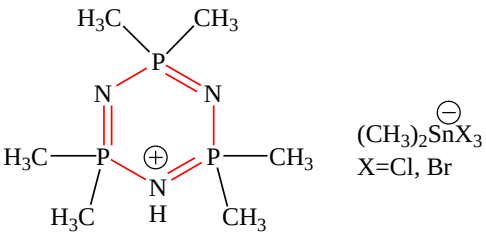

Figure 12 An example of an ionic salt phosphazene complex[44]

(ii) Interaction with the ring/backbone nitrogen or ring/backbone phosphorus, as shown in Figure 13, and

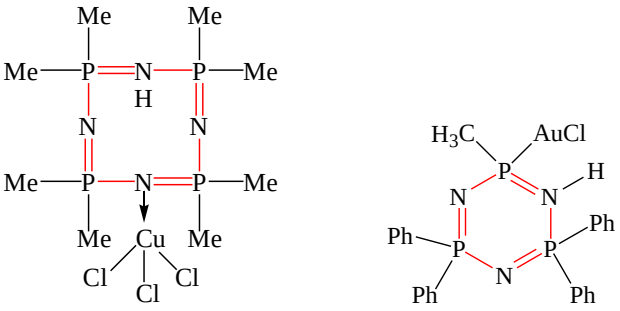

Figure 13 Examples of phosphazene ring nitrogen atom[43] (left) and ring phosphorus interaction[43] (right)

(iii) Coordination to exocyclic donors, with or without participation by the ring/backbone nitrogen, as shown in Figure 14.

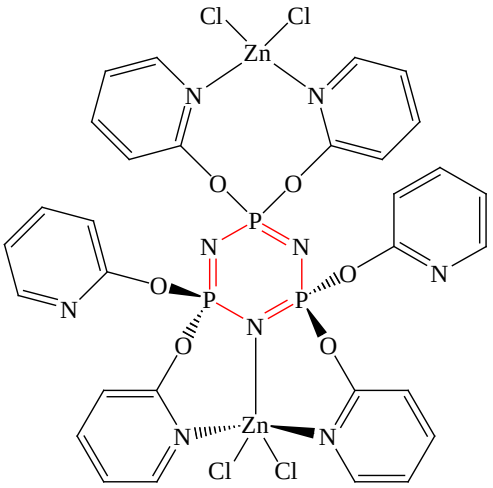

Figure 14 An example of exocyclic coordination with and without phosphazene ring nitrogen coordination[45]

This multi-modal coordination ability of phosphazenes leads to a diverse field of research, and polymers bearing transition metals are expected to display interesting properties, though few have yet been synthesised or reported.[46] Some examples are given below.

Stable phosphazene-metal coordination complexes may not serve as efficient ion exchangers if the metal cannot be easily removed from the substrate, but may prove useful in adhesive applications.[47] Equally, a number of compounds display selectivity in ion extraction[21, 48, 49] which may prove useful in commercial applications as a means of filtering selected ions from a mixture, or in environmental operations where metal contamination needs to be contained.

As an illustrative example, pyrazolylcyclotriphosphazenes have two nitrogen atoms per exocyclic ring and hence form effective coordination ligands. They have been synthesised as bis, tetrakis and hexakis compounds thus providing multiple coordination sites for mono and bimetallic complexes.

With hexakis(dimethylpyrazolyl)cyclotriphosphazene, platinum[50] and palladium[51] chlorides coordinate exclusively through geminal pyrazolyl moieties, whereas copper chloride[52] coordinates in a distorted trigonal bipyramidal fashion (Figure 15). Molybdenum carbonyl coordinates via two geminal pyrazolyl rings and one of the ring nitrogens to give an octahedral structure.

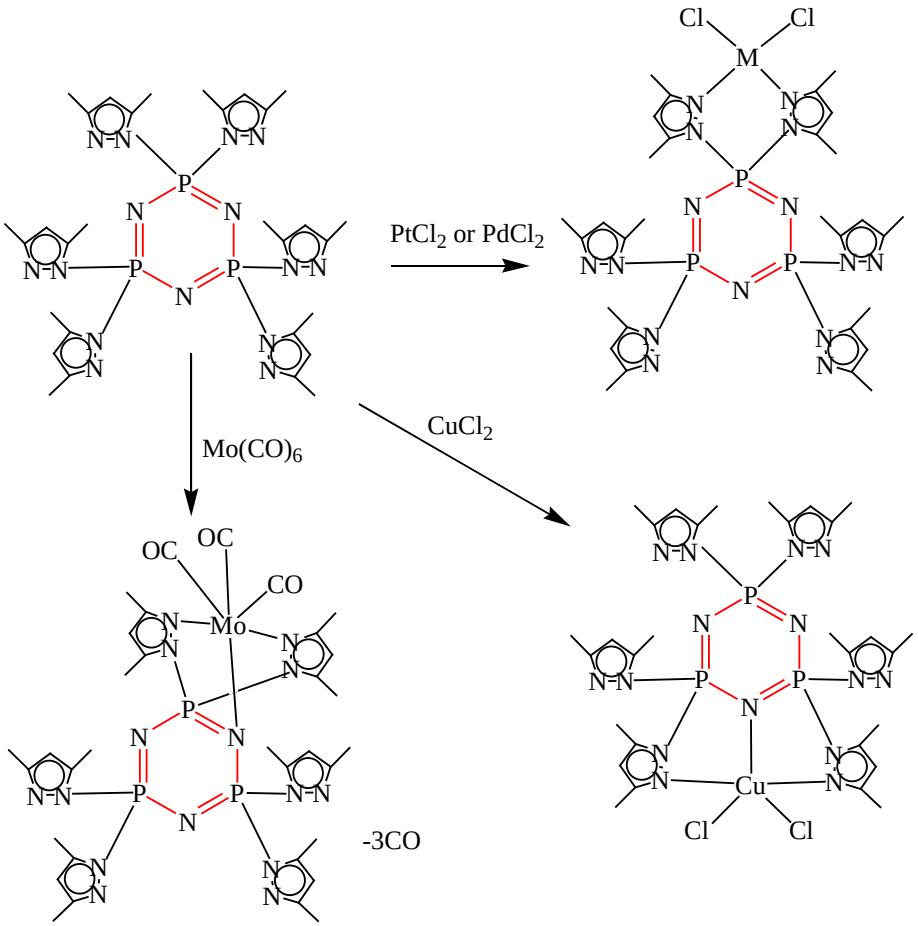

Figure 15 Examples of coordination modes to hexakis(dimethylpyrazolyl)-cyclotriphosphazene

Coordination to various pyridine moieties is discussed in some depth in the introduction to Chapter 2, where work by Ainscough *et al.*[53] on the hexakis(pyridyloxy)-cyclotriphosphazene demonstrates a range of coordination modes.

1.2 Modern day phosphazene research

Phosphazene research covers an extensive range of areas from fundamental studies on structure determination and synthesis, to real world applications such as dentistry, drug delivery, catalysis and ion exchangers to name a few. This section illustrates some aspects of this diverse field.

1.2.1 Fundamental studies on the synthesis of phosphazenes with known structures

Whilst the vast majority of reported structures rely on the nucleophilic substitution of chlorine atoms on the cyclotriphosphazene, the substitution pathway is not always straight-forward or predictable as previously stated. Wisian-Neilson *et al.*[54] recently reported a method for the synthesis of non-geminal cyclotriphosphazenes starting from the N-methylsilylphosphoranimine rather than the cyclic trimer (Figure 16).

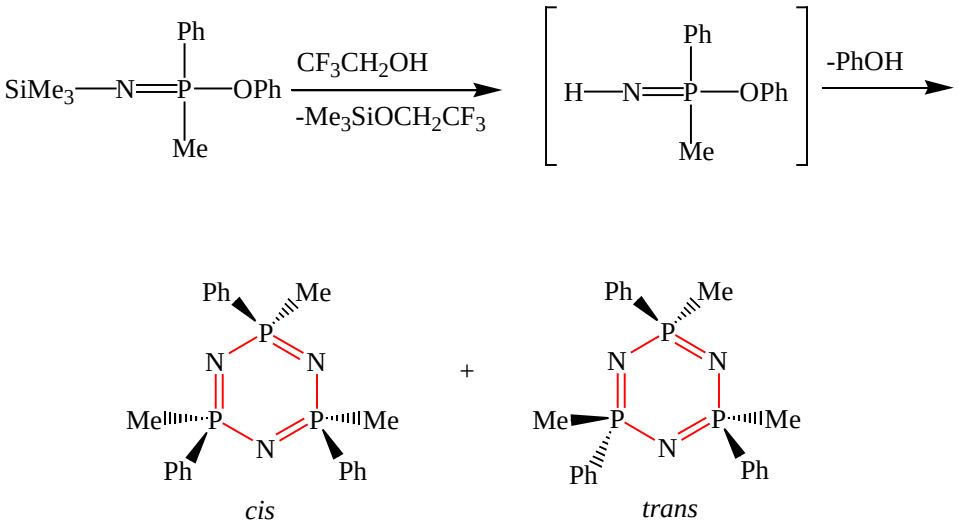

Figure 16 Scheme reported by Wisian-Neilson *et al.*[54] for non-geminal synthesis

The reported ratio of *trans* to *cis* isomers was 2.8:1 with the X-ray crystal structure of the *cis* isomer resembling a basket on the phenyl bearing side of the ring system (Figure 17). Given the previously stated uncertainty regarding regiochemistry, this process may allow for further progress in synthesising known polymer architectures.

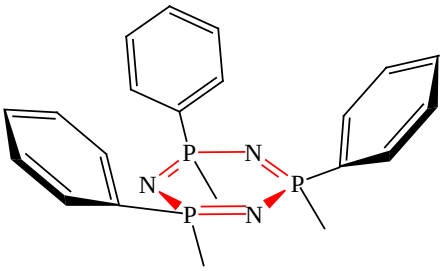

Figure 17 Basket-like structure reported by Wisian-Neilson *et al*.[54]

Allcock *et al*,[55] have demonstrated that known polymer architecture can be achieved for cyclolinear polymers via an acyclic diene metathesis (ADMET) reaction. For example, reaction of alkoxides with cyclophosphazenes bearing non-polymerisible phenoxy or alkylether groups yield diene species (Figure 18) capable of condensation polymerisation.

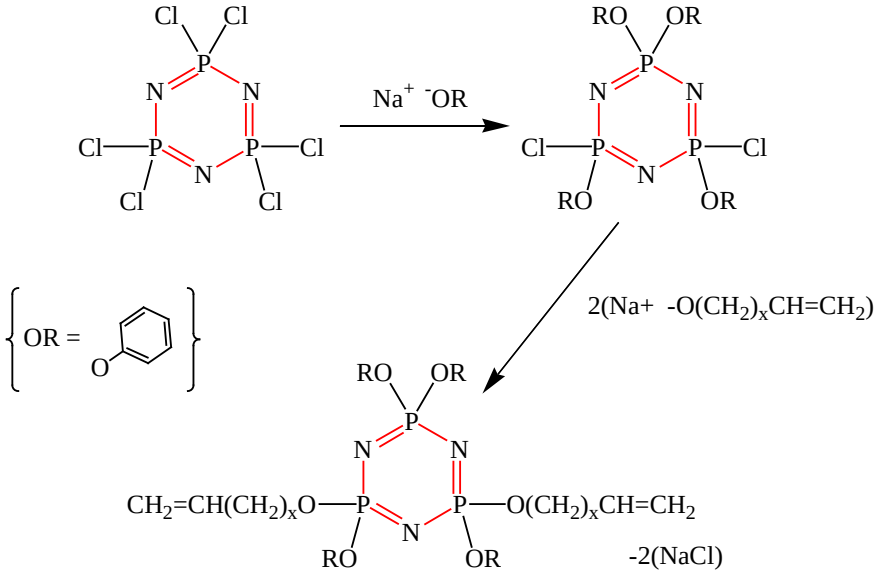

Figure 18 Cyclolinear monomer reported by Allcock *et al*.[55] for ADMET synthesis

Richards *et al*.[56] and Ainscough *et al*.[57] have also demonstrated that supramolecular self-assembly of compounds is possible using Ag(I) to form bridges between cyclophosphazene rings as shown in Figure 19.

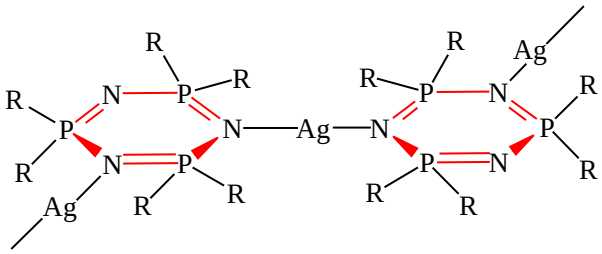

R = *n*-propyl,cyclohexyl, benzyl, or $P_3N_3(C_4H_8N)_6$

Figure 19 Supramolecular structure reported by Richards *et al*.[56]

Achieving known architecture of polyphosphazenes is more difficult and is subject to statistical variation when more than one side group is to be substituted onto the polymer backbone. This is discussed in more detail in Chapter 5.

1.2.2 Applications of phosphazenes: Biodegradable polyphosphazenes

A number of side groups can hydrolyse in the presence of water such that a hydroxyl group is formed. Side groups of this type include amino acid esters, imidazolyl, glucosyl, glyceryl (vide supra), glycolate and lactate. Following hydrolysis the hydroxyl proton can migrate to the neighbouring nitrogen atom and further hydrolytic degradation can occur to cause break-up of the polyphosphazene backbone (Figure 20) to yield harmless products that can be metabolised or excreted.[58]

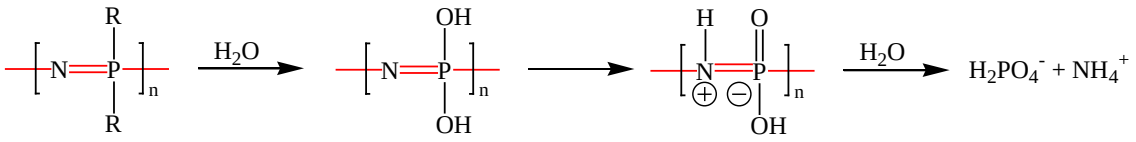

R = amino acid esters, imidazolyl, glucosyl, glyceryl, glycolate, lactate...

Figure 20 Hydrolysis of side groups leading to backbone degradation

This biodegradation allows the formulation of compounds capable of releasing pharmaceutical agents under controlled conditions. The release rate is dependent on the rate of hydrolytic decomposition of the polyphosphazene, which in turn is determined

by the nature and ratio of the side groups. The pharmaceutical agent can either be covalently attached to the backbone, or physically dispersed within a polymer matrix.

Other bioerodable polyphosphazenes have also been shown to be compatible host scaffolds for tissue engineering whereby the polyphosphazene provides a physical support for new tissue growth and eventually degrades into harmless products as the new tissue becomes self supporting.[59]

1.2.3 Applications of phosphazenes: Polyphosphazenes in dentistry and beyond

Biodegradation is not always a desirable property for new materials. Gettleman[41] describes positive results in the use of a fluoroethoxyphosphazene compounded with an acrylic resin, as being superior to a silicon lined denture when user groups were surveyed regarding the tactile preference. In addition the phosphazene compounds were also cited as being superior in their resistance to certain fungal strains.

Gettleman's paper[41] gives an insight into the politics of new materials. The particular polyphosphazene used for the dental trials was designated Eypel-F, a registered product of the Ethyl Corporation. This product was withdrawn from production in 1994, with the Ethyl Corporation citing the loss of valuable military contracts as the root cause despite continuing demand from the dental profession. Gettleman[41] also describes that engineers at the Ethyl Corporation had pointed out that the use of a polyphosphazene "O" ring would have prevented the Challenger space shuttle disaster in 1986, given its low glass transition temperature (-40 °C) and the fact that it would not burn. Whilst this may be true in principle, Feynman's[60] account of other manufacturing and managerial shortcomings within NASA during the Presidential Commission investigating the accident are aptly summarised in his comment that "For a successful technology, reality must take precedence over public relations, for nature cannot be fooled".

1.2.4 Applications of phosphazenes: Fuel cells

In today's environment of global uncertainty over fuel resources, supply and price, increasing attention is being given to alternative energy sources. New Zealand as a nation is well known for its investment in wind and hydro-electricity generation. Whilst these static systems are commercially viable, portable alternatives for transportation, to replace the dependence on fossil fuels are still in the experimental

stage. One possible power source is the direct methanol fuel cell,[61] in which polyphosphazenes can play a major role. Fuel cells are energy conversion devices that utilise air and a fuel (H_2 or methanol) to generate electricity. Early devices used fluorinated membranes to separate the electrodes, as these work well for H_2/air systems but suffer from high leakage between the anode and cathode when methanol is employed as the fuel component, thereby destroying performance. Sulfonated polyphosphazenes, as shown in Figure 21, have been demonstrated to perform well in air/methanol fuel cells although much work is still required to optimise performance and commercialise this technology.

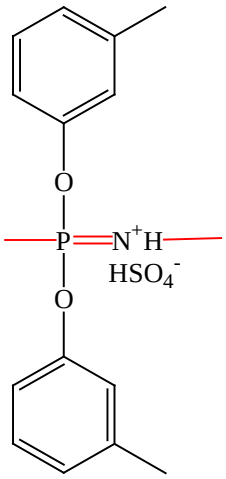

Figure 21 Poly[bis(3-methylphenoxy)phosphazene] used in methanol fuel cells

1.2.5 Applications of phosphazenes: Fire retardants

Dez *et al*.[62] reported the successful incorporation of cyclotriphosphazenes with hexamethyldiisocyanate to give cyclolinear polyurethane polymers (Figure 22) which have much higher decomposition temperatures than the parent polyurethane.

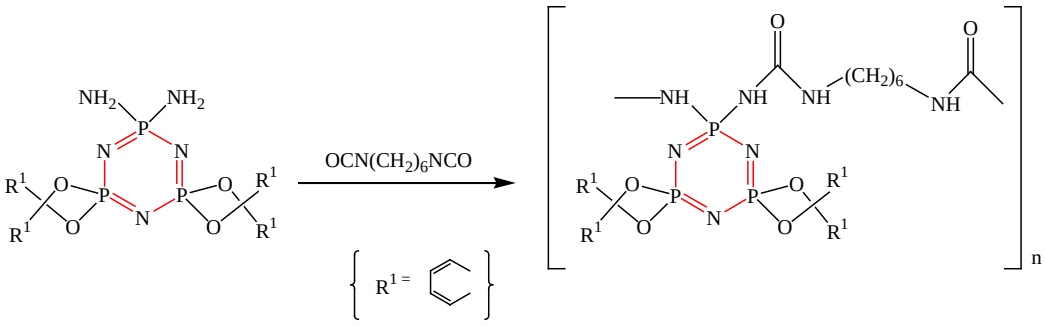

Figure 22 Cyclolinear phosphazene polymer reported by Dez *et al*.[62]

Allen *et al*.[63] made the observation that cyclo- and polyphosphazenes have the potential to be good, environmentally friendly fire retardants as an alternative to halogenated materials. The main factor in the widespread use of phosphazenes is one of cost and Allen *et al*.[63] suggest that more work is required into the nature of blended materials. A polyurethane material similar to that reported by Dez *et al*.[62], having a 20% loading of phosphazene, yielded a self-extinguishing blend. Traditional halogenated additives such as trichloroethanol and *p*-bromophenol increase the limiting oxygen index (LOI - being the percentage of oxygen required to sustain burning) of polyester resins from 18.0 to 21.6 and 24.0 respectively, whereas the LOI for phosphazene additives range from 24.0 [$N_3P_3(OMe)_6$] to 38.0 for [$N_3P_3(OCH_2C_2F_4H)_3Cl_3$].

1.2.6 Applications of phosphazenes: Hydrophobic and hydrophilic materials

Traditional organic polymers such as polytetrafluoroethene (PTFE) are produced by the polymerisation of fluorinated monomers, as shown in Figure 23.

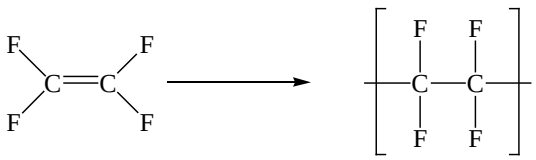

Figure 23 Schematic of PTFE polymerisation

This approach to polymerisation limits the ability to alter or tune the macroscopic properties of the polymer. Polyphosphazenes can be synthesised in a number of ways,

as detailed in greater depth in the introduction to Chapter 5, however, a simplified scheme is given in Figure 24.

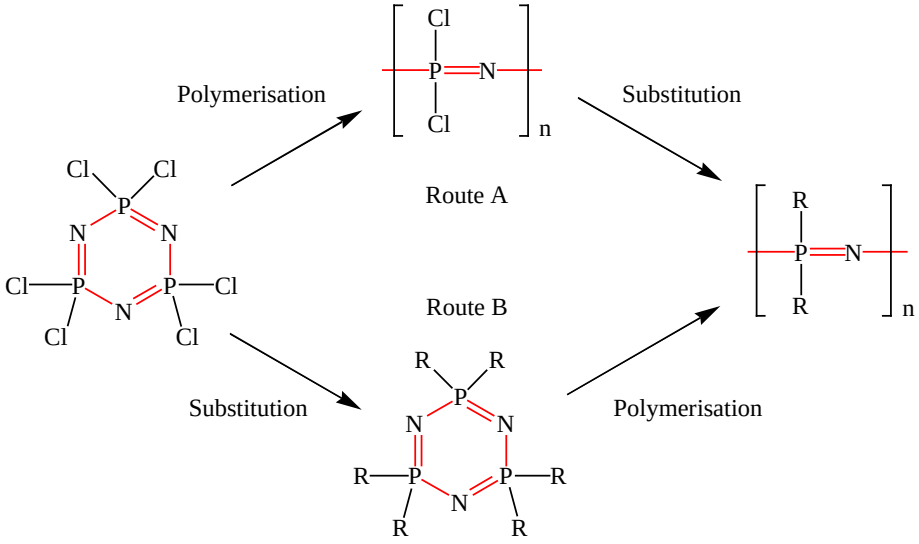

Figure 24 Polymerisation routes for polyphosphazenes

This versatility allows the properties of the final polymer to be adapted to different applications. Fluorinated polyphosphazenes with, for example, trifluoroethoxy side groups, are among the most hydrophobic polymers known to exist. Subsequent metathetical nucleophilic exchange reactions can further modify the polymer surface and hence its properties as demonstrated by Allcock *et al*.[64] and shown in Figure 25.

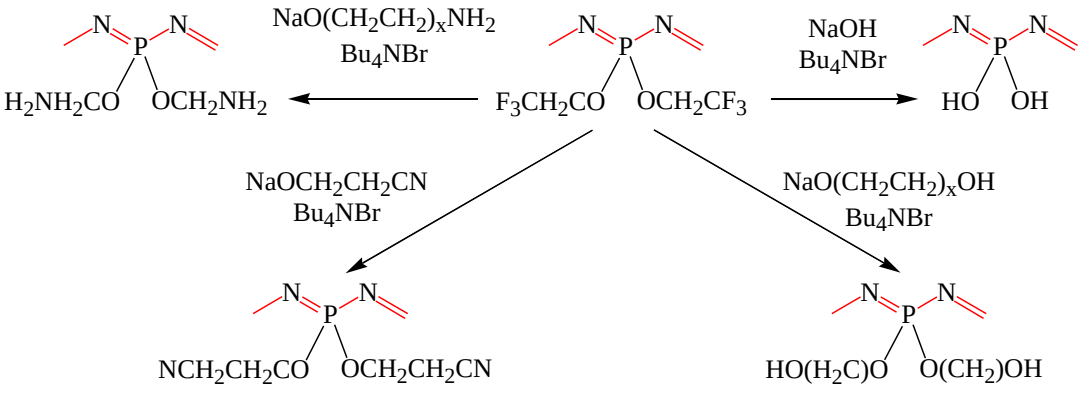

Figure 25 Surface modification of trifluoroethoxy substituted polyphosphazene as reported by Allcock *et al*.[64]

1.3 The present study

Chapter 2 introduces three new cyclotriphosphazene ligands, and a fourth related molecule that was synthesised purely for crystallographic comparison. Synthesis and characterisation of the ligands is the main theme of this chapter.
With reference to Figure 26, the new ligands are:

(i) Spiro(2,2'-biphenyl)tetrakis(2-oxypyridine)cyclotriphosphazene (**L**^{1}),

(ii) Spiro(2,2'-biphenyl)tetrakis(2-oxy-4-methylpyridine)cyclotriphosphazene (**L**^{2}), and

(iii) Spiro(2,2'-biphenyl)tetrakis(2-oxy-6-methylpyridine)cyclotriphosphazene (**L**^{3}).

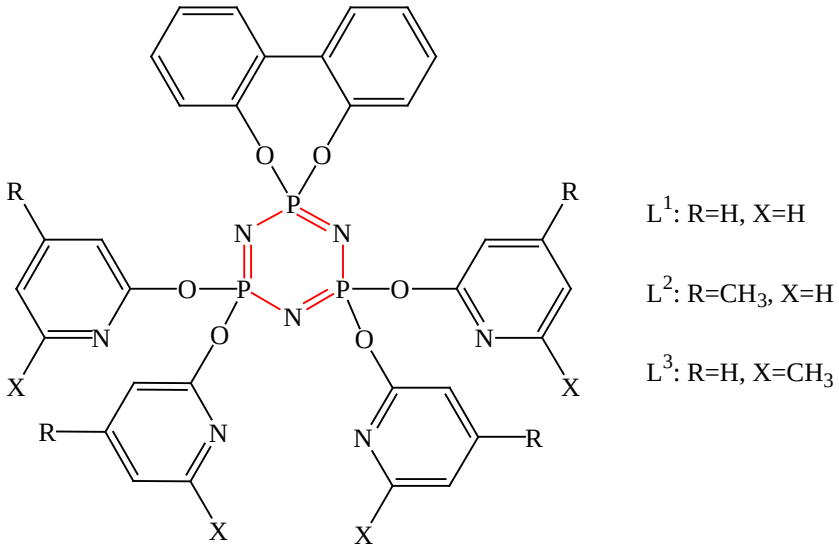

Figure 26 Schematic drawing of the new ligand design

Chapter 3 focuses on synthesis and characterisation of complexes of the ligands with selected transition metal halides and compares the single crystal X-ray structures.

Chapter 4 reports the single crystal X-ray structures and fluxional behaviour of the complexes [Zn$L^{2}Cl_{2}$], [Cd $L^{2}Cl_{2}$] and [Hg $L^{2}Cl_{2}$]. Variable temperature $^{31}P\{^{1}H\}$ NMR and ^{1}H NMR studies are undertaken and a possible mechanism for fluxional behaviour is postulated.

Chapter 5 translates the small molecule work from Chapters 3 and 4 by introducing a range of new polyphosphazenes containing pyridyloxy side groups which are reacted with selected transition metals.

Appendix 1 illustrates the practical laboratory synthesis of poly(dichloro)-phosphazene.

The accompanying CD-ROM contains an electronic copy of the entire thesis and CIF files for the single crystal X-ray structures.

1.4 References

1. Staudinger, H., *From Organic Chemistry to Macromolecules*. John Wiley & Sons, Inc.: New York, 1970; p. 303.

2. Allcock, H. R.; Best, R. J., *Can. J. Chem.* **1964,** 42, 447.

3. Mark, J. E.; Allcock, H. R.; West, R., *Inorganic Polymers*. 2nd ed, Oxford University Press, Inc.: New York, 2005; p. 144.

4. Carriedo, G. A., *J. Chil. Chem. Soc.* **2007,** 52(2), 1191 and references therein.

5. Diefenbach, U., Phosphazenes with pyridine side groups. In *Applicative Aspects of Cyclophosphazenes*, ed.; Gleria, M.; De Jaeger, R., Nova Science Publishers Inc: New York, 2004; p. 185-213.

6. Chaplin, A. B.; Harrison, J. A.; Dyson, P. J., *Inorg. Chem.* **2005,** 44(23), 8407.

7. Liebig, J.; Wöhler, J., *Ann. Chem.* **1834,** 11, 139.

8. Rose, H., *Ann. Chem.* **1834,** 11, 129.

9. Wichelhaus, H., *Chem. Ber.* **1870**, 163.

10. Stokes, H. N., *Am. Chem. J.* **1897,** 19, 782.

11. Mark, J. E.; Allcock, H. R.; West, R., *Inorganic Polymers*. 2nd ed, Oxford University Press, Inc.: New York, 2005; p. 338.

12. Tonei, D. M.; Bertani, R.; De Jaeger, R.; Gleria, M., In *Applicative Aspects of Cyclophosphazenes*, ed.; Gleria, M.; De Jaeger, R., Nova Science Publishers, Inc: New York, 2004; p. 1-30.

13. Kolich, C. H.; Meltsner, B. R.; Braxton Jr, H. G., **1991**. (5,006,324). Ethyl Corp. USA.

14. Shaw, R. A.; Fitzsimmons, B. W.; Smith, B. C., *Chem. Rev.* **1962,** 62, 247.

15. Audrieth, L. F.; Steinman, R.; Toy, A. D. F., *Chem. Rev.* **1943,** 32, 99.

16. Allcock, H. R., *Chemistry and Applications of Polyphosphazenes*. John Wiley and Sons Inc: New York, 2003; p. 11.

17. Allcock, H. R., *Phosphorus, Sulfur Silicon Relat. Elem.* **2004,** 179, 661.

18. Allen, C. W., *Chem. Rev.* **1991,** 91, 119.

19. Allcock, H. R., *Chemistry and Applications of Polyphosphazenes*. John Wiley and Sons Inc: New York, 2003; p. 110-122.

20. Allcock, H. R.; Harris, P. J., *Inorg. Chem.* **1981,** 20(9), 2844.

21. Diefenbach, U.; Kretschmann, M., *Z. Anorg. Allg. Chem.* **1998,** 624, 335.

22. Lehr, W.; Pietschmann, J., *Chem.-Ztg.* **1970,** 94, 362.

23. Lehr, W., *Z. Anorg. Allg. Chem.* **1967,** 350, 18.

24. Feistel, G. R.; Moeller, T., *J. Inorg. Nucl. Chem.* **1967,** 29, 2731.

25. Allcock, H. R., *Chemistry and Applications of Polyphosphazenes*. John Wiley and Sons Inc: New York, 2003; p. 95.

26. Gabler, D. G.; Haw, J. F., *Inorg. Chem.* **1990,** 29(20), 4018.

27. Gabler, D. G.; Haw, J. F., *Macromolecules* **1991,** 24(14), 4218.

28. Wisian-Neilson, P.; Neilson, R. H., *J. Am. Chem. Soc.* **1980,** 102, 2848.

29. Neilson, R. H.; Wisian-Neilson, P., *Chem. Rev.* **1988,** 88, 541.

30. Corradi, E.; Farina, A.; Gallazzi, M. C.; Bruckner, S.; Meille, S. V., *Polym. Int.* **1999,** 40, 4473.

31. Carriedo, G. A.; García Alonso, F. J.; González, P. A., *Macromol. Rapid Commun.* **1997,** 18, 371.

32. Carriedo, G. A.; Fernández-Catuxo, L.; García-Alonso, F. J.; Gómez-Elipe, P.; González, P. A., *Macromolecules* **1996,** 29(16), 5320.

33. Fitzsimmons, B. W.; Shaw, R. A., *Proc. Chem. Soc. (London)* **1961**, 258.

34. Fitzsimmons, B. W.; Hewlett, C.; Shaw, R. A., *J. Chem. Soc.* **1964,** Nov, 4459.

35. Ferrar, W. T.; DiStefano, F. V.; Allcock, H. R., *Macromolecules* **1980,** 13, 1345.

36. Karthikeyan, S.; Krishnamurthy, S. S., *J. Chem. Soc., Dalton Trans.* **1991,** 2, 299.

37. Allcock, H. R.; Kugel, R. L., *J. Am. Chem. Soc.* **1965,** 87, 4216.

38. Allcock, H. R.; Kugel, R. L.; Valan, K. J., *Inorg. Chem.* **1966,** 5, 1709.

39. Mark, J. E.; Allcock, H. R.; West, R., *Inorganic Polymers*. 2nd ed, Oxford University Press: New York, 2005; p. 130-131.

40. Allcock, H. R.; Kim, C., *Macromolecules* **1990,** 23(17), 3881.

41. Gettleman, L., In *Applicative Aspects of Poly(organophosphazenes)*, ed.; Gleria, M.; De Jaeger, R., Nova Science Publishers, Inc.: New York, 2004; p. 33-47.

42. Allcock, H. R., *Chemistry and Applications of Polyphosphazenes*. John Wiley and Sons Inc: New York, 2003; p. 24.

43. Chandrasekhar, V.; Krishnan, V., In *Applicative Aspects of Cyclophosphazenes*, ed.; Gleria, M.; De Jaeger, R., Nova Science Publishers, Inc: New York, 2004; p. 159-184.

44. Chandrasekhar, V.; Justin Thomas, K. R., *Appl. Organomet. Chem.* **1993,** 7, 1.

45. Ainscough, E. W.; Brodie, A. M.; Depree, C. V.; Otter, C. A., *Polyhedron* **2006,** 25, 2341.

46. Allcock, H. R., *Chemistry and Applications of Polyphosphazenes*. John Wiley and Sons Inc: New York, 2003; p. 72.

47. Diefenbach, U.; Cannon, A. M.; Stromburg, B. E.; Olmeijer, D. L.; Allcock, H. R., *J. Appl. Polym. Sci.* **2000,** 78, 650.

48. Diefenbach, U.; Kretschmann, M.; Stromburg, B. E., *Chem. Ber.* **1996,** 129, 1573.

49. Diefenbach, U.; Kretschmann, M.; Stromburg, B. E., *Phosphorus, Sulfur Silicon Relat. Elem.* **1997,** 124-125, 143.

50. Galicano, K. D.; Paddock, N. L., *Can. J. Chem.* **1982,** 60, 521.

51. Galicano, K. D.; Paddock, N. L.; Rettig, S. J.; Trotter, J., *Inorg. Nucl. Chem. Lett.* **1979,** 15, 417.

52. Justin Thomas, K. R.; Chandrasekhar, V.; Scott, S. R.; Hallford, R.; Wallace Cordes, A., *J. Chem. Soc., Dalton Trans.* **1993**, 2589.

53. Ainscough, E. W.; Brodie, A. M.; Depree, C. V.; Moubaraki, M.; Murray, K. S.; Otter, C. A., *J. Chem. Soc., Dalton Trans.* **2005,** 20, 3337 and references therein.

54. Wisian-Neilson, P.; Jung, J., H.; Potluri, S. K.; Mauldin, C. E.; Zhang, H., *Phosphorus, Sulfur Silicon Relat. Elem.* **2004,** 179, 817.

55. Allcock, H. R.; Clay Kellam III, E., *Macromolecules* **2002,** 35, 40.

56. Richards, P. I.; Steiner, A., *Inorg. Chem.* **2003,** 43, 2810.

57. Ainscough, E. W.; Brodie, A. M.; Depree, C. V.; Jameson, G. B.; Otter, C. A., *Inorg. Chem.* **2005,** 44, 7325.

58. Heyde, M.; Schacht, E., In *Applicative Aspects of Poly(organophosphazenes)*, ed.; Gleria, M.; De Jaeger, R., Nova Science Publishers, Inc.: New York, 2004; p. 1-32.

59. Tabata, Y., *PDA J. Pharm. Sci. Technol.* **2000,** 3, 80.

60. Leighton, R., *What do you care what other people think?* Unwin Hyman Ltd.: London, 1989; p. 248.

61. Pintauro, P. N.; Wycisk, R., In *Applicative Aspects of Poly(organophosphazenes)*, ed.; Gleria, M.; De Jaeger, R., Nova Science Publishers, Inc.: New York, 2004; p. 225-254.

62. Dez, I.; Levalois-Mitjaville, J.; Grützmacher, H.; Gramlich, V.; De Jaeger, R., *Eur. J. Inorg. Chem.* **1999,** 10, 1673.

63. Allen, C. W.; Hernandez-Rubio, D., In *Applicative Aspects of Poly(organophosphazenes)*, ed.; Gleria, M.; De Jaeger, R., Nova Science Publishers, Inc.: New York, 2004; p. 119-137.

64. Allcock, H. R.; Steely, L. B.; Singh, A., *Polym. Int.* **2006,** 55, 621.

Chapter 2: Phosphazene Ligand Syntheses

2.0 Abbreviations used in Chapter 2

biph	2,2'-dioxybiphenyl
2OPy	2-oxypyridine
2O-4-MePy	2-oxy-4-methylpyridine
2O-6-MePy	2-oxy-6-methylpyridine
OOP	Out of plane
ESMS	Electrospray Mass Spectrometry

2.1 Introduction

The overall aim of this body of research is to undertake the synthesis of polyphosphazenes containing 2-pyridyloxy side-groups capable of coordinating to transition metals. Such systems have wide potential for applications such as catalysts, conductors, ion exchangers and in biomedical drug delivery to name a few.[1, 2] In order to elucidate possible pathways and develop new polyphosphazenes, the role of small cyclic model systems is crucial to establish that complete halogen replacement is possible, if side reactions are likely and to identify optimal reaction conditions.[3, 4] The use of small molecules as templates allows for ease of synthesis and, since the chloropolymer $[NPCl_2]_n$ is exceedingly sensitive to hydrolysis, permits the use of standard techniques for analysis, such as ESMS and X-ray crystallography which are not conducive to polymeric materials.[5] In addition, reported CHN microanalysis figures for polymers invariably demonstrate greater variance than for small molecules. In solution, the cyclotriphosphazene has also been shown to be sensitive to hydrolysis,[6] hence reactions need to be undertaken in anhydrous conditions.

Accurate characterization of polymeric materials is fraught with uncertainty, especially when more than one side group or co-substituent is attached to the polymer backbone. By their very nature polyphosphazenes are flexible, having very low bond torsion[7] and random orientations lead to localized, semi-ordered aggregations, formation of lamellae and semi-crystalline regions in conjunction with amorphous phases. These different phases are greatly affected by the size and chemical nature of the side groups as well as the distribution of these groups along the backbone. For short chain length polymers, end group concentration may also become a factor in the microscopic and macroscopic properties. In co-substituent polymers the distribution of the side groups and degree of tacticity can only be reasoned in terms of statistical probability, although for phosphazene polymers with organic side groups, $^{31}P\{^{1}H\}$ NMR spectra can give an insight into the number distribution of the side groups by integration of the spectral peaks, though the random nature of the polymers often leads to line broadening and thus a degree of uncertainty.[8]

Also, unlike the cyclophosphazenes, the polymer may exist in various conformations due to random orientation of the backbone. The inherent flexibility may also reduce the ability to coordinate to transition metals by favouring π-π stacking of, for example, aryloxy moieties.

2.1.1 The main areas of cyclophosphazene research

From a review of the scientific literature, three broad areas of cyclotriphosphazene research are apparent:

(i) Substitution patterns of side groups,
(ii) Macroscopic properties of hexasubstituted ligands, and
(iii) Studies concerning ligand design and chelating abilities of the ring and exocyclic groups.

Brief examples of these three areas are given below.

(i) Reactions of cyclotriphosphazene with amines afford a mixture of geminal and non-geminal products as shown in Table 1.

Formula	Amine type	Gem or non-gem	Comments
NH_3	Ammonia	Gem	
NH_2R	Primary	Both	Depends on steric bulk
NHRR'	Secondary	Gem << non-gem	
NRR'R"	Tertiary	Gem < non-gem	Possible electronic effect

Table 1 General substitution patterns for amines with cyclotriphosphazenes

The substitution pattern for amines given in Table 1 is very general and not fully understood since solvent effects also appear to have a major influence on substitution patterns.[9]

As recently as 2004, Wisian-Neilson *et al.*[10] reported studies on non-geminal substitution of $[(Me)(Ph)PN]_3$ with MeI, finding that regioselectivity is also a factor in the substitution pattern. The *trans* isomer reacted cleanly with three equivalents of MeI to give a trisubstituted product as shown in Figure 1, however the *cis* isomer, under identical reaction conditions, gave a mixture of di- and trisubstituted products.

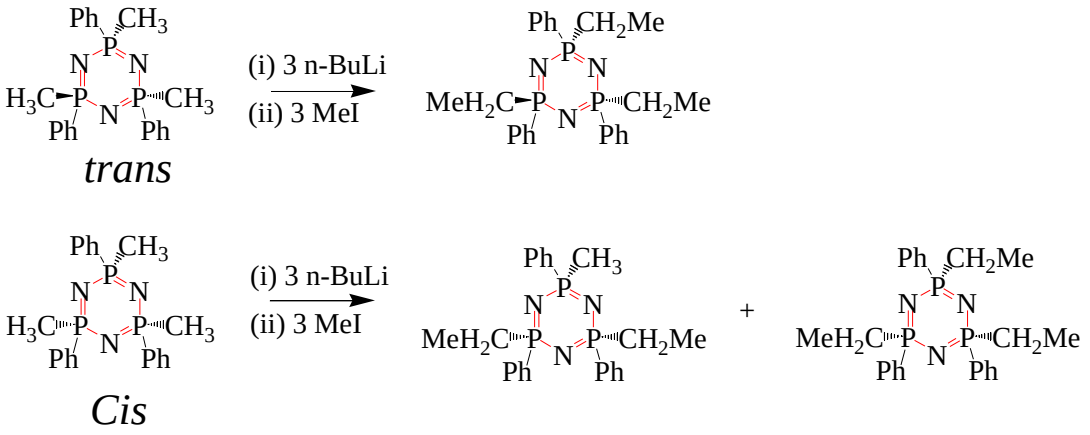

Figure 1 Reaction scheme for the *trans* isomer of $[(Me)(Ph)PN]_3$ reported by Wisian-Neilson *et al.*[10]

Jung *et al.*[11, 12] reported geminal only substitution of the hexachlorocyclotriphosphazene by 2-thiopyridine to give 1,1-bis(pyridyl-2-thio)-3,3,5,5-tetrachlorocyclotriphosphazene. Despite three potential bis-substituted isomers being possible, modification of mole ratios and reaction times failed to produce anything but the 1,1 isomer (Figure 2).

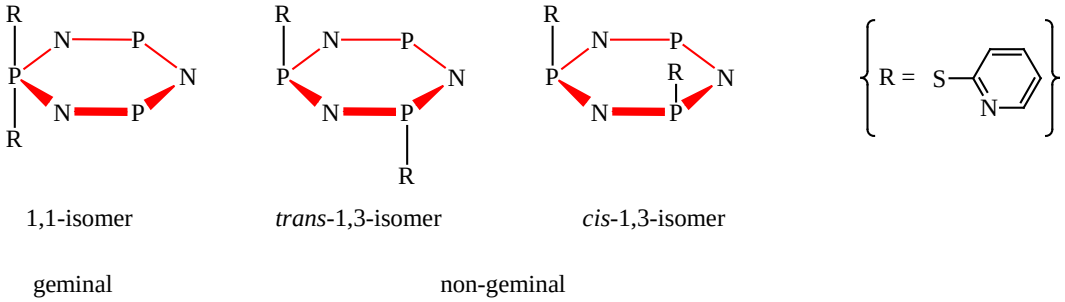

Figure 2 Potential bis-substituted isomers reported by Jung *et al.*[11, 12]

The affects of steric bulk on the substitution pattern are well illustrated by Krause *et al.*[13] and by Chandrasekhar *et al.*[14] In attempting to synthesise fully substituted adamantane and cyclohexylamine cyclotriphosphazenes respectively, it was found that the major products were the tetrakis compounds shown in Figure 3.

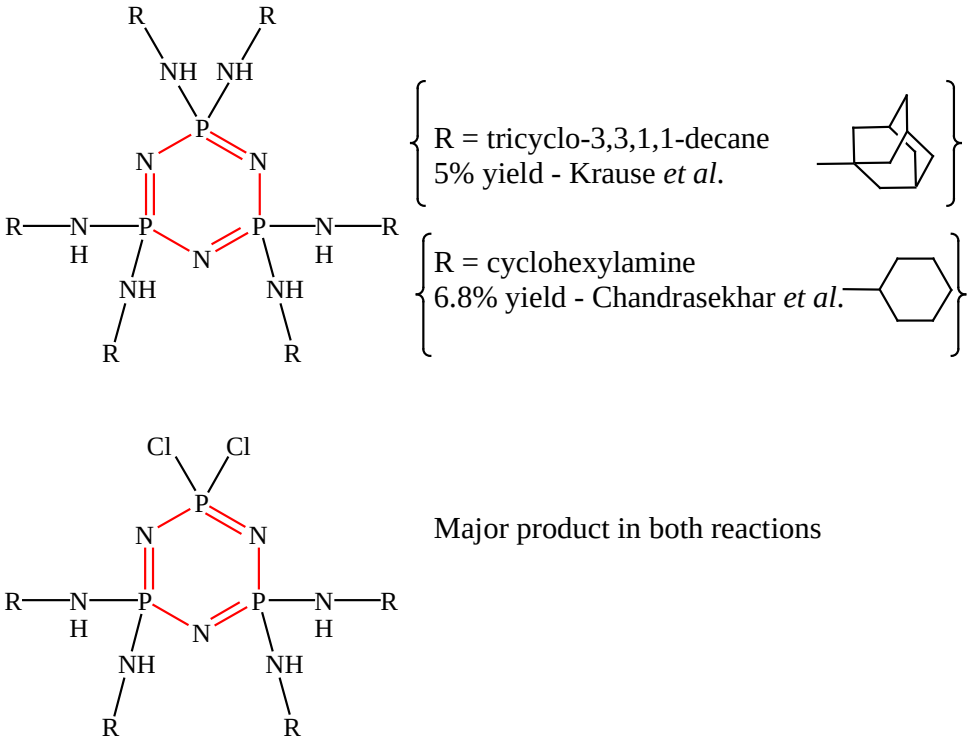

Figure 3 Reaction products reported by Krause *et al.*[13] and Chandrasekhar *et al.*[14]

In both cases, reaction with the octachlorocyclotetraphosphazene afforded the fully substituted octakis products, which was attributed to the greater skeletal flexibility of the tetramer over the trimer.

(ii) Macroscopic properties of the small molecules (and indeed the polymeric analogues) are of interest in their own right. The adamantane compounds reported by Krause *et al.*[13] are expected to confer high thermal and oxidative stability, and high density.

The fully substituted hexakis(trifluoroethoxy)cyclotriphosphazene is unusually stable to heat, light and water, and for this reason was the side group selected for the first stable polyphosphazene synthesised in 1964 by Allcock *et al.*[15, 16] This polymer remains one of the most hydrophobic known to exist.

Tonei *et al*.[17] claim that the cyclophosphazene based hydraulic fluids are one of the most important classes of phosphazene derivatives, for use as lubricants and additives with a wide range of applications. Cyclotri- and cyclotetraphosphazene hydraulic fluid additives containing fluoroalkoxy groups, for example, confer high thermal stability and resistance to halogen gases.

(iii) Ligands capable of coordination to metals through electron lone-pair donation, and with multidentate chelating ability are summarised in the introduction to Chapter 3. However, some specific examples of pyridine moieties are now given to establish certain criteria regarding potential problems with these species.

In 1994, Diefenbach *et al*.[18] described the synthesis of the first pyridine substituted phosphazenes. That pyridine substitution had not received previous investigation is attributed by Diefenbach to early work by Audrieth *et al*.[19] in 1943, and Migachev *et al*.[20] (Figure 4) in 1966, who described the formation of derivatives from halogenated phosphazenes exposed to pyridine compounds, and their subsequent decomposition.

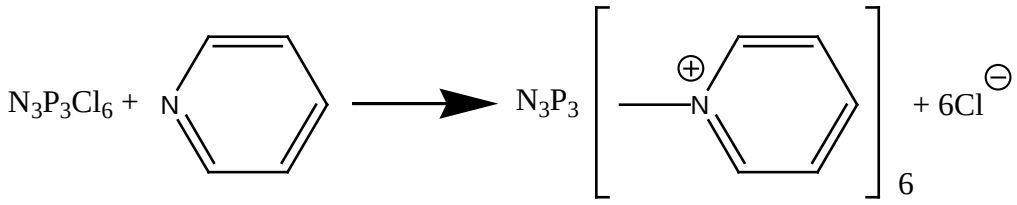

Figure 4 Phosphazenylpyridinium salt reported by Migachev *et al*.[20]

Diefenbach *et al*.[18] reported that reaction of aminopyridine groups with hexachlorocyclotriphosphazene did indeed create a mixture of substituted products, decomposition products and some unidentified side products. However, pentaphenoxymonochlorocyclotriphosphazene formed a stable product on substitution of the remaining chlorine with the aminopyridine group. The electron withdrawing phenoxy moieties, combined with their steric bulk were attributed with conferring stability on the phosphazene system (Figure 5).

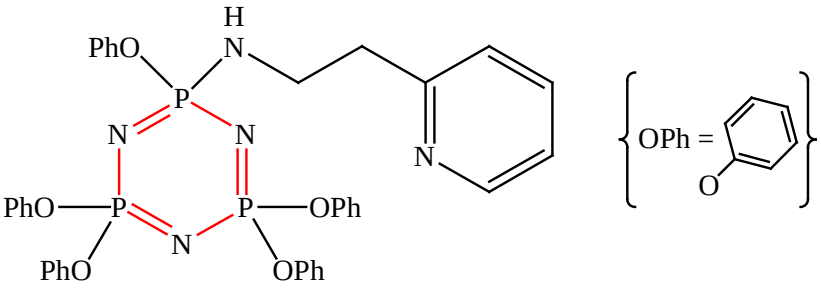

Figure 5 Structure of the 2-ethylaminopyridine reaction product reported by Diefenbach *et al.* [18]

Diefenbach *et al.*[4, 21-25] developed this work over the period 1994-1999, with further aminopyridine moieties, extending to the formation of transition metal coordination complexes. The coordination behaviour of cyclophosphazenes is complex, electron withdrawing groups (e.g. pyrazolyl or imidazolyl) favour metal coordination to the side groups, whereas electron donating groups (e.g. amines) favour phosphazene ring nitrogen coordination. Intermediate structures with both side group and phosphazene ring nitrogen coordination are also known.

In 1995, Carriedo *et al.*[26] synthesised two fully substituted compounds, hexakis(2-pyridyloxy)cyclotriphosphazene and hexakis(4-pyridyloxy)cyclotriphosphazene (Figure 6). The hexakis(4-pyridyloxy)cyclotriphosphazene reportedly formed in low yield (19%) which was partly attributed to decomposition.

Carriedo *et al.*[27, 28] synthesised the first polyspirophosphazene containing biph moieties in high yield and purity, noting that the polymers formed were both stable and lacking in side branches. Thus incorporation of these groups became a feature of the small molecule syntheses in the present work with a view to reducing potential problems with the polymer synthesis.

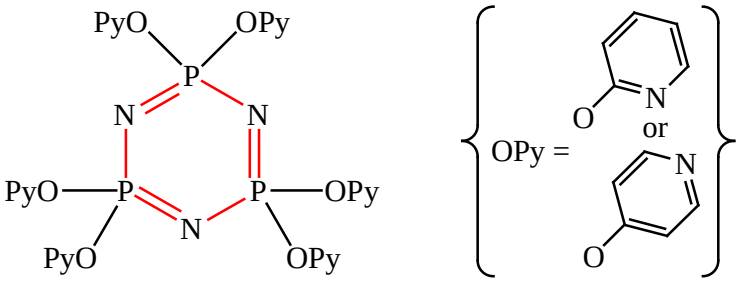

Figure 6 Structure reported by Carriedo *et al*.[26]

Work reported by Ainscough *et al*.[29-31] demonstrates that the hexakis(2-pyridyloxy)-cyclotriphosphazene ligand (pyridyloxy in this case being 2OPy or 2O-4-MePy) is very versatile and demonstrates multidentate behaviour with transition metals. The related species bis(biph)bis(2O-4-MePy)cyclotriphosphazene has also been reported.[32]
The choice of the cyclotriphosphazene as a template is somewhat moot since the cyclotetraphosphazene or higher cyclic species might better mimic conditions on the polyphosphazene backbone due to their greater flexibility.[8, 9, 29] However, the cyclotriphosphazene is easiest to prepare, is readily available from commercial sources and relatively inexpensive. In addition, prior work within the Ainscough/Brodie group[30, 31, 33, 34] and by others,[26, 35] has studied hexakis(2-pyridyloxy) and bis(biph)bis(2-pyridyloxy) cyclotriphosphazene derivatives[32] (Figure 7).

2.1.2 Investigation protocol for small molecule phosphazene models

The present study has the ultimate objective of achieving synthesis and characterization of metal bearing phosphazene polymers, thus a protocol for precursor cyclic model templates was established.

(i) The compound (biph)tetrakis(2-pyridyloxy)cyclotriphosphazene (Figure 8) completes the stereochemical studies within the Ainscough/Brodie group.[31]

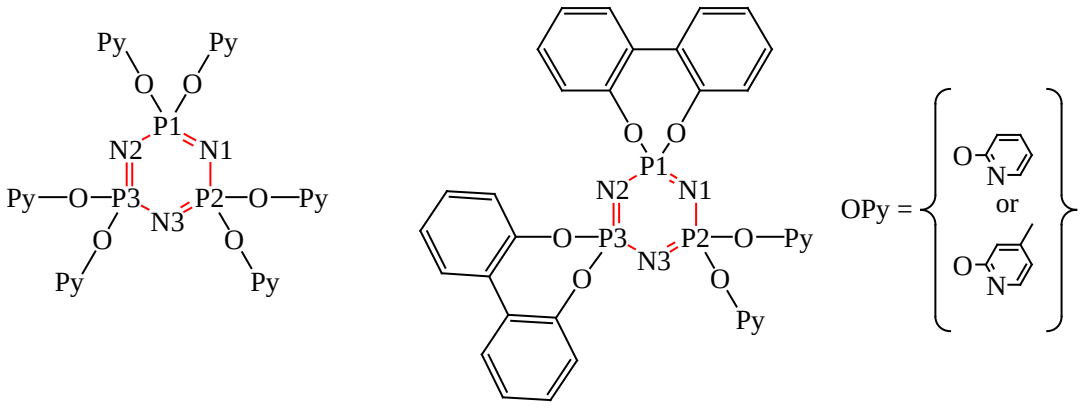

Figure 7 Cyclotriphosphazene structures studied within the Ainscough/Brodie group[31]

(ii) Geometric models established that having the pyridyl C-O bond in the two position, i.e. *ortho* to the pyridyl nitrogen atom, affords the greatest potential for electron donation from the $N_{pyridyloxy}$ and $N_{cyclotriphosphazene}$ donor set. This protocol was important to establish, and then to transfer it to the polyphosphazenes.

(iii) Solubility of the final polymer is critical for characterization, thus the solubility of the model cyclotriphosphazene system, and potentially the polymer, would be investigated by methyl substitution on the pyridyl rings.

2.1.3 Cyclophosphazenes designed in the present work

With reference to Figure 8, the new ligands to be synthesised are:

(biph)tetrakis(2-pyridyloxy)cyclotriphosphazene **(L^1)**
(biph)tetrakis(4-methyl-2-pyridyloxy)cyclotriphosphazene **(L^2)**
(biph)tetrakis(6-methyl-2-pyridyloxy)cyclotriphosphazene **(L^3)**
(biph)tetrakis(6-chloro-2-pyridyloxy)cyclotriphosphazene **(L^4)**

(N.B. **L^4** is included only for crystallographic comparison (vide infra))

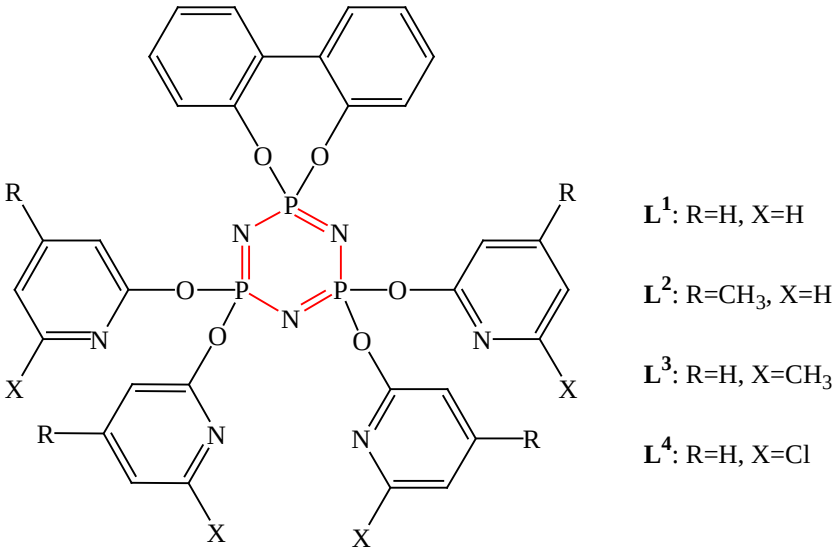

Figure 8 Schematic drawing of the new ligand design

2.2 Experimental section

All manipulations were carried out under nitrogen using standard Schlenk techniques. Analytical grade solvents were purchased from standard chemical suppliers and used without further purification. Cs_2CO_3 (Acros), was dehydrated at 140 ºC prior to use. K_2CO_3 (BDH), $[N_3P_3Cl_6]$ (Aldrich), 2-hydroxypyridine (Aldrich), 2-hydroxy-4-methylpyridine (Aldrich) and 2-hydroxy-6-methylpyridine (Aldrich), were all used as received. 2,2'-biphenol (Merck) was sublimed in vacuo prior to use to give a white crystalline solid. The cyclotriphosphazene, $[N_3P_3Cl_6]$ (Otsuka Chemical Co.) was recrystallised from hot heptane prior to use.

Microanalyses were performed by Campbell Microanalytical Laboratory, University of Otago. NMR spectra were recorded on a Bruker Avance 400 MHz spectrometer in $CDCl_3$. IR spectra were run as KBr discs on a Perkin-Elmer Paragon 1000 and a Nicolet 5700 which was also used for Far IR spectra on polyethylene media. UV/vis spectra were recorded on Shimadzu UV-160A (200-1100 nm) and Shimadzu UV-310PC (200-1200 nm) instruments. Electrospray mass spectra were collected from CH_3CN solutions on a micromass ZMD spectrometer run in positive ion mode.

2.2.1 Syntheses of the ligands

Three ligands, $\mathbf{L^1}$, $\mathbf{L^2}$ and $\mathbf{L^3}$ have been synthesised for subsequent reaction with transition metals. A fourth compound ($\mathbf{L^4}$) has also been synthesised as a model to compare with the X-ray structure of $\mathbf{L^3}$. Reactions were followed by $^{31}P\{^1H\}$ NMR.

2.2.2 X-ray crystallography

The X-ray data was collected on a Siemens P4 four circle diffractometer, using a Siemens SMART 1K CCD area detector. The crystals were mounted in an inert oil, transferred into the cold gas stream of the detector and irradiated with graphite monochromated Mo Kα (k = 0.71073 Å) X-rays. The data were collected by the SMART program and processed with SAINT to apply Lorentz and polarisation corrections to the diffraction spots (integrated 3 dimensionally). Crystal refinement data are given in Table 2, selected bond lengths and angles are in Table 3 and the numbering scheme is given in Figure 10. The structures were solved by direct methods and refined using the SHELXTL program.[36] Hydrogen atoms were calculated at ideal positions.

2.2.3 Preparation of $[N_3P_3(biph)Cl_4]$

This preparation followed that of the literature.[28]

A mixture of $[N_3P_3Cl_6]$ (2.006 g, 5.770 mmol), biph (1.070 g, 5.746 mmol) and K_2CO_3 (4.002 g, 28.956 mmol) in acetone (100 ml) was stirred under N_2 overnight. The solution was filtered through celite, washed with CH_2Cl_2 (3 x 40 ml) and dried in vacuo. White crystals were obtained by slow diffusion from CH_2Cl_2/hexane at 4 ºC. Yield: 2.27 g, (74%). $^{31}P\{^1H\}$ NMR ($CDCl_3$): δ 25.9 (d, J = 71 Hz), 14.0 (t, J = 71 Hz).

2.2.4 Preparation of (biph)tetrakis(2-pyridyloxy)cyclotriphosphazene (L^1)

To a stirred suspension of $[N_3P_3(biph)Cl_4]$ (0.260 g, 0.570 mmol) in acetone (80 ml) was added 2-hydroxypyridine (0.220 g, 2.300 mmol) and Cs_2CO_3 (0.860 g, 2.640 mmol). After stirring under N_2 for two days, the solution was filtered through Celite, washed with CH_2Cl_2 and dried under vacuum. White crystals were obtained by slow diffusion from CH_2Cl_2/hexane at 4 °C. Yield: 0.63 g (81%). Elemental Analysis: Calculated for $C_{32}H_{24}N_7O_6P_3$: C, 55.26; H, 3.48; N, 14.10. Found: C, 55.09; H, 3.87; N, 13.46. ESMS:

m/z 696 $[M+H]^+$, 828 *m/z* $[M+Cs]^+$. $^{31}P\{^1H\}$ NMR ($CDCl_3$): δ 26.8 (t, J_{PP} = 94 Hz), 8.0 (d, J_{PP} = 95 Hz). ^1H NMR ($CDCl_3$): δ 8.21 (d, *J* = 4.9 Hz), 7.62 (t, *J* = 7.4 Hz), 7.11 (d, *J* = 8.2 Hz), 7.04 (t, *J* = 6.0 Hz). IR (KBr disc) ν/cm-1 (PN): 1225, 1172. M_P 195-197 °C

2.2.5 Preparation of (biph)tetrakis(4-methyl-2-pyridyloxy)cyclotriphosphazene (L^2)

To a stirred suspension of $[N_3P_3(biph)Cl_4]$ (1.310 g, 2.850 mmol) in acetone (100 ml) was added 2-hydroxy-4-methylpyridine (1.250 g, 11.450 mmol) and Cs_2CO_3 (4.250 g, 13.040 mmol). After stirring at reflux under N_2 for eight days, the reaction mixture was filtered through a Celite pad, which was washed with acetone. The combined filtrates were added slowly to a small quantity of distilled water (5 ml) to form a milky solution, which on continued addition yielded the product as a white precipitate. The precipitate was collected by filtration and dried under vacuum. Fine white crystals were obtained from a solution of CH_2Cl_2/hexane. Yield: 1.28 g (50%).

$^{31}P\{^1H\}$ NMR ($CDCl_3$): δ 26.5 ppm (t, *J* = 96 Hz), 7.9 ppm (d, *J* = 97 Hz). ^1H NMR ($CDCl_3$): δ 8.08 (d, *J* = 5.1 Hz), 6.92 (s), 6.94 (d, *J* = 5.1 Hz), 2.31 (s, methyl). ESMS: *m/z* 752 $[M+H]^+$. Elemental Analysis: Calculated for $C_{36}H_{32}N_7O_6P_3$: C, 57.53; H, 4.29; N, 13.05. Found: C, 57.25; H, 4.42; N, 12.98. IR (KBr disc) ν/cm-1 (PN): 1195, 1142. M_P 162-165 °C

2.2.6 Preparation of (biph)tetrakis(6-methyl-2-pyridyloxy)cyclotriphosphazene (L^3)

To a stirred suspension of $N_3P_3(biph)Cl_4$ (0.607 g, 1.317 mmol) in acetone (100 ml) was added 2-hydroxy-6-methylpyridine (0.740 g, 6.780 mmol) and NaH (0.160 g, 6.666 mmol). After stirring at reflux under N_2 for fourteen days, the reaction mixture was filtered through celite and washed with acetone to give a clear light pink liquid. Fine white crystals were obtained from a solution of CH_2Cl_2/hexane. Yield: 1.327 g, (98.5%).

$^{31}P\{^1H\}$ NMR ($CDCl_3$) gave δ 27.0 ppm (t, J = 96 Hz), 7.8 ppm (d, J = 97 Hz). ^1H NMR ($CDCl_3$): δ 7.29 (t, *J* = 8.2 Hz), 6.33 (d, *J* = 9.1 Hz), 5.98 (d, *J* = 7.0 Hz), 2.29 (s, methyl). ESMS, 752 *m/z* $[M+H]^+$. Elemental analysis: Calculated for $C_{36}H_{32}N_7O_6P_3 \cdot 0.66\ C_6H_{14}$ (809.73): C, 59.33; H, 5.26; N, 12.11. Found: C, 59.08; H, 4.84; N, 11.89. IR (KBr disc) ν/cm^{-1}, 1213, 1168, 1094. M_P 152-158 ºC.

2.2.7 Preparation of (biph)tetrakis(6-chloro-2-pyridyloxy)cyclotriphosphazene (L^4)

To a stirred suspension of $[N_3P_3(biph)Cl_4]$ (0.480 g, 1.040 mmol) in CH_2Cl_2 (50 ml) was added 2-hydroxy-6-chloropyridine (0.540 g, 4.170 mmol) and Cs_2CO_3 (1.350 g, 4.170 mmol). After stirring at under N_2 for three days, the reaction mixture was filtered through celite and washed with acetone to give a clear light purple liquid which was taken to dryness to give a pink powder. Lustrous crystals were obtained on evaporation of $CHCl_3$. Yield: 0.780 g, (77%).

$^{31}P\{^1H\}$ NMR ($CDCl_3$): δ 25.23 ppm (t, J = 96 Hz), 7.09 ppm (d, J = 97 Hz). ^1H NMR ($CDCl_3$): δ 7.58 (t, *J* = 7.9 Hz), 7.08 (d, *J* = 2.1 Hz), 7.06 (d, *J* = 2.5 Hz). ESMS: 832 *m/z* $[L+H]^+$, 964 *m/z* $[L+Cs]^+$. Elemental analysis: Calculated for $C_{32}H_{20}N_7O_6P_3Cl_4$: C, 45.96; H, 2.42; N, 11.92; Cl, 17.44. Found: C, 46.12; H, 2.42; N, 11.77; Cl, 17.02. IR (KBr disc) ν/cm^{-1}, 1213, 1094. M_P 182-184 ºC.

2.3 Observations regarding the syntheses of the ligands

The ligands $\mathbf{L^1}$, $\mathbf{L^2}$ and $\mathbf{L^3}$ were synthesised by reaction of the precursor spiro(biph)tetrachlorocyclotriphosphazene with the appropriate salts of the 2-hydroxypyridine system in acetone ($\mathbf{L^1}$, $\mathbf{L^2}$, $\mathbf{L^3}$) or CH_2Cl_2 ($\mathbf{L^4}$) and at reflux ($\mathbf{L^2}$, $\mathbf{L^3}$) as per the generic reaction scheme given in Figure 9. All reactions required the pyridyloxy derivative and the K_2CO_3, Cs_2CO_3 or NaH used for proton abstraction in excess. Carriedo *et al*.[37] reported that the use of Cs_2CO_3 as base affords faster reaction times than with K_2CO_3 for a range of alkoxy and aryloxy groups, however, a rigorous assessment of optimum reaction conditions has not been attempted.

It was found that subliming the “as received” 2,2'-biphenol to give a white crystalline solid of high purity, removed the need for solvent extraction during work up. Initial difficulties obtaining an X–ray crystal structure for $\mathbf{L^3}$ led to the synthesis of an analogue using 2-hydroxy-6-chloropyridine ($\mathbf{L^4}$) which, for completeness, is included herein.

An alternative way of performing the synthesis is using a one-pot process starting from $[N_3P_3Cl_6]$ using Cs_2CO_3 for nucleophilic substitution of the 2,2'-dioxybiphenyl and the 2-pyridyloxy derivative, but subsequent separation of the product from the reaction mixture is

difficult due to the similar solubilities of the component by-products. $^{31}P\{^{1}H\}$ NMR identifies the one-pot reaction mixture (for the 2O-4-MePy derivative) as constituting the phosphazene with the hexasubstituted pyridine derivative (s, 6.6 ppm), the phosphazene with two substituted 2,2'-biphenolate moieties (d, 27.9 ppm, t, 10.5 ppm), and the desired product with one 2,2'-biphenolate moiety (d, 8.9 ppm, t, 27.8 ppm). Thus it was found to be preferable to undertake the 2,2'-dioxybiphenyl protection using a 1:1 molar ratio of the starting materials and K_2CO_3 as proton abstractor, followed by crystallisation to obtain the pure tetrachloro compound for subsequent nucleophilic substitution of the remaining chlorine groups with the 2-pyridyloxy derivative using Cs_2CO_3 as shown in Figure 9.

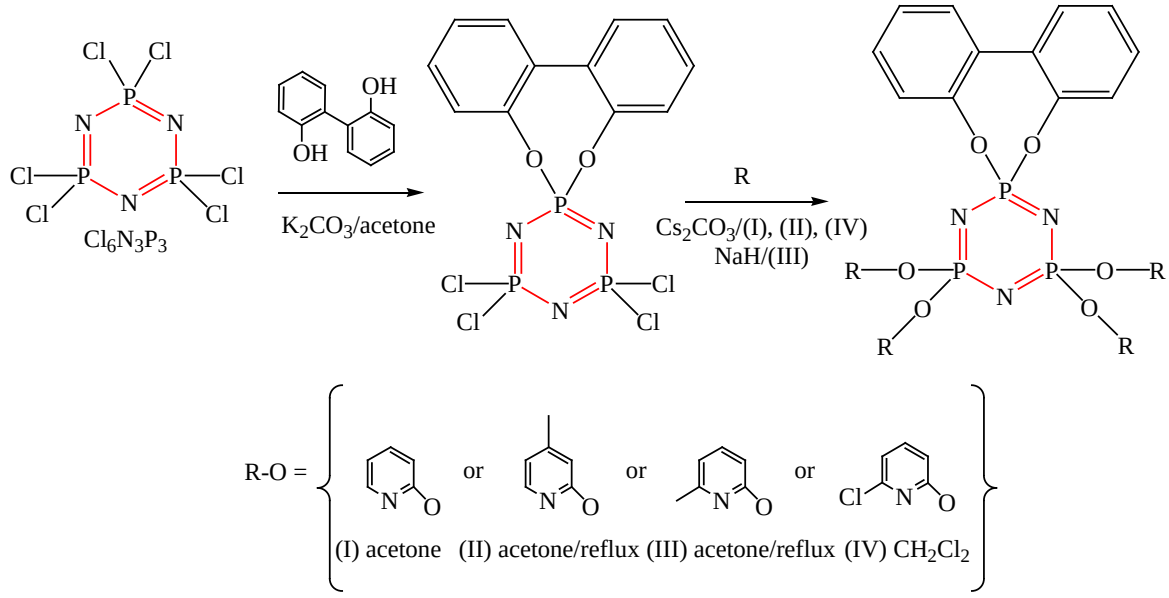

Figure 9 Generic reaction scheme for ligand syntheses

Reaction times for the ligands vary markedly, at two, eight and fourteen days respectively for $\mathbf{L^1}$, $\mathbf{L^2}$ and $\mathbf{L^3}$ ($\mathbf{L^2}$ and $\mathbf{L^3}$ requiring refluxing conditions). However $\mathbf{L^4}$, the 6-chloro-2-pyridinoxy derivative, takes just three days without reflux in CH_2Cl_2. It is postulated that for $\mathbf{L^1}$, $\mathbf{L^2}$ and $\mathbf{L^3}$ the reaction is increasingly hampered by steric hindrance due to the presence of the methyl group and its position on the pyridyl ring.

For the chloro analogue, $\mathbf{L^4}$, it was considered that steric hindrance would be a factor, having the chlorine *ortho* to the pyridyl nitrogen, and that the greater electronegativity of chlorine might act to reduce the nucleophilicity of the attacking oxygen. However, Allen[38] points out that with respect to exocyclic electronic effects, if the nucleophile is electron donating then the rate of bimolecular reaction is reduced as the electrophilic nature of the phosphazene is subsequently reduced. Thus in the case of the chloropyridine moiety it can be reasoned that the presence of the first chloropyridine substituent must be electron withdrawing leading to an increased rate of substitution for the second chloropyridine. Since $\mathbf{L^4}$ was only synthesised in order to elucidate a possible structure for $\mathbf{L^3}$, due to persistent failure to grow X-ray quality crystals, further investigation into the $\mathbf{L^4}$ mechanism and possible solvent interaction is beyond the scope of this work.

ESMS for the free ligands always gave $[L+H]^+$ as the major species, although it is not uncommon to see minor species of $[L+Cs]^+$ where caesium is still present in the post work-up solution.

2.3.1 Crystal structures of the ligands

Refinement data for the X-ray crystal structures are given in Table 2.

Compound	$\mathbf{L^1}$	$\mathbf{L^2}$	$\mathbf{L^3}$	$\mathbf{L^4}$
Molecular formula	$C_{32}H_{24}N_7O_6P_3$	$C_{36}H_{32}N_7O_{6.25}P_3$	$C_{36}H_{32}N_7O_6P_3$	$C_{32}H_{20}Cl_4N_7O_6P_3$
Molecular weight	695.49	751.60	751.60	833.26
T (K)	84(2)	84(2)	111(2)	98(2)
Crystal System	Monoclinic	Monoclinic	Orthorhombic	Monoclinic
Space Group	$C2/c$	$P2/n$	$Pna2_1$	$P2(1)/c$
a (Å)	20.315(4)	15.1534(4)	35.3551(17)	12.3798(4)
b (Å)	10.629(2)	10.9489(3)	10.8858(5)	15.3067(4)
c (Å)	16.762(3)	22.4662(6)	18.1055(8)	18.3953(5)
α (˚)	90	90	90	90
β (˚)	120.16(3)	106.5550(10)	90	99.308(2)
γ (˚)	90	90	90	90
V (Å^3)	3129.4(11)	3572.92(17)	6968.2(6)	3439.90(17)
Z	4	4	8	4
μ(MoKα) (mm^{-1})	0.249	0.223	0.229	0.541
ρ_{calc}(g cm^{-3})	1.467	1.397	1.433	1.609
2θmax (˚)	54.18	51.46	50.70	50.7
No. of unique reflections	3423	6816	12745	6285
Data/restraints/parameters	3423 / 0 / 218	6816 / 0 / 475	12745 / 1 / 945	6285 / 0 / 469
Final R indices [$I > 2\sigma(I)$]	$R1$ = 0.0394 $wR2$ = 0.0919	$R1$ = 0.0515 $wR2$ = 0.1298	$R1$ = 0.0392 $wR2$ = 0.0765	$R1$ = 0.0283 $wR2$ = 0.0809
R indices (all data)	$R1$ = 0.0582 $wR2$ = 0.1021	$R1$ = 0.0899 $wR2$ = 0.0.1557	$R1$ = 0.0643 $wR2$ = 0.0856	R1 = 0.0374 $wR2$ = 0.0874
Goodness of Fit on F^2	1.035	0.963	1.027	1.019

Table 2 Crystal and Refinement Data for the Ligands

Table 2 indicates that the refinement data for each structure are acceptable for publication. CIF files are included on the accompanying compact disc for reference. On conducting an online CIF check,[39] no significant alerts were returned.

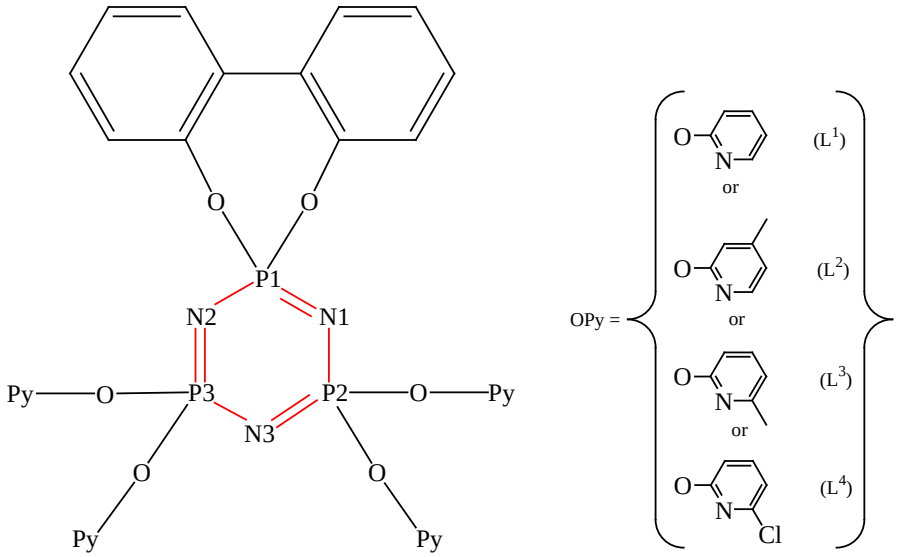

Figure 10 Generic numbering scheme used in Table 3 for cyclotriphosphazene ligands

	L^{1}	L^{2A}	L^{2B}	L^{3A}	L^{3B}	L^{4}
P1-N1	1.5874(17)	1.580(3)	1.578(3)	1.582(2)	1.578(3)	1.5809(15)
P1-N2	1.5874(17)	1.580(3)	1.578(3)	1.572(2)	1.575(3)	1.5801(15)
P2-N1	1.5855(17)	1.582(3)	1.572(3)	1.580(2)	1.578(2)	1.5727(15)
P3-N2	1.5856(13)	1.582(3)	1.572(3)	1.575(2)	1.575(3)	1.5769(15)
P2-N3	1.5856(13)	1.574(2)	1.5826(19)	1.581(3)	1.582(3)	1.5732(15)
P3-N3	1.5856(13)	1.574(2)	1.5826(19)	1.586(3)	1.578(3)	1.5768(16)
N1-P1-N2	119.34(12)	118.6(2)	118.9(2)	119.12(13)	118.42(12)	118.91(8)
N1-P2-N3	117.77(10)	118.78(16)	119.31(16)	117.66(13)	117.34(13)	119.32(8)
N2-P3-N3	117.77(10)	118.78(16)	119.31(16)	119.02(13)	117.93(14)	118.91(8)
P1-N1-P2	119.49(10)	120.67(17)	121.07(17)	120.11(15)	120.53(16)	120.12(9)
P1-N2-P3	119.49(10)	120.67(17)	121.07(17)	120.49(15)	120.99(16)	120.86(10)
P2-N3-P3	121.22(15)	120.9(2)	120.3(2)	120.99(15)	121.20(15)	120.81(10)

Table 3 Selected bond lengths (Å) and angles (°) for the ligands (superscripts $^{2A,\ 2B}$ etc. refer to ligand conformers described later)

As expected, the phosphazene ring bond lengths and angles do not change much through the range of ligands $\mathbf{L^1}$ to $\mathbf{L^4}$, and the values lie close to other cyclophosphazenes where P-N bond lengths are generally in the range 1.54 Å to 1.63 Å, N-P-N bond angles are in the range 116° to 120° and P-N-P bond angles are in the range 119° to 148°. Specific comments about each ligand are now given.

2.3.2 Crystal structure of (biph)tetrakis(2-pyridyloxy)cyclotriphosphazene ($\mathbf{L^1}$)

Monoclinic $\mathbf{L^1}$ crystallises in space group *C*2/*c* with no occluded solvent molecules present in the unit cell and refines as one half of the molecule related by a centre of symmetry.
At the time of writing this thesis, Chandrasekhar *et al*.[40] have recently published an X-ray crystal structure of $\mathbf{L^1}$ and a number of metal complexes with this ligand. The limited crystallographic detail given in that publication was compared to that obtained in this work. The P-N bond lengths and P-N-P/N-P-N angles for $\mathbf{L^1}$ are in good agreement with those published. However, Chandrasekhar *et al*.[40] stated that the cyclotriphosphazene ring is nearly planar, having an out of plane deviation of +/- 0.1254 Å. The out of plane deviation found in the present study is +/- 0.2507 Å, being double the value reported by Chandrasekhar *et al*.[40] indicating a degree of flexibility in the phosphazene ring according to the crystallisation conditions.
Crystallisation conditions differed in the choice of solvent, Chandrasekhar *et al*.[40] obtained crystals by allowing the supernatant CH_2Cl_2 to evaporate, whereas crystals in the present study were obtained by slow diffusion of hexane into a CH_2Cl_2 solution of $\mathbf{L^1}$, however neither data set has occluded solvent.

Jung *et al*.[11, 12] noted that with the 1,1-bis(pyridyl-2-thio)-3,3,5,5-tetrachloro-cyclotriphosphazene system, there was an interaction between the pyridyl nitrogen and the cyclotriphosphazene ring phosphorus to which it was attached via the hinging sulfur atom, such that the two atoms were within the P···N van der Waals distance (3.40 Å) as depicted in Figure 11. Jung *et al*.[11, 12] concluded from space-filling models that this behaviour was due to the pyridyl nitrogen atoms being sterically pinched between the chloro groups. In the present study, a similar interaction is observed though the exact stereochemical arrangement differs from ligand to ligand as discussed in later sections.

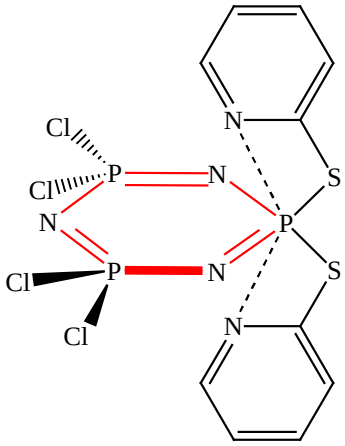

Figure 11 Intramolecular P···N interaction reported by Jung *et al*.[11, 12]

Single crystal X-ray structures in this work invariably demonstrate a reaction between one of the 2-oxypyridine moieties and the phosphazene ring phosphorus atom to which it is attached via the hinging oxygen. A more plausible explanation for this interaction is that of Davidson[41] who, by means of density functional theory (DFT) calculations, demonstrated that the lone pair of electrons residing on the 2-oxypyridine nitrogen atom may donate sufficient electron density to all three phosphorus atoms to form a π-like bond.

For **L**$^{\mathbf{1}}$, non-geminal pyridyloxy pendant arms demonstrate intramolecular slipped stacking[42] with a 10.4° angle between the ring mean planes and 3.924 Å between the planar centroids (Figure 12). The central phosphazene ring is puckered to accommodate this although similar metric parameters from the work of Chandrasekhar *et al*.[40] are not available for comparison. Figure 12 shows the intramolecular slipped stacking of the pyridyloxy rings (solid line between pyridyloxy rings containing N5 and N4A) and the van der Waals P···N interaction (dotted line) between N4 and P2. Being symmetry related, N4···P2 = N4A···P2A = 2.845 Å. The distance N5-P2 (and its *trans* non-geminal symmetry related twin, N5A-P2A) is greater than the van der Waals distance at 3.522 Å.

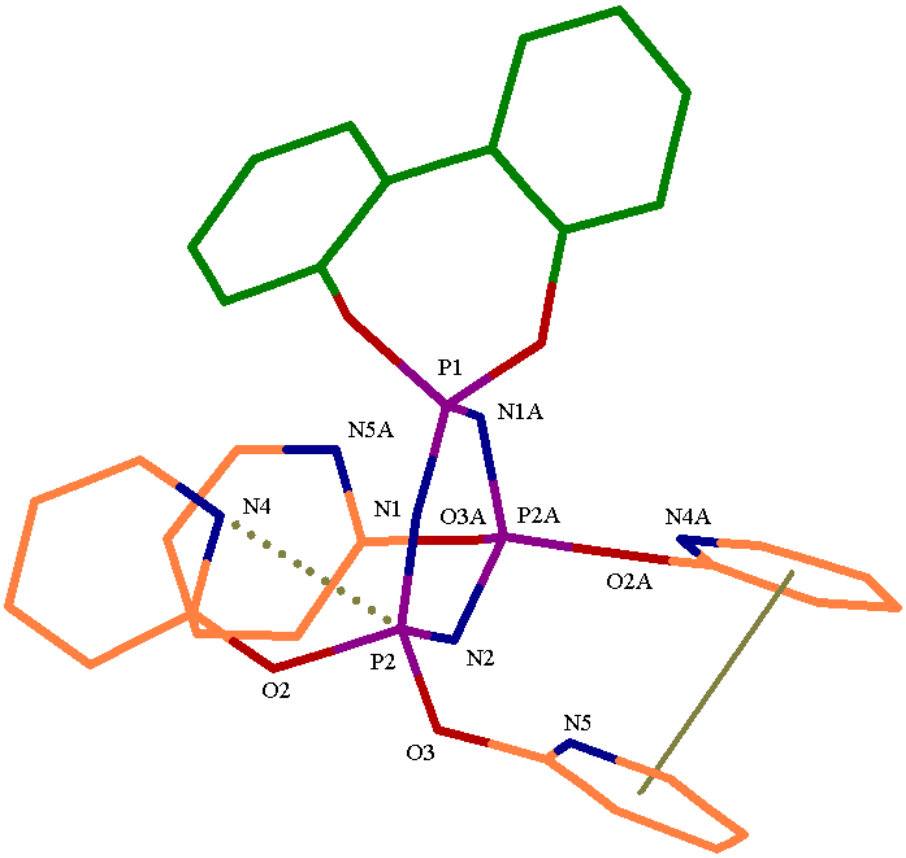

Figure 12 Intramolecular relationships in $\mathbf{L^1}$ (hydrogen atoms removed for clarity)

2.3.3 Crystal structure of (biph)tetrakis(4-methyl-2-pyridyloxy)cyclotriphosphazene ($\mathbf{L^2}$)

$\mathbf{L^2}$ crystallises in space group *P*2/*n* with 0.25 molecules of water. Four molecules exist in the unit cell which refine as two halves of each molecule related by a 2-fold axis of symmetry. $\mathbf{L^2}$ displays no slipped stacking of the pyridyloxy rings, possibly due to steric effects of the methyl groups being *para* to the pyridyloxy ring nitrogen. Of the two conformations, one ($\mathbf{L^{2A}}$) (Figure 13) has the pendant pyridyloxy arms arranged pseudo-equatorially in a plane perpendicular to the vertical axis of the main ring, which is puckered to accommodate this arrangement. The second conformation ($\mathbf{L^{2B}}$) (Figure 13) has two of

the *trans* pyridyloxy pendant arms pseudo-equatorial, as above, and two adopting a pseudo-axial arrangement in line with the vertical ring axis. In the latter case, the phosphazene ring is almost planar.

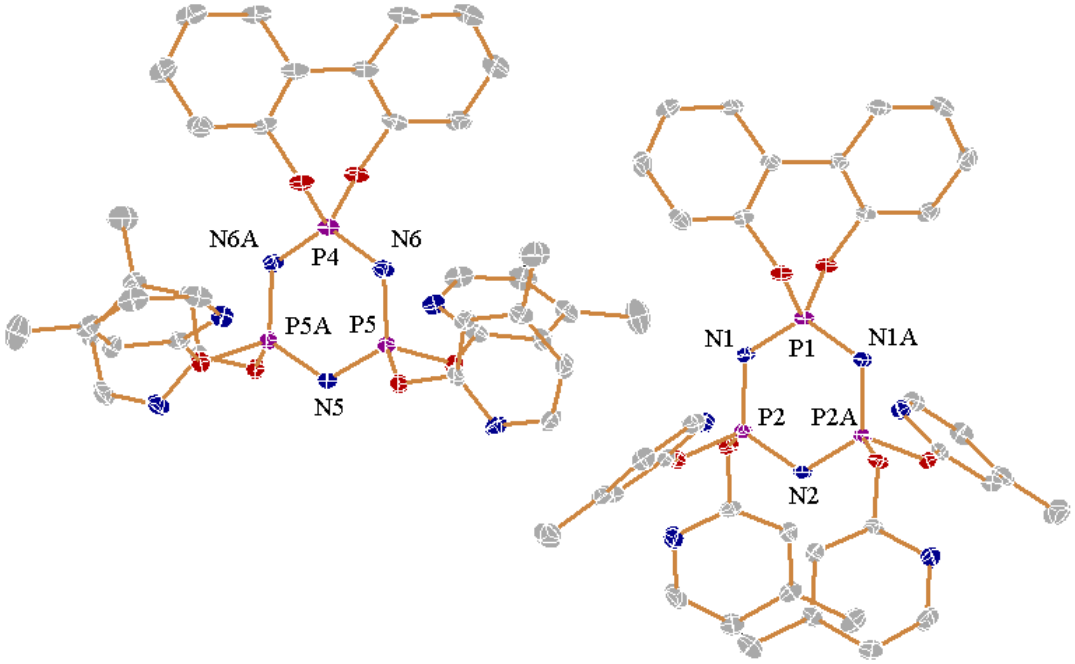

Figure 13 Ligand conformations of $\mathbf{L^{2A}}$ (left) and $\mathbf{L^{2B}}$ (right). Thermal ellipsoids are drawn at 50% probability (hydrogen atoms and occluded solvent removed for clarity)

For both $\mathbf{L^{2A}}$ and $\mathbf{L^{2B}}$, a similar N···P interaction occurs as for $\mathbf{L^{1}}$, with one *trans* non-geminal symmetry related pyridyloxy nitrogen atom per side of the central phosphazene ring being within the P···N van der Waals distance as shown in Figures 14 and 15.

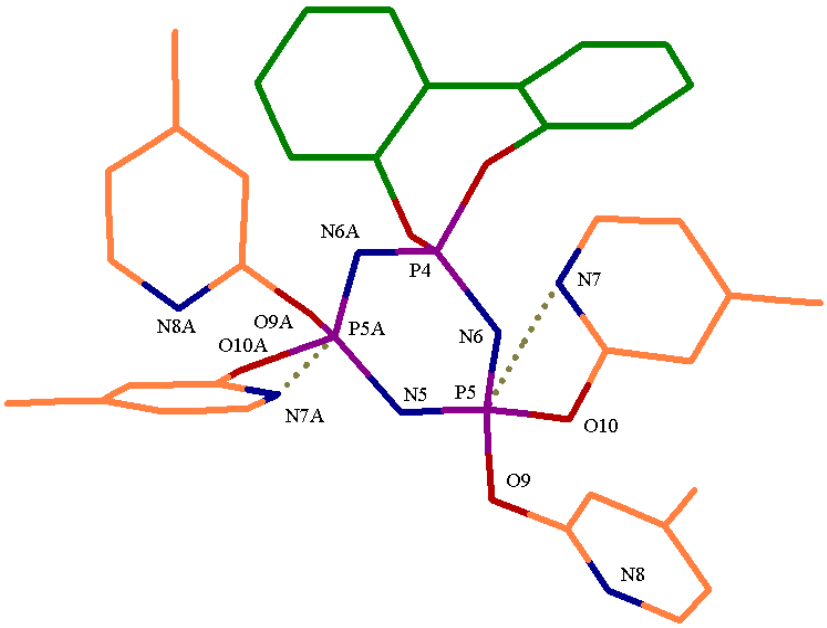

Figure 14 Intramolecular N···P interactions in $\mathbf{L^{2A}}$
(hydrogen atoms and occluded solvent removed for clarity)

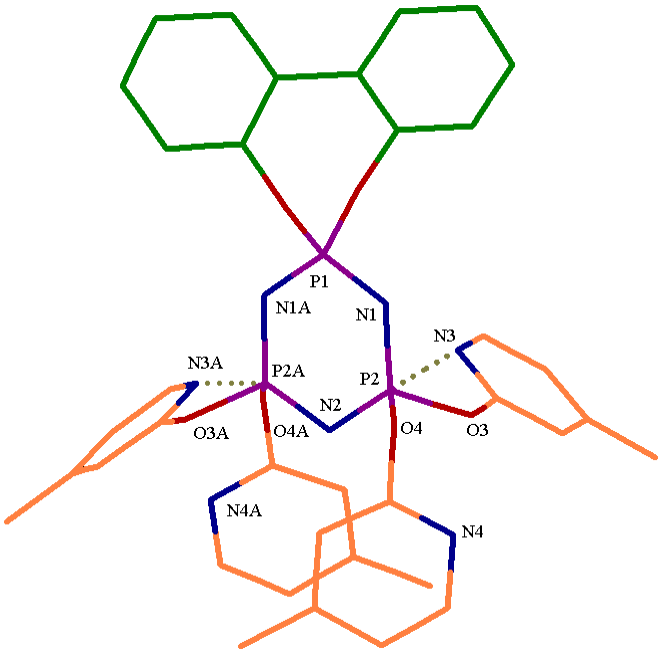

Figure 15 Intramolecular N···P interactions in $\mathbf{L^{2B}}$
(hydrogen atoms and occluded solvent removed for clarity)

For **L**^{2A} in Figure 14, the *trans* non-geminal symmetry related P···N interactions (dotted lines) are N7-P5 = N7A-P5A = 2.920 Å.

L^{2B} in Figure 15, exhibits the same P···N interaction for the pseudo-equatorial *trans* non-geminal pyridyloxy arms. For **L**^{2B}, the *trans* non-geminal symmetry related P···N interactions (dotted lines) are N3···P2 = N3A···P2A = 2.859 Å. The P2···N4 distance = 3.439 Å and is outside the van der Waals distance.

Addition of the CH_3 groups on the pyridyloxy moiety prevents intramolecular slipped stacking. However enthalpically favourable[42] intramolecular point-to-face stacking does occur in **L**^{2B} (Figure 16) between *cis* non-geminal pyridyloxy rings, with: H7···N3A (dashed lines) = 2.690 Å and H7-planar centroid (dotted lines) = 2.913 Å.

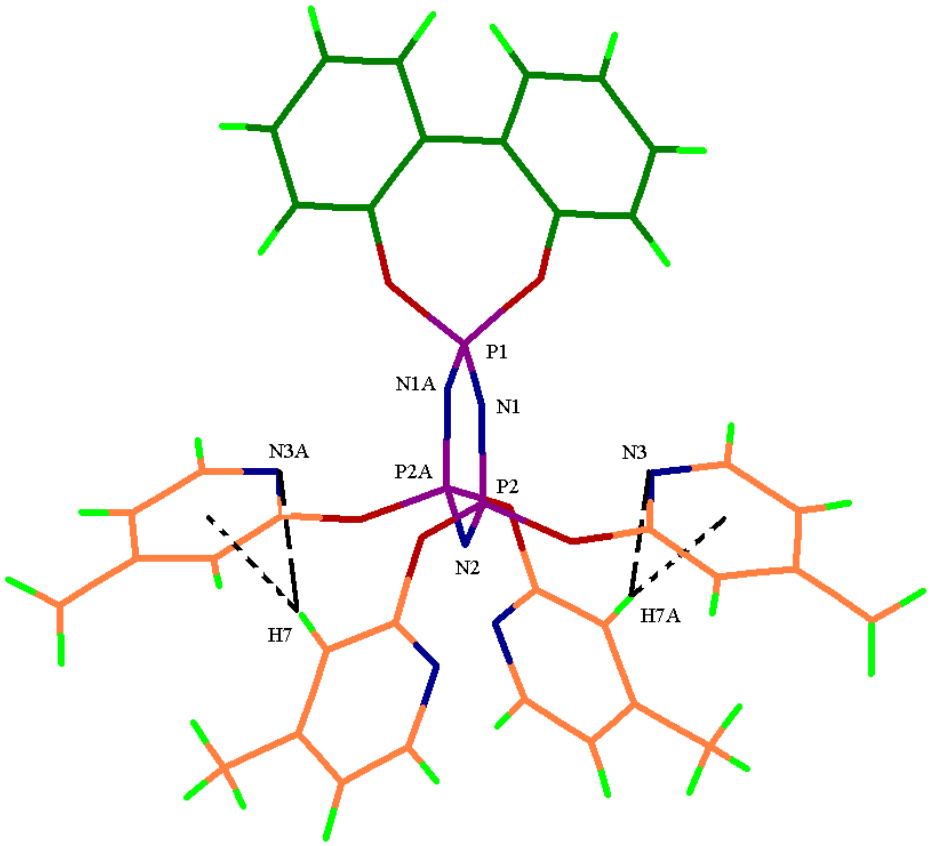

Figure 16 **L**^{2B} showing point-to-face stacking (occluded solvent removed for clarity)

2.3.4 Crystal structure of (biph)tetrakis(6-methyl-2-pyridyloxy)cyclotriphosphazene (L^3)

L^3 crystallises in space group *Pna*2(1) with no occluded solvent. Two molecules exist in the unit cell which refines as two complete molecules, each having no centre of symmetry.

One molecule (L^{3A}) has a random orientation of the pyridyloxy arms although two of the *cis* non-geminal rings appear to undergo a degree of slipped stacking where the distance between centroids is 4.044 Å and the angle between the mean planes is 11.2°. The distance between the planar centroids (solid line in Figure 17) is such that it is unlikely to be a π-π interaction and that the alignment is steric rather than electronic in nature.[42]

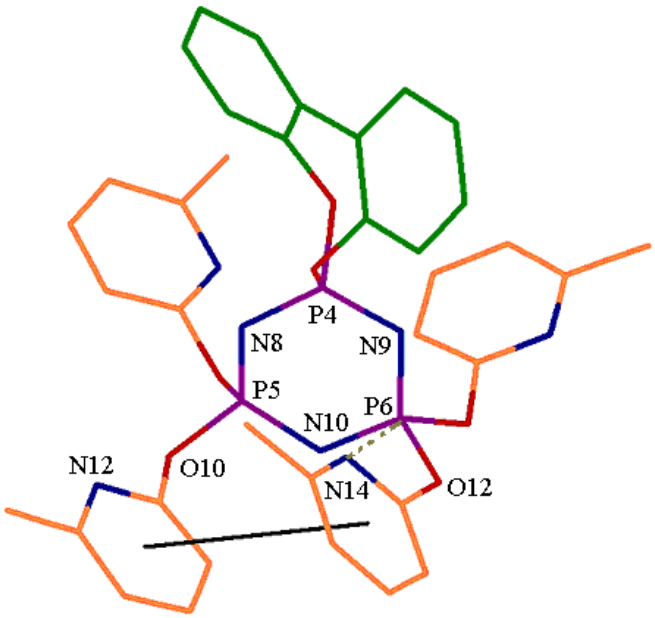

Figure 17 L^{3A} slipped stacking between one set of *cis* non-geminal pyridyloxy rings (solid line) and P···N interaction (dotted line), (hydrogen atoms removed for clarity)

The second molecule in the cell, L^{3B}, has two sets of nearly coplanar geminal pyridyloxy arms as seen in Figures 18 and 19.

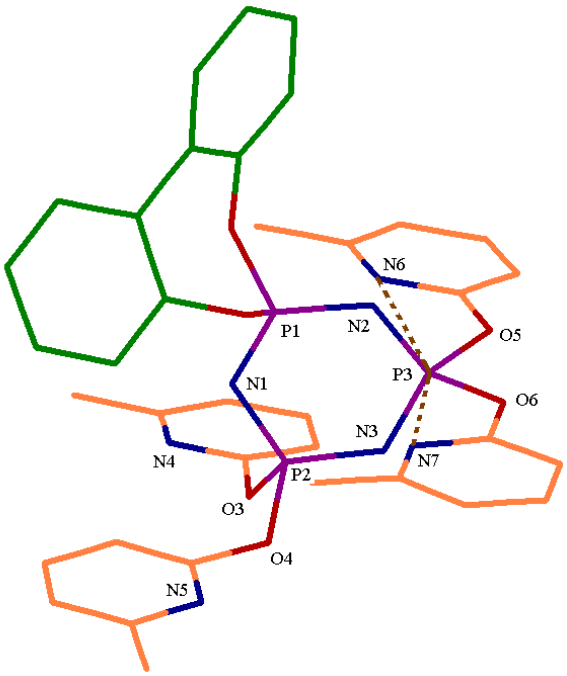

Figure 18 Intramolecular P···N interactions in $\mathbf{L}^{3B}$ (hydrogen atoms removed for clarity)

For $\mathbf{L}^{3B}$ in Figure 18 above, the *trans* geminal P···N interactions (dotted lines) are: N6···P3 = 2.840 Å and N7···P3 = 2.871 Å.

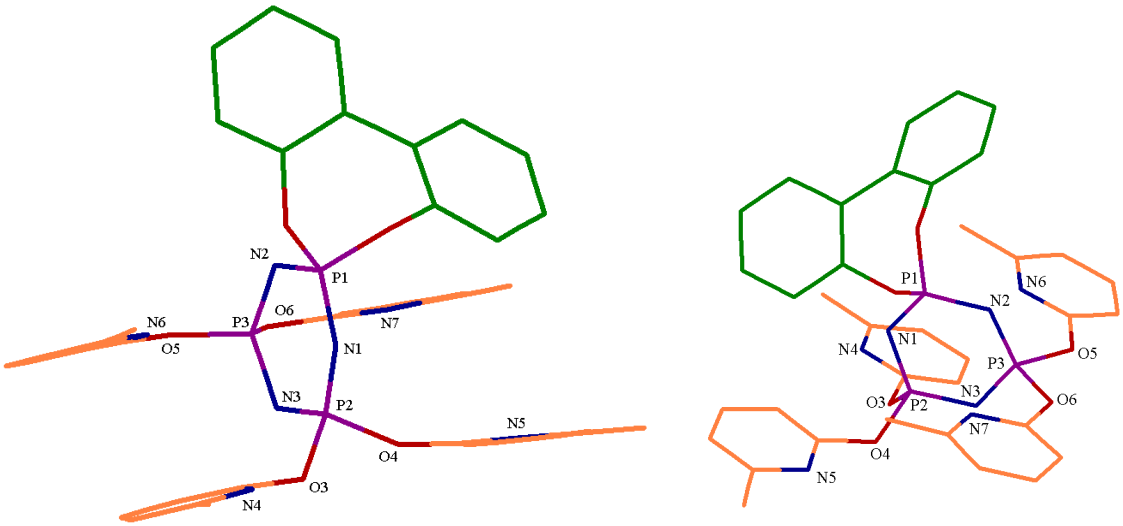

Figure 19 Left: $\mathbf{L}^{3B}$ showing almost parallel coplanarity of the two sets of pyridyloxy rings
Right: Rotated view to clarify orientation (hydrogen atoms removed for clarity)

Table 4 gives the angles between the mean planes of the pyridyl rings and it can be seen that the rings exhibiting the Van der Waals interaction (i.e. the rings containing N6 and N7) have the least deviation from coplanarity at 3.9°.

Ring system in $\mathbf{L}^{3B}$	Angle between mean planes (°)
N7 - N6 Geminal	3.9
N4 - N5 Geminal	8.7
N4 - N6 Non-Geminal	4.7
N5 - N7 Non-Geminal	4.2

Table 4 Angles between pyridyloxy rings in $\mathbf{L}^{3B}$

The planar alignments of the 2-oxypyridine moieties in $\mathbf{L}^{3B}$ combined with $\mathbf{L}^{3A}$ does not lead to a high degree of stacking in the crystal structure, indeed only one example of intermolecular slipped stacking is observed (Figure 20).

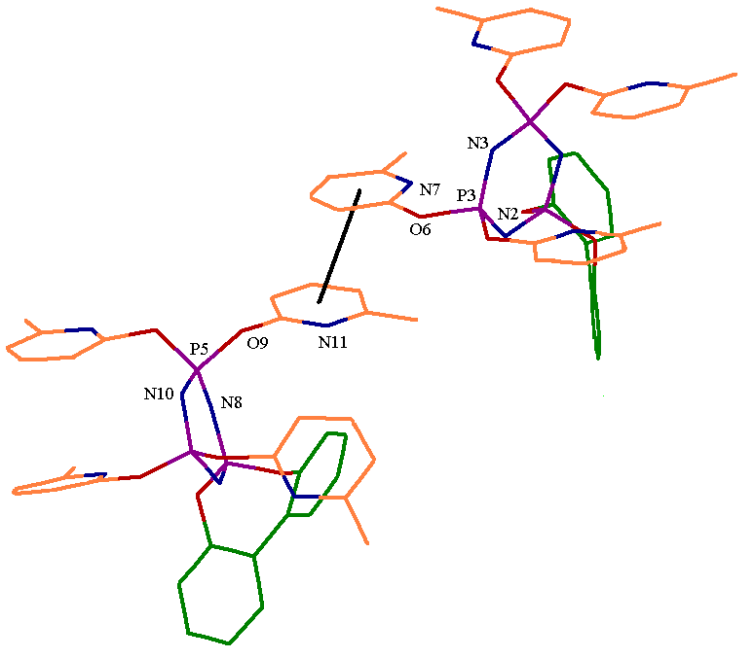

Figure 20 Intermolecular slipped stacking in $\mathbf{L}^{3}$ with approximately 3.816 Å between the pyridyloxy rings (solid line) (hydrogen atoms removed for clarity)

2.3.5 Crystal structure of (biph)tetrakis(6-chloro-2-pyridyloxy)cyclotriphosphazene (L^4)

Ligand L^4 crystallises in space group *P*2(1)/*c* with no occluded solvent, and refines with one molecule in the unit cell (Figure 21). Two *trans* geminal pyridyloxy arms demonstrate the P···N interaction similar to that reported by Jung *et al*.[11, 12] for the 1,1-bis(pyridyl-2-thio)-3,3,5,5-tetrachlorocyclotriphosphazene system.

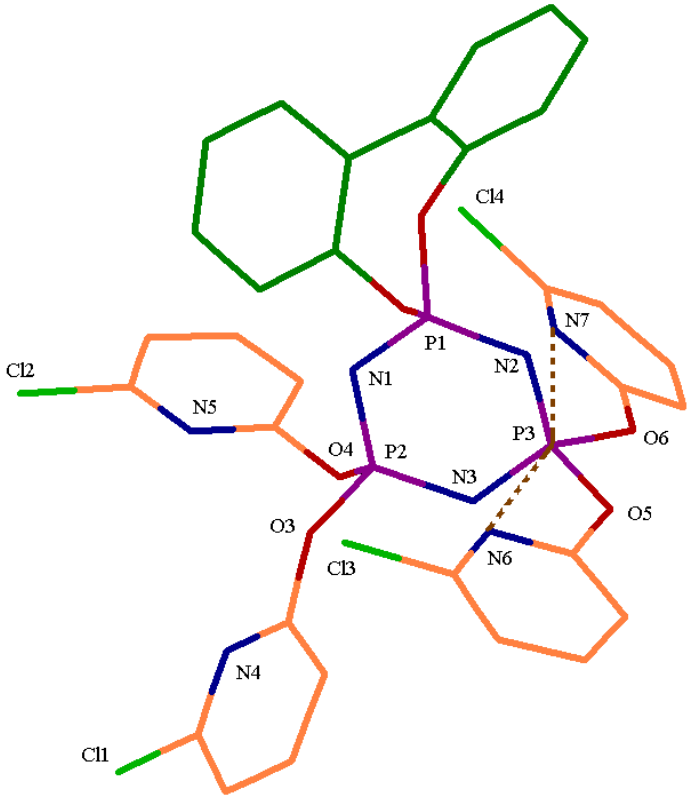

Figure 21 Intramolecular P···N interactions in L^4 (hydrogen atoms removed for clarity)

For L^4 in Figure 21 above, the *trans* geminal P···N interactions (dotted lines) are N6···P3 = 2.821 Å, and N7···P3 = 2.902 Å.

L^4 is the only compound that demonstrates long range slipped stacking of the pyridyloxy rings as seen in Figures 22-23, where the stacking produces column-like structures through

the crystal. The interatomic distances are in the order of 3.6 to 3.7 Å between closest carbon atoms in the adjacent pyridyloxy rings.

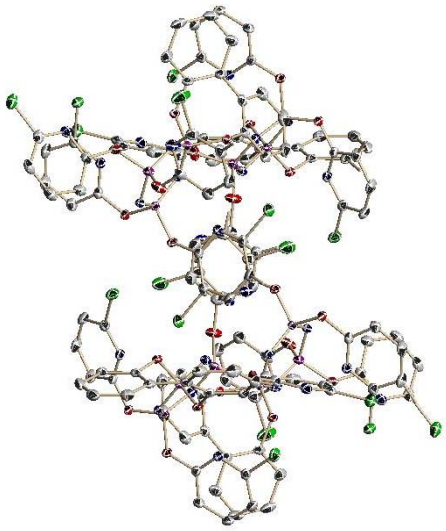

Figure 22 Stacking of pyridyloxy rings creating column-like structures for **L**^{4} (hydrogen atoms removed for clarity)

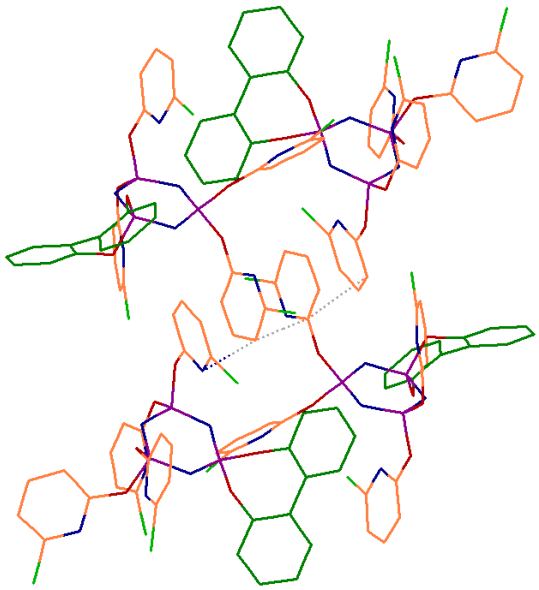

Figure 23 Rotated view of **L**^{4} showing a column-like structure along its length, the dotted line has been added for ease of identification (hydrogen atoms removed for clarity)

2.3.6 Comparison of the X-ray structures

Taking a consistent mean plane through four atoms of the phosphazene ring (i.e. P1, N1, N1A and N2 for $\mathbf{L^1}$) and adding the out-of-plane (OOP) distances for the remaining phosphorus atoms allows a comparison between molecules of the degree of distortion in the phosphazene ring (Table 5).

	Mean plane	OOP (Å)	OOP (Å)	OOP Total (Å)
$\mathbf{L^1}$	P1, N1, N1A, N2	P2 = 0.2507	P2A = -0.2507	0.5014
$\mathbf{L^{2A}}$	P4, N6, N6A, N5	P5 = 0.1456	P5A = -0.1456	0.2912
$\mathbf{L^{2B}}$	P1, N1, N1A, N2	P2 = -0.0326	P2A = 0.0326	0.0652
$\mathbf{L^{3A}}$	P1, N1, N2, N3	P2 = -0.1838	P3 = 0.0904	0.2742
$\mathbf{L^{3B}}$	P4, N8, N9, N10	P5 = 0.2540	P6 = -0.1555	0.4095
$\mathbf{L^4}$	P1, N1, N2, N3	P2 = -0.1089	P3 = 0.0636	0.1725

Table 5 Comparison of cyclotriphosphazene ring distortion in the ligands $\mathbf{L^1}$, $\mathbf{L^{2A}}$, $\mathbf{L^{2B}}$, $\mathbf{L^{3B}}$ and $\mathbf{L^4}$

As can be seen from Table 5, the ring planarity covers a range of 0.4362 Å. Since the molecules at the upper and lower bounds of the range both demonstrate some degree of stacking and P···N interaction then it is likely that, as reported by Allcock,[8] the phosphazene ring planarity is apparently a response to crystal packing forces and the degree of planarity seems to have little effect on the stability of the molecule.

Jung *et al.*[11, 12] described the S-P-S angle (*c.f.* Figure 11, page 50) for geminal thiopyridine moieties as being noticeably pinched (94.95(7)°) from a regular tetrahedral angle (approximately 109°) thus being proof of the interaction. As can be seen from Table 6, even where there is no P···N interaction, the O-P-O angles are all less than a regular tetrahedral angle, therefore in the phosphazenes under consideration in this work the O-P-O angle does not appear to be dependent on, or proof of, the P···N interaction.

Ligand	Angle O-P-O	Angle (°)	Interaction	Distance (Å)	Symmetry related	G/ NG
$\mathbf{L^1}$	O2-P2-O3	95.32(8)	P2···N4	2.854	Yes	NG
$\mathbf{L^{2A}}$	O9-P5-O10	96.95(12)	P5···N7	2.920	Yes	NG
$\mathbf{L^{2B}}$	O3-P2-O4	99.00(12)	P3···N3	2.861	Yes	NG
$\mathbf{L^{3A}}$	O11-P6-O12	94.56(12)	P6···N14	2.848	No	Only one
$\mathbf{L^{3B}}$	O5-P3-O6	92.62(11)	P3···N6	2.840	No	G
			P3···N7	2.871		
	O3-P2-O4	97.21(11)	-	-		
$\mathbf{L^4}$	O5-P3-O6	92.35(7)	P3···N6	2.821	No	G
			P3···N7	2.902		
	O3-P2-O4	104.57(8)	-	-		

Table 6 Summary of the van der Waals intramolecular N···P interactions: G=geminal, NG=non-geminal

The geminal interacting pyridyl rings of $\mathbf{L^{3B}}$ and $\mathbf{L^4}$, do have a smaller O-P-O angle than the geminal non-interacting pyridyl rings, O3-P2-O4 for $\mathbf{L^{3B}}$ and $\mathbf{L^4}$ as highlighted in Table 6. Although intra- and intermolecular interactions are occurring, no single factor seems to dominate the packing, which might be a reflection on the flexibility of the cyclotriphosphazene ring and the ease of rotation about the hinge oxygen of the pyridyloxy rings. As will be shown in Chapter 4, these systems exhibit fluxional behaviour in the presence of Zn^{2+}, Cd^{2+} and Hg^{2+} and it seems likely therefore that the configuration adopted in the X-ray structure is sensitive to its environment.

Ligand	P-O-C	Angle (°)	Intramolecular P···N interaction
$\mathbf{L^1}$	P2A-O2A-C7A	121.23	Yes
	P2-O3-C12	126.69	No
$\mathbf{L^{2A}}$	P5-O10-C54	123.03	Yes
	P5-O9-C49	122.00	No
$\mathbf{L^{2B}}$	P2-O3-C18	121.51	Yes
	P2-O4-C13	124.46	No
$\mathbf{L^{3A}}$	P6-O12-C64	120.78	Yes
	P6-O11-C59	118.40	No
	P5-O9-C49	126.02	No
	P5-O10-C54	126.38	No
$\mathbf{L^{3B}}$	P3-O5-C23	121.09	Yes
	P3-O6-C28	122.01	Yes
	P2-O4-C18	125.06	No
	P2-O3-C13	128.55	No
$\mathbf{L^4}$	P3-O5-C23	121.08	Yes
	P3-O6-C28	122.20	Yes
	P2-O3-C13	130.30	No
	P2-O4-C18	127.79	No

Table 7 Comparison of P-O-C angles with intramolecular P···N interactions

The van der Waals intramolecular N···P interactions for the ligands are summarised for the X-ray structures in Table 7, and there appears to be little correlation between P-O-C angle and the P···N interaction for the 2-pyridyloxy species. For L^{3B} and L^4, it could be argued that smaller P-O-C bonds favour the P···N interaction but since no data is present for the standard deviation in the angular measurements, the significance of this observation is subjective.

2.4 Conclusions

Three ligands have been synthesised and characterised as models for the polymeric analogues, and a fourth compound synthesised as a crystallisation model. Each ligand comprises a cyclotriphosphazene ring with one spiro-2,2'-dioxybiphenyl moiety blocking one ring-phosphorus site. The remaining two phosphorus atoms are fully substituted with a 2-pyridyloxy derivative. The choice of stereochemistry completes the available scenarios for cyclotriphosphazene substitution with pyridine moieties for the Aincough/Brodie group.[30, 31, 33, 34]

Reaction times for synthesis of the ligands appear to be determined by steric factors dependent on the presence and position of the pyridyl methyl group, which had been introduced to assess solubility factors that might assist in ensuring good solubility in the polymeric analogues. Reaction time for the chloro analogue is comparatively fast, which may be due to exocyclic electronic effects although the factors affecting the rate have not been investigated further.

The P···N interaction, whereby one or more pyridyloxy nitrogen atoms appear to interact with the phosphazene ring nitrogen atom to which they are attached via their respective hinge oxygen atoms, is a common feature in these ligands. The conclusion by Jung *et al*.,[11, 12] that this interaction was due to steric constraint of the pyridyl nitrogen atoms by chloro groups in the 1,1-bis(pyridyl-2-thio)-3,3,5,5-tetrachlorocyclotriphosphazene system may be specific to that system only. That a similar P···N interaction is observed in the new ligands, where the 2-oxypyridine moieties do not sterically constrain the nitrogen atoms of each other may point to an electronic, rather than steric, mechanism for this behaviour as proposed by Davidson.[41] As yet, no evidence can be found in the literature for a cyclotriphosphazene containing a combination of thio- and 2-oxypyridine moieties that might further elucidate matters.

Given the high concentration of aryloxy moieties, the degree of stacking within the cyclotriphosphazene models is unexpectedly low and it is difficult to predict the effect of stacking in the polyphosphazene analogues, given the low bond torsion of the

polyphosphazene skeleton. This serves to emphasise, or question, the validity of arguments regarding the use of the trimeric ring structure as an appropriate model for the polymer architecture, rather than the tetrameric or higher cyclic structures.
It is noteworthy that the use of 2-pyridyloxy moieties has resulted in the successful syntheses of stable ligands, with no apparent degradation. The ligand design provides a potentially nitrogen rich environment for coordination to transition metals, having four nitrogen donors from the pyridyloxy moieties and three available nitrogen donors from the cyclotriphosphazene ring. Flexibility of the ligands is evident from the conformations adopted in the X-ray crystal structures and rotation of the 2-pyridyloxy rings about the hinge oxygen atoms may afford greater coordination ability.

A number of questions arise from the ligand synthesis:

(i) Will the methyl groups added to afford greater solubility in the polymer actually hinder coordination by their steric bulk?

(ii) While it is obvious that the methyl groups affect the packing forces in the solid state, will coordination to metals result in a higher degree of stacking?

(iii) Each ligand displays some degree of interaction between the pyridyloxy nitrogen atoms and the phosphorus to which they are attached via the hinge oxygen atom. Will this interaction compete for control of the metal coordination site?

(iv) Given that the ligands hexakis(2OPy)cyclotriphosphazene and hexakis(2O-4-Py)cyclotriphosphazene demonstrate a range of coordination geometries to transition metals, how will the coordination modes be affected by the presence of the 2,2'-dioxybiphenyl moiety?

(v) To what extent are the ligand results applicable to the polyphosphazene analogues?

These questions will be considered in subsequent chapters.

2.5 References

1. Allcock, H. R.; Desorcie, J. L.; Riding, G. H., *Polyhedron* **1987,** 6, 119.

2. Andrews, M. P.; Ozin, G. A., *Chem. Mater.* **1989,** 1, 174.

3. Allcock, H. R., *Phosphorus, Sulfur Silicon Relat. Elem.* **2004,** 179, 661.

4. Diefenbach, U.; Adamaszek, P.; Bloy, M., *Heteroat. Chem.* **1999,** 10(1), 9.

5. Allcock, H. R., *J. Inorg. Organomet. Polym. Mater.* **2006,** 16, 277.

6. Gabler, D. G.; Haw, J. F., *Inorg. Chem.* **1990,** 29(20), 4018.

7. Allcock, H. R., *Chemistry and Applications of Polyphosphazenes*. John Wiley and Sons Inc: New York, 2003; p. 86-89.

8. Allcock, H. R., *Chemistry and Applications of Polyphosphazenes*. John Wiley and Sons Inc: New York, 2003; p. 11.

9. Chandrasekhar, V.; Justin Thomas, K. R., *Struct. Bond.* **1993,** 81, 41.

10. Wisian-Neilson, P.; Jung, J., H.; Potluri, S. K.; Mauldin, C. E.; Zhang, H., *Phosphorus, Sulfur Silicon Relat. Elem.* **2004,** 179, 817.

11. Jung, O.; Kim, Y. T.; Lee, H.; Kim, K. M.; Chae, H. K.; Sohn, Y. S., *Bull. Chem. Soc. Jpn.* **1997,** 70(9), 2125.

12. Jung, O.; Park, S. H.; Lee, Y.; Cho, Y.; Kim, K. M.; Lee, S.; Chae, H. K.; Sohn, Y. S., *Inorg. Chem.* **1996,** 35(23), 6899.

13. Krause, W. E.; Parvez, M.; Visscher, K. B.; Allcock, H. R., *Inorg. Chem.* **1996,** 35(21), 6337.

14. Chandrasekhar, V.; Vivekanandan, K.; Nagendran, S.; Senthil Andavan, G. T.; Weathers, N. R.; Yarbrough, J. C.; Cordes, A. W., *Inorg. Chem.* **1998,** 37(24), 6192.

15. Allcock, H. R.; Kugel, R. L., *J. Am. Chem. Soc.* **1965,** 87, 4216.

16. Allcock, H. R.; Kugel, R. L.; Valan, K. J., *Inorg. Chem.* **1966,** 5, 1709.

17. Tonei, D. M.; Bertani, R.; De Jaeger, R.; Gleria, M., In *Applicative Aspects of Cyclophosphazenes*, ed.; Gleria, M.; De Jaeger, R., Nova Science Publishers, Inc: New York, 2004; p. 1-30.

18. Diefenbach, U.; Allcock, H. R., *Inorg. Chem.* **1994,** 33(20), 4562.

19. Audrieth, L. F.; Steinman, R.; Toy, A. D. F., *Chem. Rev.* **1943,** 32, 109.

20. Migachev, G. I.; Stepanov, B. I., *Russ. J. Inorg. Chem.* **1966,** 11(7), 929.

21. Diefenbach, U.; Kretschmann, M., *Z. Anorg. Allg. Chem.* **1998,** 624, 335.

22. Diefenbach, U.; Kretschmann, M.; Çavdarci, Ö. *Phosphorus, Sulfur Silicon Relat. Elem.* **1994,** 93-94, 415.

23. Diefenbach, U.; Kretschmann, M.; Çavdarci, Ö. *Monatshefte für Chemie* **1996,** 127, 989.

24. Diefenbach, U.; Kretschmann, M.; Stromburg, B. E., *Chem. Ber.* **1996,** 129, 1573.

25. Diefenbach, U.; Kretschmann, M.; Stromburg, B. E., *Phosphorus, Sulfur Silicon Relat. Elem.* **1997,** 124-125, 143.

26. Carriedo, G. A.; Gómez-Elipe, P.; García-Alonso, F. J.; Fernández-Catuxo, L.; Díaz, M. R.; Granda, S. C., *J. Organomet. Chem.* **1995,** 498, 207.

27. Carriedo, G. A., *J. Chil. Chem. Soc.* **2007,** 52(2), 1191 and references therein.

28. Carriedo, G. A.; Fernández-Catuxo, L.; García-Alonso, F. J.; Gómez-Elipe, P.; González, P. A., *Macromolecules* **1996,** 29(16), 5320.

29. Ainscough, E. W.; Brodie, A. M.; Derwahl, A., *Polyhedron* **2003,** 22, 189.

30. Ainscough, E. W.; Brodie, A. M.; Depree, C. V.; Otter, C. A., *Polyhedron* **2006,** 25, 2341.

31. Ainscough, E. W.; Brodie, A. M.; Depree, C. V.; Moubaraki, M.; Murray, K. S.; Otter, C. A., *J. Chem. Soc., Dalton Trans.* **2005,** 20, 3337 and references therein.

32. Ainscough, E. W.; Brodie, A. M.; Derwahl, A.; Kirk, S.; Otter, C. A., *Inorg. Chem.* **2007,** 46(23), 9841.

33. Ainscough, E. W.; Brodie, A. M.; Depree, C. V., *J. Chem. Soc., Dalton Trans.* **1999,** 23, 4123.

34. Ainscough, E. W.; Brodie, A. M.; Depree, C. V.; Jameson, G. B.; Otter, C. A., *Inorg. Chem.* **2005,** 44, 7325.

35. Chandrasekhar, V.; Pandian, B. M.; Azhakar, R., *Inorg. Chem.* **2006,** 45(9), 3510.

36. Sheldrick, G. M. *SHELXL Suite of Programs for Crystal Structure Analysis*, Institüt für Anorganische Chemie der Universität, Tammanstrasse 4, Göttingen, Germany: 1998.

37. Carriedo, G. A.; García Alonso, F. J.; González, P. A., *Macromol. Rapid Commun.* **1997,** 18, 371.

38. Allen, C. W., *Coord. Chem. Rev.* **1994,** 130, 137.

39. IUCr CheckCIF/PLATON. http://journals.iucr.org/services/cif/checkcif.html accessed 13-06-2008

40. Chandrasekhar, V.; Pandian, B. M.; Azhakar, R., *Polyhedron* **2007,** 27, 255.

41. Davidson, R. J. Masterate Thesis. Massey University, **2007**.

42. Janiak, C., *J. Chem. Soc., Dalton Trans.* **2000**, 3885.

Chapter 3: Reactions of Phosphazene Ligands with Selected Transition Metals

3.0 Abbreviations used in Chapter 3

biph	2,2'-dioxybiphenyl
CH_2Cl_2	dichloromethane
CH_3CN	acetonitrile
2OPy	2-oxypyridine
4OPy	4-oxypyridine
2O-4-MePy	2-oxy-4-methylpyridine
2O-6-MePy	2-oxy-6-methylpyridine
DMP	3,5-dimethyl-1-pyrazolyl
bipy	bipyridyl
ESMS	electrospray mass spectrometry
TBP	trigonal bipyramidal
CTP	cyclotriphosphazene

3.1 Introduction

The design of cyclophosphazene ligands capable of coordination to transition metals has received wide research interest over the last 30 years, whilst coordination of transition metals to the polymeric analogues has not been as widely studied except, for example, in specific applications such as the water soluble potential anticancer derivative reported by Allcock *et al*.[1]

It is speculated, however, that polymers with coordinated transition metals should exhibit unusual chemical and physical properties.[2] Suggested applications for coordination polymers include heterogeneous catalysts,[3] selective metal extraction compounds,[4, 5] electroactive materials,[3] solar energy conversion,[6] ion exchangers,[7] and so on. This expectation has driven research interest in the cyclotriphosphazenes as molecular scaffolds for coordination compounds, culminating in the conclusion by Allcock[8, 9] that the role of small molecule synthesis is crucial in order to gain a fundamental understanding of the chemistry, side reactions and optimisation techniques that might be applicable to the polymeric systems. Chlorocyclophosphazenes $[NPCl_2]_n$ undergo nucleophilic substitution of chlorine by a wide range of potential donor ligands and a range of substituted cyclotriphosphazenes may be prepared and characterised.

Transition metals can coordinate to phosphazene systems in a number of ways:[10-12]

(i) In heterocyclic coordination compounds, where the metal forms an intimate part of the ring, are known for both phosphazanes and phosphazenes as shown in Figure 1.

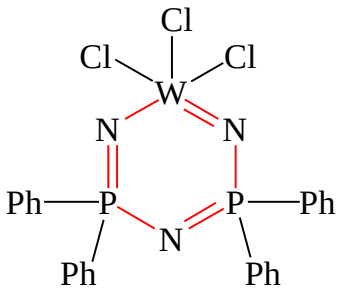

Figure 1 An example of a metal containing heterocyclic phosphazene[11]

(ii) In ionic salts whereby a cyclophosphazene ring nitrogen becomes protonated and the metal species exists as a counter ion as shown in Figure 2.

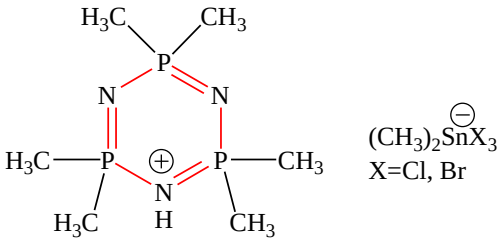

Figure 2 An example of an ionic salt phosphazene complex[13]

(iii) In exclusive coordination to a cyclophosphazene ring nitrogen atom as shown in Figure 3.

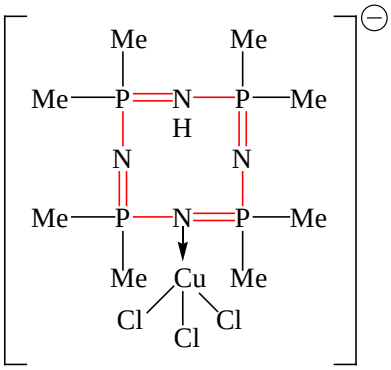

Figure 3 An example of exclusive coordination to a phosphazene ring nitrogen atom[12]

(iv) In coordination with a cyclophosphazene ring phosphorus atom as shown in Figure 4.

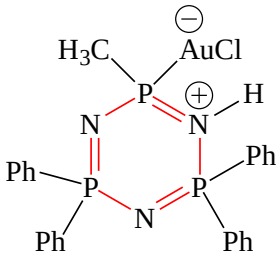

Figure 4 An example of coordination to a phosphazene phosphorus atom[12]

(v) In coordination via exocyclic groups which may also include a cyclophosphazene ring nitrogen atom as shown in Figure 5.

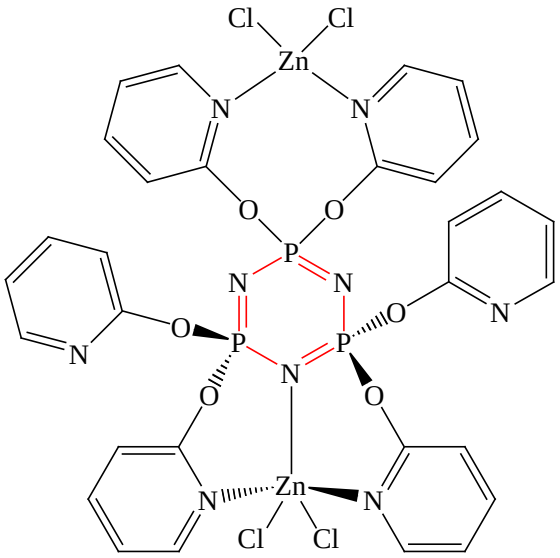

Figure 5 An example of exocyclic coordination with and without phosphazene ring nitrogen coordination[14]

Of these coordination modes, the ligands synthesised in this work were predicted to coordinate by method (v) above, based on reports by Ainscough *et al.*[14, 15] with hexakis(2-pyridyloxy)cyclotriphosphazene ligands. After the research in this chapter was completed, Chandrasekhar *et al.*[16] reported a variety of structures with the ligand N_3P_3(biph)(2OPy)$_4$ (**L^1**). These included hepta-coordinate [CoL^1(NO$_3$)$_2$], hexa-coordinate [CuL^1(NO$_3$)$_2$], as discussed in section 3.1.1.3, and penta-coordinate [ZnL^{1}Cl$_2$]. In the hepta- and penta-coordinate structures the ligand **L^1** acts as a κ^3N donor with two non-geminal pyridyl nitrogen atoms and one phosphazene ring nitrogen, whereas in the hexa-coordinate mode **L^1** acts as a κ^3N donor with two nitrogen atoms from geminal pyridyl rings and one phosphazene ring nitrogen. Thus it is apparent that the ligand **L^1** is quite versatile in accommodating a number of geometries dependent upon the nature of the transition metal moiety.

3.1.1 Review of the multidentate coordination behaviour of cyclophosphazenes

Unlike many previous ligand systems developed by Chandrasekhar, Carriedo and Diefenbach, the ligands synthesised in this work are designed to allow the ring nitrogen

atoms to be involved in coordination. There follows a brief review of the literature on the metal-complexing ability of cyclophosphazene ligands. Examples range from mono- through to hexadentate behaviour and are discussed in turn.

3.1.1.1 Phosphazenes exhibiting monodentate behaviour

Carriedo *et al.*[17] synthesised the hexakis ligands $N_3P_3(2OPy)_6$ and $N_3P_3(4OPy)_6$ for complexation to a $[Mn(CO)_3(bipy)]^+$ moiety. The Mn(I) moiety has sufficient steric bulk to prevent formation of stable complexes with the 2OPy derivative. However a stable complex was formed with the 4OPy derivative to form the compound shown in Figure 6.

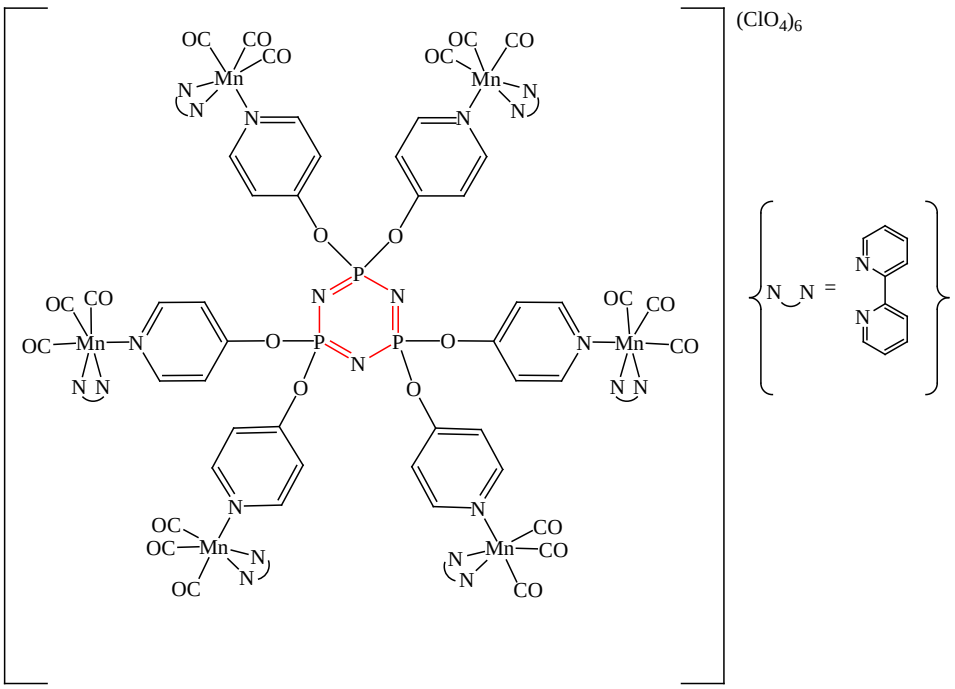

Figure 6 Hexacationic complex reported by Carriedo *et al.*[17]

Carriedo *et al.*[18-20] and Diaz *et al.*[21] have reported a range of similar monodentate $W(CO)_5$ complexes and their polymeric derivatives.

Ainscough *et al.*[22] reported the formation of an unusual dimeric complex where two hexakis(2OPy)cyclotriphosphazene ligands act as monodentate agents to bridge a copper centre as shown in Figure 7.

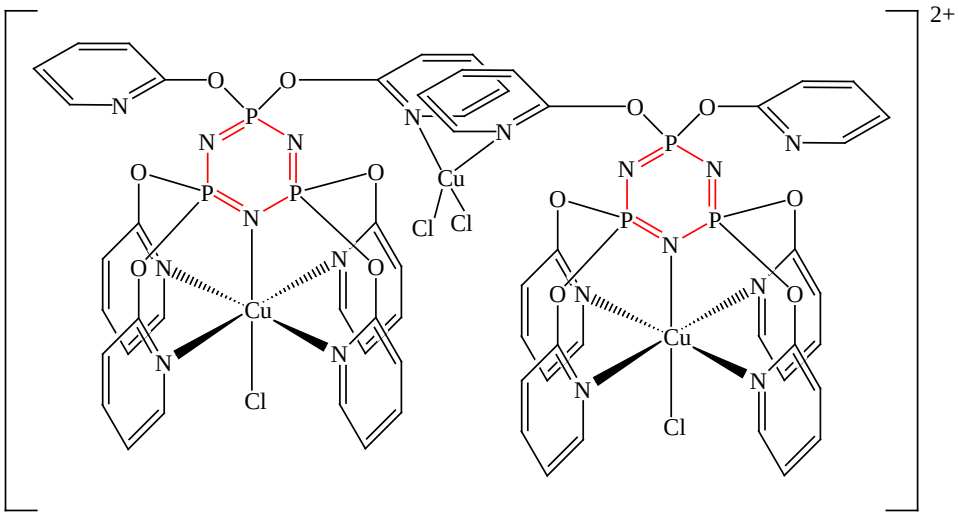

Figure 7 The dimeric trinuclear complex reported by Ainscough *et al.*[22] showing tetrahedral coordination around the bridged copper centre

The same hexakis(2OPy)cyclotriphosphazene ligand and the hexakis(2O-4-MePy) cyclotriphosphazene variant were also reported by Ainscough *et al.*[14] to form zwitterionic complexes on reaction with $CoCl_2$ (or $CoBr_2$) whereby one cobalt site consisted of a distorted tetrahedral monodentate site having a $CoNX_3$ (X=Cl or Br) arrangement by coordination to one pyridine arm as shown in Figure 8. Similar $CoNX_3$ sites had also been reported by others.[23-26]

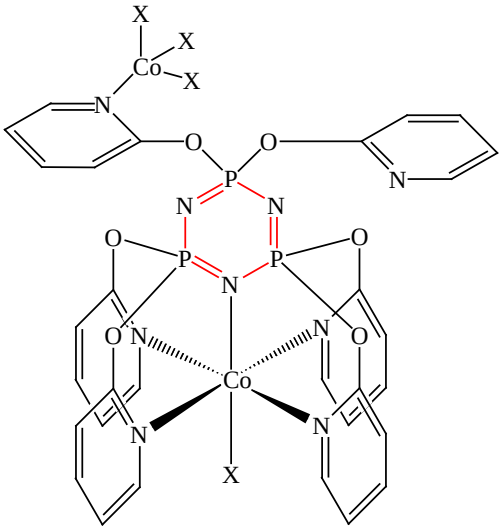

Figure 8 Zwitterionic complex reported by Ainscough *et al.*[14] demonstrating one monodentate coordination site

Diefenbach *et al*.[27] reported that reaction of the ligand pentaphenoxy(3-pyridyl-methylamino)cyclotriphosphazene with copper(II) nitrate, gave a Cu(II) bridged centre to form a dimeric compound shown in Figure 9.

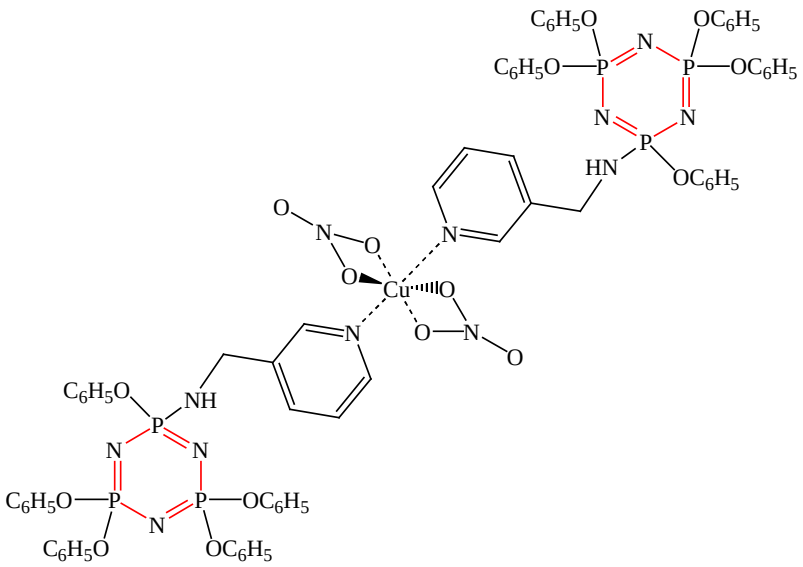

Figure 9 Cu(II) bridged dimeric compound reported by Diefenbach *et al*.[27]

3.1.1.2 Phosphazenes exhibiting bidentate behaviour

Ainscough *et al*.[28] have reported κ^2N systems for complexes with $ZnCl_2$, $HgCl_2$ and $CuCl_2$ with the ligands bis(biph)(2OPy)$_2$cyclotriphosphazene and bis(biph)(2O-4-MePy)$_2$cyclotriphosphazene. In the tetrahedral $ZnCl_2$ complex both nitrogen donors are from geminal pyridine arms in the similar ligands (Figure 10).

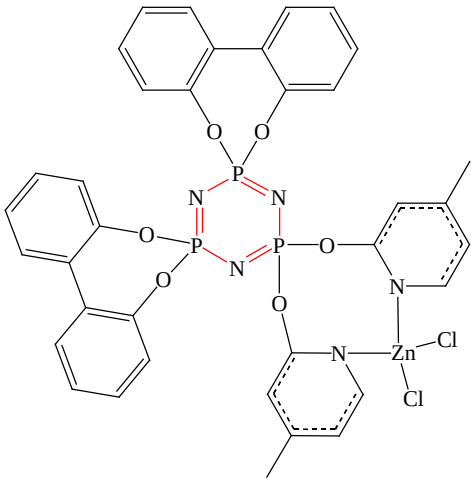

Figure 10 Tetrahedral bidentate structure reported by Ainscough *et al*.[28]

$HgCl_2$ and $CuCl_2$ give tetrahedral and distorted tetrahedral environments, respectively, with the cyclotetraphosphazene ligand tris(biph)bis(2OPy)cyclotetraphosphazene, where again the chelating nitrogen donors are from geminal pyridine arms. $CuCl_2$ also reacts with the ligand *trans*-bis(biph)tetrakis(2OPy)cyclotetraphosphazene in a 2:1 mole ratio to give two distorted tetrahedral sites whereby two sets of geminal pyridine arms bridge the two copper centres.

It is perhaps surprising that in the bidentate complexes (Figures 9 and 10), none involve the phosphazene ring nitrogen which is possibly a reflection of the steric bulk imposed by the adjacent spiro(2,2'-dioxybiphenyl) groups, or lower basicity of the phosphazene ring nitrogen in these configurations. Diefenbach *et al.*[29] reported an unusual bidentate cobalt(II) nitrate complex with the ligand pentaphenoxy(2-pyridylmethylamino) cyclotriphosphazene. The complex shown in Figure 11, contains weakly electron withdrawing groups in the phenoxy moieties, yet the adjacent phosphazene ring nitrogen is still sufficiently basic to coordinate to the Co(II) centre. The phosphazene ring P-N bond forming part of the seven-membered chelate ring is longer than usual at 1.647(10) Å and the remaining exocyclic P-N bond is slightly shorter by 0.2 Å than usual. Diefenbach *et al.*[29] reasoned that this is due to the reduced electron density in the phosphazene ring and delocalisation of the amino lone pair as reported in studies by others.[30]

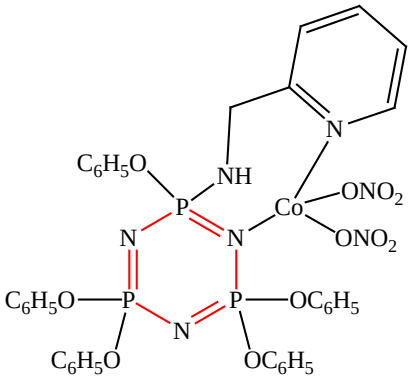

Figure 11 Unusual bidentate Co(II)NO_3 complex reported by Diefenbach *et al.*[29]

3.1.1.3 Phosphazenes exhibiting tridentate behaviour

Tridentate arrangements in cyclotriphosphazenes is typically achieved by involvement of a cyclotriphosphazene ring nitrogen atom. Justin Thomas *et al*.[31] reported the reaction of $CuCl_2$ with the anion of a pyrazolylcyclotriphosphazene (Figure 12) to form a dinuclear bridging complex in which both Cu(II) centres reside in a distorted TBP tridentate environment. A similar dinuclear bridged complex was also reported for hexakis(3,5-dimethylpyrazolyl)cyclotriphosphazene.[32]

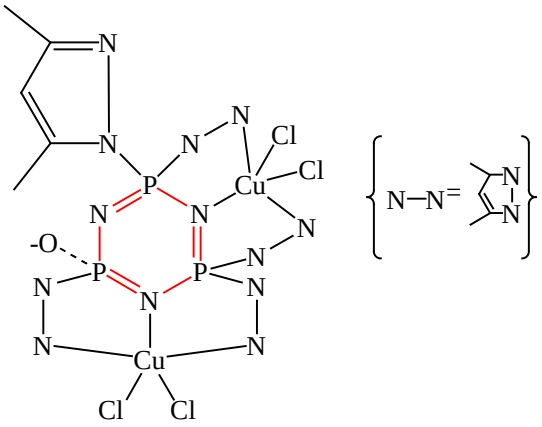

Figure 12 Dinuclear tridentate complex reported by Justin Thomas *et al*.[31]

By blocking one of the phosphorus atoms with geminal phenyl groups, Justin Thomas *et al*.[33] reported a reaction of the ligand bis(2,2-diphenyl)tetrakis(3,5-dimethylpyrazolyl) cyclotriphosphazene with Cu(II) halides to again form tridentate TBP complexes.

Ainscough *et al*.[14] reported the versatility of the hexakis(2OPy)cyclotriphosphazene and the hexakis(2O-4-MePy)cyclotriphosphazene ligands. Tridentate complexes with $CoBr_2$ give a κ^3*N* non-geminal *cis* TBP arrangement, whereas complexes with $NiCl_2$ and $ZnCl_2$ result in a κ^3*N* non-geminal *trans* TBP arrangement (Figure 13).

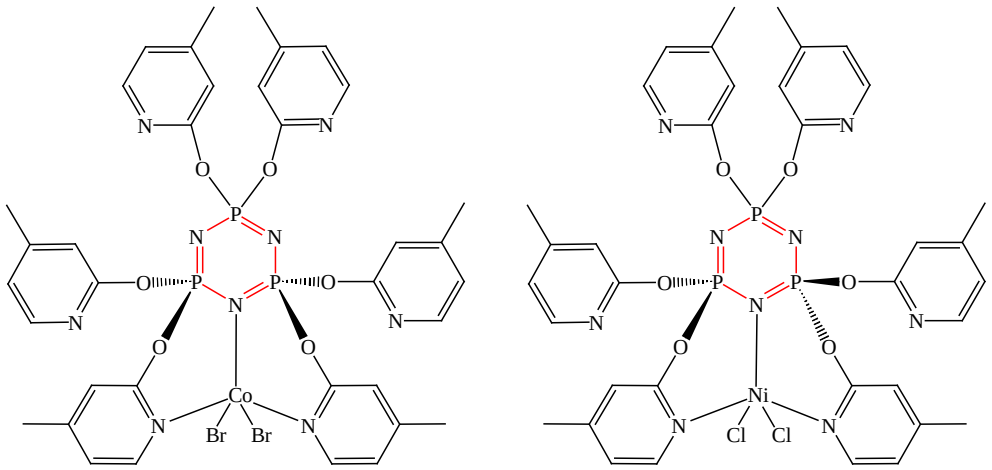

Figure 13 *cis* and *trans* tridentate structures reported by Ainscough *et al*[14] with the ligand hexakis(2O-4-MePy)cyclotriphosphazene

Chandrasekhar *et al*.[16] reported the reaction of $\mathbf{L^1}$ with $Cu(NO_3)_2{\cdot}3H_2O$ and $Co(NO_3)_2{\cdot}6H_2O$. The former gives an unusual geminal tridentate structure whilst the latter gives a non-geminal tridentate arrangement (Figure 14).

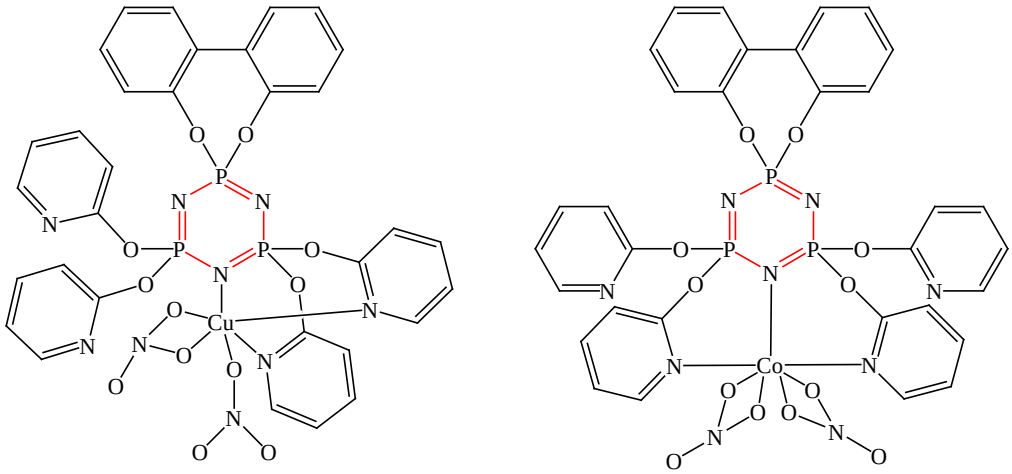

Figure 14 Tridentate complexes reported by Chandrasekhar *et al*.[16]

3.1.1.4 Phosphazenes exhibiting tetradentate behaviour

Tetradentate coordination by cyclotriphosphazenes to transition metals has been reported. The hexakis(2OPy)cyclotriphosphazene ligand reported by Ainscough *et al*.[14] reacts with $NiCl_2$ to form two isomers. One isomer gives the previously mentioned tridentate TBP arrangement (Figure 13 right), whereas the second isomer gives a

distorted octahedral arrangement coordinating to three pyridine rings, a cyclotriphosphazene ring nitrogen and the two chloride atoms.
Also reported by Ainscough *et al*.[34] was the tetradentate complex ion formed by reaction of $CuCl_2$ with 1,10-phenanthroline tethered to a cyclotriphosphazene platform (Figure 15)

Figure 15 Tetradentate complex ion reported by Ainscough *et al*.[34]

3.1.1.5 Phosphazenes exhibiting pentadentate behaviour

Pentadentate arrangements of cyclotriphosphazene ligands coordinated to transition metals typically involve an octahedral or distorted octahedral environment.
The hexakis(2OPy)cyclotriphosphazene ligand reported by Ainscough *et al*.[22] forms a trinuclear dimeric complex on reaction with $CuCl_2$. One copper centre is monodentate as described previously, the remaining two Cu(II) metal centres are pentadentate as shown in Figure 7.

With the ligands hexakis(2OPy)cyclotriphosphazene and hexakis(2O-4-MePy)-cyclotriphosphazene (Figure 16), reaction with $CoCl_2$, $NiCl_2$ and $CuCl_2$ gives a tridentate TBP type arrangement, however treatment of the complexes with $[Ag(CH_3CN)_4]PF_6$ yields pentadentate structures in a distorted octahedral environment.[15]

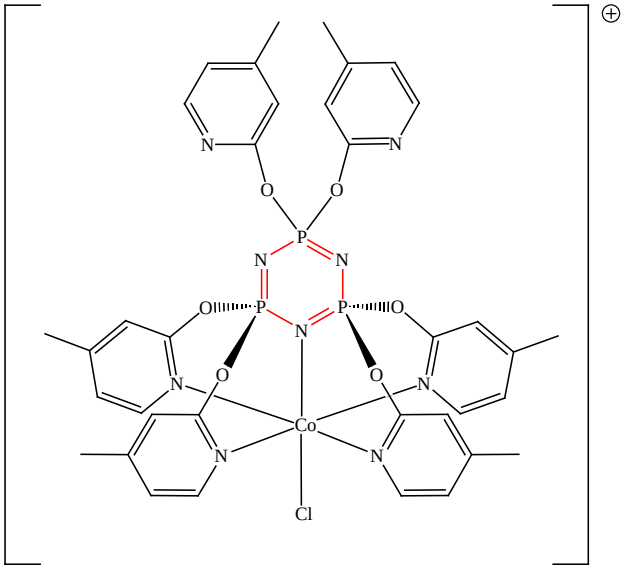

Figure 16 Pentadentate complex reported by Ainscough *et al.*[15]

3.1.1.6 Phosphazenes exhibiting hexadentate behaviour

Hexadentate arrangements with cyclotriphosphazene ligands are rare, with one example (Figure 17) being reported by Diefenbach *et al.*[5] where the mixed valent $[Cu_{13}O_9I]^{4+}$ cluster is stabilised by four tetraphenoxy(2-pyridylmethylamino)cyclotriphosphazene ligands, each in a hexadentate mode.

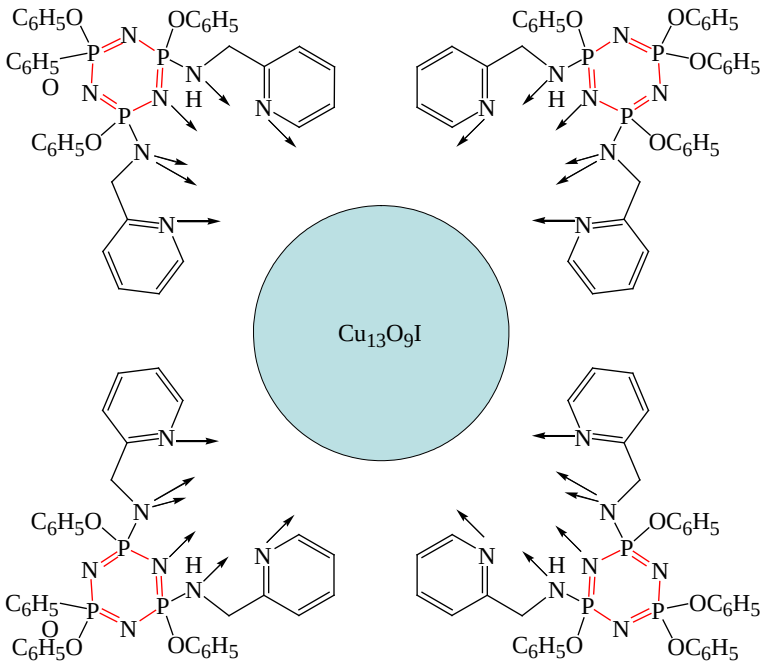

Figure 17 Schematic drawing of the hexadentate stabilisation by cyclotriphosphazene ligands reported by Diefenbach *et al.*[5]

3.1.1.7 Hydrolysis products from phosphazene complexes

Cyclotriphosphazenes coordinated to metal ions have been reported to undergo hydrolysis. Chandrasekhar *et al.*[35] reported P-O bond cleavage to give a dimeric species with the ligand hexakis(2OPy)cyclotriphosphazene (L in Figure 18) using $Co(NO_3)_2 \cdot 6H_2O$ (Figure 18).

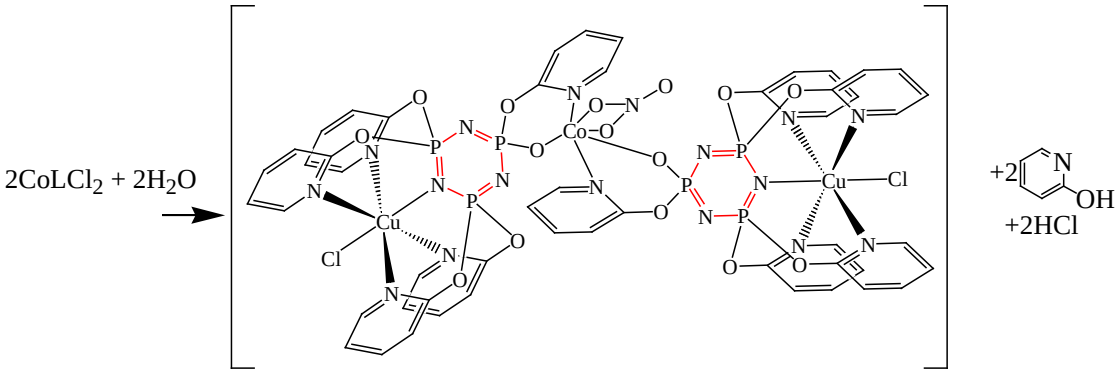

Figure 18 Hydrolysis product reported by Chandrasekhar *et al.*[35]

Ainscough *et al.*[34] reported a similar hydrolysis product from CH_3CN for the complex $[CuLCl]Cl \cdot 2CH_2Cl_2$, (where L = $[N_3P_3(biph)_2(2\text{-oxy-}1,10\text{-phenanthroline})_2]$) The X-ray structure showed that the environment around copper was distorted trigonal-bipyramidal with the ligand acting as a κ^4N donor (Figure 19).

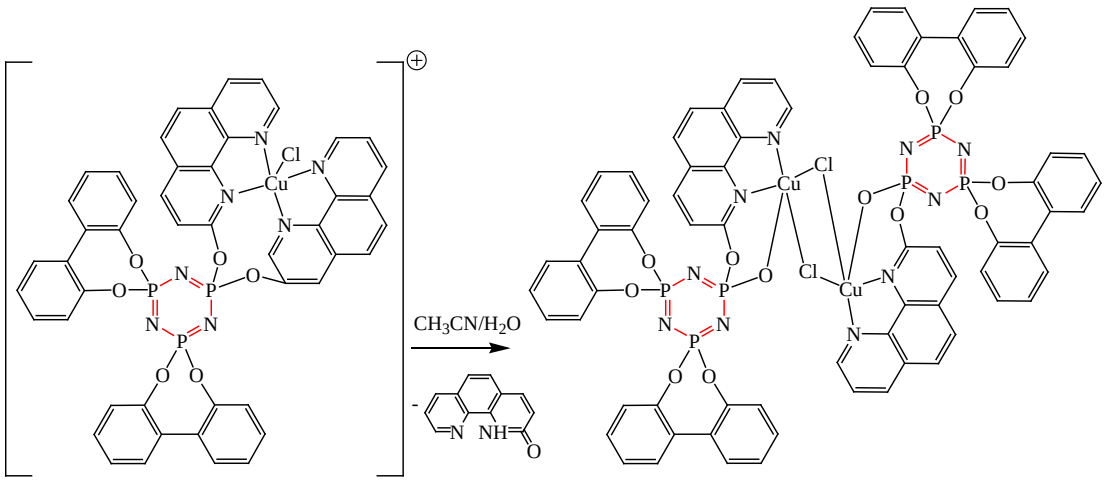

Figure 19 Hydrolysis product reported by Ainscough *et al.* [34]

In this non-exhaustive review of the coordination modes of cyclotriphosphazene ligands, it is evident that there exists a wide variety of possibilities for transition metal coordination. The coordination may be metal ion dependent and some of the ligands display various modes of coordination indicating a degree of flexibility in their behaviour.

3.2 Experimental

All manipulations were carried out under nitrogen using standard Schlenk techniques. Analytical grade solvents were purchased from standard chemical suppliers and used without further purification. Cs_2CO_3 (Acros), $CoCl_2{\cdot}6H_2O$ (Ajax), $CuCl_2{\cdot}2H_2O$ (Ajax), $CoBr_2$ (BDH) and $NiCl_2{\cdot}6H_2O$ (BDH) were dehydrated at 140 ºC prior to use. $ZnCl_2$ (M&B), $CuBr_2$ (Aldrich), $HgCl_2$ (M&B) and K_2CO_3 (BDH), were all used as received. The cyclotriphosphazene, $N_3P_3Cl_6$ (Aldrich), 2-hydroxypyridine (Aldrich), 2-hydroxy-4-methylpyridine (Aldrich) and 2-hydroxy-6-methylpyridine (Aldrich), were all used as received. 2,2'-biphenol (Merck) was sublimed prior to use. The ligand precursor, spiro(2,2'-biphenolato)tetrachlorocyclotriphosphazene was prepared by a literature method.[36]

Microanalyses were performed by Campbell Microanalytical Laboratory, University of Otago. NMR spectra were recorded on a Bruker Avance 400 MHz spectrometer in $CDCl_3$. IR spectra were run as KBr discs on Perkin-Elmer Paragon 1000 and Nicolet 5700 instruments. The latter was also used for Far IR spectra in polyethylene media. Raman spectra were recorded by Dr Geoff Waterhouse on a Renishaw RM-2 Raman microscope system, fitted with an Olympus 20 × objective lens at Auckland University. UV/vis spectra were recorded on Shimadzu UV-160A (200-1100 nm) and Shimadzu UV-310PC (200-1500+ nm) spectrophotometers. Electrospray mass spectra were collected from CH_3CN solutions on a micromass ZMD spectrometer run in positive ion mode. ESR spectra were recorded at 113 K on an X-band Varian E-104A spectrometer equipped with an E257 variable temperature controller operating at about 9.0 GHz. The spectral g values were calibrated with (diphenylpicryl)hydrazyl (DPPH) as a standard. Room temperature magnetic susceptibilities were measured by the Faraday method on a Cahn model 7550 millibalance. Conductivities were measured using a Philips 9509 digital conductivity meter.

3.2.1 Reaction of the Ligands L^1, L^2 and L^3 with selected transition metals

In this chapter, it is the coordination behaviour of the ligands **L^1**, **L^2** and **L^3** prepared in Chapter 2, with selected transition metals that is the primary focus, in order to elucidate any possible information that might be applicable to the polymeric complexes. The coordination modes of the ligands **L^1**, **L^2** and **L^3** all have one phosphorus site blocked by a 2,2'-dioxybiphenyl moiety.

3.2.2 Syntheses of the complexes with phosphazene ligands L^1, L^2 and L^3

A number of transition metal halide coordination compounds have been synthesised and characterised with the spiro(biph)tetrakis(pyridyloxy)cyclotriphosphazene ligands **L^1**, **L^2** and **L^3** prepared in Chapter 2 (Figure 20),

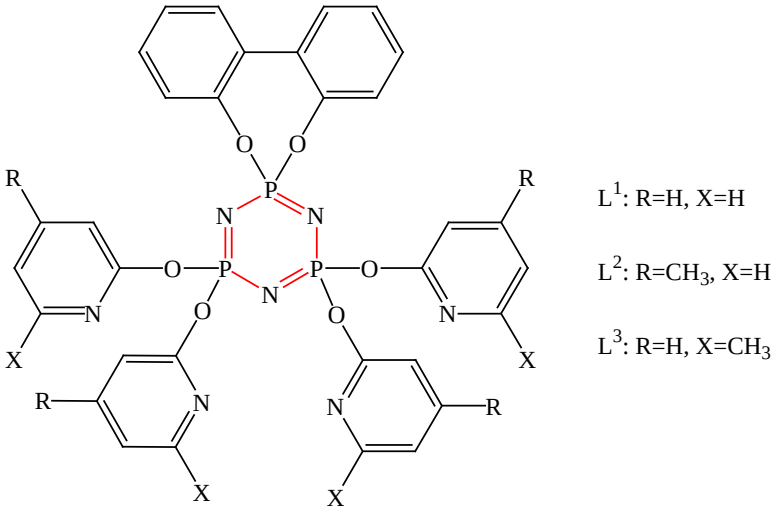

Figure 20 Schematic diagram for the ligands **L^1**, **L^2** and **L^3**

3.2.2.1 Complexes with L^1

$[CuL^1Cl_2]\cdot 0.5\ C_6H_{14}\cdot CH_3CN$

A mixture of **L^1** (0.101 g, 0.145 mmol) and anhydrous $CuCl_2$ (0.019 g, 0.146 mmol) was stirred under N_2 in 25 ml of CH_2Cl_2 overnight. The resulting yellow/gold solution was filtered through celite CH_2Cl_2 to give a green solution. The volume was reduced under vacuum to approximately 10 ml and a layer of hexane added. Slow diffusion at room temperature gave green micro-crystals. Yield 0.057 g (48%).

ESMS, 793 *m/z* $[CuL^1Cl]^+$ (100%), 758 *m/z* $[CuL^1]^+$ (40%). Elemental analysis: Calculated for $C_{32}H_{24}Cl_2CuN_7O_6P_3\cdot 0.5\ C_6H_{14}\cdot CH_3CN$ (915.10): C, 49.12; H, 4.01; N,

12.06. Found: C, 49.27; H, 3.17; N, 12.42. IR (KBr disc) ν/cm^{-1} (PN), 1238, 1217, 1190.

[CoL^{1}Cl$_2$]

A mixture of **L^{1}** (0.127 g, 0.183 mmol) and anhydrous $CoCl_2$ (0.0238 g, 0.183 mmol) was stirred under N_2 in 40 ml of CH_2Cl_2 overnight. The precipitate was filtered and washed with hexane then refluxed in CH_3CN until dissolved. Cooling produced blue crystals. Yield 0.077 g (51%).

ESMS on the blue CH_3CN solution prior to crystallisation gives 789 *m/z* [CoL^{1}Cl]$^+$ (100%). Elemental analysis: Calculated for $C_{32}H_{24}Cl_2CoN_7O_6P_3$ (825.34): C, 46.57; H, 2.93; N, 11.88. Found: C, 46.36; H, 2.98; N, 12.08. IR (KBr disc) ν/cm^{-1} (PN), 1234, 1217, 1184.

[CoL^{1}Br$_2$]

A mixture of **L^{1}** (0.0682 g, 0.098 mmol) and anhydrous $CoBr_2$ (0.021 g, 0.096 mmol) was stirred under N_2 in 10 ml of CH_2Cl_2 overnight. The precipitate was filtered and washed with hexane then refluxed in CH_3CN until dissolved. Cooling produced blue crystals. Yield 0.044 g (50%).

ESMS, 832.95 *m/z* [CoL^{1}Br]$^+$ (100%). Elemental analysis: Calculated for $C_{32}H_{24}Br_2CoN_7O_6P_3$ (914.24): C, 42.04; H, 2.65; N, 10.72. Found: C, 41.89, H, 2.80, N, 10.68. IR (KBr disc) ν/cm^{-1} (PN), 1233, 1216, 1202, 1183.

[CuL^{1}Br$_2$]

A mixture of **L^{1}** (0.0667 g, 0.095 mmol) and anhydrous $CuBr_2$ (0.021 g, 0.096 mmol) was stirred under N_2 in 10 ml of CH_2Cl_2 overnight. The resulting dark green opaque solution was filtered through celite with CH_2Cl_2 (3 x 15 ml). The volume of the solution was reduced on a rotary evaporator to approximately 10 ml and a layer of hexane added, from which small yellow crystals formed at room temperature. Yield 0.049 g (56%).

ESMS, 758 *m/z* [CuL^{1}]$^+$ (100%). Elemental analysis: Calculated for $C_{32}H_{24}Br_2CuN_7O_6P_3$ (918.85): C, 41.83; H, 2.63; N, 10.67. Found: C, 41.71, H, 2.81, N, 10.57. IR (KBr disc) ν/cm^{-1} (PN), 1232, 1217, 1182.

3.2.2.2 Complexes with L^2

$[CuL^2Cl_2]$

A mixture of $\mathbf{L^2}$ (0.048 g, 0.06 mmol) and anhydrous $CuCl_2$ (0.0089 g, 0.006 mmol) was stirred under N_2 in 30 ml of CH_2Cl_2 overnight. The initial pale yellow solution gradually formed a dark yellow solution over 3-4 hours. The solution was reduced under vacuum to approximately 10 ml and a hexane layer added. After 10 days at room temperature the solution had turned pale green with evidence of micro-crystal formation. Yield 0.025 g (44%).

ESMS, 814 *m/z* $[CuL^2]^+$ (100%), 849 *m/z* $[CuL^2Cl]^+$ (67%). Elemental analysis: Calculated for $C_{36}H_{32}Cl_2CuN_7O_6P_3$ (886.06): C, 48.80; H, 3.64; N, 11.07. Found: C, 48.90; H, 3.99; N, 10.57. IR (KBr disc) ν/cm^{-1} (PN), 1232, 1217, 1190, 1165.

$[CoL^2Cl_2]\cdot 2CH_3CN$

A mixture of $\mathbf{L^2}$ (0.066 g, 0.088 mmol) and anhydrous $CoCl_2$ (0.013 g, 0.1 mmol) was stirred under N_2 in 30 ml of CH_2Cl_2 overnight. The resulting pale blue liquid remained clear throughout the reaction. The solution was dried under vacuum to give thin blue crystals Yield 0.036 g (46%). X-ray quality crystals were obtained by recrystallisation from hot CH_3CN.

ESMS, 845 *m/z* $[CoL^2Cl]^+$ (100%). Elemental analysis: Calculated for $C_{36}H_{32}Cl_2CoN_7O_6P_3\cdot CH_2Cl_2$ (966.37): C, 45.99; H, 3.55; N, 10.15. Found: C, 46.43; H, 3.79; N, 10.08. IR (KBr disc) ν/cm^{-1} (PN), 1233, 1218, 1195, 1163.

$[CoL^2Cl_2]\cdot CH_2Cl_2$

A mixture of $\mathbf{L^2}$ (0.027 g, 0.036 mmol) and $CoCl_2\cdot 6H_2O$ (0.008 g, 0.036 mmol) was stirred under N_2 in 30 ml of CH_2Cl_2 overnight. The resulting pale blue liquid remained clear throughout the reaction. The solution was reduced under vacuum to approximately 10 ml and a hexane layer added. Dark blue crystals were obtained following complete evaporation of the liquid. This complex was synthesised purely to obtain an X-ray structure for comparison and further analysis was not undertaken.

$[CoL^2Br_2]$

A mixture of $\mathbf{L^2}$ (0.103 g, 0.137 mmol) and anhydrous $CoBr_2$ (0.0299 g, 0.137 mmol) was stirred under N_2 in 20 ml of CH_2Cl_2 overnight. The resulting dark blue solution was taken to dryness on a rotary evaporator and the resulting blue powder was refluxed in

CH_3CN from which, on cooling, X-ray quality crystals were formed. Yield 0.055 g (42%).
ESMS, 889 *m/z* $[CoL^2Br]^+$ (100%). Elemental analysis: Calculated for $C_{36}H_{32}Br_2CoN_7O_6P_3 \cdot CH_3CN$ (1011.40): C, 45.13; H, 3.49; N, 11.08. Found: C, 45.08, H, 3.71, N, 10.76. IR (KBr disc) ν/cm^{-1} (PN), 1235, 1223, 1194, 1164.

$[CuL^2Br_2]$
A mixture of $\mathbf{L^2}$ (0.076 g, 0.102 mmol) and anhydrous $CuBr_2$ (0.023 g, 0.103 mmol) was stirred under N_2 in 30 ml of CH_2Cl_2 overnight. The initial pale yellow colouration, developed into a clear yellow/green solution as the reaction progressed. The solution was reduced under vacuum to approximately 15 ml and a hexane layer added. After 4 weeks at 4 ºC, fine yellow crystals of X-ray quality were formed. Yield 0.057 g (58%).
ESMS, 814 *m/z* $[CuL^2]^+$ (100%). Elemental analysis: Calculated for $C_{36}H_{32}Br_2CuN_7O_6P_3 \cdot CH_2Cl_2$ (1059.89): C, 41.93; H, 3.23; N, 9.25. Found: C, 41.50; H, 3.43; N, 8.98. IR (KBr disc) ν/cm^{-1} (PN), 1233, 1218, 1191, 1152.

$[NiL^2Cl_2]$
A mixture of $\mathbf{L^2}$ (0.1 g, 0.13 mmol) and anhydrous $NiCl_2$ (0.017g, 0.13mmol) was stirred under N_2 in 30 ml CH_2Cl_2 overnight. A clear yellow solution was obtained by filtering through celite with 40 ml CH_2Cl_2. The volume was reduced under vacuum to approximately 10 ml and a layer of hexane added. Nucleation was initiated to produce a green powder. Yield 0.081 g, (79%).
ESMS, 844 *m/z* $[NiL^2Cl]^+$ (100%). Elemental analysis: Calculated for $C_{36}H_{32}Cl_2NiN_7O_6P_3 \cdot 2C_6H_{14} \cdot CH_2Cl_2$ (967.38): C, 52.15; H, 4.79; N, 10.14. Found: C, 51.64; H, 4.37; N, 9.07. IR (KBr disc) ν/cm^{-1} (PN), 1238, 1216, 1199, 1142.

3.2.2.3 Complexes with L^3

$[CuL^3Cl_2]$
A mixture of $\mathbf{L^3}$ (0.118 g, 0.158 mmol) and anhydrous $CuCl_2$ (0.021 g, 0.161 mmol) was stirred under N_2 in 40 ml of CH_2Cl_2 for 48 hours. The initial pale yellow colouration developed into a dark green clear solution as the reaction progressed. The solution was filtered through celite with 30 ml CH_2Cl_2 and the resulting volume reduced under vacuum to approximately 15 ml. A hexane layer was added and nucleation was

initiated to produce a light green solid which was filtered and washed with hexane prior to drying. Yield 0.101 g (73%).
ESMS, 814 *m/z* $[CuL^{3}]^{+}$ (100%). Elemental analysis: Calculated for $C_{36}H_{32}Cl_2CuN_7O_6P_3 \cdot CH_2Cl_2$ (970.99): C, 45.77; H, 3.53; N, 10.10. Found: C, 46.04; H, 3.66; N, 9.95. IR (KBr disc) ν/cm^{-1} (PN), 1222, 1184.

$[CoL^{3}Cl_2]$
A mixture of **L^{3}** (0.103 g, 0.137 mmol) and anhydrous $CoCl_2$ (0.018 g, 0.138 mmol) was stirred under N_2 in 40 ml CH_2Cl_2 overnight. The pale blue opaque solution was filtered through celite with 30 ml CH_2Cl_2. Nucleation was initiated to produce a light blue solid which was filtered and washed with hexane prior to drying. Yield 0.080 g (66%).
ESMS, 752 *m/z* $[L+H]^{+}$ (100%). 845 *m/z* $[CoL^{3}Cl]^{+}$ (trace only). Elemental analysis: Calculated for $C_{36}H_{32}ClCoN_7O_6P_3 \cdot C_6H_{14}$ (932.17): C, 54.12; H, 4.97; N, 10.52; Cl, 3.80. Found: C, 54.56; H, 4.85; N, 10.91; Cl, 3.59. IR (KBr disc) ν/cm^{-1} (PN), 1233, 1219, 1181.

3.2.3 X-ray crystallography

The X-ray data was collected on a Siemens P4 four circle diffractometer, using a Siemens SMART 1K CCD area detector. The crystals were mounted in an inert oil, transferred into the cold gas stream of the detector and irradiated with graphite monochromated Mo Kα (k = 0.71073 Å) X-rays. The data were collected by the SMART program and processed with SAINT to apply Lorentz and polarisation corrections to the diffraction spots (integrated 3 dimensionally). Crystal refinement data are given in Tables 2 and 3, selected bond lengths and angles are in Tables 6 and 7, and the numbering scheme is given in Figure 26. The structures were solved by direct methods and refined using the SHELXTL program.[37] Hydrogen atoms were calculated at ideal positions.

3.3 Results and discussion

3.3.1 Syntheses of the complexes

Complexes were prepared by reaction of **L^{1}**, **L^{2}** and **L^{3}** in a 1:1 molar ratio with the appropriate anhydrous salt in CH_2Cl_2 with the exception of $[CoL^{2}Cl_2] \cdot CH_2Cl_2$ for which

the water molecules of hydration of the cobalt chloride precursor were retained. Somewhat surprisingly, the water molecules of hydration had no noticeable effect on the complex formed, possibly due to the use of CH_2Cl_2 as solvent, which is immiscible with water. However, hydrolysis of $[CoL^2Cl_2]\cdot 2CH_3CN$ does occur over an extended period for crystals remaining in the CH_3CN mother liquor, with formation of a dimeric species (henceforth designated $[CoL^{2HP}Cl]_2$ (HP = Hydrolysis Product) for ease of reference) as described later in this chapter and shown in Equation 1. The complexes $[ZnL^2Cl_2]$, $[CdL^2Cl_2]$, and $[HgL^2Cl_2]$ were similarly synthesised and are reported separately in Chapter 4.

$$2[CoL^2Cl_2] + 2H_2O \longrightarrow [CoL^{2HP}Cl]_2 + 2HCl + 2(OHPy) \quad \text{Eq 1}$$

Solubilities of the complexes vary markedly with the ligand and with the metal halide. $[CoL^1Cl_2]$ formed a precipitate during reaction that proved to be insoluble except in refluxing CH_3CN, from which crystals formed on cooling. The crystals could not be made to redissolve in CH_2Cl_2 or even refluxing CH_3CN for subsequent solution spectra or conductivity measurements. Solubility results for the other complexes are tabulated in Table 1.

	Hot CH_3CN	CH_3CN	Acetone	CH_2Cl_2
$[CoL^1Br_2]$	Yes			
$[CoL^2Cl_2]\cdot CH_2Cl_2$		Yes	Yes	No
$[CoL^2Br_2]$		Yes	Yes	No
$[CoL^3Cl_2]$				Yes
$[CuL^3Cl_2]$				Yes

Table 1 Relative solubilities for the complexes

Thus it would appear that the presence and position of the methyl group does affect solubility as postulated in Chapter 2, being in the order (2OPy) < (2O-4-MePy) < (2O-6-MePy), and that the nature of the metal ion is also a factor in solubility.

ESMS for the cobalt halide complexes with $\mathbf{L^1}$ and $\mathbf{L^2}$ give $[CoLX]^+$, a trend which is also demonstrated for $\mathbf{L^2}$ with Ni, Zn and Hg chlorides, whereas $\mathbf{L^3}$ shows only a low intensity peak assignable to $[CoL^3Cl]^+$ with the majority species being $[L^3+H]^+$. The Cu halides show a greater tendency to form $[CuL]^+$ as the major species, the exception being $\mathbf{L^1}$ which gives $[CuL^1X]^+$.

3.3.2 Structural similarities in the crystallography

Single crystal X-ray structures were obtained for $[CoL^1Cl_2]$, $[CoL^2Cl_2]\cdot 2CH_3CN$, $[CoL^2Cl_2]\cdot CH_2Cl_2$, $[CoL^2Br_2]$ and $[CuL^2Br_2]$. All exhibit similar five-coordinate trigonal bipyramidal (TBP) complexes with the ligands acting as κ^3*N* donors coordinating via one phosphazene ring nitrogen, two nitrogens from non-geminal *trans* pyridyloxy pendant arms and two halo-ions as illustrated, for example, by the cobalt complex in Figure 21. In each case the pyridine nitrogens are axial, with equatorial positions taken by the phosphazene ring nitrogen and the halo-ions.

All of the X-ray structures demonstrate the same interaction between the non-coordinating pyridyloxy rings and the ring phosphorus to which they are bound via the hinge oxygen, as in the case for the free ligands discussed in Chapter 2,[38, 39] the bond data are given in Table 8.

Typically volatile solvent molecules are trapped within solid samples of cyclophosphazenes[14] and it is well documented that cyclic phosphazenes bearing aromatic substituents have the ability to act as clathrates.[40-44] Each structure will now be discussed separately.

3.3.2.1 X-ray structure of $[CoL^1Cl_2]$

Two X-ray structures were obtained for $[CoL^1Cl_2]$ and both were twinned such that there was a high degree of extraneous electron density. The structures could not be satisfactorily refined and are unsuitable for publication. They do however display sufficient connectivity to confirm the TBP arrangement although any data regarding bond lengths and angles is not considered to be reliable.

3.3.2.2 X-ray structures of $[CoL^2Cl_2]\cdot 2CH_3CN$ and $[CoL^2Cl_2]\cdot CH_2Cl_2$

Both complexes crystallised in space group *P*2(1)/*c*, however the X-ray structure of $[CoL^2Cl_2]\cdot 2CH_3CN$ (Figure 21) obtained from refluxing CH_3CN, refined with two

molecules of CH_3CN in the unit cell, whereas the X-ray structure of $[CoL^2Cl_2]\cdot CH_2Cl_2$ from CH_2Cl_2/hexane, refined with one disordered molecule of CH_2Cl_2.

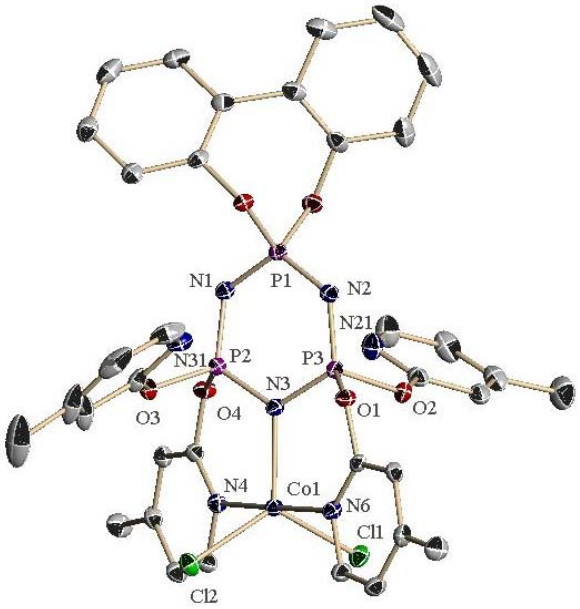

Figure 21 X-ray crystal structure of $[CoL^2Cl_2]\cdot 2CH_3CN$. Thermal ellipsoids are drawn at 50% probability (hydrogen atoms and occluded solvent removed for clarity)

The occluded solvent molecules lead to slight variations in the crystal packing (Figures 22 and 23) as can be seen from the cell dimensions in Table 2 where the cell length *c* (Å) for $[CoL^2Cl_2]\cdot 2CH_3CN$ (31.104 Å) is over twice that for $[CoL^2Cl_2]\cdot CH_2Cl_2$ (14.8927(15) Å).

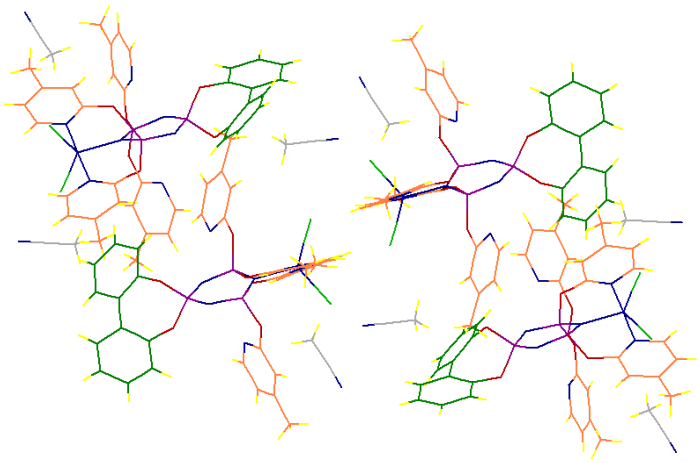

Figure 22 Packing arrangement for $[CoL^2Cl_2]\cdot 2CH_3CN$

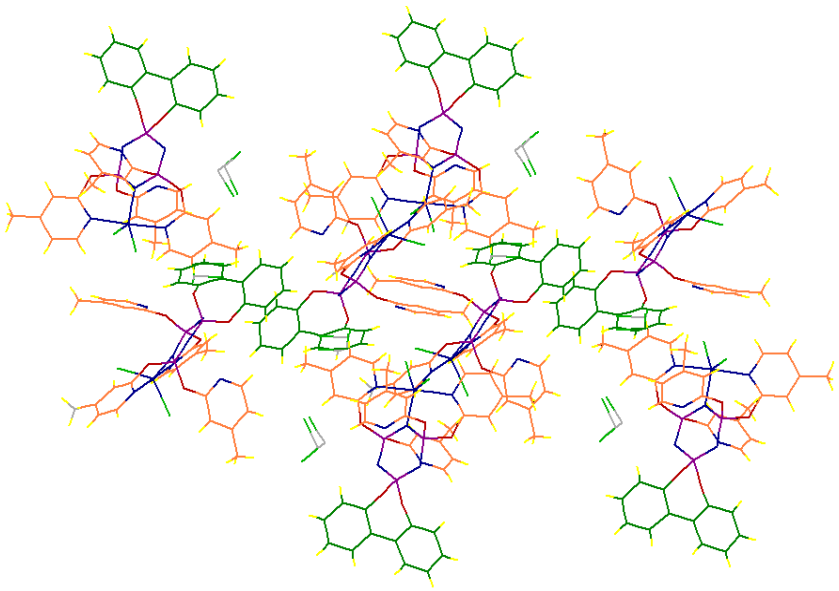

Figure 23 Packing arrangement for $[CoL^2Cl_2]\cdot CH_2Cl_2$

Both $[CoL^2Cl_2]\cdot 2CH_3CN$ and $[CoL^2Cl_2]\cdot CH_2Cl_2$ give five-coordinate trigonal bipyramidal structures with an N_3Cl_2 donor set. The two axial nitrogen atoms are from *trans* non-geminal coordinated pyridyloxy rings. The third nitrogen is from the cyclotriphosphazene ring and together with the two chloride ions, complete the donor set forming the equatorial donors.

3.3.2.3 X-ray structures of $[CoL^2Br_2]$ and $[CuL^2Br_2]$

Both complexes crystallised in space group *P*2(1)/*c*. $[CoL^2Br_2]$ refined with two molecules of CH_3CN, and $[CuL^2Br_2]$ refined with one molecule of CH_2Cl_2 (Figures 24 and 25). Both X-ray structures demonstrate distorted TBP geometry around the metal centre with no evidence for stacking between the aromatic rings.

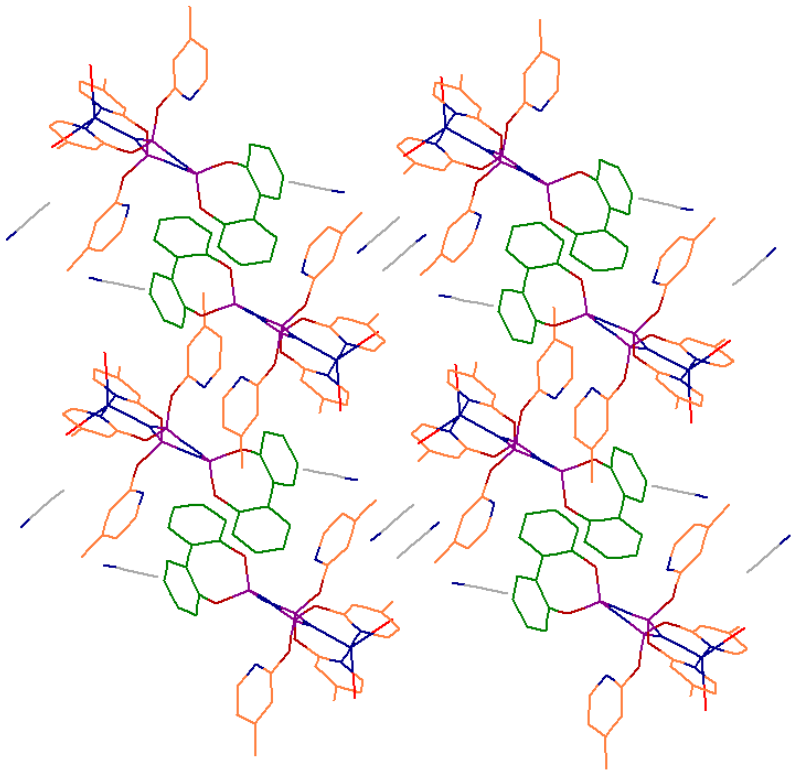

Figure 24 Packing arrangement of [CoL^2Br_2] (hydrogen atoms omitted for clarity)

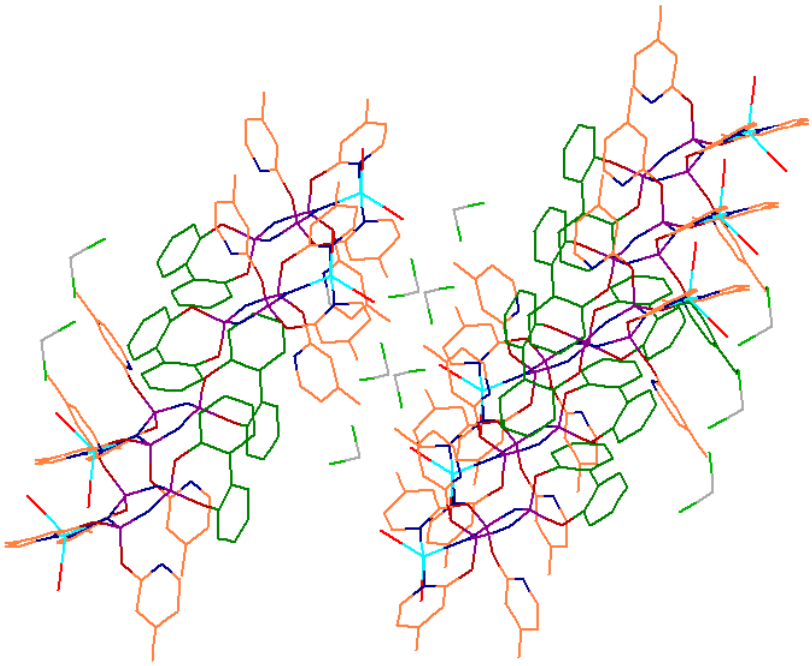

Figure 25 Packing arrangement of [CuL^2Br_2] (hydrogen atoms omitted for clarity)

The donor set for $[CoL^2Br_2]$ and $[CuL^2Br_2]$ is the same N_3X_2 as for the Co(II) complexes with the two axial nitrogen atoms from *trans* non-geminal coordinated pyridyloxy rings and the equatorial donors being the cyclotriphosphazene ring nitrogen and the two bromide ions.

3.3.3 Comparison of the X-ray structures of the complexes

Crystallographic and refinement data for the complexes are given in Tables 2 and 3. The hydrolysis product $[CoL^{2HP}Cl_2]$ is described in section 3.3.3.3.

Compound	$[CoL^2Cl_2]\cdot 2CH_3CN$	$[CoL^{2HP}Cl]_2$	$[CoL^2Cl_2]\cdot CH_2Cl_2$
Molecular formula	$C_{40}H_{38}Cl_2CoN_9O_6P_3$	$C_{34}H_{32}ClCoN_8O_6P_3$	$C_{36}H_{32}Cl_2CoN_7O_6P_3$
Molecular weight	963.53	835.97	881.43
T (K)	84(2)	93(2)	93(2)
Crystal System	Monoclinic	Triclinic	Monoclinic
Space Group	$P2(1)/c$	P-1	$P2(1)/c$
a (Å)	13.03310(10)	10.8684(15)	17.6521(19)
b (Å)	10.46700(10)	13.1852(19)	16.0697(17)
c (Å)	31.104(1)	13.3977(19)	14.8927(15)
α (˚)	90	90.424(9)	90
β (˚)	95.4240(10)	91.364(9)	92.946(3)
γ (˚)	90	91.055(9)	90
V (Å^3)	4224.14(5)	1919.0(5)	4218.9(8)
Z	4	2	4
μ (MoKα) (mm^{-1})	0.706	0.696	0.698
ρ_{calc}(g cm^{-3})	1.515	1.447	1.388
2θmax (˚)	52.82	50.7	50.7
No. of unique reflections	8623	7010	7705
Data/restraints/ parameters	8623 / 0 / 556	7010 / 0 / 483	7705 / 61 / 555
Final R indices [I >2σ(I)]	$R1$ = 0.0324 $wR2$ = 0.0847	$R1$ = 0.0677 $wR2$ = 0.1450	$R1$ = 0.0346 $wR2$ = 0.1055
R indices (all data)	$R1$ = 0.0401 $wR2$ = 0.0894	$R1$ = 0.1577 $wR2$ = 0.1776	$R1$ = 0.0496 $wR2$ = 0.1169
Goodness of Fit on F^2	1.111	0.953	1.066

Table 2 Crystallographic and refinement data for complexes $[CoL^2Cl_2]\cdot 2CH_3CN$, $[CoL^{2HP}Cl]_2$ and $[CoL^2Cl_2]\cdot CH_2Cl_2$

Compound	$[CoL^2Br_2]$	$[CuL^2Br_2]$
Molecular formula	$C_{38}H_{35}Br_2CoN_8O_6P_3$	$C_{37}H_{34}Br_2Cl_2CuN_7O_6P_3$
Molecular weight	1011.4	1059.88
T (K)	84(2)	84(2)
Crystal System	Monoclinic	Monoclinic
Space Group	$P2(1)/c$	$P2(1)/c$
a (Å)	12.9529(2)	12.9284(2)
b (Å)	10.58350(10)	10.4443(2)
c (Å)	31.52860(10)	31.9761(4)
α (˚)	90	90
β (˚)	94.63(1)	94.1280(10)
γ (˚)	90	90
V (Å^3)	4308.08(8)	4306.47(12)
Z	4	4
μ (MoKα) (mm^{-1})	2.419	2.651
ρ_{calc}(g cm^{-3})	1.559	1.635
2θmax (˚)	52.9	52.7
No. of unique reflections	8824	8728
Data/restraints/parameters	8824 / 0 / 557	8728 / 0 / 527
Final R indices [$I > 2\sigma(I)$]	$R1$ = 0.0344 $wR2$ = 0.0741	$R1$ = 0.0553 $wR2$ = 0.1057
R indices (all data)	$R1$ = 0.0473 $wR2$ = 0.0790	$R1$ = 0.0986 $wR2$ = 0.1215
Goodness of Fit on F^2	1.106	1.049

Table 3 Crystallographic and refinement data for complexes $[CoL^2Br_2]$ and $[CuL^2Br_2]$

Tables 2 and 3 indicate that the refinement data for each structure are acceptable for publication. CIF files are included on the accompanying compact disc for reference. On conducting an online CIF check[45] no significant alerts were returned.

3.3.3.1 The structural index (τ)

For five-coordinate complexes, the structural index (τ) can be evaluated from the two largest angles ($\alpha < \beta$) in the 5-coordinate system, where $\tau = (\beta - \alpha)/60$. For each complex, τ is given in Table 4 with atom numbering as shown in the generic scheme in Figure 26. All values indicate distorted trigonal bipyramidal geometry (where $\tau = 1.0$ for a regular trigonal bipyramidal stereochemistry and $\tau = 0.0$ for a regular square based pyramidal stereochemistry).[46]

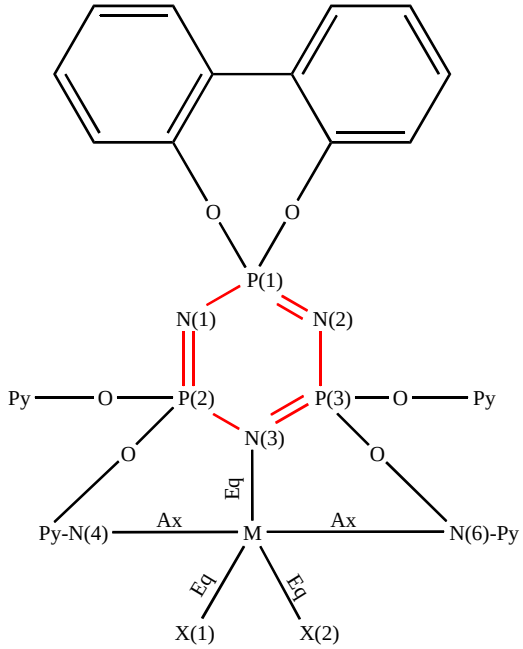

Figure 26 Generic labelling scheme for the five-coordinate complexes

Complex	β°	α°	τ [(β – α)/60]
$[CoL^2Cl_2]\cdot 2CH_3CN$	N(4)–Co–N(6) = 178.55(6)	Cl(1)–Co–Cl(2) = 123.48(2)	0.92
$[CoL^2Cl_2]\cdot CH_2Cl_2$	N(4)–Co–N(6) = 178.02(8)	Cl(2)–Co–N(3) = 122.81(6)	0.92
$[CoL^2Br_2]$	N(4)–Co–N(6) = 178.34(9)	Br(1)–Co–Br(2) = 123.29(18)	0.92
$[CuL^2Br_2]$	N(4)–Cu–N(6) = 178.06(17)	Br(1)–Cu–Br(2) = 127.40(3)	0.84

Table 4 The structural index (τ) for the five-coordinate complexes

The τ values contrast sharply with those of five-coordinate structures from work on the hexakis(2-pyridyloxy)cyclotriphosphazene (L) molecule, where τ = 0.47 for $[CuLCl_2]$ to 0.83 for $[CoLBr_2]$ implying a square based distorted trigonal bipyramidal geometry.[15] This is most likely to be a result of the hexakis(2-pyridyloxy)cyclotriphosphazene coordinating in a *cis* non-geminal fashion to the metal centre i.e. the coordinating pyridyloxy rings are on different phosphorus atoms but on the same face of the cyclotriphosphazene ring, whereas X-ray crystal structures for complexes of $\mathbf{L^1}$ and $\mathbf{L^2}$ indicate *trans* non-geminal coordination, i.e. the coordinating pyridyloxy rings are on different phosphorus atoms but on opposite faces of the cyclotriphosphazene ring.

3.3.3.2 Distortion in the coordinated complexes

There are a number of factors that can be compared between the X-ray crystal structures that are useful comparators in attempting to deduce those effects that are due to the coordinating metals and those that are ligand controlled. These factors are summarised in Table 5 and will be dealt with in turn.

3.3.3.2.1 Cyclotriphosphazene (CTP) ring distortion

The X-ray structures demonstrate a degree of phosphazene ring distortion from planar (Table 5). Taking a mean plane through atoms P(1), N(1), N(2), and N(3), and adding the total out-of-plane distances of P(2) and P(3), allows a consistent comparison of ring distortion between molecules.

	CTP ring distortion (Å)	Py ring$_{Coord}$ deviation (˚)	M-N$_{CTP\ ring}$ bond length (Å)	M-N$_{Py}$ bond length (Å)	N$_{Py}$-M-N$_{Py}$ Angle (˚)
[CoL^{2}Cl$_2$]·2CH$_3$CN	0.3708	170.9	2.048(17)	2.205(17) 2.228(17)	178.55(6)
[CoL^{2}Cl$_2$]·CH$_2$Cl$_2$	0.3803	165.1	2.050(2)	2.226(2) 2.227(2)	178.02(8)
[CoL^{2}Br$_2$]	0.3718	170.8	2.043(2)	2.239(2) 2.213(2)	178.34(9)
[CuL^{2}Br$_2$]	0.3815	169.3	2.070(4)	2.088(4) 2.097(4)	178.06(17)

CTP = cyclotriphosphazene. N$_{Py}$ = nitrogen of the coordinated pyridyl ring

Table 5 Comparison of selected distortion parameters

As can be seen from Table 5, the order of ring distortion is: [CoL^{2}Cl$_2$]·2CH$_3$CN < [CoL^{2}Br$_2$] < [CoL^{2}Cl$_2$]·CH$_2$Cl$_2$ < [CuL^{2}Br$_2$]. While the data may not be statistically significant, comparison with the free ligand molecules, **L^{2A}** (0.2912 Å), **L^{2B}** (0.0652 Å) from Chapter 2, would seem to indicate that coordination to the metal does induce a degree of ring distortion in these systems. Allcock[47] reported that the phosphazene ring planarity is apparently a response to crystal packing forces, and that the degree of planarity seems to have little effect on the stability of the molecule. It appears that

intramolecular forces, such as coordination to metals, could also influence ring planarity.

3.3.3.2.2 Deviation of coordinated pyridyloxy rings (Py $ring_{Coord}$ deviation)

Taking a mean plane through the coordinated 2-pyridyloxy rings, as shown in Figure 27, allows a comparison of the relative planarity of the rings either side of the metal centre. It would appear from Table 5, that the nature of the coordinating adduct has little effect on this parameter since both Co(II) and Cu(II) species have similar values. The greatest deviation is between $[CoL^2Cl_2]\cdot 2CH_3CN$ and $[CoL^2Cl_2]\cdot CH_2Cl_2$ and it would seem that the deviation of the 2-pyridyloxy rings from planarity is a further indicator of the sensitivity of the cyclotriphosphazene to packing forces induced by the occluded solvent molecules.

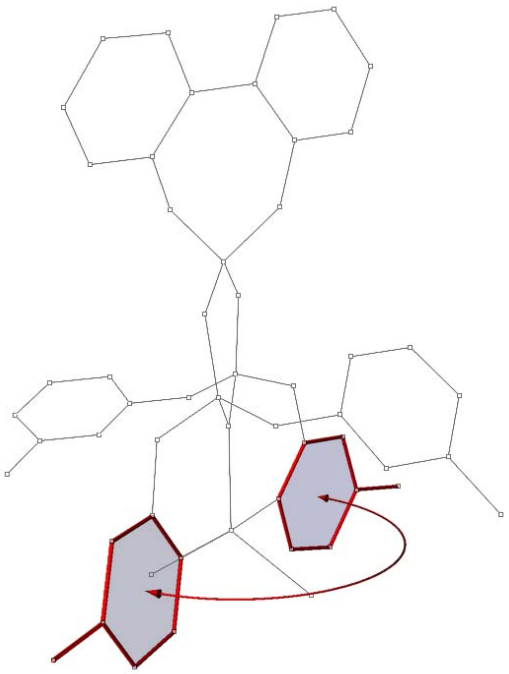

Figure 27 Deviation of coordinated pyridyloxy rings (Py $ring_{Coord}$ deviation)

3.3.3.2.3 M-N bond lengths

The bond length from the metal centre to the pyridyl nitrogen atoms shows that the Cu-$N_{(Py)}$ bond length (2.088-2.097 Å) is significantly shorter than that of Co-$N_{(Py)}$ (2.205-2.239 Å), while the $N(3)_{ring}$-M bond length increases from: $N(3)_{(ring)}$-$Co_{(Br2)}$ (2.043 Å) <

$N(3)_{(ring)}$-$Co_{(Cl2)}$ (2.048-2.050 Å) < $N(3)_{(ring)}$-Cu (2.070 Å). Thus it would appear that with the pyridyl arms coordinating from different faces of the phosphazene ring, the ionic radius of the metal is a factor in the degree of twist in the ring. For dipositive ions in 5-coordinate geometry, the ionic radii are: Cu (0.065 nm) < Co (0.067 nm).[48] Figure 28 gives the generic labelling system used for discussion of the various bond data.

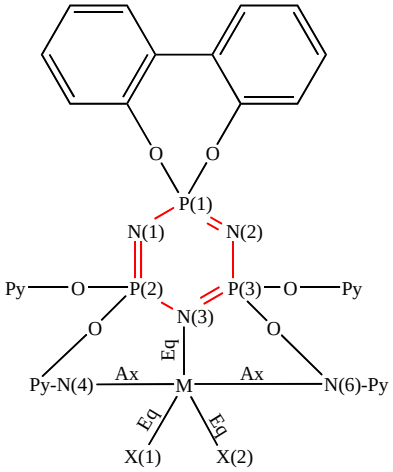

Figure 28 Generic labelling for reference

Selected bond data are given in Tables 6, 7, and 8. It is interesting to note that in all of the Co(II) complexes, the equatorial M-$N(3)_{(ring)}$ bond length is consistently shorter than the axial M-$N_{(Py)}$ bond lengths. Whilst for Cu(II) there is some overlap due to the associated standard deviation. This trend also holds for the hexakis(2OPy)cyclotriphosphazene and hexakis(2O-4-MePy)cyclotriphosphazene ligands. Justin Thomas *et al.*[33] reported that for the ligand 2,2-diphenyl-tetrakis(3,5-dimethyl-1-pyrazolyl) cyclotriphosphazene (DMP), the complexes $[Cu(DMP)X_2]$ (X=Cl, Br) had longer equatorial Cu-$N_{(ring)}$ bonds (2.320(5) Å) than the axial Cu-$N_{(Py)}$ bonds (1.979(5) Å). This result could be due to the greater flexibility induced by the oxygen hinge in the oxypyridine moiety.

3.3.3.2.4 P-N bond lengths, P-N-P and N-P-N angles

Typically, for a range of cyclotriphosphazene ring complexes, there is a small variation in the ring P-N bond lengths on coordination with metals,[49] with the bonds to the coordinated nitrogen being consistently longer (1.601(4)-1.618(2) Å) than the non-coordinated P-N bond lengths (1.5585(17)-1.593(4) Å). The coordinating pyridyloxy

groups lie on opposite sides of the phosphazene ring in each case i.e. in a *trans* arrangement, and it would therefore appear that ligand effects control the geometry in the solid state.

For the cyclotriphosphazene rings, the P-N bond lengths and P-N-P bond angles are within the expected ranges of 1.54-1.63 Å, and 119-148˚ respectively, with the N-P-N bond angles varying less than the P-N-P bond angles (116-120˚).[50]

3.3.3.2.5 Metal-halide bond lengths and angles

The metal halide bond lengths range from 2.2741(7) to 2.4703(8) and follow the order CoCl < CoBr < CuBr. The X-M-X bond angles vary by approximately 2.5˚ between $[CoL^2Cl_2]\cdot 2CH_3CN$ and $[CoL^2Cl_2]\cdot CH_2Cl_2$ which may be linked to the deviation between the mean planes of the coordinated pyridyl rings (170.9˚ and 165.1˚ respectively) resulting from the packing forces induced by the different occluded solvent molecules. Thus it seems that the cyclotriphosphazene rings may well be flexible and susceptible to packing forces as suggested by Allcock.[47]

As the X-M-X (X = Cl, Br) angle increases, the halide ions encroach on the non-coordinating pyridyl arms although as shown in the space filling diagrams in Figure 29, this encroachment is not sufficient to cause any significant steric hindrance. From Table 6, the X-M-X angles range from 120.97˚ for $[CoL^2Cl_2]\cdot CH_2Cl_2$ to 127.40˚ for $[CuL^2Br_2]$ reflecting the decrease in trigonal bipyramidal geometry as seen in the τ values given in Table 4.

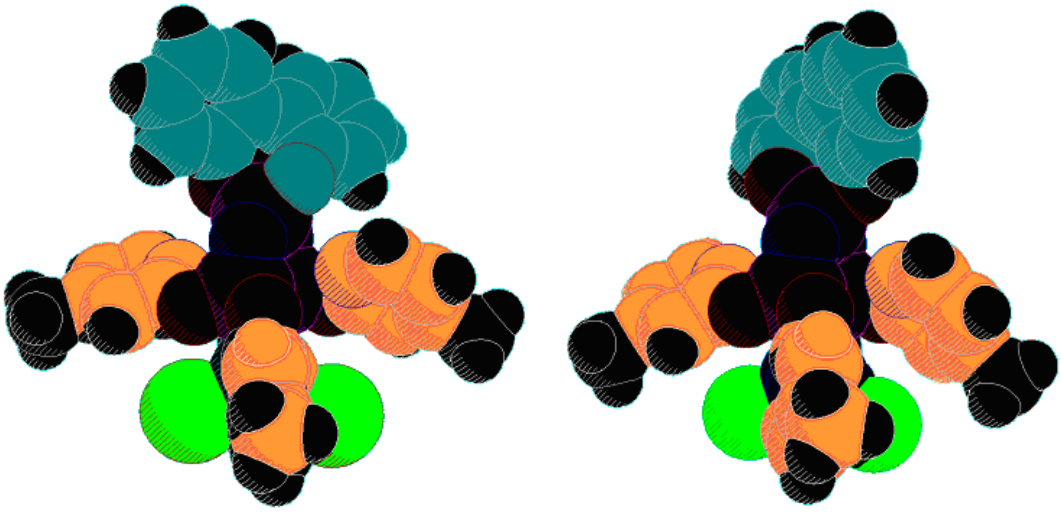

Figure 29 Space filling diagrams of $[CuL^2Br_2]$ (left) and $[CoL^2Cl_2]\cdot CH_2Cl_2$ (right)

$[CoL^2Cl_2]\cdot 2CH_3CN$	Å	$[CoL^2Cl_2]\cdot CH_2Cl_2$	Å	$[CoL^2Br_2]$	Å	$[CuL^2Br_2]$	Å
Co(1)-Cl(1)	2.2763(5)	Co(1)-Cl(1)	2.2741(7)	Co(1)-Br(1)	2.4170(5)	Cu(1)-Br(1)	2.4703(8)
Co(1)-Cl(2)	2.2880(5)	Co(1)-Cl(2)	2.2769(7)	Co(1)-Br(2)	2.4362(5)	Cu(1)-Br(2)	2.4655(8)
Co(1)-N(3)	2.0480(17)	Co(1)-N(3)	2.050(2)	Co(1)-N(3)	2.043(2)	Cu(1)-N(3)	2.070(4)
Co(1)-N(4)	2.2051(17)	Co(1)-N(4)	2.226(2)	Co(1)-N(4)	2.239(2)	Cu(1)-N(4)	2.088(4)
Co(1)-N(6)	2.2289(17)	Co(1)-N(6)	2.227(2)	Co(1)-N(6)	2.213(2)	Cu(1)-N(6)	2.097(4)
P(1)-N(1)	1.5808(17)	P(1)-N(1)	1.588(2)	P(1)-N(1)	1.585(2)	P(1)-N(1)	1.591(4)
P(1)-N(2)	1.5847(17)	P(1)-N(2)	1.582(2)	P(1)-N(2)	1.581(2)	P(1)-N(2)	1.593(4)
P(2)-N(1)	1.5640(17)	P(2)-N(1)	1.569(2)	P(2)-N(1)	1.558(2)	P(2)-N(1)	1.565(4)
P(2)-N(3)	1.6117(17)	P(2)-N(3)	1.610(2)	P(2)-N(3)	1.607(2)	P(2)-N(3)	1.603(4)
P(3)-N(2)	1.5585(17)	P(3)-N(2)	1.569(2)	P(3)-N(2)	1.562(2)	P(3)-N(2)	1.561(4)
P(3)-N(3)	1.6059(17)	P(3)-N(3)	1.607(2)	P(3)-N(3)	1.618(2)	P(3)-N(3)	1.601(4)
	(˚)		(˚)		(˚)		(˚)
N(3)-Co(1)-N(4)	89.60(6)	N(3)-Co(1)-N(4)	89.76(8)	N(3)-Co(1)-N(6)	89.77(9)	N(3)-Cu(1)-N(4)	90.21(16)
N(3)-Co(1)-N(6)	89.77(6)	N(3)-Co(1)-N(6)	89.14(8)	N(3)-Co(1)-N(4)	89.68(9)	N(3)-Cu(1)-N(6)	91.25(16)
N(4)-Co(1)-N(6)	178.55(6)	N(4)-Co(1)-N(6)	178.02(8)	N(4)-Co(1)-N(6)	178.34(9)	N(4)-Cu(1)-N(6)	178.06(17)
N(3)-Co(1)-Cl(1)	116.36(5)	N(3)-Co(1)-Cl(1)	116.21(6)	N(3)-Co(1)-Br(1)	116.40(7)	N(3)-Cu(1)-Br(1)	117.53(12)
N(4)-Co(1)-Cl(1)	89.12(5)	N(4)-Co(1)-Cl(1)	89.08(6)	N(4)-Co(1)-Br(1)	89.86(6)	N(4)-Cu(1)-Br(1)	91.51(12)
N(6)-Co(1)-Cl(1)	89.98(5)	N(6)-Co(1)-Cl(1)	92.88(6)	N(6)-Co(1)-Br(1)	88.98(6)	N(6)-Cu(1)-Br(1)	88.96(12)
N(3)-Co(1)-Cl(2)	120.15(5)	N(3)-Co(1)-Cl(2)	122.81(6)	N(3)-Co(1)-Br(2)	120.30(7)	N(3)-Cu(1)-Br(2)	115.06(12)
N(4)-Co(1)-Cl(2)	91.74(5)	N(4)-Co(1)-Cl(2)	90.10(6)	N(4)-Co(1)-Br(2)	89.54(6)	N(4)-Cu(1)-Br(2)	88.99(12)
N(6)-Co(1)-Cl(2)	89.71(5)	N(6)-Co(1)-Cl(2)	89.12(6)	N(6)-Co(1)-Br(2)	92.09(6)	N(6)-Cu(1)-Br(2)	89.23(12)
Cl(1)-Co(1)-Cl(2)	123.48(2)	Cl(1)-Co(1)-Cl(2)	120.97(3)	Br(1)-Co(1)-Br(2)	123.297(18)	Br(1)-Cu(1)-Br(2)	127.40(3)

Table 6 Selected bond lengths (Å) and angles (º) for the complexes

[CoL2Cl2]·2CH_3CN		[CoL^2Cl_2]·CH_2Cl_2		[CoL^2Br_2]		[CuL^2Br_2]		[$CoL^{2HP}Cl]_2$	
PNP	(˚)	PNP	(˚)	PNP	(˚)	PNP	(˚)	PNP	(˚)
P(2)-N(1)-P(1)	121.71(11)	P(2)-N(1)-P(1)	121.45(13)	P(2)-N(1)-P(1)	121.78(15)	P(2)-N(1)-P(1)	121.1(3)	P(1)-N(1)-P(2)	124.9(3)
P(3)-N(2)-P(1)	121.71(11)	P(3)-N(2)-P(1)	122.14(13)	P(3)-N(2)-P(1)	121.73(15)	P(3)-N(2)-P(1)	121.4(3)	P(3)-N(2)-P(1)	120.4(3)
P(3)-N(3)-P(2)	120.27(10)	P(3)-N(3)-P(2)	121.34(13)	P(2)-N(3)-P(3)	120.06(15)	P(3)-N(3)-P(2)	120.7(2)	P(3)-N(3)-P(2)	123.3(3)
NPN		NPN		NPN		NPN		NPN	
N(1)-P(1)-N(2)	118.00(9)	N(2)-P(1)-N(1)	117.85(11)	N(2)-P(1)-N(1)	117.97(13)	N(1)-P(1)-N(2)	118.0(2)	N(1)-P(1)-N(2)	118.1(3)
N(1)-P(2)-N(3)	117.65(9)	N(1)-P(2)-N(3)	116.75(11)	N(1)-P(2)-N(3)	118.04(13)	N(1)-P(2)-N(3)	117.8(2)	N(1)-P(2)-N(3)	112.2(3)
N(2)-P(3)-N(3)	117.95(9)	N(2)-P(3)-N(3)	117.29(11)	N(2)-P(3)-N(3)	117.63(13)	N(2)-P(3)-N(3)	118.1(2)	N(2)-P(3)-N(3)	118.1(3)

Table 7 Ring angles

[CoL^2Cl_2]·2CH_3CN		[CoL^2Cl_2]·CH_2Cl_2		[CoL^2Br_2]		[CuL^2Br_2]	
	(Å)		(Å)		(Å)		(Å)
P2-N31	2.795	P2-N5	2.849	P2-N31	2.794	P2-N31	2.826
P3-N21	2.804	P3-N7	2.849	P3-N21	2.794	P3-N21	2.816

Table 8 Interaction distance between pyridyl nitrogen and cyclophosphazene ring phosphorus

3.3.3.3 X-ray crystal structure of the hydrolysis product of $[CoL^2Cl^2]\cdot 2CH_3CN$

When crystals of $[CoL^2Cl_2]\cdot 2CH_3CN$ were stored in the supernatant CH_3CN solution and out of direct sunlight for 3 months, the blue crystals underwent a colour change to clear pink. Single crystal X-ray crystallography confirmed the formation of a centrosymmetric hydrolysis product that crystallised in space group *P*-1 and refined as one half of the centrosymmetric molecule related by a centre of symmetry and with two molecules of CH_3CN in the unit cell. Crystallographic and refinement data are given in Table 2.

Hydrolysis occurs through loss of one of the pyridyloxy rings to afford a ligand that is monoanionic, coordinating to one cobalt(I) centre in a tetradentate fashion through the phosphazene ring nitrogen and the remaining three pyridyl arms. The phosphazenate oxygen and the remaining chloride ligand make up the octahedral N_4OCl donor set, with the oxygen coordinating to the second symmetry related cobalt centre (Figure 30).

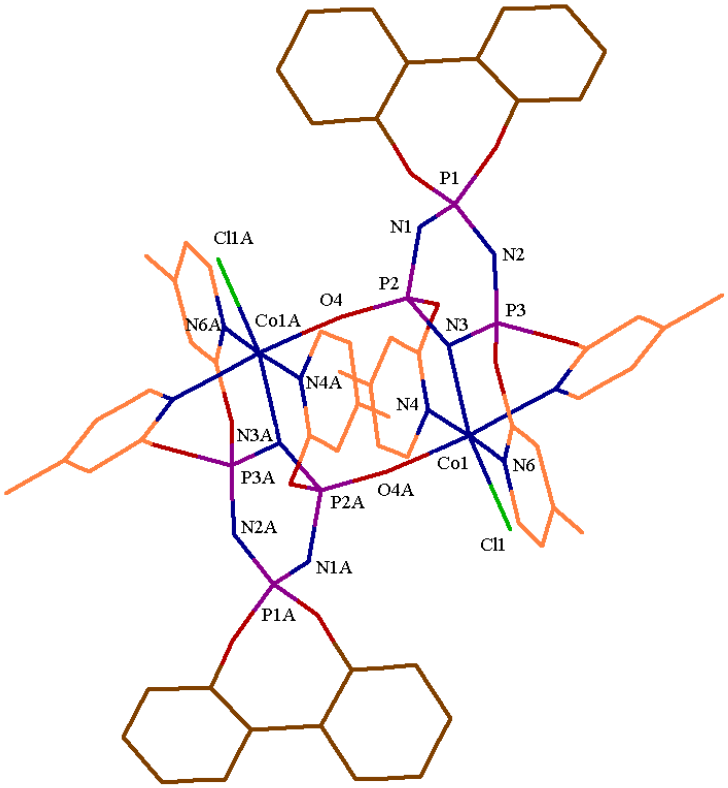

Figure 30 The structure of the $[CoL^{2HP}Cl]$ hydrolysis product (hydrogen atoms and occluded solvent molecules omitted for clarity)

Figure 31 gives the labelling scheme for atom identification in Table 9.

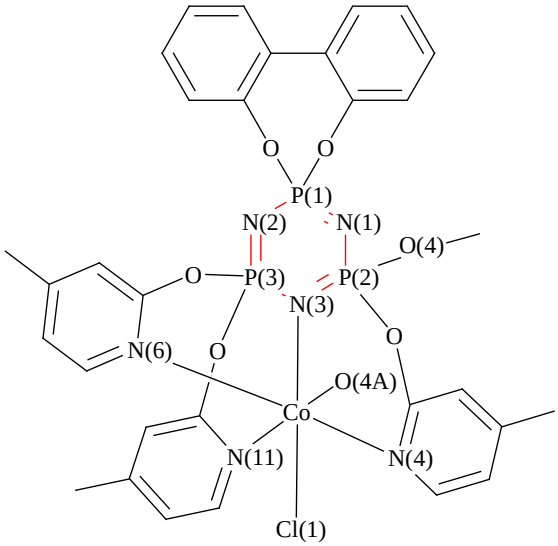

Figure 31 Labelling diagram for the centrosymmetric half of the [CoL^{2HP}Cl] complex (hydrogen atoms removed for clarity)

[CoL^{2HP}Cl]$_2$			
Bond	Length (Å)	Angle	(˚)
Co(1)-O(4)A	2.035(4)	O(4)A-Co(1)-N(3)	93.58(17)
Co(1)-N(3)	2.150(5)	O(4)A-Co(1)-N(4)	88.74(17)
Co(1)-N(11)	2.206(5)	O(4)A-Co(1)-N(6)	86.76(17)
Co(1)-N(4)	2.223(5)	O(4)A-Co(1)-N(11)	175.52(18)
Co(1)-Cl(1)	2.3901(17)	O(4)A-Co(1)-Cl(1)	95.48(12)
Co(1)-N(6)	2.408(5)		
		N(3)-Co(1)-N(4)	91.48(18)
		N(3)-Co(1)-N(6)	85.73(18)
P(1)-N(1)	1.572(5)	N(3)-Co(1)-N(11)	82.74(18)
P(1)-N(2)	1.594(5)	N(3)-Co(1)-Cl(1)	170.36(14)
P(2)-N(1)	1.603(5)		
P(2)-N(3)	1.646(5)	N(11)-Co(1)-N(4)	88.81(19)
P(3)-N(2)	1.573(5)	N(11)-Co(1)-N(6)	95.47(18)
P(3)-N(3)	1.594(5)	N(11)-Co(1)-Cl(1)	88.35(14)
P(2)-O(4)	1.488(4)		
		N(4)-Co(1)-N(6)	174.55(17)
		N(4)-Co(1)-Cl(1)	92.00(14)
		Cl(1)-Co(1)-N(6)	91.49(13)

Table 9 Selected bond lengths and angles for [CoL^{2HP}Cl]$_2$

The $[CoL^{2HP}Cl]_2$ complex shows a marked deviation in N1-P2-N3 (*c.f.* Figure 28) from the normal range of 119-148˚, being 112.2(3)˚ which is probably a consequence of distortion due to dimerisation and formation of the P-O-Co linkage.

3.3.4 Physicochemical studies of the complexes

Although X-ray structures demonstrate a similar TBP arrangement, they are not available for every complex. A variety of physicochemical techniques were used to elucidate as much structural information as possible and these are discussed next.

3.3.4.1 ESR spectroscopy

X-band ESR spectra of the ligand-copper halide complexes, recorded in frozen CH_2Cl_2 at liquid nitrogen temperature, are shown in Table 10. Generally, two g values were observed for each of the copper complexes, having an average splitting of 15 mT. The spectra are typical for a major species having mononuclear axial symmetry with a $d_{x^2-y^2}$ ground state [51] . The data are consistent with a square pyramidal geometry at 113 K, suggesting the compounds are all exhibiting neutral complex distortion isomerism, where the room temperature solid state structure is a distorted trigonal bipyramidal. No spectra displayed absorption at the half field values around 1500 gauss ($\Delta M_s = \pm 2$) at g $\approx$ 4, which is consistent with there being no dimeric species present.

Complex*	CH_2Cl_2 glass at 113 K		
	$g_{\shortparallel}$	$A_{\shortparallel}$ (10^{-4} cm^{-1})	$g_{\perp}$
$[CuL^1Cl_2]$	2.26	165	2.09
$[CuL^1Br_2]$	2.29	167	2.12
$[CuL^2Cl_2]$	2.27	165	2.10
$[CuL^2Br_2]$	2.29	163	2.12
$[CuL^3Cl_2]$	2.27	161	2.11

* Occluded solvent molecules not included

Table 10 ESR spectral parameters for the copper complexes

3.3.4.2 Magnetic moment data

The room temperature magnetic moments for the complexes are presented in Table 11. For trigonal bipyramidal high spin cobalt(II) complexes, the effective magnetic moments can vary between 4.26 and 5.03 μ_B[52] which is above the spin only value for three unpaired electrons indicating a degree of spin orbit coupling which varies with the ligand field strength.[53] The complexes above are generally in the expected range and the trigonal bipyramidal geometry is supported by X-ray crystallography.

For octahedral nickel(II) complexes, the magnetic moments range from 2.9 to 3.3 μ_B.[54] The value recorded at 3.06 μ_B is in the expected range for octahedral geometry but is higher that the spin-only value of 2.83 μ_B for a d^8 ion, indicating a degree of spin-orbit coupling. However, the magnetic moment value alone does not particularly differentiate it from a trigonal bipyramidal structure and supporting evidence for the octahedral structure comes from electronic spectra.

The magnetic moments of mononuclear copper(II) complexes are generally in the range 1.75 to 2.20 μ_B.[53] The observed magnetic moments are consistent with one unpaired electron with some contribution from spin-orbit coupling.

Complex*	Effective magnetic moment μ_B
$[CoL^2Br_2]$	4.24
$[CoL^2Cl_2]$	4.26
$[CuL^2Br_2]$	2.03
$[CuL^2Cl_2]$	2.29
$[NiL^2Cl_2]$	3.06
$[CoL^1Br_2]$	4.55
$[CoL^1Cl_2]$	4.48
$[CuL^1Br_2]$	2.22
$[CuL^1Cl_2]$	2.15
$[CuL^3Cl_2]$	1.91

* Occluded solvent molecules not included

Table 11 Room temperature magnetic moments for the complexes

3.3.4.3 UV/visible solution and solid state spectroscopy

The nujol mull transmittance spectra for the cobalt complexes (Table 12), display d-d bands in the 850-900 nm and 590-655 nm regions, consistent with the trigonal bipyramidal structure[52 53] as found by the X-ray structures. However, in CH_3CN or CH_2Cl_2 solutions, characteristic d-d absorptions at about 700, 630 and 620 nm, with high extinction coefficients, are more consistent with a distorted tetrahedral structure.[55] This is indicative of a structural rearrangement on going from the solid state to solution. Each of the complexes $[CuL^1Cl_2]$ and $[CuL^2Cl_2]$, display a broad d-d band around 800 - 850 nm respectively which tails into the infra-red, while $[CuL^1Br_2]$ and $[CuL^2Br_2]$ have a similar band at lower energy, at about 1150 or 1120 nm respectively because of the lower ligand field strength of the bromide ion. These are consistent with copper having a trigonal bipyramidal environment as shown by X-ray crystallography to be correct for $[CuL^2Br_2]$.[52, 56] The spectrum for $[CuL^3Cl_2]$ is different from the chloro complexes above, having a broad band at higher energy (710 nm) which is consistent with a geometry change to square-based pyramidal or a distorted intermediate between square-based pyramidal and trigonal bipyramidal.[57]

The solution spectra for the copper complexes are not straightforward and there is a lack of definitive statements that can be made regarding structural assignments since these often overlap.[58] Generally, values found for the complexes with $\mathbf{L^1}$ and $\mathbf{L^2}$ have a component above 830 nm which might favour assignment of TBP geometry,[58] in line with the X-ray structures, as opposed to tetrahedral geometry. Values at higher energy may indicate a TBP to square-based pyramidal distortion[59] rather than a change in coordination. For the complex with $\mathbf{L^3}$, the slight shift to lower energy from solid to solution spectra is perhaps indicative of a similar distortion though no other evidence is available.

The presence of three d-d bands in the solid state and solution spectra for NiL^2Cl_2 is consistent with Ni having an octahedral geometry in both media.[54]

Complex[a]	Solvent	Soln[b]	Solid State[c]	Solution	Solid
				λ_{max}/nm (ε/dm^3 mol^{-1} cm^{-1})	λ_{max}/nm
[CoL^{1}Br$_2$]	CH_3CN	Tet	TBP	700 (176), 630 (117), 620 (131)	590 (bd), 850 (vb)
[CoL^{1}Cl$_2$]	Insoluble	-	TBP	Insoluble	520 (sh), 590 (bd), 680 (sh), 850 (vb)
[CoL^{2}Br$_2$]	CH_3CN*	Tet	TBP	700 (196), 630 (133), 620 (147)	545 (sh), 585, 625, 900 (vb)
[CoL^{2}Cl$_2$]·CH_2Cl_2	CH_3CN*	Tet	TBP	685 (185), 675 (sh) (160), 590 (160)	535 (sh), 585, 665, 900 (bd)
[CoL^{3}Cl$_2$]	CH_2Cl_2	Tet	TBP	675 (103), 620 (96), 565 (75)	660 (bd), 850 (vb)
[CuL^{1}Br$_2$]	CH_2Cl_2	TBP	TBP	965 (bd) (229), 650 (95)	1150 (bd)
[CuL^{1}Cl$_2$]	CH_2Cl_2	TBP	TBP	720 (sh) (84), 875 (vb) (104)	800 (vb)
[CuL^{2}Br$_2$]	CH_2Cl_2	TBP	TBP	940 (200), 650 (sh) (58)	1120 (vb), 655
[CuL^{2}Cl$_2$]	CH_2Cl_2	TBP	TBP	895 (116)	850 (vb)
[CuL^{3}Cl$_2$]	CH_2Cl_2	TBP	TBP	765 (vb) (151)	710 (vb),
[NiL^{2}Cl$_2$]	CH_2Cl_2	Oct	Oct	1270 (bd) (13), 810 (bd) (8), 420 (24)	1205 (vb), 705 (b), 415

*Also in acetone. [a] Lattice solvent not included. [b] Possible structures in solution. [c] Possible structures in the solid state. Tet = tetrahedral. TBP = trigonal bipyramidal. Oct = Octahedral. sh = shoulder. bd = broad. vb = very broad.

Table 12 Electronic spectral data for the complexes

3.3.4.4 IR spectroscopy

Mid range IR spectral data (ν(P-N) stretch) are shown for comparison in Table 13. Far IR and Raman spectral data of the complexes are given in Table 14, while selected Raman spectra of selected complexes are compared to assignments for the spiro(2,2'-biphenolato)tetrachlorocyclotriphosphazene and are listed in Table 15.

Small changes in the ν(P-N) stretch are noted on complexation as seen in Table 13 and this is consistent with phosphazene ring nitrogen coordination. Similar changes in the ν(P-N) stretch have been noted for five-coordinate pyrazolyl complexes.[33]

ν(P-N)	cm^{-1}	cm^{-1}		cm^{-1}	cm^{-1}		cm^{-1}	cm^{-1}
L^1	1225	1172	**L^2**	1195	1142	**L^3**	1213	1168
$[CuL^1Cl_2]$	1238	1190	$[CuL^2Cl_2]$	1190	1165	$[CuL^3Cl_2]$	1222	1184
$[CoL^1Cl_2]$	1234	1184	$[CoL^2Cl_2]\cdot CH_2Cl_2$	1195	1163	$[CoL^3Cl_2]$	1219	1181
$[CoL^1Br_2]$	1233	1183	$[CoL^2Br_2]$	1194	1164			
$[CuL^1Br_2]$	1232	1182	$[CuL^2Br_2]$	1191	1152			
			$[NiL^2Cl_2]$	1199	1142			

Table 13 Comparison of ν(P-N) stretch for the complexes

In the far IR spectra, terminal ν(MCl) and *ν*(MBr) vibrations appear in the region 400-200 cm^{-1} and 300-200 cm^{-1} respectively [60], and the ratio ν(MBr) / ν(MCl) should be in the range 0.77 – 0.74 [60]. For CoL^1X_2, CoL^2X_2, CuL^1X_2 and CuL^2X_2, ν(MBr) / ν(MCl) = 0.78, 0.75, 0.71 and 0.75 respectively which are close to the expected range.
The results show a general trend that νMCl > νMBr throughout, consistent with the larger atomic mass of bromine.

Compound	Far IR	Raman
	ν(M-X) cm^{-1}	ν(M-X) cm^{-1}
$[CoL^1Br_2]$	251 + sh	
$[CoL^1Cl_2]$	320	
$[CoL^2Br_2]$	240, 232	231
$[CoL^2Cl_2]\cdot CH_2Cl_2$	320	285
$[CoL^3Cl_2]$	234	
$[CuL^1Br_2]$	195 (167 L)	
$[CuL^1Cl_2]$	273, (320 L)	
$[CuL^2Br_2]$	228, (188 L)	223
$[CuL^2Cl_2]$	302	313
$[CuL^3Cl_2]$	329	
$[NiL^2Cl_2]$	259	
$[ZnL^2Cl_2]$	327, 303	

(L) indicates a further band which may contain a ligand component

Table 14 Far IR and Raman M-X vibrations of the complexes

$[CuL^2Cl_2]$	$[CuL^2Br_2]$	$[CoL^2Cl_2]\cdot CH_2Cl_2$	$[CoL^2Br_2]$	Assignment[61]
ν / cm^{-1}	ν / cm^{-1}	ν / cm^{-1}	ν / cm^{-1}	
1608	1608	1606	1610	biph ring stretch
1499	1499	1497	1498	biph ring stretch
1309	1310	1309	1310	biph ring stretch
1270	1267	1270	1277	C-H bending
1159	1158	1159	1156	P-N stretch
1038	1038	1039	1037	biph ring breathing
1018	1019	1010	1009	biph ring stretch + O-P-O stretch
996	996	997	997	C-O-P stretch
751	751	749	751	PN ring breathing
698	698	694	698	biph ring deformation

Table 15 Comparison of the complexes by selected Raman spectroscopic data

In Table 15, selected Raman stretching and bending modes for the biphenolate fragment and ring P-N stretches are given.[61] The biphenolate ring stretch at about 1610 cm^{-1} is dominant in the Raman and IR spectra. Other bands in Table 15 are only weakly active, or not present in the mid IR. It appears that complexation to a metal centre does not significantly affect the Raman frequencies of the phosphazene ring platform. As expected, the IR and Raman data are complimentary for molecular fingerprinting.

3.3.4.5 Conductivity

The results indicate that all of the compounds are essentially non-electrolytes in solution, thus there is no major dissociation to ionic species in the solvents used, although there may be partial displacement of some halide atoms to account for the small values obtained, e.g. for $[NiL^2Cl_2]$. For the cobalt complexes, the conductivity indicates that the solution rearrangement from five-coordinate to tetrahedral is primarily due to breaking of an M-N bond rather than displacement of a halide by the solvent molecules. Molar conductivities are given in Table 16 below.

Complex	Conductivity Λ	Solvent
	S cm^2 mol^{-1}	
$[CoL^1Br_2]$	36	CH_3CN[b]
$[CoL^1Cl_2]$	Insoluble	-
$[CoL^2Br_2]$	19	Acetone
$[CoL^2Cl_2]\cdot CH_2Cl_2$	18/48	Acetone/CH_3CN
$[CuL^1Br_2]$	53	Acetone[a]
$[CuL^1Cl_2]$	20	Acetone
$[CuL^2Br_2]$	44	Acetone
$[CuL^2Cl_2]$	7	Acetone
$[CuL^3Cl_2]$	18	Acetone
$[HgL^2Cl_2]$	4	Acetone
$[NiL^2Cl_2]$	50	Acetone
$[ZnL^2Cl_2]$	6	Acetone

[a] a 10^{-3} M acetone solution for a 1:1 electrolyte has a molar conductivity of 100-130 S cm^2 mol^{-1}.[62] [b] a 10^{-3} M CH_3CN solution of tetrabutylammoniumhexafluorophosphate, has a measured molar conductivity of 158 S cm^2 mol^{-1} for a 1:1 electrolyte.

Table 16 Conductivity data measurements [a,b] at 25 °C

3.4 Conclusions

Twelve transition metal complexes have been synthesised, with emphasis on the ligand $\mathbf{L^2}$. Cobalt complexes with $\mathbf{L^1}$ were not soluble and the X-ray structures were incapable of full refinement. Complexes with $\mathbf{L^3}$ are highly soluble but X-ray quality crystals failed to materialise. Thus, in order to best elucidate the chemistry of the ligands that may be transferable to the polymeric analogues, $\mathbf{L^2}$ appears to yield the most amenable complexes for analysis.

Reactions with various transition metal-halides lead to a ligand controlled five-coordinate structure with κ^3*N* donor sets in the solid state (the notable exception being nickel chloride which, on the basis of electronic spectra, appears to be octahedral). In solution, cobalt complexes undergo a structural transformation to a tetrahedral arrangement, but with only small changes to the conductivity, which suggests that one of the Co-N bonds is being broken rather than a Co-Cl bond. This rearrangement appears not to be solvent specific. At 113 K, the ESR data indicates that the copper complexes rearrange to a square pyramidal geometry, thus it is evident that the ligands exhibit a degree of lability dependent upon physical conditions. In each case the rearrangement may be described as a neutral complex distortion isomerism with the

halide ions remaining coordinated to the metal. IR spectroscopy is complementary to other techniques used and can be used as a molecular fingerprint for coordination of the ligands to transition metals.

Chapter 2 posed a number of questions regarding ligand design. Firstly, it seems that the addition of the methyl group and its position on the pyridyl ring does advantageously affect solubility in the order $\mathbf{L^3} > \mathbf{L^2} > \mathbf{L^1}$. There is no apparent reason at this stage to assume that this property will not translate to the polymeric analogues.

Secondly, intermolecular stacking does not appear to be enhanced by coordination of the ligands to transition metals, indeed, the packing appears to be greatly influenced by the nature and quantity of the occluded solvent which may have ramifications for conformations within the polymers, since they are inherently more flexible.

Thirdly, each X-ray structure indicates a ligand controlled five-coordinate structure in the solid state, which is always of a *trans* non-geminal nature. However there is evidence for structural rearrangements at low temperature for Cu(II) complexes and in solution for Co(II) complexes. It appears that the intramolecular interaction between the non-coordinated pyridyl rings and the phosphorus atom to which they are attached is a dominant feature in the solid state but may be affected by temperature and in solution dependent upon the transition metal involved.

Lastly, the presence of the 2,2'-dioxybiphenyl moiety seems to dictate a five-coordinate TBP arrangement on the complexes by restricting the available sites for coordination, although the presence or absence of occluded solvent molecules has a major affect on the solid state crystal packing.

The presence of the 2,2'-dioxybiphenyl moiety present on the cyclotriphosphazene reduces the coordination versatility of the ligands when compared to fully substituted hexakis ligand designs. Comparison of the structural index values for this work with the hexakis(pyridyloxy)cyclotriphosphazene ligands, suggests that the presence of the biph moiety restricts the geometry to *trans* non-geminal on coordination to metals leading to more regular TBP structures.

This is not a surprising result since the number of potential pyridyl nitrogen donors is reduced by one third and the 2,2'-dioxybiphenyl moiety serves to sterically hinder the sites available for intermolecular interactions. With five-coordinate structures prevailing, and with evidence for the uncoordinated pyridyloxy ring nitrogen to seemingly favour intramolecular interaction with the cyclotriphosphazene ring phosphorus to which it is attached, the viability of this model for the polymeric analogue has to be questioned, given that the polymer will be inherently more flexible than the cyclotriphosphazene ring. However, the rearrangement of the cobalt complexes in solution, as suggested by the electronic spectra, begs the question that it is perhaps the nature of the transition metal that will provide more of an insight than the ligand design when metals are coordinated to the polymeric analogues. Having less rigid geometry, it is possible that the polymer complexes may offer alternative coordination modes that are energetically more favourable and preferred by the particular metal species.

3.5 References

1. Allcock, H. R.; Allen, R. W.; O'Brien, J. P., *J. Am. Chem. Soc.* **1977,** 99(12), 3984.

2. Justin Thomas, K. R.; Chandrasekhar, V.; Zanello, P.; Laschi, F., *Polyhedron* **1997,** 16(7), 1003.

3. Allcock, H. R.; Manners, I.; Mang, M. N.; Parvez, M., *Inorg. Chem.* **1990,** 29(3), 522.

4. Diefenbach, U.; Bloy, M.; Stromburg, B. E., *Phosphorus, Sulfur Silicon Relat. Elem.* **1999,** 144, 65.

5. Diefenbach, U.; Kretschmann, M.; Stromburg, B. E., *Phosphorus, Sulfur Silicon Relat. Elem.* **1997,** 124-125, 143.

6. Díaz, C.; Barbosa, M.; Godoy, Z., *Polyhedron* **2004,** 23, 1027.

7. Diefenbach, U.; Adamaszek, P.; Bloy, M., *Heteroat. Chem.* **1999,** 10(1), 9.

8. Allcock, H. R., *Chemistry and Applications of Polyphosphazenes*. John Wiley and Sons Inc: New York, 2003; p. 11.

9. Allcock, H. R., *Phosphorus, Sulfur Silicon Relat. Elem.* **2004,** 179, 661.

10. Rivard, E.; Ragogna, P. J.; McWilliams, A. R.; Lough, A. J.; Manners, I., *Inorg. Chem.* **2005,** 44(19), 6789.

11. Witt, M.; Roesky, H. W., *Chem. Rev.* **1994,** 94, 1163.

12. Chandrasekhar, V.; Krishnan, V., In *Applicative Aspects of Cyclophosphazenes*, ed.; Gleria, M.; De Jaeger, R., Nova Science Publishers, Inc: New York, 2004; p. 159-184.

13. Chandrasekhar, V.; Justin Thomas, K. R., *Appl. Organomet. Chem.* **1993,** 7, 1.

14. Ainscough, E. W.; Brodie, A. M.; Depree, C. V.; Otter, C. A., *Polyhedron* **2006,** 25, 2341.

15. Ainscough, E. W.; Brodie, A. M.; Depree, C. V.; Moubaraki, M.; Murray, K. S.; Otter, C. A., *J. Chem. Soc., Dalton Trans.* **2005,** 20, 3337 and references therein.

16. Chandrasekhar, V.; Pandian, B. M.; Azhakar, R., *Polyhedron* **2007,** 27, 255.

17. Carriedo, G. A.; Gómez-Elipe, P.; García-Alonso, F. J.; Fernández-Catuxo, L.; Díaz, M. R.; Granda, S. C., *J. Organomet. Chem.* **1995,** 498, 207.

18. Carriedo, G. A.; García-Alonso, F. J.; Díaz Valenzuela, C.; Valenzuela, M. L., *Polyhedron* **2006,** 25, 105.

19. Carriedo, G. A.; García-Alonso, F. J.; García-Álvarez, L. J.; Díaz Valenzuela, C.; Sáez, N. Y., *Polyhedron* **2002,** 21, 2587.

20. Carriedo, G. A.; García-Alonso, F. J.; García, J. L.; Carbajo, R. J.; Ortiz, F. L., *Eur. J. Inorg. Chem.* **1999,** 6, 1015.

21. Díaz, C.; Valenzuela, M. L., *Macromolecules* **2006,** 39(1), 103.

22. Ainscough, E. W.; Brodie, A. M.; Depree, C. V., *J. Chem. Soc., Dalton Trans.* **1999,** 23, 4123.

23. Bloy, M.; Kretschmann, M.; Scholz, S.; Teichert, M.; Diefenbach, U., *Z. Anorg. Allg. Chem.* **2000,** 626, 1946.

24. Davidson, G. J. E.; Loeb, S. J.; Parekh, N. A.; Wisner, J. A., *J. Chem. Soc., Dalton Trans.* **2001,** 21, 3135.

25. Divjakovic, V.; Leovac, V. M.; Ribar, B.; Argay, G.; Kalman, A., *Acta Crystallogr., Sect. B38,* **1982**, 1738.

26. Xu, H.; Li, J.; Wu, Z.; Zou, J.; Xu, Z.; You, X., *Polyhedron* **1993,** 12, 2261.

27. Diefenbach, U.; Kretschmann, M.; Çavdarci, Ö. *Monatshefte für Chemie* **1996,** 127, 989.

28. Ainscough, E. W.; Brodie, A. M.; Derwahl, A.; Kirk, S.; Otter, C. A., *Inorg. Chem.* **2007,** 46(23), 9841.

29. Diefenbach, U.; Kretschmann, M.; Stromburg, B. E., *Chem. Ber.* **1996,** 129, 1573.

30. Chandrasekharan, A.; Krishnamurthy, S. S.; Nethaji, M., *Inorg. Chem.* **1994,** 33, 3085.

31. Justin Thomas, K. R.; Chandrasekhar, V.; Scott, S. R.; Hallford, R.; Wallace Cordes, A., *J. Chem. Soc., Dalton Trans.* **1993**, 2589.

32. Justin Thomas, K. R.; Chandrasekhar, V.; Pal, P.; Scott, S. R.; Hallford, R.; Wallace Cordes, A., *Inorg. Chem.* **1993,** 32, 606.

33. Justin Thomas, K. R.; Tharmaraj, P.; Chandrasekhar, V.; Scott, S. R.; Wallace Cordes, A., *Polyhedron* **1995,** 14(8), 977.

34. Ainscough, E. W.; Brodie, A. M.; Jameson, G. B.; Otter, C. A., *Polyhedron* **2007,** 26, 460.

35. Chandrasekhar, V.; Pandian, B. M.; Azhakar, R., *Inorg. Chem.* **2006,** 45(9), 3510.

36. Carriedo, G. A.; Fernández-Catuxo, L.; García-Alonso, F. J.; Gómez-Elipe, P.; González, P. A., *Macromolecules* **1996,** 29(16), 5320.

37. Sheldrick, G. M. *SHELXL Suite of Programs for Crystal Structure Analysis*, Institüt für Anorganische Chemie der Universität, Tammanstrasse 4, Göttingen, Germany: 1998.

38. Jung, O.; Park, S. H.; Lee, Y.; Cho, Y.; Kim, K. M.; Lee, S.; Chae, H. K.; Sohn, Y. S., *Inorg. Chem.* **1996,** 35(23), 6899.

39. Jung, O.; Kim, Y. T.; Lee, H.; Kim, K. M.; Chae, H. K.; Sohn, Y. S., *Bull. Chem. Soc. Jpn.* **1997,** 70(9), 2125.

40. Allcock, H. R.; Siegel, L. A., *J. Am. Chem. Soc.* **1964,** 86, 5140.

41. Allcock, H. R.; Levin, M. L.; Whittle, R. R., *Inorg. Chem.* **1986,** 25, 41.

42. Siegel, L. A.; van der Hende, J. H., *J. Chem. Soc.* **1967,** A, 817.

43. Allcock, H. R.; Stein, M. T., *J. Am. Chem. Soc.* **1974,** 96, 49.

44. Ainscough, E. W.; Brodie, A. M.; Derwahl, A., *Polyhedron* **2003,** 22, 189.

45. IUCr CheckCIF/PLATON. http://journals.iucr.org/services/cif/checkcif.html accessed 13-06-2008

46. Addison, A. W.; Rao, T. N.; Reedijk, J.; Van Rijn, J.; Verschoor, G. C., *J. Chem. Soc., Dalton Trans.* **1984,** 7, 1349.

47. Allcock, H. R., *Chemistry and Applications of Polyphosphazenes*. John Wiley and Sons Inc: New York, 2003; p. 89-90.

48. Shannon, R. D., *Acta Crystallogr. A 32.* **1976**, 751.

49. Chandrasekhar, V., Nagendran, S., *Chem. Soc. Rev.* **2001,** 30, 193.

50. Allcock, H. R., *Chemistry and Applications of Polyphosphazenes*. John Wiley and Sons Inc: New York, 2003; p. 91-92.

51. Hathaway, B. J., In *Comprehensive Coordination Chemistry, First Edition*, ed.; Wilkinson, G., Pergamon Press: New York, 1987; 5, p. 662-663.

52. Patra, A. K.; Ray, M.; Mukherjee, R., *J. Chem. Soc., Dalton Trans.* **1999,** 15, 2461.

53. Cotton, F. A.; Wilkinson, G., *Advanced Inorganic Chemistry, A Comprehensive Text, Pt.2*. 5th ed; John Wiley & Sons: New York, 1988; 1, p. 730-731.

54. Sacconi, L., In *Comprehensive Coordination Chemistry, Fifth Edition*, ed.; Wilkinson, G., Pergamon Press: 1987; 5, p. 46-51.

55. Lever, A. B. P., *Inorganic Electronic Spectroscopy*. 2nd Elsevier: New York, 1984; 33, p. 496-503.

56. Hathaway, B. J., In *Comprehensive Coordination Chemistry*, 1st ed.; Wilkinson, G.; Gillard, R. D.; McLeverty, J. A., Pergamon Press: New York, 1987; 5, p. 533-744.

57. Murphy, G.; Murphy, C.; Murphy, B.; Hathaway, B., *J. Chem. Soc., Dalton Trans.* **1997**, 2653.

58. Lever, A. B. P., *Inorganic Electronic Spectroscopy*. 2nd Elsevier: New York, 1984; 33, p. 572.

59. Lever, A. B. P., *Inorganic Electronic Spectroscopy*. 2nd Elsevier: New York, 1984; 33, p. 568.

60. Nakamoto, K., *Infrared and Raman Spectra of Inorganic and Coordination Compounds, Part B, Fifth Edition*. John Wiley and Sons: New York, 1997; p. 183-190.

61. Menendez, J. R.; Carriedo, G. A.; Garcia-Alonso, F. J.; Clavijo, E.; Nazri, M.; Aroca, R., *J. Raman Spectrosc.* **1999,** 30, 1121.

62. Marr, G.; Rockett, B. W., *Practical Inorganic Chemistry*. Van Nostrand Reinhold: New York, 1972; p. 122.

Chapter 4: Fluxional behaviour of $[ZnL^2Cl_2]$, $[CdL^2Cl_2]$ and $[HgL^2Cl_2]$

4.0 Abbreviations used in Chapter 4

MAS	Magic Angle Spinning
VT NMR	Variable Temperature Nuclear Magnetic Resonance
THF	tetrahydrofuran
TBP	trigonal bipyramidal
RBF	round bottom flask
T_c	coalescence temperature
TMS	tetramethylsilane

4.1 Introduction to fluxional behaviour

Fluxional behaviour is a well known and reported phenomenon in chemistry. Since the advent of variable temperature NMR (VT NMR) spectroscopy, the observance of fluxional behaviour has become almost commonplace for chemists. However, to paraphrase Canovese *et al.*[1] "Many organometallic compounds undergo fluxional rearrangements which are revealed by dynamic NMR spectroscopy……In most cases the fluxional behaviour is only reported without discussion of the molecular mechanism involved".

This introduction is concerned, where possible, with fluxional behaviour in coordination chemistry.

4.1.1 Fluxional behaviour in coordination chemistry

The kinetics of molecular behaviour is temperature dependent. Complexes can demonstrate rapid exchange on the NMR timescale at room temperature, whereas for other systems, higher temperatures are often required to elucidate molecular motion. For example, Di Vaira *et al.*[2] describe the neutral complex $[ML^6]\cdot 3H_2O$ (L^6 = a mixed pendant-arm macrocyclic ligand, M = Cd(II), Hg(II) or Pb(II)) which is conformationally rigid at 273 K, but exhibits fluxional behaviour with increasing temperature (Figure 1). In the absence of X-ray structure data being reported, this research invoked the use of molecular dynamics calculations and is relevant for the study of both Cd and Hg complexes reported in this chapter. The authors speculate on a number of possible exchange processes to explain their NMR data. Whilst not being conclusive, they infer that a number of processes could be occurring and because they all occur at the same temperature, their rate constants should be similar.

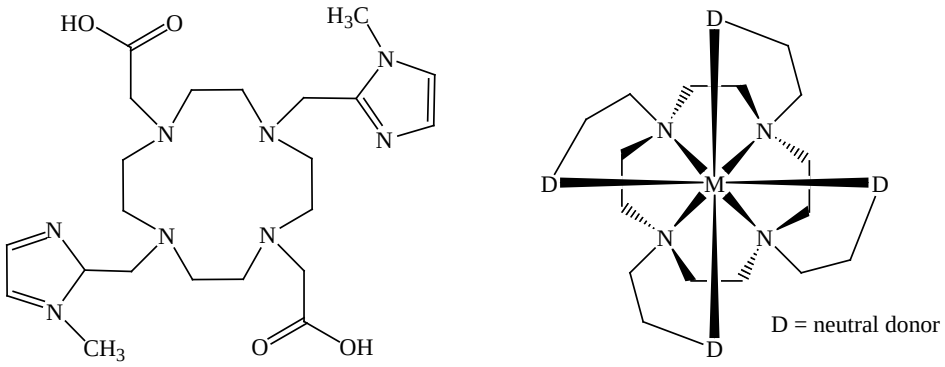

Figure 1 Free ligand (left) and metal complex (right) reported by Di Vaira *et al.*[2]

Song *et al.*[3] describe a 7-azaindole-containing scorpionate complexed with copper triphenylphosphine that demonstrated an asymmetry in the X-ray structure (Figure 2). This was described as a surprising result since the ambient temperature ^{1}H NMR spectra indicated a magnetically symmetrical environment. VT ^{1}H NMR studies from 298 K to 203 K were consistent with a dynamic exchange process between two coordinated and one non-coordinated 7-azaindoyl groups. (Note, the term "scorpionate" is descriptive of the way in which the molecule chelates to the metal ion, resembling the pincer and stinging action of a scorpion).

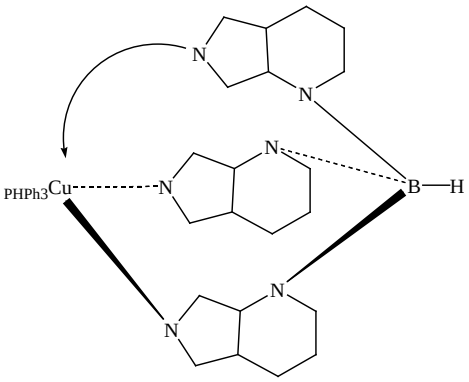

Figure 2 Simplified diagram of the scorpionate complex described by Song *et al.*[3]

Schlager *et al.*[4] investigated the behaviour of a hexadentate tris(aminobenzyl)-triazacyclononane ligand (Figure 3) complexed with Zn, Cd and Hg. It was observed that the Cd and Hg complexes displayed a clear asymmetric structure at the lowest experimentally available temperature whereas the Zn complex did not. Evidently the Zn(II) complex is still undergoing fluxional motion at the temperatures achieved.

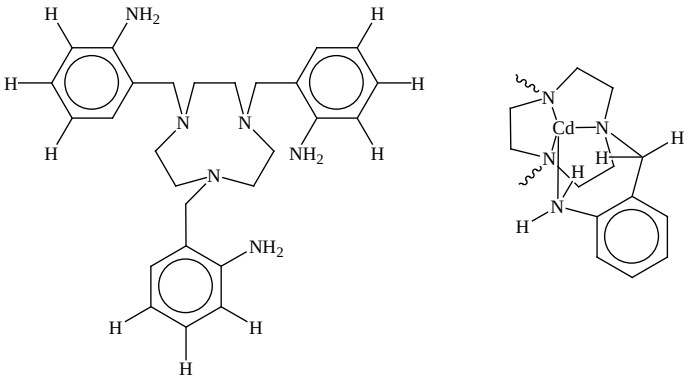

Figure 3 Free ligand (left) and complex (right) reported by Schlager *et al.*[4]

4.1.2 Fluxional behaviour in cyclotriphosphazenes and related complexes

Fluxional behaviour has been reported in the scientific literature for only a small number of complexes containing the cyclotriphosphazene ring. In the main, previous reports tend to propose mechanisms that are consistent with NMR data and, where crystal structures have been obtained, the suggestion is that the low temperature limit conformation is closest to that of the X-ray structure. There are no reports that propose a structure obtained from X-ray crystallography as a possible intermediate, in explaining the NMR data of fluxional behaviour in phosphazene systems.

Byun *et al.*[5] proposed a fluxional mechanism for dinuclear zinc, cadmium and copper complexes (Figures 4-6), whereby fast interconversion between trigonal bipyramidal (TBP) and tetrahedral sites occurs on increasing the sample temperature from 203 K to 243 K to make all of the phosphorus sites equivalent. They also describe three A_2B patterns in the $^{31}P\{^1H\}$ NMR of the dicadmium complex indicating three possible solution species being present between 188 K and 233 K.

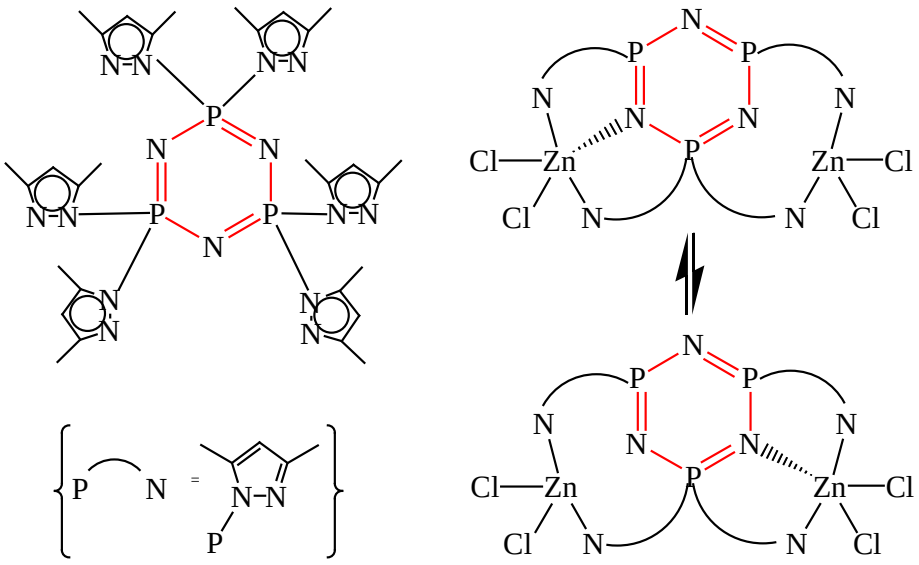

Figure 4 Free ligand (left) and interconversion between TBP and tetrahedral sites (right) for a dinuclear zinc(II) complex reported by Byun *et al.*[5]

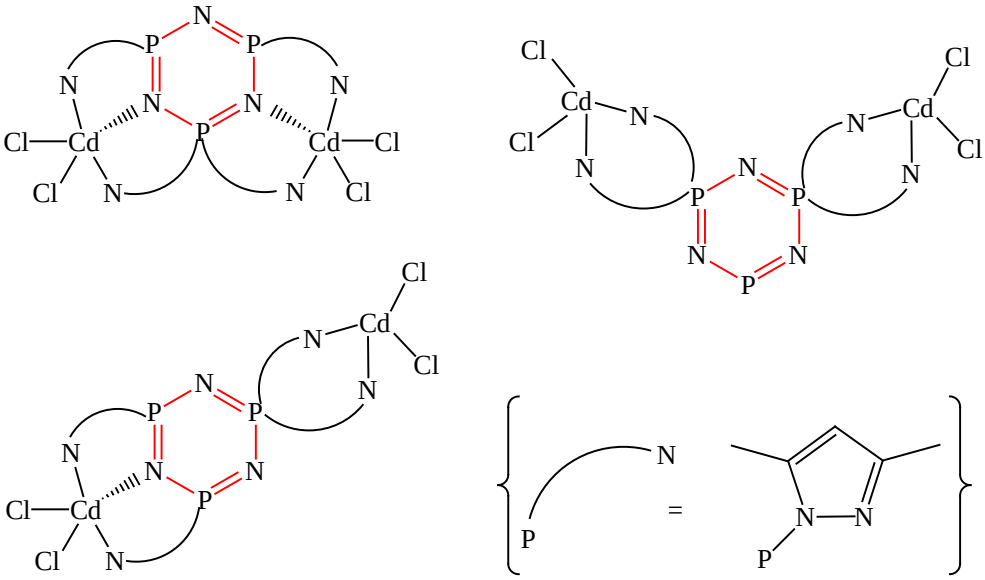

Figure 5 Proposed structures for a dinuclear cadmium(II) complex resulting in three A_2B $^{31}P\{^1H\}$ NMR spectra as reported by Byun *et al.*[5]

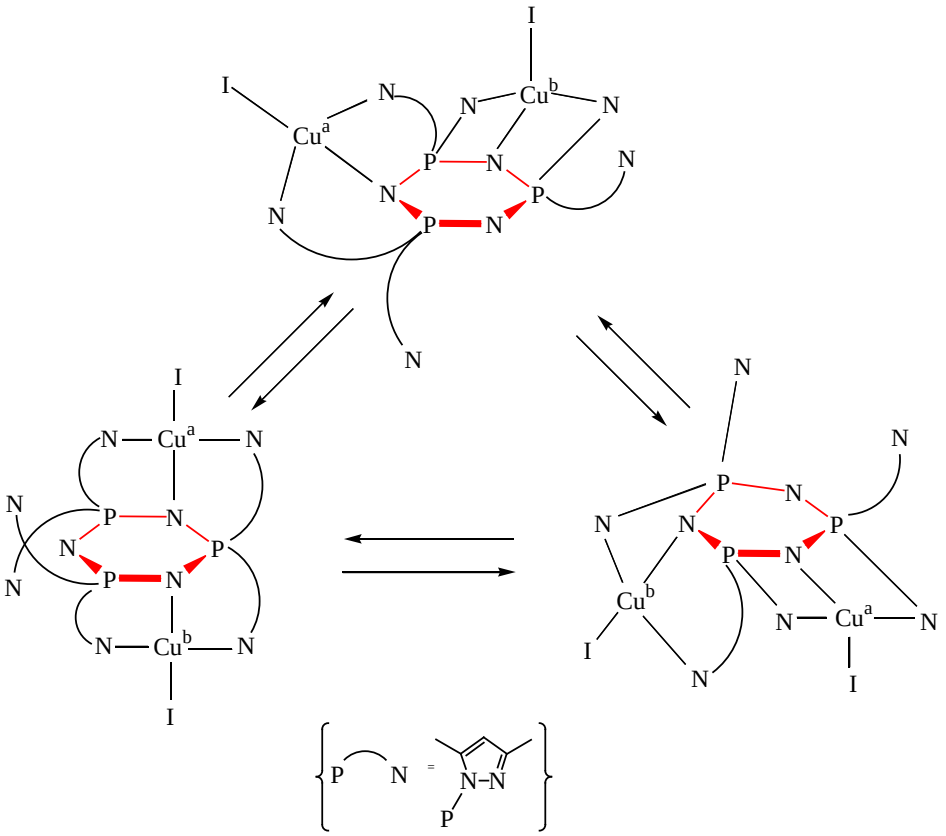

Figure 6 Proposed structures for a dinuclear copper(I) complex as reported by Byun *et al.*[5]

Ainscough *et al.*[6] reported a dinuclear [L($ZnCl_2$)$_2$] complex (L = hexakis(2OPy)-cyclotriphosphazene in which the X-ray structure demonstrated both tetrahedral and TBP coordination environments around the two Zn(II) metal centres (Figure 7). However, the $^{31}P\{^1H\}$ NMR spectrum displayed only one signal in CD_2Cl_2 at δ 5.5 ppm indicating that all three phosphorus sites were equivalent in solution at room temperature. Attempts to elucidate the solution behaviour by VT $^{31}P\{^1H\}$ NMR, gave complex spectra on cooling that could not be rationalised.[7]

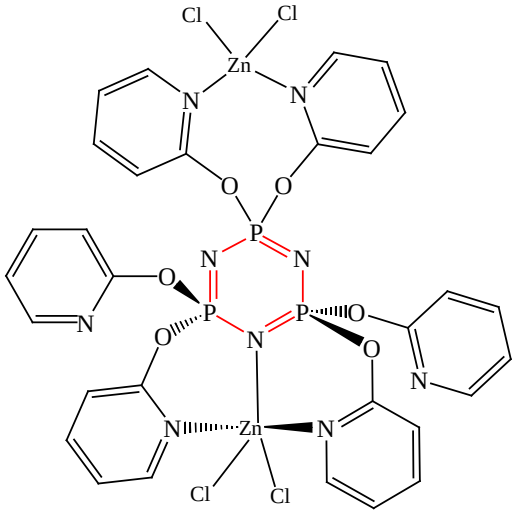

Figure 7 Dinuclear Zn(II) complex reported by Ainscough *et al.*[6]

Justin Thomas *et al.*[8] describe a tetrakis(pyrazolyl)cyclotriphosphazene with one phosphorus atom blocked by non-coordinating groups. Coordination to palladium is from geminal pyrazolyl groups. Whilst they identify a fluxional process at room temperature, it is explained in terms of isomerisation (Figure 8) and variable temperature studies were not undertaken stating only that “the nature of the dynamic processes are not clear at this stage”.

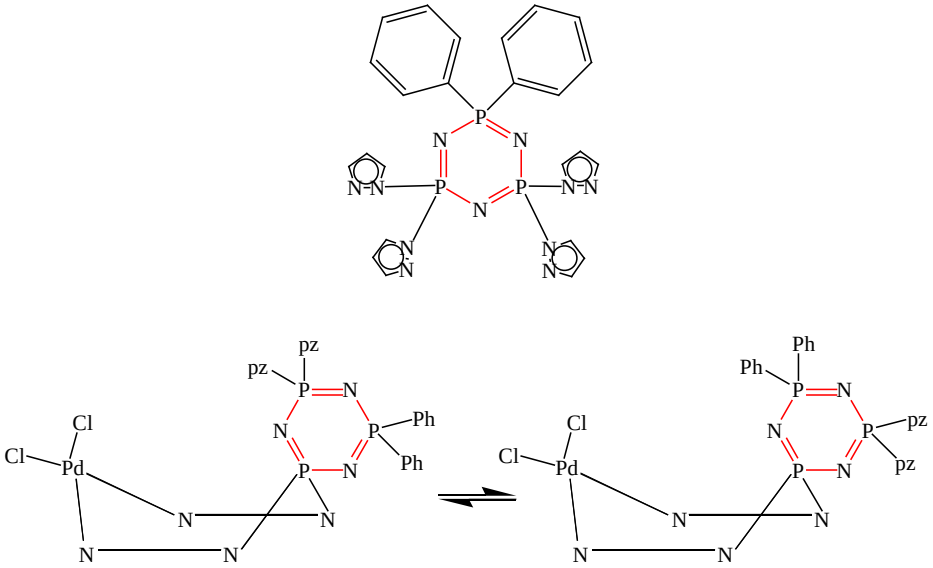

Figure 8 Free ligand (top) and isomerism in a tetrakis(pyrazolyl)cyclotriphosphazene complex reported by Justin Thomas *et al.*[8]

Rivals *et al.*[9] proposed a mechanism for fluxional behaviour in the first reported mixed metal complex $[\{(THF)_2Li\}_3Me_2Al\{(PhNH)_2(PhN)_4P_3N_3\}]$ based on NMR data. In this complex the organoaluminium moiety effectively blocks one of the phosphorus sites by coordination to two geminal PhN groups. The organolithium groups coordinate to the phosphazene ring nitrogen atoms either in a tri- or tetra-valent mode, the latter of which includes one of the nitrogen atoms from a PhN group (Figure 9).

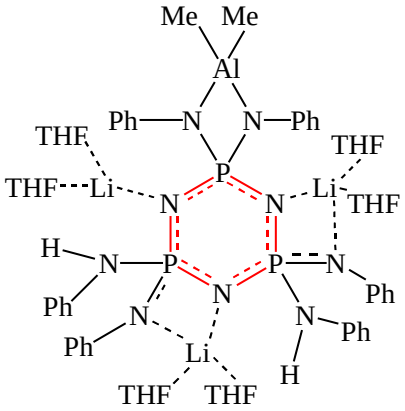

Figure 9 Simplified mixed metal complex reported by Rivals *et al.*[9]

The X-ray structure of the complex revealed three chemically different phosphorus sites, however VT NMR demonstrated an A_2X system suggesting non-rigid stereochemistry and a mirror symmetry oscillating system was proposed to explain the data (Figure 10).

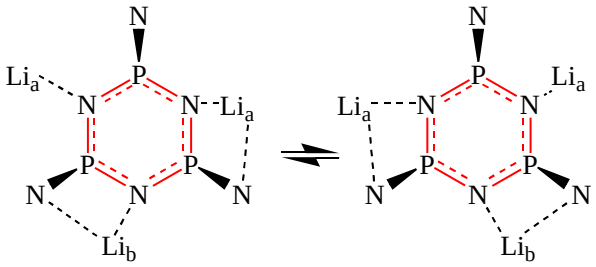

Figure 10 Simplified model showing mirror symmetry oscillation as reported by Rivals *et al.*[9]

Heston *et al.*[10] describe a $GaCl_3$ adduct of $[P_3N_3Cl_6]$ (Figure 11) and explain the broad $^{31}P\{^1H\}$ resonance in the NMR spectrum in terms of gallium dissociation and recombination of the adduct.

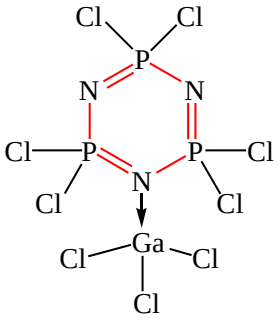

Figure 11 $GaCl_3$ adduct reported by Heston *et al.*[10]

4.1.3 Fluxional behaviour in polyphosphazenes

Fluxional behaviour has also been detected in polyphosphazenes, though no examples are found for polymeric coordination complexes. Simonutti *et al.*[11] propose side chain mobility and rotation about P-CH_2 in poly(diethylphosphazene) (Figure 12) and hence

different conformations to explain solid state ^{13}C NMR spectra but conclude that "the detailed mechanism of this motion is, however, not understood".

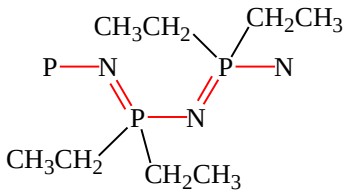

Figure 12 Poly(diethylphosphazene) reported by Simonutti *et al.*[11]

Taylor *et al.*[12] used solid state $^{31}P\{^{1}H\}$ MAS NMR data to explain the amplitude of side chain motion in the semicrystalline poly[bis(3-methylphenoxy)phosphazene] (Figure 13) over a temperature range from -50°C to 100°C.

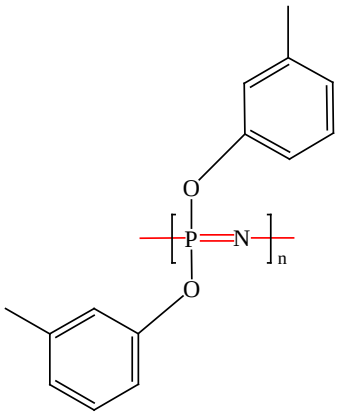

Figure 13 Poly[bis(3-methylphenoxy)phosphazene] reported by Taylor *et al.*[12]

Taylor *et al.*[12] concluded that negligible motion occurs in the crystalline phase below T_g and that large amplitude motions occur in the amorphous phase above T_g including unrestricted rotation of the side groups and torsional motion along the backbone. This work by Taylor *et al.*[12] is one of the few reports on polyphosphazenes that attempts to derive thermodynamic parameters from the VT NMR data.

Allcock *et al.*[13] describe the existence of spinning side bands in $^{31}P\{^{1}H\}$ MAS NMR as being indicative of increasing rigidity as the temperature decreases, for a nonlinear optical (NLO) chromophore linked to a polyphosphazene backbone (Figure 14). Longer

spacer groups between the aromatic portion of the NLO side group and the phosphazene backbone decrease the temperature at which main chain motion is quenched. In order to study relative motion of NLO chromophore side groups the use of a phosphazene backbone is an ideal medium because ^{13}C NMR is not complicated by the backbone and, as well, $^{31}P\{^{1}H\}$ NMR can be used to detect backbone motion independently.

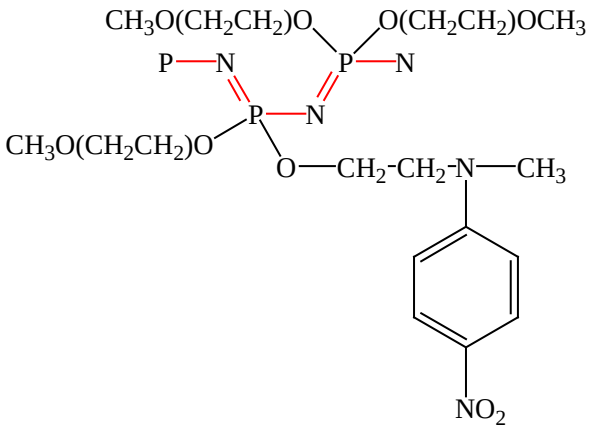

Figure 14 NLO Chromophore linked to a polyphosphazene backbone as reported by Allcock *et al*. [13]

Crosby *et al.*[14] reported the first high resolution solid state $^{31}P\{^{1}H\}$ MAS NMR study of poly(diethoxy)phosphazenes (Figure 15) in 1987, and inferred that a sharp signal above T_g is indicative of large amplitude, rapid anisotropic motion of the main chain to give a time averaged signal. This signal broadens below T_g as the amplitude decreases and slight variations in the phosphorus atom environments coalesce and start to become distinguishable on the NMR timescale.

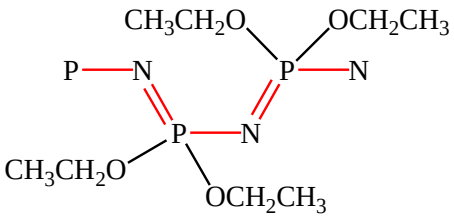

Figure 15 Poly(diethoxy)phosphazene structure reported by Crosby *et al.*[14]

4.1.4 Investigation protocol for fluxional behaviour in $[ML^2Cl_2]$

During analysis of the transition metal complexes with the ligand **L²**, it was noted that the complex $[CoL_2Cl_2]$ appeared to undergo a structural rearrangement in solution (see Chapter Three). NMR analysis of the paramagnetic complex gave spectra that were very broad and essentially featureless. Few reports in the literature attempt to derive thermodynamic parameters from fluxional behaviour in cyclo or polyphosphazenes. As mentioned in previously, many reports leave the mechanism of fluxional behaviour unexplained. In an attempt to elucidate possible fluxional mechanisms, diamagnetic complexes with a range of ionic radii, $[ZnL^2Cl_2]$, $[CdL^2Cl_2]$ and $[HgL^2Cl_2]$, were prepared.

In this study the ligand was designed to provide a nitrogen rich environment for coordination to transition metals via electron donation from 2-pyridyloxy moieties and from the phosphazene ring nitrogen. The use of one blocking biphenolate on the phosphazene ring was expected to effectively constrain the coordination site and reduce the complexity of VT NMR spectra.

To investigate fluxional behaviour in metal complexes, the 4-methyl-2-pyridyloxy variant, **L²** (Figure 16), was the preferred ligand option due to good solubility in NMR solvents and ready assignment of the ^{1}H NMR signal of the proton *ortho* to the pyridyl nitrogen.

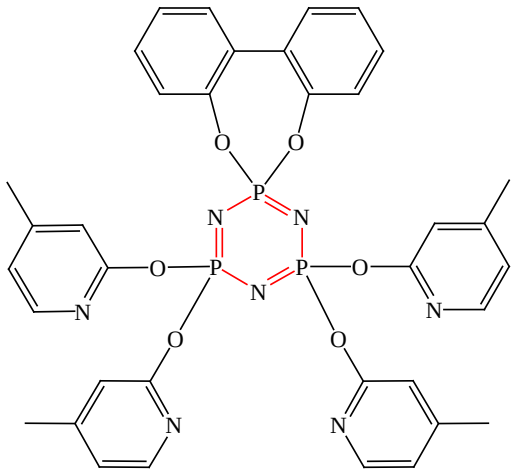

Figure 16 Ligand L^2

The diamagnetic complexes $[ZnL^2Cl_2]$, $[CdL^2Cl_2]$ and $[HgL^2Cl_2]$ were prepared and characterised. Single crystal X-ray structures were obtained for $[ZnL^2Cl_2]$ and

[CdL^2Cl_2] to elucidate structural information. ^1H and $^{31}P\{^1H\}$ VT NMR studies were undertaken to examine any fluxional behaviour and to establish possible mechanisms, as well as to determine thermodynamic parameters.

4.2 Experimental Section

4.2.1 General

All manipulations were carried out under nitrogen using standard Schlenk techniques. Analytical grade solvents were purchased from standard chemical suppliers and used without further purification. The cyclotriphosphazene, $N_3P_3Cl_6$ (Aldrich, plus a gift from the Otsuku Company, Japan), 2-hydroxy-4-methylpyridine (Aldrich), $ZnCl_2$ (M&B) and $HgCl_2$ (M&B) were used as received, $CdCl_2 \cdot 2.5\ H_2O$ (Hopkin & Williams) was dried at 140 °C prior to use. Synthesis of the ligand is described in Chapter Two. Microanalyses were performed by Campbell Microanalytical Laboratory, University of Otago. NMR spectra were recorded on a Bruker Avance 400 MHz spectrometer in CD_2Cl_2; temperature calibration was performed using 4% methanol in CD_3OD (D_4 deuterated methanol) with a trace of HCl.[15] Lineshape analysis was performed using the freeware program SpinWorks v.2.5.1.[16] Electrospray mass spectra were collected from CH_3CN solutions on a Micromass ZMD spectrometer run in positive ion mode.

Arrhenius plots[17] were obtained by plotting the natural log of the rates (ln k) obtained from the SpinWorks lineshape software against 1/T, with a correction factor to account for the deviation of the NMR displayed temperature and that obtained by calibration. Since the Arrhenius equation is $k = A \exp(-E_a/RT)$, where:

k = measured rate s^{-1}

A = pre-exponential factor

E_a = activation energy

R = Gas constant = 8.3145 $JK^{-1}\ mol^{-1}$

T = temperature K.

The activation energy is given by the slope of the Arrhenius plot multiplied by –R, with the assumption that A and E_a are both temperature independent.

Eyring plots[18] were obtained by plotting ln k/T versus 1/T. The Eyring equation is defined as $k = x\ (k_B \cdot T/h)\exp(-\Delta G/RT)$, where x is assumed to be 1, and:

k_B = Boltzmann constant = $1.38066 \cdot 10^{-23}\ JK^{-1}$

h = Plank constant = $6.626 \cdot 10^{-34}$ Js

G = Gibbs free energy of activation.

From the Eyring plots, thermodynamic parameters can be derived since:

Enthalpy of activation $\Delta H = -R \cdot \text{slope}(1/T \cdot \ln(k/T))$

Entropy of activation $\Delta S = R(\text{intercept}(1/T \cdot \ln(k/T) - \ln(k_B/h))$.

4.2.2 Syntheses of the complexes

tbp-[ZnL^2Cl_2]·CH_2Cl_2 and tet-[ZnL^2Cl_2]·$5CH_2Cl_2$

A mixture of L^2 (0.101 g, 0.134 mmol) and anhydrous $ZnCl_2$ (0.018 g, 0.132 mmol) was stirred overnight under N_2 in 30 ml CH_2Cl_2. The resulting white cloudy solution was filtered through celite with CH_2Cl_2 to yield a clear liquid which was taken to dryness to give a white powder, this was filtered and washed with hexane (0.06 g, 59%). The powder was dried overnight at 70°C under vacuum and used for analysis. X-ray quality clear crystals of tbp-[ZnL^2Cl_2]·CH_2Cl_2 were obtained by layering hexane over a concentrated solution of [ZnL^2Cl_2] in CH_2Cl_2. X-ray quality clear crystals of tet-[ZnL^2Cl_2]·$5CH_2Cl_2$ were obtained by dissolving the remaining solid left in the reaction RBF in excess CH_2Cl_2 and layering with hexane.

Elemental analysis: Calculated for $C_{36}H_{32}Cl_2N_7O_6P_3Zn \cdot 0.33\ C_6H_{14}$ (917.97): C, 49.72; H, 4.17; N, 10.68. Found: C, 49.51; H, 3.96; N, 10.68. $^{31}P\{^1H\}$ NMR ($CDCl_3$): δ 22.08 (t, *J*=102.8 Hz), 7.76 (d, *J* =100.9 Hz). ^1H NMR ($CDCl_3$): δ 8.32 (d, J=5.0 Hz), 7.10 (d, J=5.0 Hz), 6.93 (s), 2.37 (s, methyl). ESMS, 850 m/z [$ZnL^2Cl]^+$.

[CdL^2Cl_2]·$4CH_2Cl_2$

A mixture of L^2 (0.139 g, 0.180 mmol) and $CdCl_2$ (0.034 g, 0.180 mmol) was stirred overnight in 60 ml CH_2Cl_2 under N_2. The slightly cloudy white solution was filtered through celite with CH_2Cl_2 to give a clear liquid. The volume of the liquid was reduced to approximately 10 ml and a layer of hexane added, X-ray quality crystals formed from the solution (0.144 g, 82%). The crystals were dried under vacuum at 70°C overnight for analysis.

Elemental analysis: Calculated for $C_{36}H_{32}CdCl_2N_7O_6P_3$ (934.92): C, 46.25; H, 3.45; N, 10.49; Cl, 7.58. Found: C, 46.48; H, 3.52; N,10.41; Cl, 7.59. $^{31}P\{^1H\}$ NMR ($CDCl_3$): δ 23.03 (t, *J*=100.9 Hz), 6.52 (d, *J*=103.3 Hz). ^1H NMR ($CDCl_3$): δ 8.25 (d, J=5.2 Hz), 7.01 (d, J=5.1 Hz), 6.86 (s), 2.35 (s, methyl). ESMS, 900 *m/z* [$CdL^2Cl]^+$.

[HgL^2Cl_2]

A mixture of L^2 (0.110 g, 0.146 mmol) and $HgCl_2$ (0.036 g, 0.132 mmol) was stirred overnight in 30 ml CH_2Cl_2, under N_2. The slightly cloudy white solution was filtered through celite with 30 ml CH_2Cl_2 to give a clear liquid. The volume of the liquid was reduced to approximately 10 ml and a layer of hexane added. Nucleation produced a white powder (0.07 g, 49%). The powder was dried overnight at 70°C under vacuum and used for analysis.

Elemental analysis: Calculated for $C_{36}H_{32}Cl_2HgN_7O_6P_3 \cdot 0.5\ C_6H_{14}$ (1067.20): C, 43.89; H, 3.78; N, 9.19. Found: C, 43.60; H, 3.67; N, 9.30. $^{31}P\{^1H\}$ NMR ($CDCl_3$): δ 24.80 (t, *J*=97.1 Hz), 7.35 (d, *J*=99.3 Hz). ^1H NMR ($CDCl_3$): δ 7.98 (d, J=5.1 Hz), 6.95 (d, J=4.9 Hz), 6.88 (s), 2.34 (s, methyl). ESMS, 988 *m/z* $[HgL^2Cl]^+$.

4.2.3 Crystallography

X-ray data were collected on a Siemens P4 four circle diffractometer, using a Siemens SMART 1K CCD area detector. The crystals were mounted in an inert oil, transferred into the cold gas stream of the detector and irradiated with graphite monochromated Mo-Kα (λ = 0.71073 Å) X-rays. The data were collected by the SMART program and processed with SAINT to apply Lorentz and polarisation corrections to the diffraction spots (integrated three-dimensionally). The structures were solved by direct methods and refined using the SHELXTL program.[19] Hydrogen atoms were calculated at ideal positions. For the solution of $[CdL^2Cl_2] \cdot 4CH_2Cl_2$, the electron density of one molecule of disordered C_6H_{14} was removed from the unit cell using PLATON/SQUEEZE.[20] One molecule of C_6H_{14} and one molecule of water per cell, was removed (60 e- per cell and 261.5 $Å^3$ was left by the void). Crystal data are given in Table 1.

The single crystal X-ray structure of tbp-$[ZnL^2Cl_2] \cdot CH_2Cl_2$ is unsuitable for publication, having too few reflections collected as detected during CIF checking, but does demonstrate the connectivity to confirm the presence of a five-coordinate species where L^2 behaves as a κ^3*N* donor, coordinating to the metal centre through the phosphazene ring nitrogen and two *trans* non-geminal pyridyloxy arms. Attempts to grow more crystals resulted in tet-$[ZnL^2Cl_2] \cdot 5CH_2Cl_2$ and decomposition products.

Compound	tbp-$[ZnL^2Cl_2]\cdot CH_2Cl_2$	tet-$[ZnL^2Cl_2]\cdot 5CH_2Cl_2$	$[CdL^2Cl_2]\cdot 4CH_2Cl_2$
Molecular formula	$C_{37}H_{34}Cl_4N_7O_6P_3Zn$	$C_{37.25}H_{34.50}Cl_{4.50}N_7O_6P_3Zn$	$C_{37.50}H_{35.11}CdCl_{4.67}N_7O_{6.03}P_3$
Molecular weight	972.79	994.02	1051.02
T (K)	98(2)	97(2)	93(2)
Crystal System	Monoclinic	Triclinic	Triclinic
Space Group	*P*2(1)/*c*	*P*-1	*P*-1
a (Å)	17.512(4)	14.6984(10)	13.8423(5)
b (Å)	15.990(3)	16.7607(11)	17.6519(7)
c (Å)	14.686(3)	21.9219(15)	27.6057(11)
α (˚)	90	97.417(4)	90.811(2)
β (˚)	92.93(3)	104.210(4)	94.710(2)
γ (˚)	90	111.410(4)	101.398(2)
V (Å^3)	4106.7(14)	4728.8(6)	6586.7(4)
Z	4	4	4
μ (MoKα) (mm^{-1})	1.031	0.924	0.944
ρ_{calc}(g cm^{-3})	1.573	1.396	1.59
2θmax (˚)	62.46	50.7	50.16
No. of unique reflections	7017	17242	22601
Data/restraints/ parameters	7017 / 42 / 543	17242 / 0 / 1149	22601 / 49 / 1654
Final R indices [$I > 2\sigma(I)$]	$R1$ = 0.0576 $wR2$ = 0.1517	$R1$ = 0.0686 $wR2$ = 0.1713	$R1$ = 0.0596 $wR2$ = 0.1055
R indices (all data)	$R1$ = 0.0728 $wR2$ = 0.1653	$R1$ = 0.1371 $wR2$ = 0.2241	$R1$ = 0.0894 $wR2$ = 0.1148
Goodness of Fit on F^2	1.024	1.041	1.075

Table 1 Crystal and refinement data for the complexes

4.3 Results and Discussion

Three complexes have been synthesised and characterised, $[ZnL^2Cl_2]$, $[CdL^2Cl_2]$ and $[HgL^2Cl_2]$, and X-ray crystal structures were obtained for the two former complexes. VT NMR spectra were analysed for all the complexes.

4.3.1 Syntheses of the complexes

For each complex, anhydrous metal chlorides were reacted with the ligand $\mathbf{L^2}$ in CH_2Cl_2 in a 1:1 mole ratio. $^{31}P\{^1H\}$ NMR spectra indicated that the reactions had gone to completion after stirring overnight. Relevant analytical data are given in the experimental section and indicate that each complex is formed in a 1:1 metal-ligand

ratio. All of the complexes exhibited good solubility in CH_2Cl_2 in line with the other metal complexes made with the ligand $\mathbf{L^2}$ as reported in Chapter Three. ESMS gave spectra consistent with formation of the $[ML^2Cl]^+$ cation.

4.3.2 Crystallography of tetrahedral $[ZnL^2Cl_2]\cdot 5CH_2Cl_2$

The tetrahedral form of $[ZnL^2Cl_2]\cdot 5CH_2Cl_2$ (tet-$[ZnL^2Cl_2]\cdot 5CH_2Cl_2$ Figure 17) crystallised in space group *P*-1 and refined with two complete molecules of the complex (molecules A and B in Figure 17) and five molecules of CH_2Cl_2 in the unit cell. The differences between each molecule are:

(i) a spatial orientation of one of the *gem* non-coordinated pyridyl rings about the P-O bond, which increases the Van der Waals interaction between the phosphorus and nitrogen atoms as shown in Table 2 (P···N Van der Waals distance = 3.40 Å)

(ii) the complex has two chiral centres forming intramolecular macrocycles that demonstrate different directions of rotation in each molecule. There is a seven membered spiro ring with the biphenolate moiety, and an eight membered spiro ring containing the Zn(II) centre. In molecule A, atoms O4 and O3 take on a clockwise twist relative to P2 (*R* configuration) whereas in molecule B, atoms O9 and O10 display an *S* configuration. Similarly, atoms O1 and O2, and O7 and O8 also display *S* and *R* configurations respectively. The fact that *RR* or *SS* configurations are not evident is probably due to packing forces within the crystal. The distribution of five solvent molecules (Figure 18) in the cell probably confers a different packing arrangement and coordination to that of tbp-$[ZnL^2Cl_2]\cdot CH_2Cl_2$.

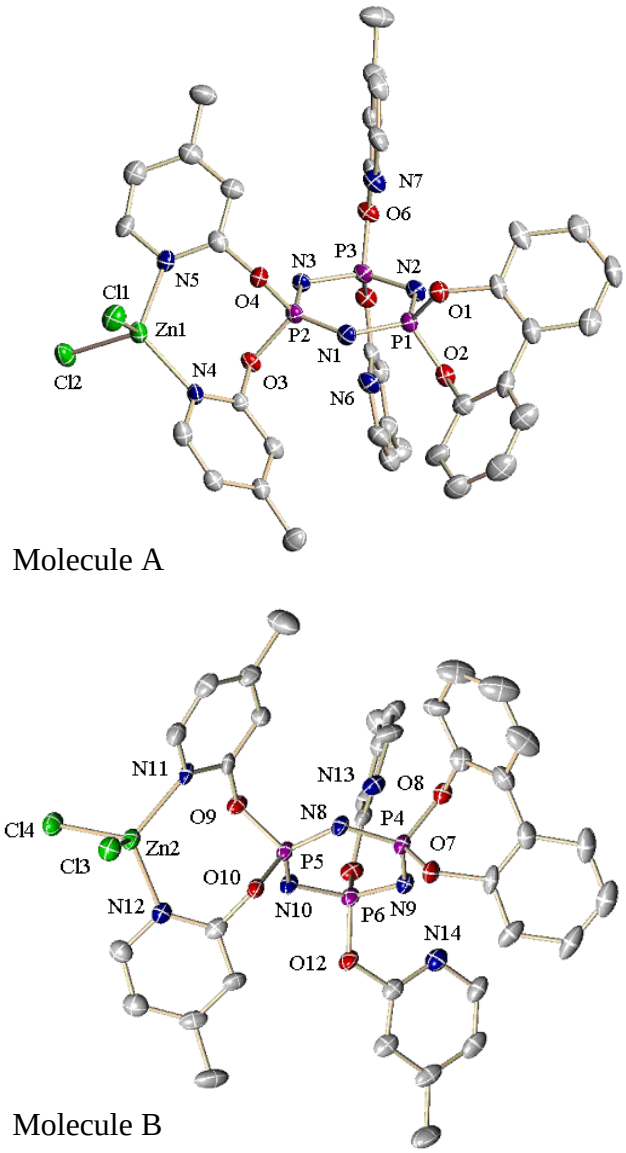

Figure 17 The two tetrahedral molecules in the unit cell of tet-$[ZnL^2Cl_2]\cdot 5CH_2Cl_2$. Thermal ellipsoids are drawn at 50% probability (hydrogen atoms and occluded solvent removed for clarity)

Van der Waals interaction	Distance (Å)
Molecule A - N6···P3	2.783
Molecule A - N7···P3	2.853
Molecule B - N13···P6	2.849
Molecule B - N14···P6	2.921

Table 2 Van der Waals interactions for molecules A and B

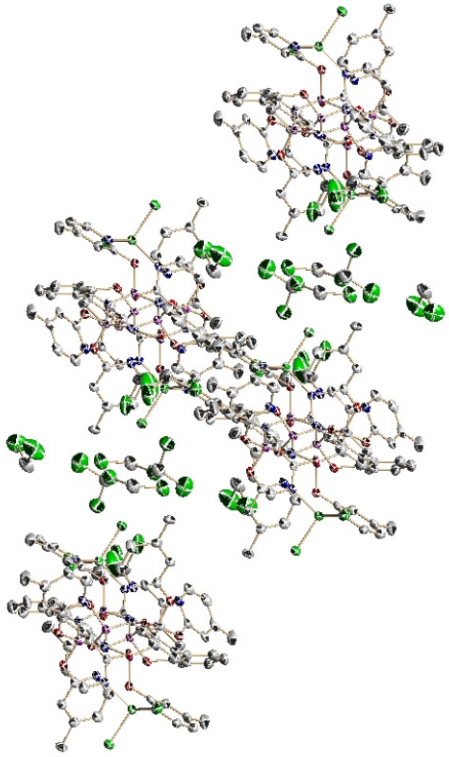

Figure 18 Solvent pockets constraining the packing of tet-[ZnL^2Cl_2]·$5CH_2Cl_2$ Thermal ellipsoids are drawn at 50% probability (hydrogen atoms removed for clarity)

4.3.3 Crystallography of trigonal bipyramidal [ZnL^2Cl_2]·CH_2Cl_2

Trigonal bipyramidal [ZnL^2Cl_2]·CH_2Cl_2 (tbp-[ZnL^2Cl_2]·CH_2Cl_2) crystallised in space group *P*2(1)/*c* and refined with one fractional CH_2Cl_2 molecule (0.25 occupancy). One molecule of the complex is present in the unit cell and the coordination sphere around the Zn(II) centre is five-coordinate trigonal bipyramidal (TBP) giving an N_3Cl_2 donor set (Figure 19). Two nitrogen donors are from pyridyl rings coordinating in a *trans* non-geminal manner to form the axial bonds. One phosphazene ring nitrogen and the two chloride ions form the equatorial bonds. The non-coordinating pyridyl rings are spatially orientated such that the nitrogen atoms are within the P···N Van der Waals distance (3.40 Å) of the phosphazene ring phosphorus to which they are attached via the hinge oxygen atoms. The distances being; P2···N5 = 2.814 Å and P3···N7 = 2.806 Å. Atoms N4 and N6 form the axial bonds whereas the phosphazene ring nitrogen, N3, and the two chloride ions form the equatorial bonds.

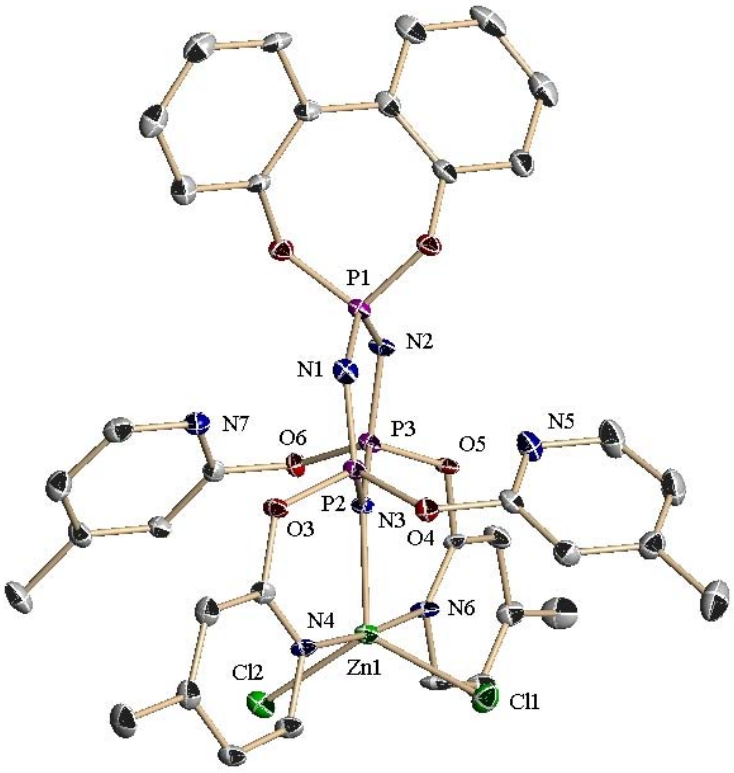

Figure 19 The X-ray structure of tbp-[ZnL^2Cl_2]·CH_2Cl_2
Thermal ellipsoids are drawn at 50% probability (hydrogen atoms and occluded solvent removed for clarity)

4.3.4 Crystallography of [CdL^2Cl_2]·4CH_2Cl_2

The Cd complex crystallised in space group *P*-1 and refined with four complete molecules of CH_2Cl_2 and one disordered molecule of hexane. The crystal structure for the Cd complex has three molecules in the unit cell. One molecule has a similar five-coordinate TBP structure to the Zn complex (Figure 20) with the same N_3Cl_2 donor set of N18 and N20 forming the axial bonds. Equatorial bonds are formed by the phosphazene ring nitrogen, N17 and the two chloride ions. The tbp-[ZnL^2Cl_2]·CH_2Cl_2 and [CdL^2Cl_2]·4CH_2Cl_2 are not strictly isostructural due to the different space group and solvent dispersal within the cell. This molecule is hereinafter referred to as tbp-[CdL^2Cl_2].

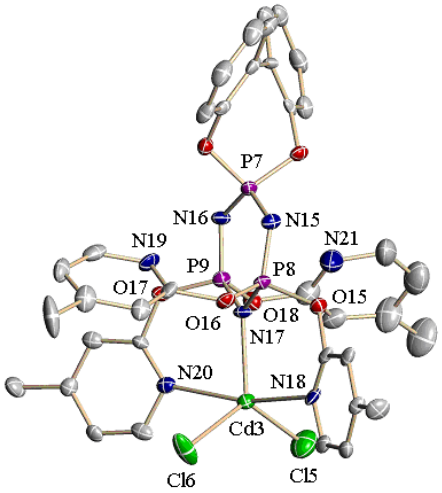

Figure 20 The X-ray structure of tbp-[CdL^2Cl_2]
Thermal ellipsoids are drawn at 50% probability (hydrogen atoms and occluded solvent removed for clarity)

A second molecule has a six-coordinate distorted octahedral geometry around the Cd centre, hereinafter referred to as oct-[CdL^2Cl_2] (Figure 21), with an 'N_4Cl_2' donor set whereby the third nitrogen, N12, comes from coordination of a third pyridine ring, thus there are two nitrogens from two geminal pyridines, one nitrogen from a non-geminal pyridine and the fourth from the phosphazene ring. The remaining uncoordinated pyridyl ring is again within the P···N Van der Waals distance at 2.830 Å.

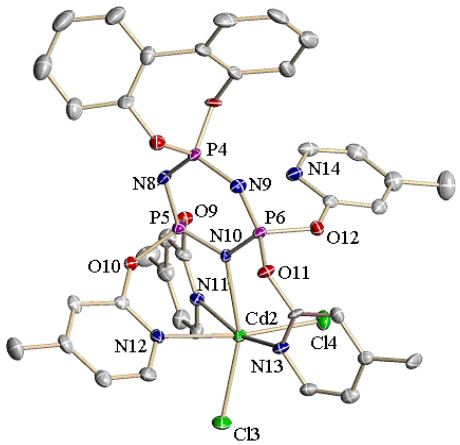

Figure 21 The distorted octahedral structure of oct-[CdL^2Cl_2]
Thermal ellipsoids are drawn at 50% probability (hydrogen atoms and occluded solvent removed for clarity)

The chloride atoms make up the remainder of the donor set but undergo a spatial shift to give a distorted octahedral OC-6-23 geometry (Cahn-Ingold-Prelog (CIP) system)[21] where the principal axis is Cl-Cd-$N_{phosphazene\ ring}$ and the plane perpendicular to this axis comprises the second chloride and the three pyridyl nitrogen atoms (Figure 22).

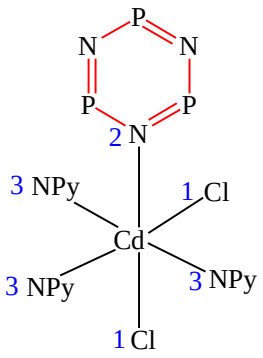

Figure 22 Priority numbers (blue) used in the CIP system[21] for identifying structure geometry in complexes.

The third molecule in the unit cell represents a disordered state lying somewhere between the first two molecules, hereinafter referred to as dis-[CdL^2Cl_2] (Figure 23), having a third pyridyl ring with partial occupancy in a non-coordinated TBP arrangement and partial occupancy in a coordinated octahedral position. This structure demonstrates that the Cd complex appears to be undergoing fluxional behaviour at the point of crystallisation and that three potential structures were “frozen” in the crystalline state.

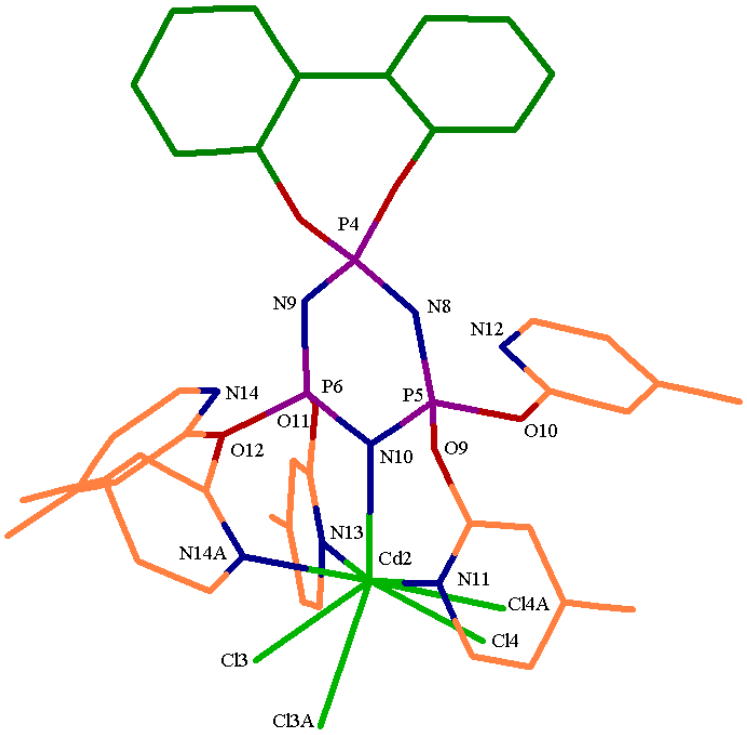

Figure 23 The disordered structure of dis-[CdL^2Cl_2]

(NB. A "Pipes" model has been used for clarity of the disordered pyridyl rings. Suffix "A" denotes the parts of the molecule associated with the disordered structure)

4.3.5 Comparison of the complexes

The crystallographic data for tbp-[ZnL^2Cl_2]·CH_2Cl_2 is included for illustrative purposes only. With incomplete data collection the bond lengths and angles may not be sufficiently accurate for exact comparison between complexes. However it is the trends noted for the [CdL^2Cl_2]·$4CH_2Cl_2$ structures that are core to the argument and remain valid.

The observed distortion from planarity of the phosphazene ring appears to be related to both the ionic radius of the coordinating metal(II) ion in these complexes, and the coordination number. Zn(II) has the smaller ionic radius but exhibits the greatest phosphazene ring distortion. Taking a mean plane through phosphazene ring atoms P1, N1, N2, and N3, and adding the distances of P2 and P3 from this plane (or the comparable atoms in the other molecules) a measure of distortion for the ring that is

consistent between molecules is obtained (Figure 24). This is listed as CTP ring distortion in Table 3.

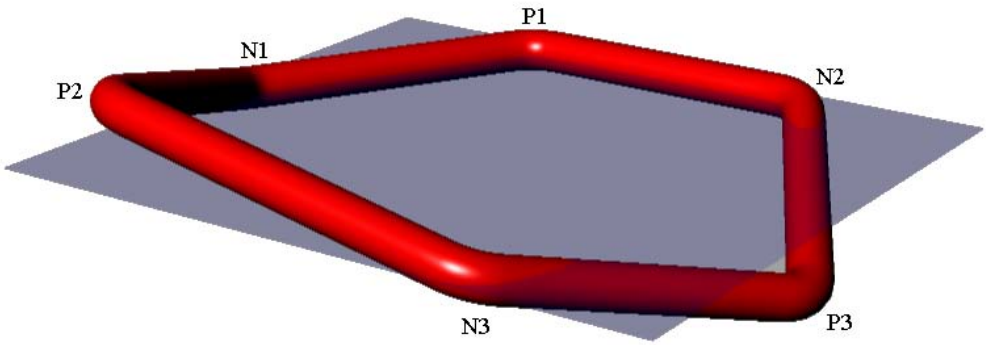

Figure 24 Representation of the mean plane for structure comparison (CTP ring distortion)

Taking a similar mean plane for each of the coordinated pyridyl rings one can derive a measure of the angular displacement of the rings about the metal centre for comparison between structures. For example, for the Zn complex the angle between coordinated pyridyl rings is 164.4° (Figure 25). For each molecule the relevant data are listed in Table 3 as Py ring$_{Coord}$ deviation.

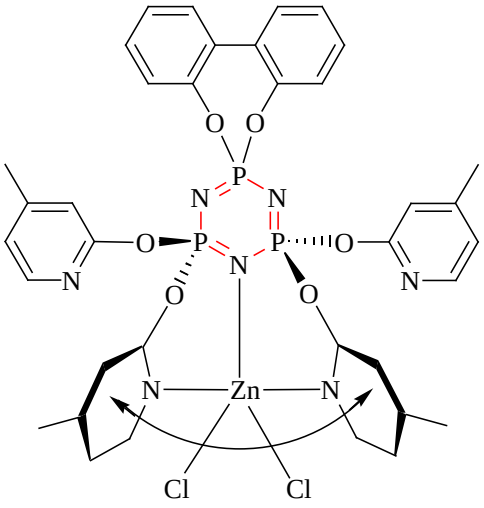

Figure 25 Diagram showing the angle between mean planes of the coordinated pyridyl rings (Py ring $_{Coord}$ deviation)

	CTP ring distortion (Å)	Py ring$_{Coord}$ deviation (°)	M-N$_{CTP\ ring}$ bond length (Å)	M-N$_{Py}$ bond length (Å)	N$_{Py}$-M-N$_{Py}$ angle (°)
tbp-[ZnL^{2}Cl$_2$]	0.3588	164.4	2.056(4)	2.265(3) 2.275(3)	175.21(14)
tbp-[CdL^{2}Cl$_2$]	0.2916	163.3	2.31(2)	2.44(2) 2.49(2)	166.5(7)
dis-[CdL^{2}Cl$_2$]	0.2854	144.2	2.32(2)	2.48(2) 2.52(2) 2.45(7)$_{3rd\ Py}$	163.5(7)
oct-[CdL^{2}Cl$_2$]	0.2124	143.8	2.41(2)	2.53(2) 2.55(2) 2.48(2)$_{3rd\ Py}$	163.6(6)

CTP = Cyclotriphosphazene. The subscript "3rd Py" indicates the third pyridine ring that encroaches to form an octahedral complex. Occluded solvent molecules have been omitted from the table

Table 3 Comparison of selected structural data

It can be seen from Table 3 that the phosphazene ring distortion is greatest in the five-coordinate structures and decreases with increasing ionic radius and with coordination number (ionic radii are: tbp-Zn = 0.68 Å, tet-Zn = 0.60 Å, tbp-Cd = 0.87 Å, tet-Cd = 0.78 Å and oct-Cd = 0.95 Å).[22] In addition the bond length from the phosphazene ring nitrogen atom to the metal centre and from the pyridine rings to the metal centre, increases with ionic radius and with coordination number. Thus as the centroid of the metal atom moves further from the phosphazene ring nitrogen, the phosphazene ring tends towards planarity. This reflects the degree of twist induced on the phosphazene ring by the *trans* nature of the coordinating pyridine rings.

In Figure 26 below, the effect that the increased coordination has on the angle between the mean planes of the coordinating pyridines can easily be visualised. The top illustration denotes the viewing axis after removal of the biphenolate moiety for clarity.

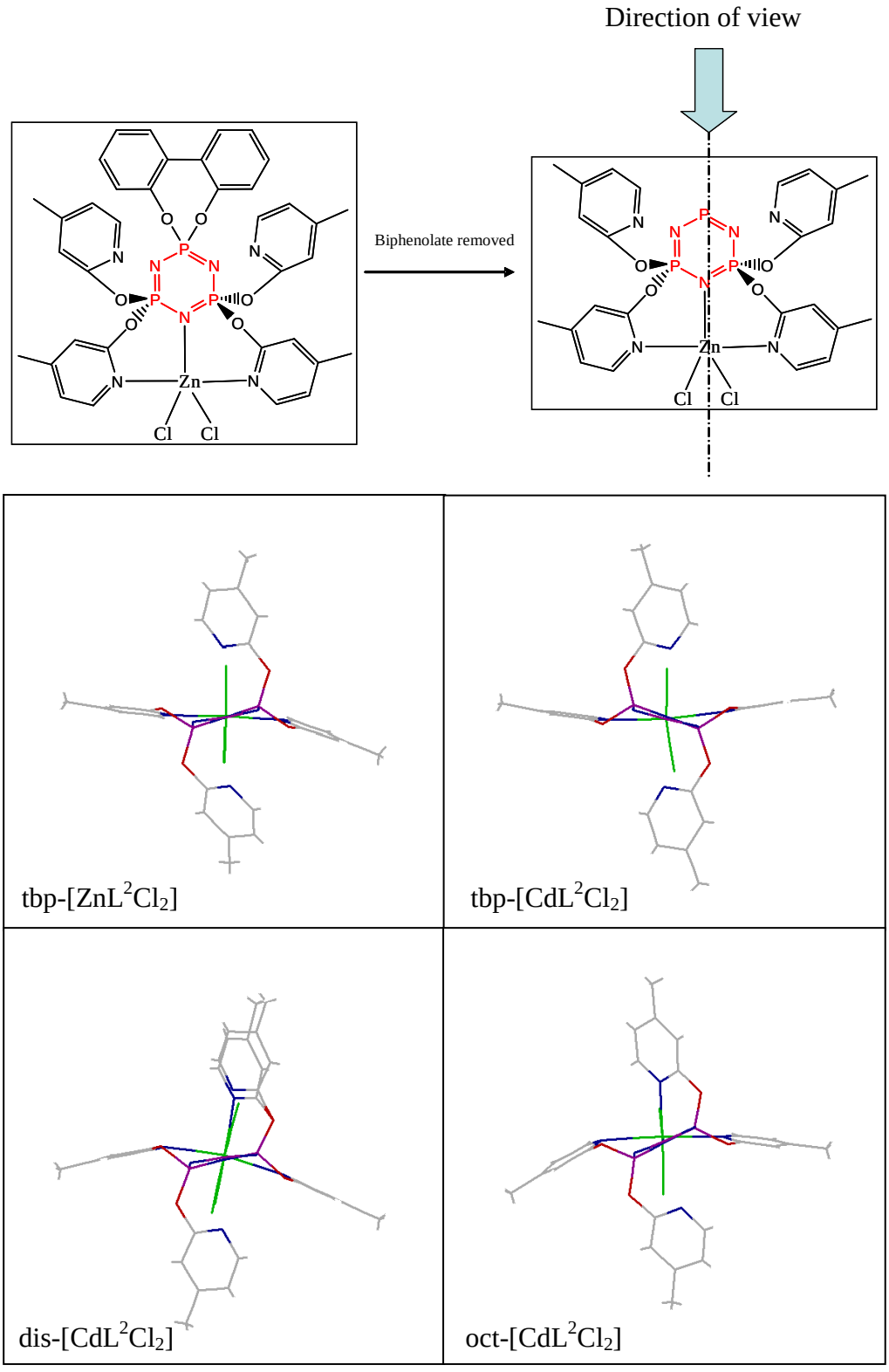

Figure 26 Complexes viewed down the central axis of the phosphazene ring.

Deviation of the metal ion from the mean plane of the phosphazene ring varies as follows; tbp-[ZnL^2Cl_2]·CH_2Cl_2 = 0.0334 Å, tbp-[CdL^2Cl_2] = 0.1730 Å, dis-[CdL^2Cl_2] = 0.2628 Å and oct-[CdL^2Cl_2] = 0.2675 Å. For the Cd species the out of plane deviation is towards the encroaching third pyridyl ring. The bond angles in the chelate rings vary by only one or two degrees between all of the structures except for the oct-[CdL^2Cl_2] structure (Figure 27) which has the third pyridyl arm attached. In this structure the angle O15-P8-N17 opens up on coordination of the third pyridyl arm by some 6.5˚ thus relaxing the phosphazene ring distortion.

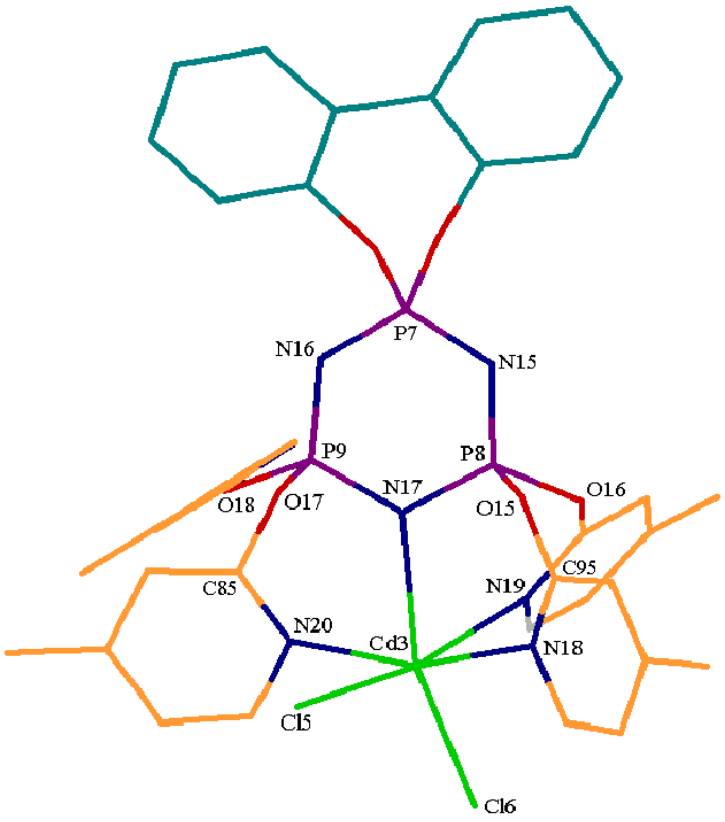

Figure 27 Labelling of atoms for structural comparison of the chelate rings

The structural index (τ) for the Cd and Zn five-coordinate complexes is given in Table 4, being evaluated by the two largest angles (α < β) in the five-coordinate system. The values indicate TBP geometry (where τ = 1.0 for a regular TBP stereochemistry and τ = 0.0 for a regular square based pyramidal stereochemistry).[23]

Complex[a]	β	α	τ [(β – α)/60]
tbp-[CdL^2Cl_2]	N(4)-Cd(1)-N(6) = 166.52˚	Cl(1)-Cd(1)-N(3) = 120.82˚	0.76
tbp-[ZnL^2Cl_2]	N(4)–Zn–N(6) = 175.56˚	Cl(1)–Co–Cl(2) = 122.30˚	0.89

[a]Occluded solvent molecules omitted from the table

Table 4 Structural index (τ) for the tbp-[CdL^2Cl_2] and tbp-[ZnL^2Cl_2]·CH_2Cl_2 five-coordinate complexes

The τ values demonstrate a similar degree of distortion from regular TBP as seen with five-coordinate structures with the ligand hexakis(2-pyridyloxy)cyclotriphosphazene molecule (L), where for [$L(ZnCl_2)_2$] τ = 0.82.[6]

The change in environment around the metal centre (Figure 28) is tabulated in Table 5. Angles and bond lengths for the third coordinating pyridyl arm in the Cd complex are not given.

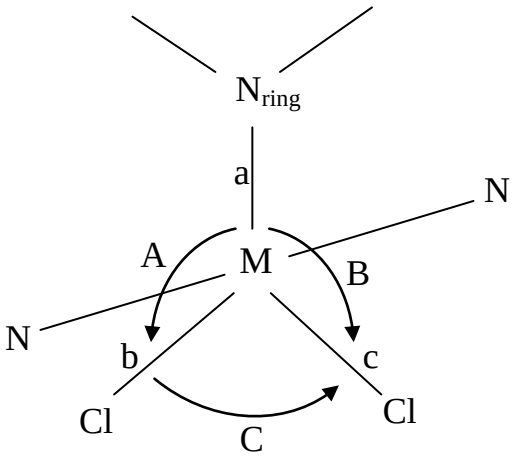

Figure 28 Labelling used for the bond lengths and angles in the Zn and Cd complexes
A = side of approach of 3rd coordinating pyridyl ring, M = Zn, Cd

	A°	B°	C°	a (Å)	b (Å)	c (Å)
tbp-[ZnL^{2}Cl$_2$]	115.74(8)	121.92(8)	122.32(5)	2.056(4)	2.2318(12)	2.2308(10)
tbp-[CdL^{2}Cl$_2$]	120.8(6)	120.1(6)	118.4(6)	2.31(2)	2.441(7)	2.459(7)
dis-[CdL^{2}Cl$_2$]$_{TBP}$ [a]	122.0(6)	117.3(6)	120.6(4)	2.32(2)	2.429(9)	2.413(18)
dis-[CdL^{2}Cl$_2$]$_{oct}$ [b]	160.6(12)	102.6(13)	96.8(16)	2.32(2)	2.59(4)	2.55(6)
oct-[CdL^{2}Cl$_2$]$_{oct}$	157.7(5)	97.0(5)	105.3(2)	2.41(6)	2.493(7)	2.468(7)

[a] = five-coordinate part of dis-[CdL^{2}Cl$_2$], [b] = six-coordinate part of dis-[CdL^{2}Cl$_2$].

Occluded solvent molecules omitted from the table

Table 5 Summary of the environment around each metal centre in the complexes

The values of angle A of 160.6(12)° (Cd$_{disord\ oct}$) and 157.7(5)° (Cd$_{oct}$) clearly demonstrate the degree of distortion from true octahedral geometry where angle A would be 180°. This distortion is most likely caused by steric hindrance of the third pyridyl arm being tethered to the phosphazene ring but has the effect of reducing the deviation from planarity of the phosphazene ring.

The bond lengths within the phosphazene ring show the expected trend on coordination to a metal ion,[24] in that the P-N bonds that flank N3 (N3 being coordinated to the metal - Figure 29) tend to be slightly longer than the rest of the P-N bonds in the ring.[24] However this variance decreases with increasing coordination number (Table 6).

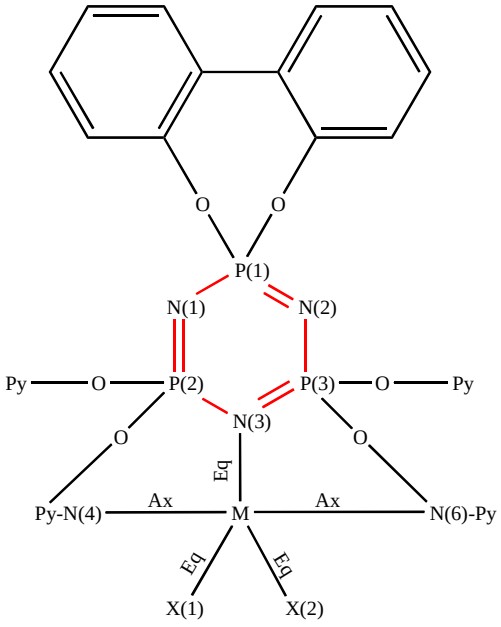

Figure 29 Labelling scheme for Table 6

Bond Lengths	tbp-[ZnL^2Cl_2] Å	tbp-[CdL^2Cl_2] Å	dis-[CdL^2Cl_2] Å	oct-[CdL^2Cl_2] Å
P1-N1	1.558(4)	1.58(2)	1.58(2)	1.59(2)
P1-N2	1.578(3)	1.59(2)	1.58(2)	1.59(2)
P2-N1	1.561(4)	1.57(2)	1.58(2)	1.58(2)
P3-N2	1.555(4)	1.57(2)	1.58(2)	1.58(2)
P2-N3	1.599(3)	1.62(2)	1.61(2)	1.59(2)
P3-N3	1.597(4)	1.61(2)	1.61(2)	1.61(2)
Range	0.044(4)	0.05(2)	0.03(2)	0.03(2)

Occluded solvent molecules omitted from the table

Table 6 Phosphazene ring internal bond lengths

Comparison with Table 3 shows that the M-$N_{CTP\ ring}$ bond lengthens with increasing coordination number, and from Table 6; the internal P-N ring bond lengths correspondingly tend towards equality with the range decreasing from 0.05 to 0.03 Å for the three [CdL^2Cl_2]·$4CH_2Cl_2$ variants in the order tbp-[CdL^2Cl_2], dis-[CdL^2Cl_2] and oct-[CdL^2Cl_2]. Thus the increased electron density (and ionic radius) around the metal centre with increased coordination allows the phosphazene ring P-N bonds flanking the coordinated ring nitrogen to lengthen.

4.4 Evidence for fluxional behaviour in the complexes

Variable temperature NMR studies were conducted to examine in detail the fluxional behaviour. This section covers both ^1H and $^{31}P\{^1H\}$ NMR studies, starting with ^1H NMR.

4.4.1 ^1H VT NMR studies on the complexes

The use of the 4-methyl-2-pyridyloxy ligand, $\mathbf{L^2}$, allows clear assignment of proton signals for ^1H variable temperature NMR studies. At 298 K in CD_2Cl_2 the proton *ortho* to the pyridyl nitrogen (H3 in Figure 30) appears furthest downfield (due to de-shielding by the nitrogen atom) as a well-defined doublet, through coupling to the *meta* hydrogen atom (H2 in Figure 30). NB there are four *ortho* protons to consider in total, one ea from the four 2-oxypyridine rings.

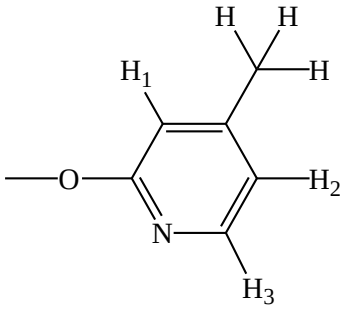

Figure 30 Hydrogen atom numbering on the pyridyl moiety

For $[CdL^2Cl_2]$ and $[HgL^2Cl_2]$ complexes (Figures 31 and 32 respectively), on reducing the temperature, the doublet peak coalesces into a singlet at ≈ 253 K that broadens before splitting into two distinct singlets below 213 K (Cd: 8.6, 8.1 ppm, Hg: 7.8, 7.6 ppm).

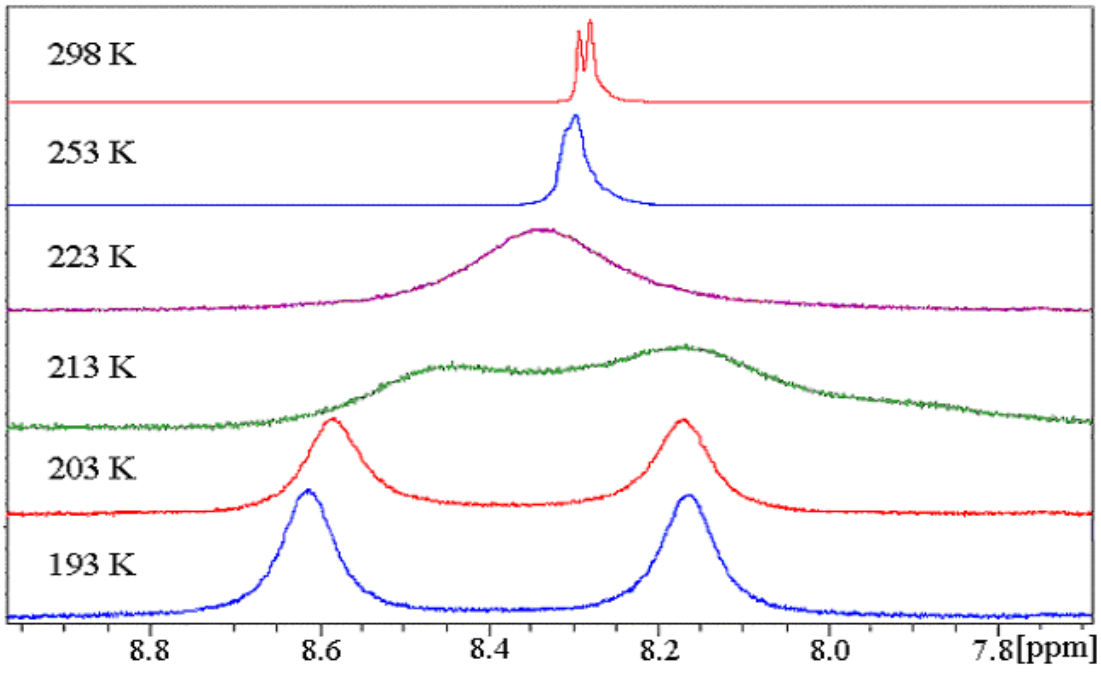

Figure 31 ^1H VT NMR spectra for proton H3 in $[CdL^2Cl_2]$ in CD_2Cl_2 relative to TMS

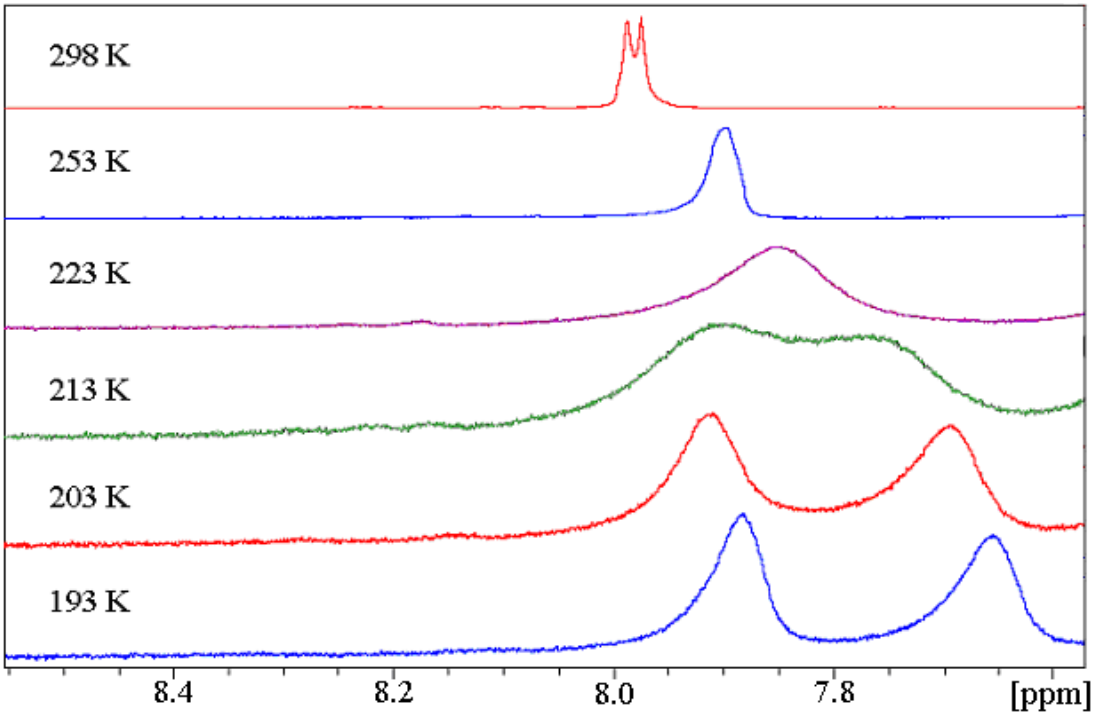

Figure 32 ^{1}H VT NMR spectra for proton H3 in [HgL^{2}Cl$_2$] in CD_2Cl_2 relative to TMS

From the ^{1}H VT NMR spectra for the [CdL^{2}Cl$_2$] and [HgL^{2}Cl$_2$] complexes a number of observations can be made. The first is the general shift in ppm with reducing temperature, downfield for the [CdL^{2}Cl$_2$] complex and upfield for the [HgL^{2}Cl$_2$] complex and it would appear that this drift is a real phenomenon. It has been reported that the reference spectrum of the NMR standard, tetramethylsilane (TMS), drifts upfield with decreasing temperature by -6x10^{-4} ppm/K,[25] and this was observed during the VT NMR studies. The drift exhibited by [CdL^{2}Cl$_2$] and [HgL^{2}Cl$_2$] is greater than that due to temperature effects on the TMS alone. For the two complexes, a satisfactory explanation for the difference in direction of the drift has not, as yet, been determined. Secondly the coalescence temperature (T_c) for both complexes appears to be similar and in the region of 223 K. Thirdly, it is apparent that the low temperature limitation imposed by the choice of solvent (in this case CD_2Cl_2 - freezing point 176 K) is such that the fluxional behaviour observed in the spectra is still occurring as demonstrated by the broadness of the peaks below T_c. Under ideal experimental conditions it would be expected that as the rate decreased to a point where the magnetic environments of the two *ortho* hydrogen sites were effectively frozen, then the broad singlet signals would

once again show the splitting due to the *meta* hydrogen atoms and resolve into two well defined doublets as per the room temperature signal.

For the [ZnL^2Cl_2] complex spectra (Figure 33), the signals do not demonstrate the field shift of the [CdL^2Cl_2] and [HgL^2Cl_2] complexes and the centre of each signal remains at approximately 8.32 ppm. Below T_c however, the broad peak splits to form an asymmetric peak, which subsequently evolves into four peaks below 203 K.

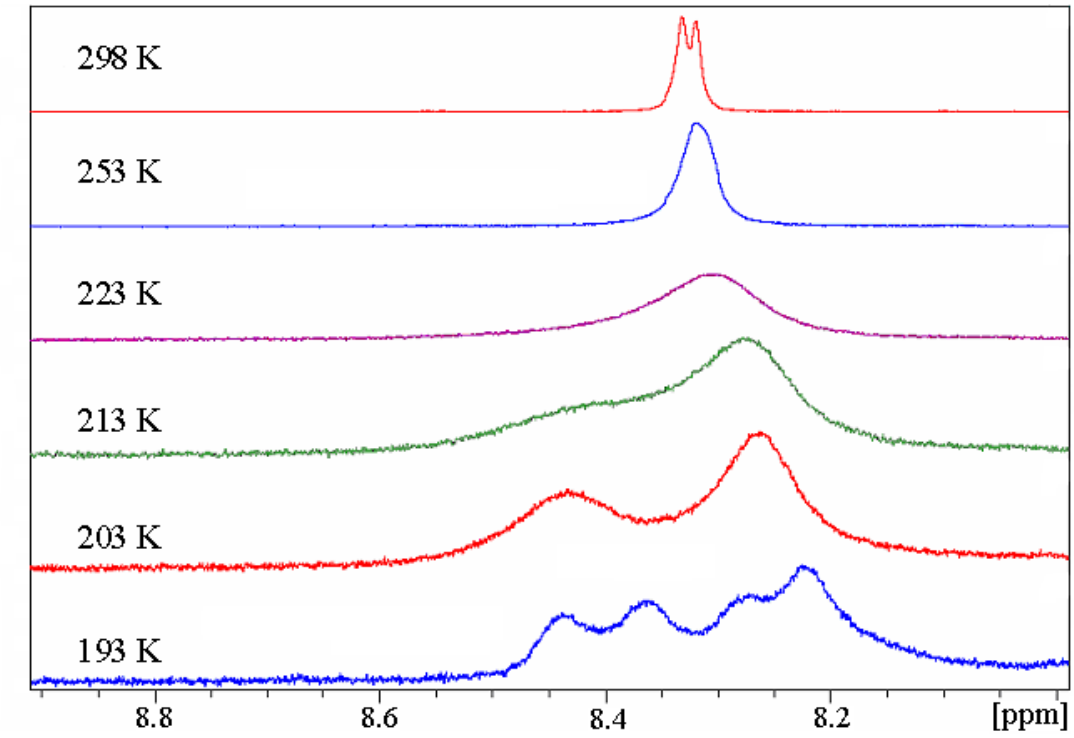

Figure 33 ^{1}H VT NMR spectra for [ZnL^2Cl_2]

Further analysis of the [ZnL^2Cl_2] ^{1}H VT NMR spectra indicates a weak fifth signal in the region of the four broad singlets at approximately 7.95 ppm (Figure 34). The [ZnL^2Cl_2] complex follows a similar pattern to that for [CdL^2Cl_2] and [HgL^2Cl_2] but towards the low temperature limit at 188 K, four distinct peaks are observed for the *ortho* proton environment and a fifth weaker signal appears slightly upfield.

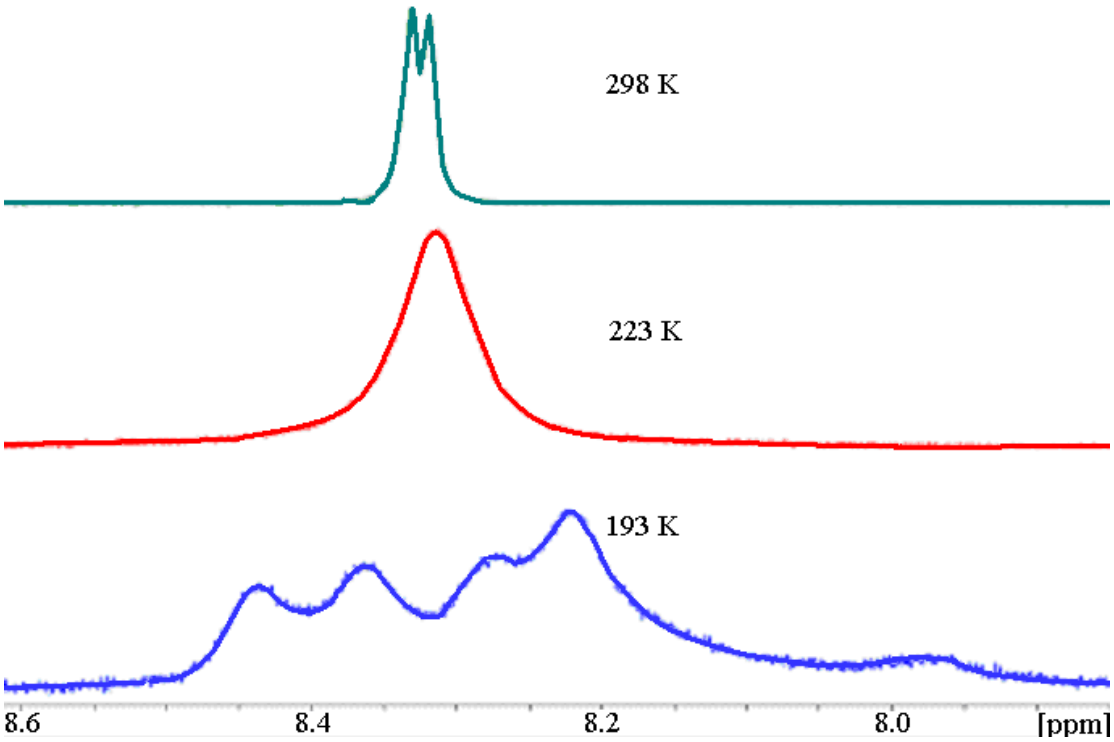

Figure 34 ^{1}H VT NMR spectra for [ZnL^{2}Cl$_2$] - A fifth weak signal is just evident upfield (7.95 ppm) of the four singlet signals for the [ZnL^{2}Cl$_2$] complex at 193 K.

The temperature dependent behaviour is fully reversible in that no difference in splitting is observed whether the solution is being cooled or warmed to a specific temperature. Thus the linear nature of the Arrhenius and Eyring plots (vide infra) is assumed to be correct provided that the sample is permitted to equilibrate at any given temperature to prevent localised temperature gradients within the sample.

Arrhenius and Eyring plots were obtained by lineshape analysis using SpinWorks software[16] which incorporates Alex Bains "Mexico" program.[26] This allows the rate of the fluxional behaviour to be estimated and approximate values for thermodynamic quantities to be derived. Experimental and calculated lineshapes are shown in Figure 35. For the [CdL^{2}Cl$_2$] and [HgL^{2}Cl$_2$] systems, fitting was performed manually. In defining the software parameters, best fits were achieved for [CdL^{2}Cl$_2$] and [HgL^{2}Cl$_2$] assuming an ABCD system, where A and B, and C and D represent *ortho* H atoms on geminal pyridyloxy groups that mutually exchange.

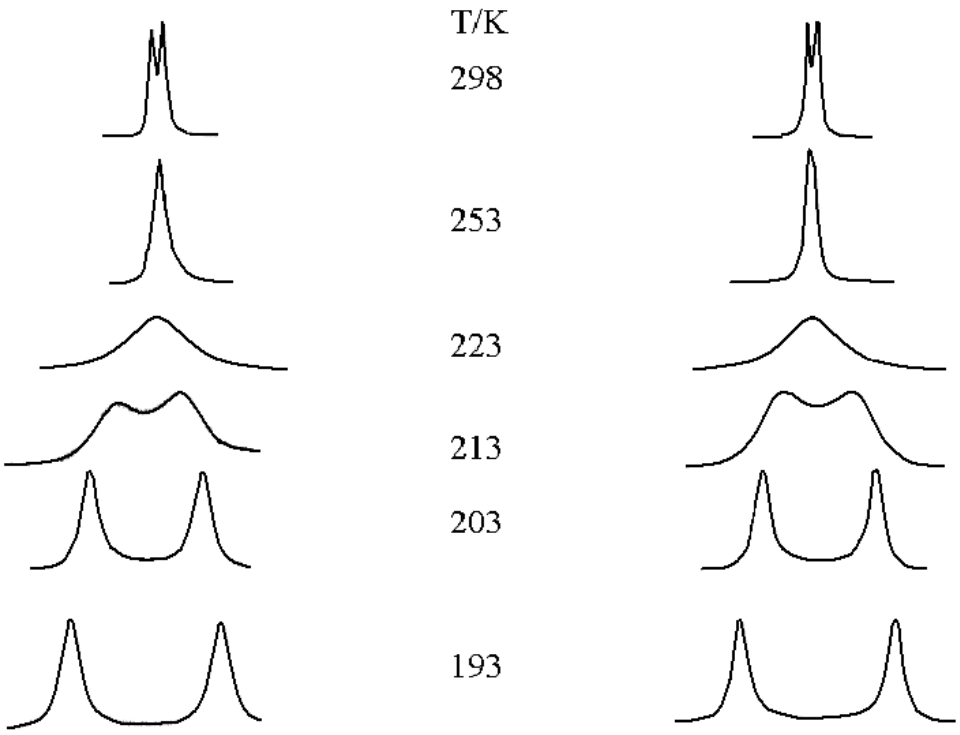

Figure 35 Experimental (left) and calculated (right) lineshape fitting for $[CdL^2Cl_2]$

Based on the rate data obtained from lineshape fitting, Arrhenius and Eyring plots could be obtained (Graphs 1-4). Thermodynamic quantities are tabulated in Table 7.

Data for $[CdL^2Cl_2]$			Data for $[HgL^2Cl_2]$		
T/K	$\Delta G^{\ddagger}$/kJ mol^{-1}	E_a/kJ mol^{-1}	T/K	$\Delta G^{\ddagger}$/kJ mol^{-1}	E_a/kJ mol^{-1}
297	46.5(8)	28.2(5)	297	50.2(8)	23.0(4)
246	41.4(7)		281	48.0(8)	
225	40.5(7)	$\Delta H^{\ddagger}$ kJ mol^{-1}	246	44.0(7)	$\Delta H^{\ddagger}$ kJ mol^{-1}
215	40.1(7)	26.2(4)	236	43.1(7)	21.1(4)
205	39.8(7)		225	42.0(7)	
187	38.7(6)	$\Delta S^{\ddagger}$ J mol^{-1}	215	41.6(7)	$\Delta S^{\ddagger}$ J mol^{-1}
		-65.5(11)	205	40.9(7)	-95.4(16)

Table 7 Thermodynamic parameters derived from Arrhenius and Eyring plots

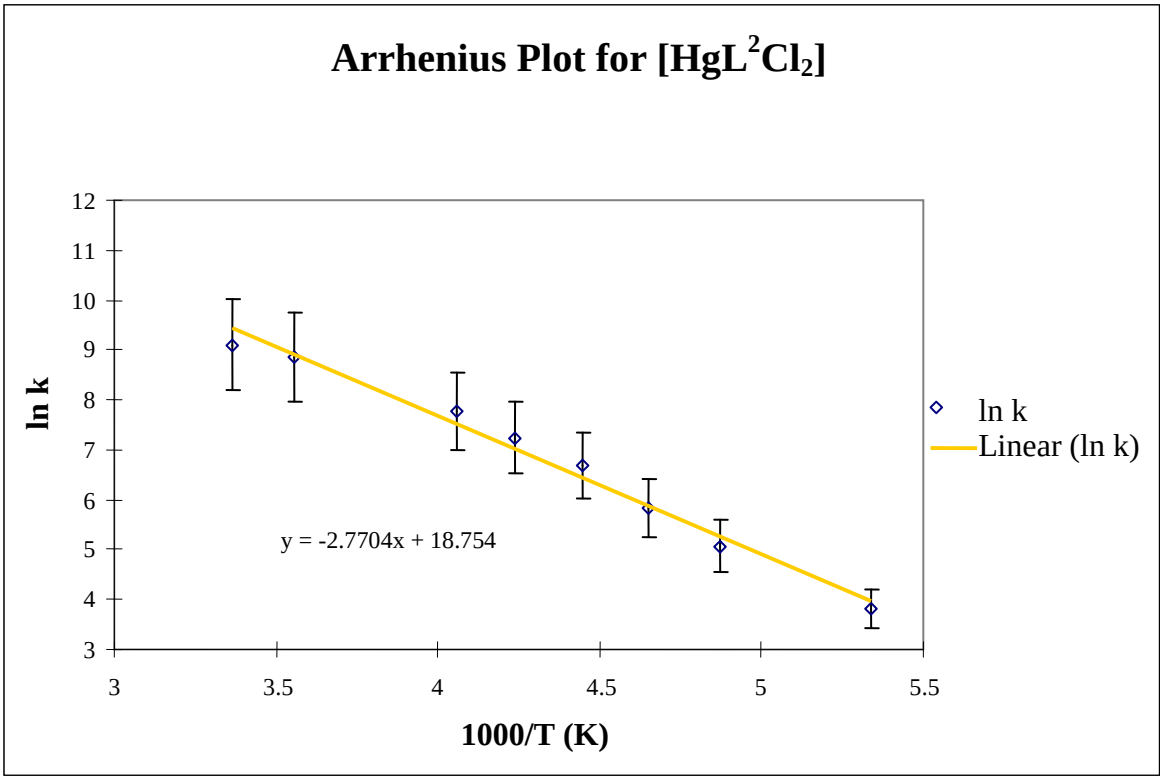

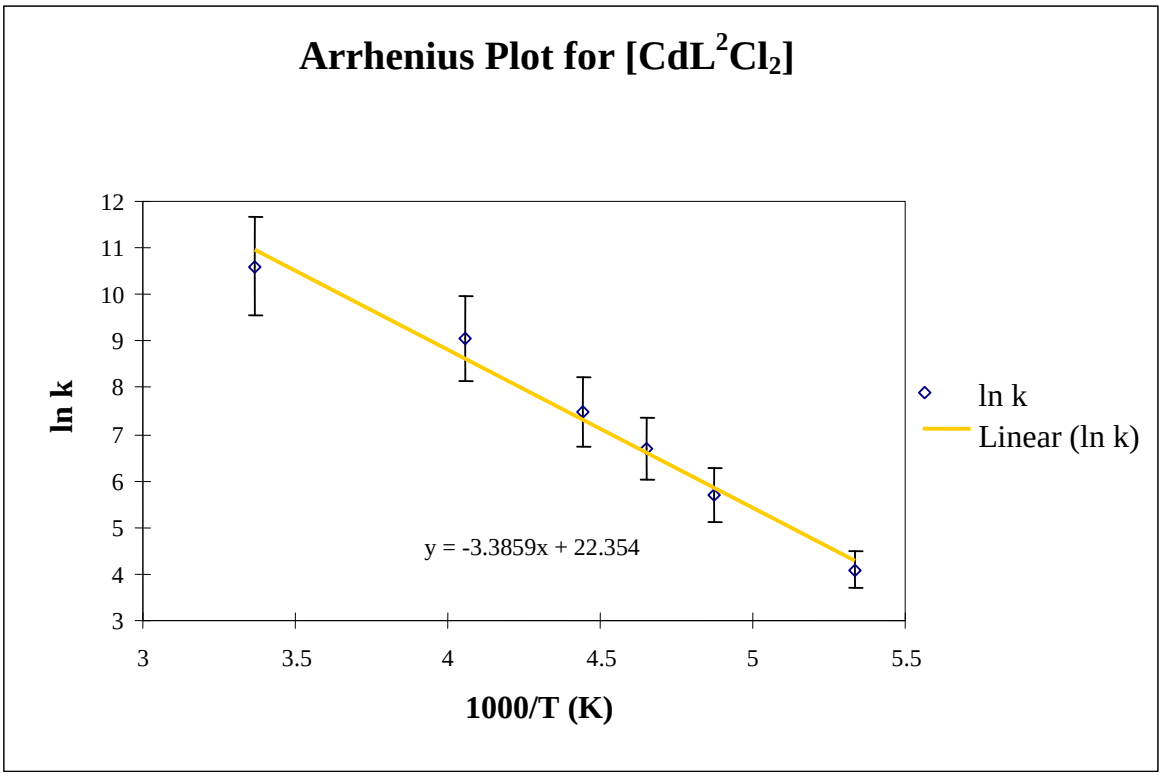

Graphs 1 and 2 Arrhenius plots for $[HgL^2Cl_2]$ and $[CdL^2Cl_2]$ complexes

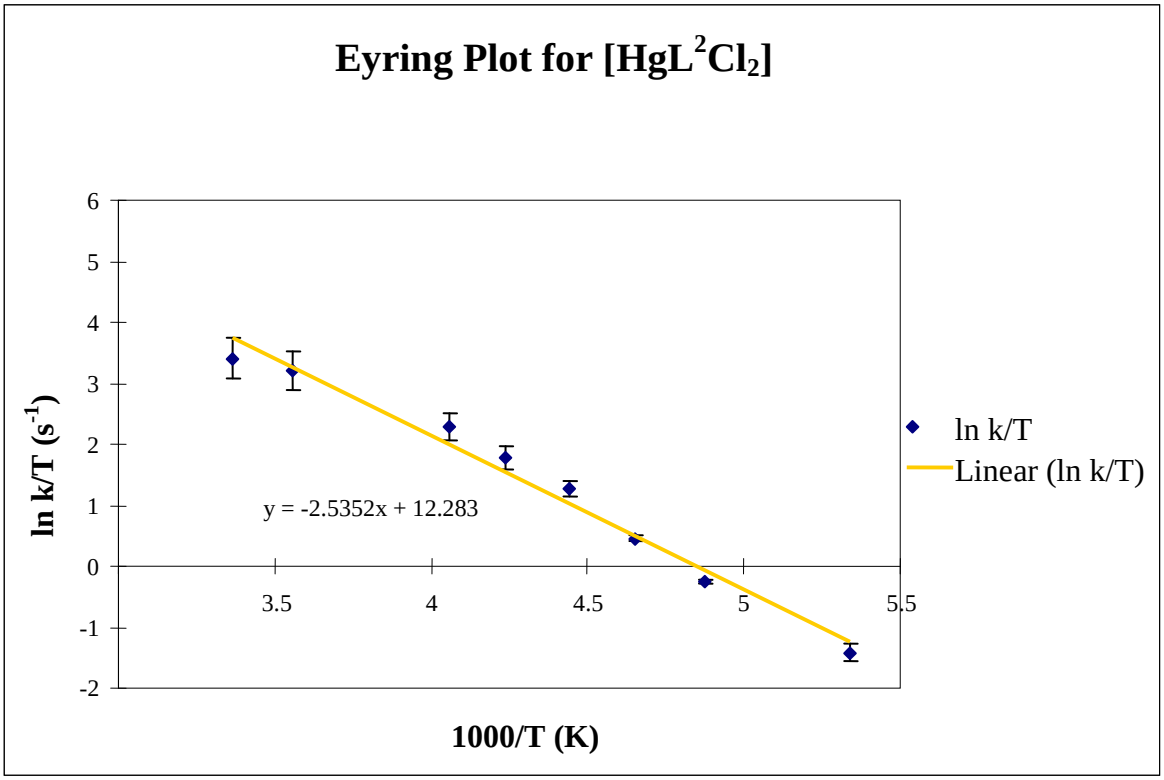

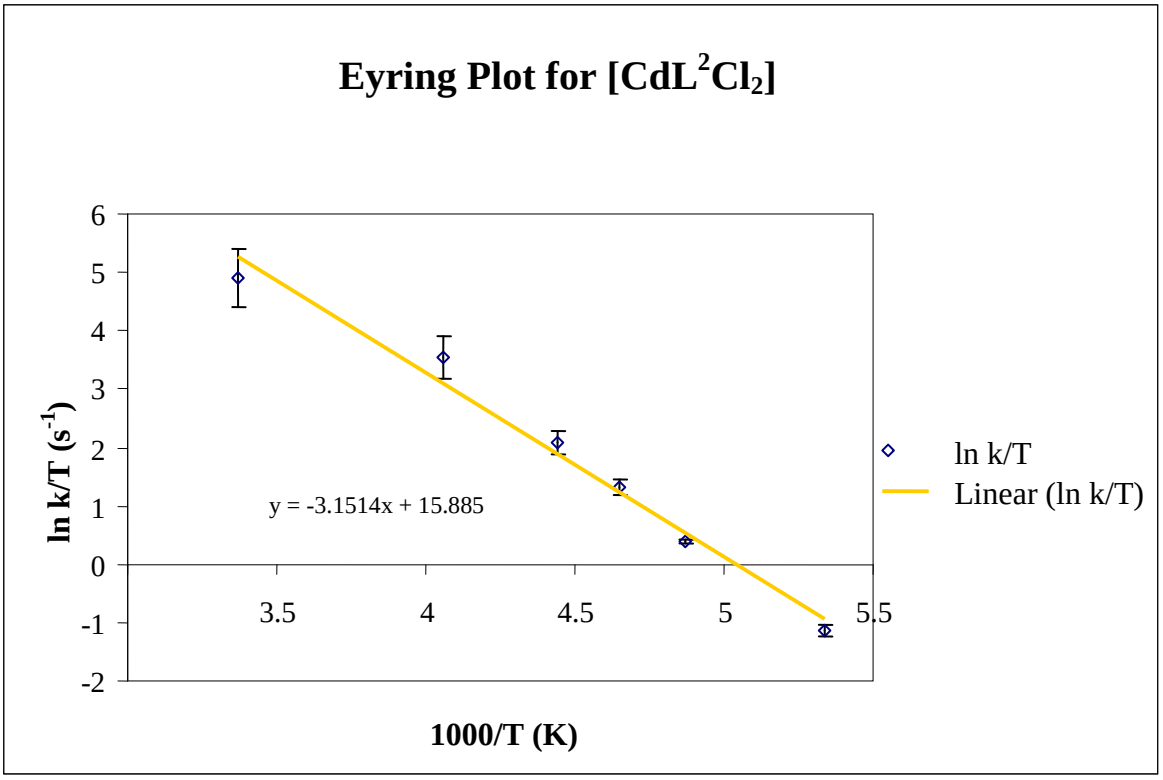

Graphs 3 and 4 Eyring plots for $[HgL^2Cl_2]$ and $[CdL^2Cl_2]$

A reasonable explanation for the negative value of $\Delta S^{\ddagger}$ would be synchronous rupture and formation of bonds,[1] or additional bond formation.[27] This combined with the lengthening of the M-$N_{Phosphazene\ ring}$ bonds, and tendency towards equality for the internal P-N bonds and towards planarity for the phosphazene ring all indicate a lower energy, more ordered state. However the presence of five and six-coordinate species in the X-ray structure for $[CdL^2Cl_2]\cdot 4CH_2Cl_2$, as well as an apparent intermediate state indicates that the dynamic behaviour is not solely governed by thermodynamics.

Modelling the $[ZnL^2Cl_2]$ system at the low temperature limit is particularly limited in terms of the existing software capabilities, although four peaks can be generated, the intensity of all four cannot be simulated simultaneously or accurately enough to provide reliable data for thermodynamic calculations. If a five-coordinate minor species does exist as indicated by the weak fifth signal at 7.95 ppm in Figure 36, then it can be reasoned that this is one of two singlets, the second of which may underlie the four peak pattern. However, the broadness of the peaks does not allow accurate integration to confirm this.

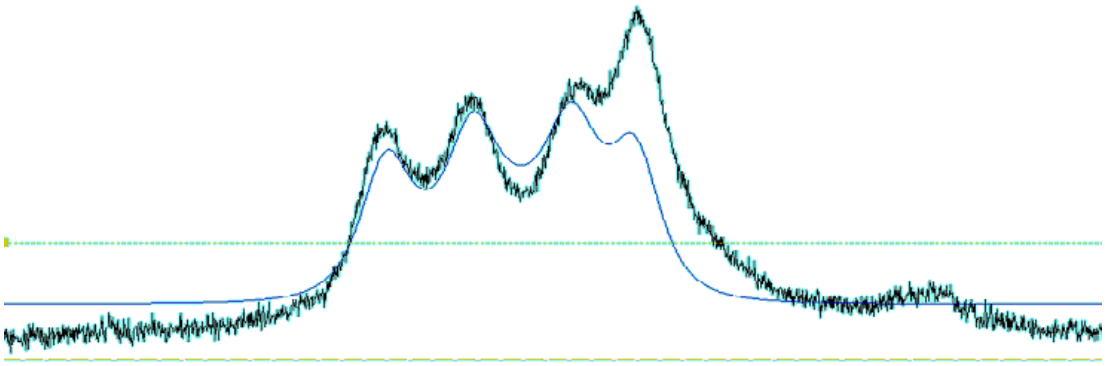

Figure 36 Attempted lineshape modelling of the [ZnL2Cl2] 1H VT NMR spectrum

4.4.2 $^{31}P\{^1H\}$ VT NMR studies on the complexes

The $^{31}P\{^1H\}$ NMR spectra for $[CdL^2Cl_2]$ and $[HgL^2Cl_2]$ demonstrate a doublet and triplet at all temperatures (Figure 37) ($[CdL^2Cl_2]$: 6.47 ppm *d*, 23.88 ppm *t*, $^2J_{(PA\text{-}PB)}$ = 106 Hz. $[HgL^2Cl_2]$: 7.57 ppm *d*, 25.06 ppm *t*, $^2J_{(PA\text{-}PB)}$ = 99 Hz) indicating that there is no change in the environment of the phosphorus atoms on cooling.

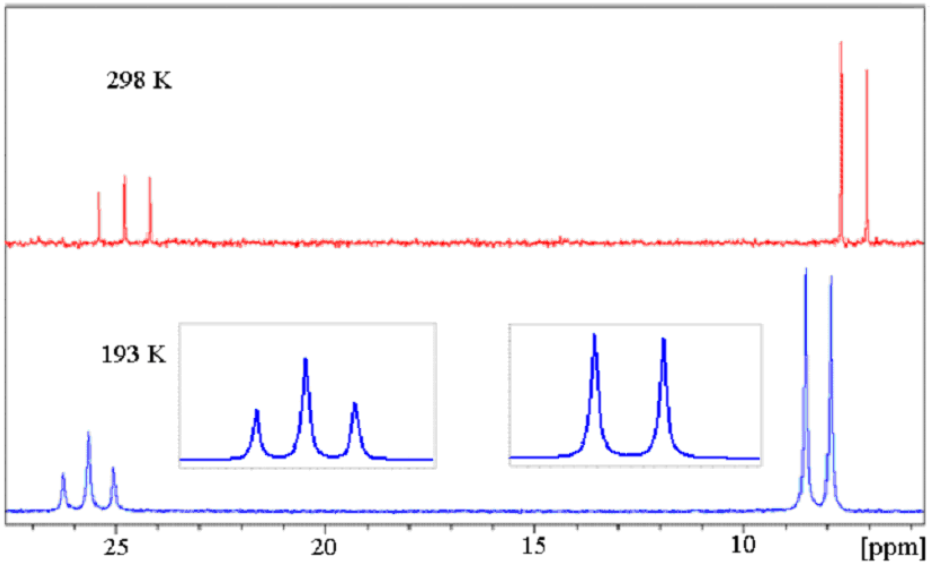

Figure 37 $[HgL^2Cl_2]$ $^{31}P\{^1H\}$ NMR at 298 K (top) and 223 K

However, the $[ZnL^2Cl_2]$ complex demonstrates a different behaviour at the low temperature limit (Figure 38). At 298 K the doublet - triplet pattern indicates that two of the three P atoms are in an equivalent environment. After coalescence three triplets are observed and clearly defined at 193 K, and an underlying minor species appears as a weak doublet - triplet (Major: 6.96 ppm *t*, 11.31 ppm *t*, 24.65 ppm *t*, $^2J_{(PA\text{-}PB)}$ = 89 Hz. Minor: 7.33 ppm *d*, 22.26 ppm *t*, $^2J_{(PA\text{-}PB)}$ = 91 Hz). These are shown schematically in Figure 39.

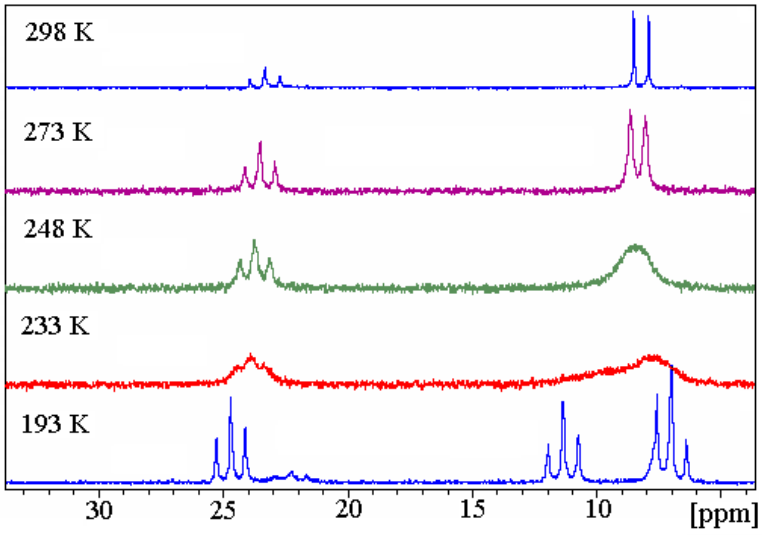

Figure 38 $^{31}P\{^1H\}$ NMR for $[ZnL^2Cl_2]$ at 298 K - 193 K

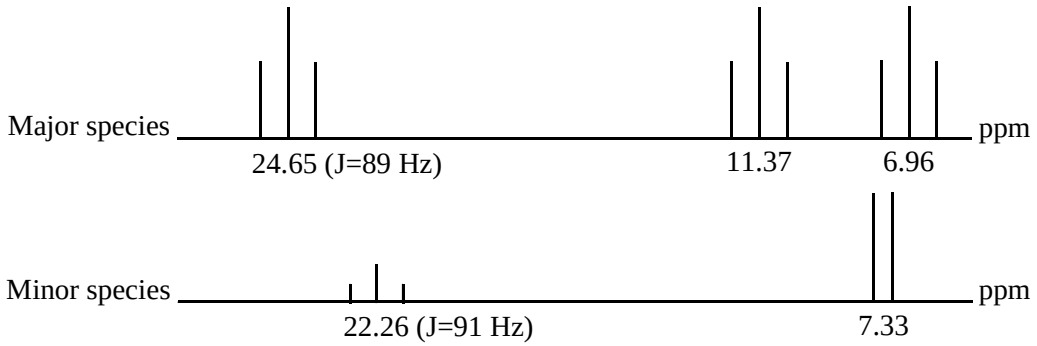

Figure 39 Schematic diagram of the major and minor species present in the $^{31}P\{^{1}H\}$ NMR of the $[ZnL^{2}Cl_2]$ complex at 193 K

Integrating the triplet pattern at 193 K gave a 1:1:1.7 ratio, indicating that underlying the triplet at 6.96 ppm there is a second component. A 2D COSY NMR (Figure 40) was performed at low temperature and it is readily apparent that there is an underlying doublet coupled to the minor species triplet suggesting that for the minor species, two of the phosphorus atoms are equivalent.

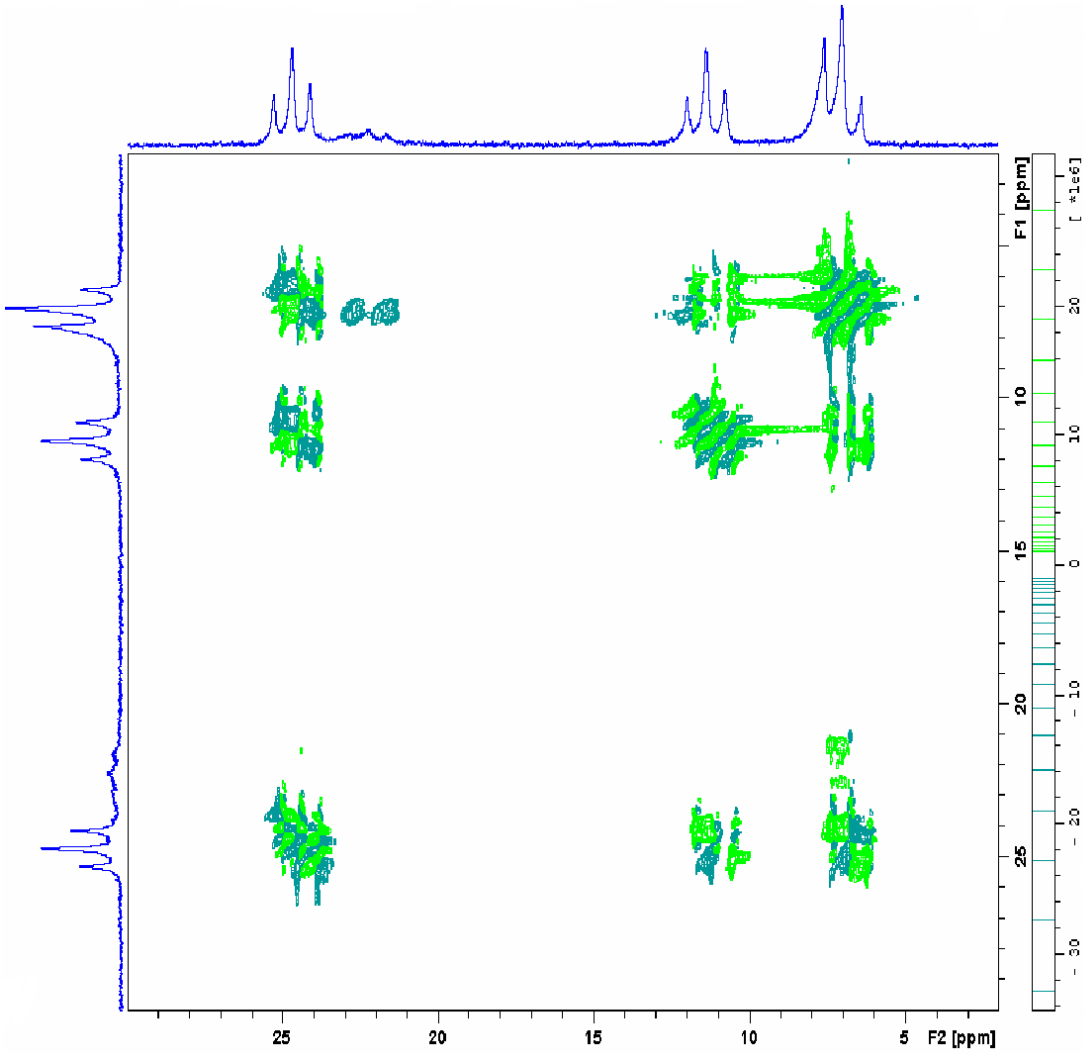

Figure 40 $^{31}P\{^{1}H\}$ COSY NMR for $[ZnL^{2}Cl_2]$ in CD_2Cl_2 at 193 K

Towards the low temperature limit, the 2D Cosy $^{31}P\{^{1}H\}$ NMR revealed a minor species in the $[ZnL^{2}Cl_2]$ complex as an underlying doublet and triplet (t, 22.3 ppm, d, 7.3 ppm), and two possible hypotheses could account for this phenomenon.

Firstly, the $ZnCl_2$ could dissociate to leave free ligand which, since only a small proportion is evident in the spectra, would imply a dynamic equilibrium between $[ZnL^{2}Cl_2]$ and $\mathbf{L^2}$ + $ZnCl_2$, because if the process occurred purely as a result of low temperature energetics one would expect to see complete transformation to free ligand. The main objection to this being the actual phenomenon observed, is that the process is fully reversible and that as the temperature is increased the minor species doublet/triplet pattern disappears to leave the three triplets. To avoid mechanical stress on the NMR

tube, the low temperature experiments were performed in a static environment i.e. with no spinning of the tube, thus the only source of agitation within the sample is that of temperature gradients while adjusting the temperature between recording successive spectra, which seems an unlikely explanation for complete homogeneity and reformation of the complex.

Secondly, a structural rearrangement could occur at low temperature, one that does not involve dissociation of the $ZnCl_2$ moiety and liberation of free ligand. To test these hypotheses, a small quantity of free ligand was added to solutions of the $[ZnL^2Cl_2]$, $[HgL^2Cl_2]$ and $[CdL^2Cl_2]$ complexes and low temperature $^{31}P\{^1H\}$ NMR spectra were recorded. The spectra (Figures 41-43) clearly demonstrate that the free ligand is present as a separate species at all temperatures, and that the minor species observed is therefore more likely to be due to a non-dissociative structural rearrangement in which two of the P atoms are magnetically equivalent, and not free ligand undergoing an upfield shift with temperature.

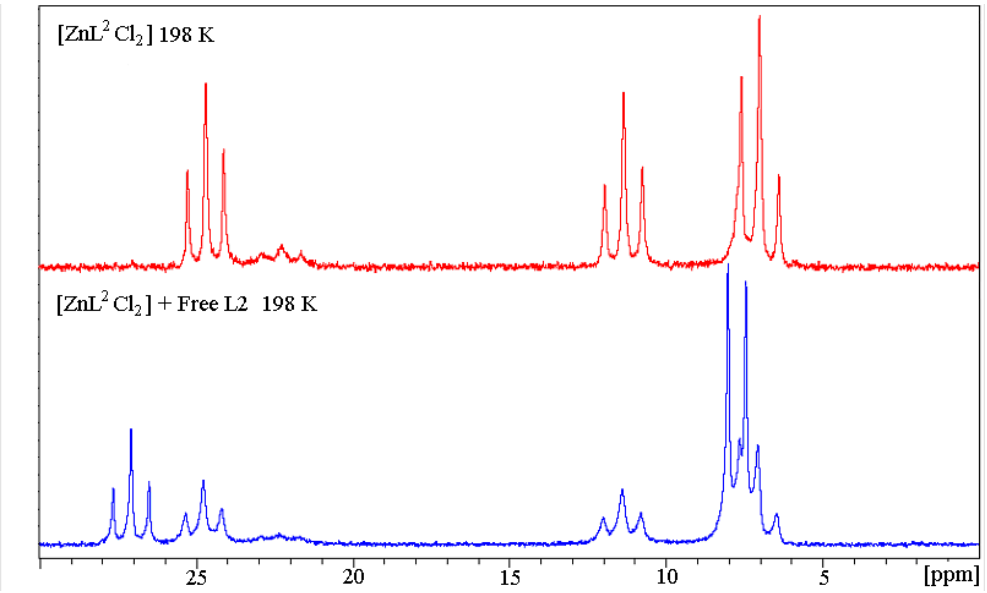

Figure 41 $^{31}P\{^1H\}$ NMR at 198 K – Top $[ZnL^2Cl_2]$, bottom $[ZnL^2Cl_2]$ plus free $\mathbf{L^2}$

For the $[ZnL^2Cl_2]$ complex above, the triplet of the minor species (centred at approximately 22.3 ppm) can clearly be discerned at 198 K.

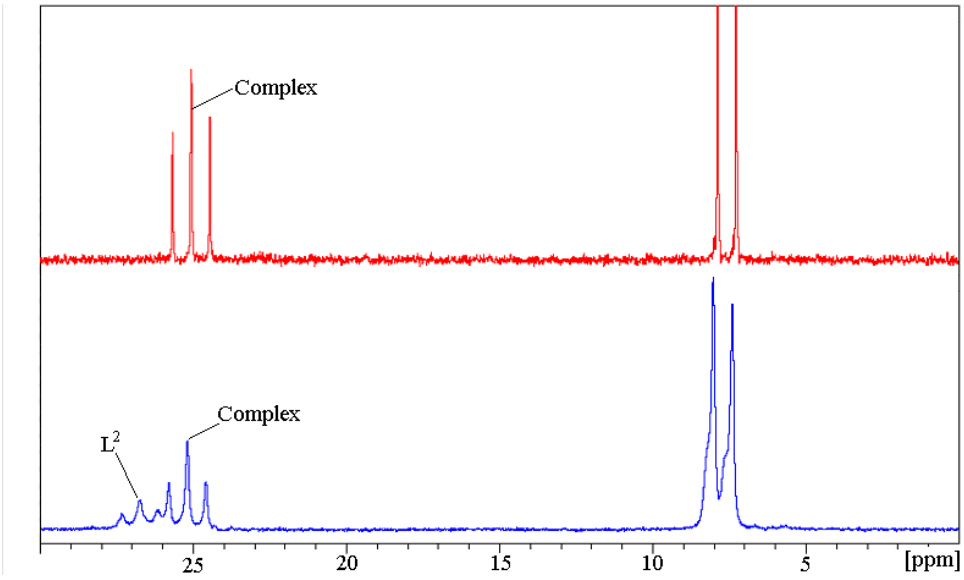

Figure 42 $^{31}P\{^{1}H\}$ NMR at 223 K - Top $[HgL^{2}Cl_{2}]$ and bottom $[HgL^{2}Cl_{2}]$ plus free $\mathbf{L^{2}}$

It is worth noting that for the $[HgL^{2}Cl_{2}]$ complex it is the triplet (assigned to the phosphorus bearing the 2,2'- biphenolate moiety) that shifts on complexation to the metal ion, not the doublet (assigned to the equivalent phosphorus atoms bearing the 4-methyl-2-pyridyloxy moieties). It can also be seen that the signals overlap to an extent.

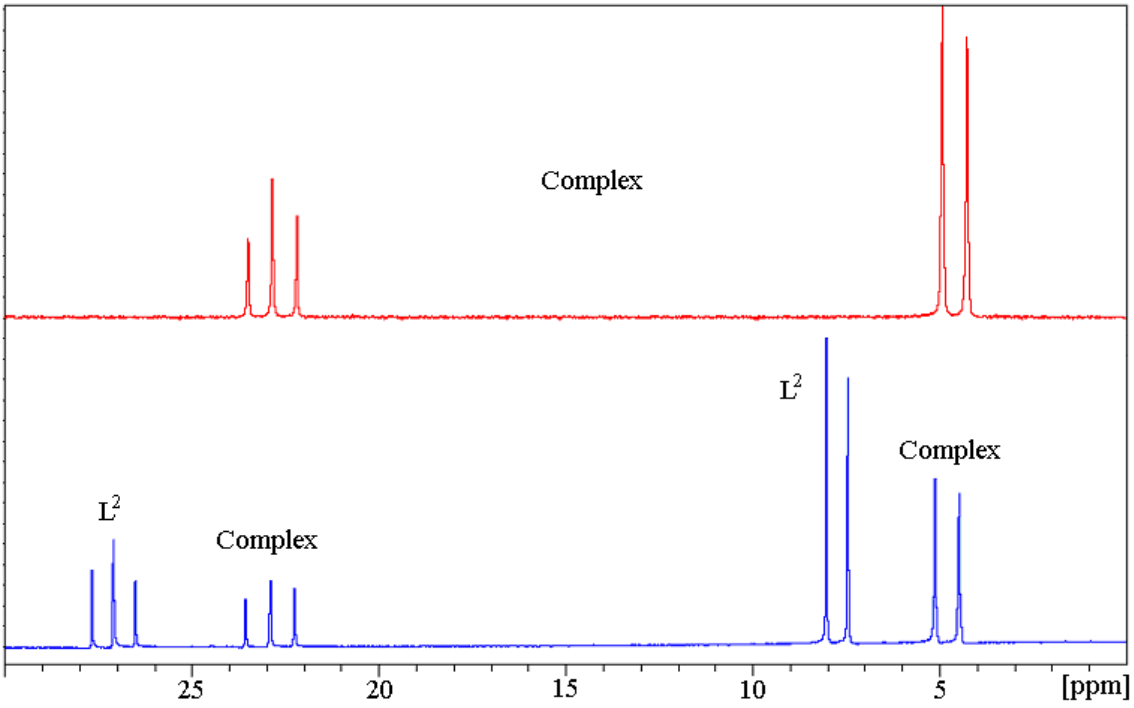

Figure 43 $^{31}P\{^{1}H\}$ NMR at 198 K – Top $[CdL^{2}Cl_{2}]$ and bottom $[CdL^{2}Cl_{2}]$ plus free $\mathbf{L^{2}}$

For the $[CdL^2Cl_2]$ complex the spectra are clearly unambiguous without the overlap evident in the $[HgL^2Cl_2]$ complex or any evidence for the presence of minor species.

4.4.3 Possible mechanisms of fluxional behaviour

Work by Byun *et al*.[5] and by Ainscough *et al*.[6] on hexakis-substituted cyclotriphosphazenes complexed to either Zn or Cd in mono or dinuclear ratios, has suggested that NMR spectra can, in part, be explained by rationalising the spectra in terms of known structures from X-ray data. For $[CdL^2Cl_2]$ and by inference, $[HgL^2Cl_2]$, it is therefore postulated that the TBP structure is retained at all temperatures measured, given the solvent-limited range, and that the observed fluxional spectra are due to coordination exchange of the pyridyl arms with the metal centre which, at room temperature, is sufficiently rapid on the NMR timescale to result in a time averaged doublet in the ^1H spectrum for the protons *ortho* to the pyridyl nitrogen atoms. Below T_c this rate of exchange decreases and two proton environments can be distinguished as equally intense singlets integrating at 1:1. The crystal structure of the Cd complex indicates a possible intermediate, dis-$[CdL^2Cl_2]$, for the exchange process and since this is not visible in the ^1H or $^{31}P\{^1H\}$ spectra of $[CdL^2Cl_2]$ or $[HgL^2Cl_2]$, this would suggest that at the temperatures achievable this intermediate either has a shorter lifetime than the NMR timescale, or its formation is not yet energetically favourable.
For $[ZnL^2Cl_2]$, by analogy with the solution rearrangement of the $[CoL^2Cl_2]$ complex reported in Chapter three, and with X-ray data to confirm that both TBP and tetrahedral structures are possible, it is argued that at room temperature in solution, the Zn forms a tetrahedral structure which undergoes rapid exchange with the pyridine rings (Figure 44) such that the two phosphorus atoms to which the pyridines are attached appear equivalent and give a time averaged A_2B signal in the $^{31}P\{^1H\}$ VT NMR spectrum.

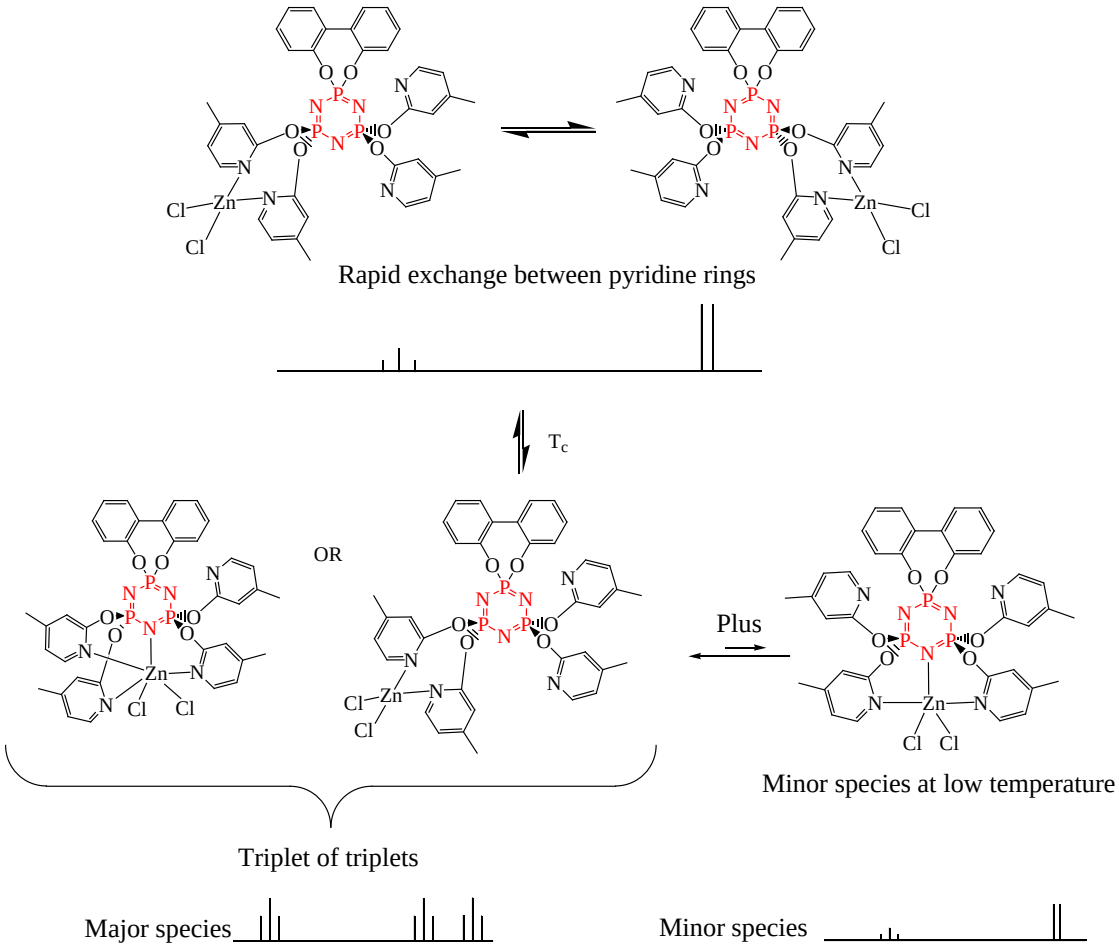

Figure 44 Top: Room temperature configuration with rapid exchange between pyridine rings. Bottom: Possible configurations at low temperature

Below T_c the three observed triplets in the $^{31}P\{^1H\}$ VT NMR spectrum can be viewed as three overlapping doublets of doublets where the J coupling is such that the signals appear as pseudo triplets (see Figures 38 and 44). It is then not unreasonable to propose that the required non-equivalence in the phosphorus environments can be achieved by two possible mechanisms.

(i) $[ZnL^2Cl_2]$ could adopt the six-coordinate structure demonstrated by oct-$[CdL^2Cl_2]$ and that this has a sufficiently long lifetime to be observable on the NMR timescale

(ii) that the rapid exchange of pyridine arms merely slows below T_c to a point whereby the tet-$[ZnL^2Cl_2]$ structure becomes distinguishable.

In each case, as the low temperature limit is approached the five-coordinate structure appears as the underlying doublet-triplet of the minor species. This hypothesis also explains the observed four signals for the *ortho* proton in the ^{1}H VT NMR spectrum, arising from 4 non-equivalent sites with, at the low temperature limit, a fifth signal being part of the five-coordinate environment of the minor species.

Of the two possible mechanisms, the six-coordinate oct-$[CdL^{2}Cl_{2}]$ structure may well be applicable to $[ZnL^{2}Cl_{2}]$. If this structure were to follow the same trends as Cd in terms of reduced ring strain and greater bond lengths on formation of a six-coordinate structure, then it may represent a viable low energy conformation existing in parallel with the five-coordinate structure. For the $[CdL^{2}Cl_{2}]\cdot 4CH_{2}Cl_{2}$ X-ray structure to exhibit three different structures in the unit cell implies that this must be favourable on energetic grounds.

4.5 Conclusions

Fluxional behaviour has been investigated for the complexes $[ZnL^{2}Cl_{2}]$, $[CdL^{2}Cl_{2}]$ and $[HgL^{2}Cl_{2}]$, using VT NMR with subsequent lineshape analysis and X-ray crystal structures. Evidence emerged to suggest that transition metal halides formed TBP complexes with $\mathbf{L^{2}}$, but further results revealed that fluxional behaviour was taking place. The design of $\mathbf{L^{2}}$, having a readily identifiable *ortho* proton signal for ^{1}H VT NMR gave a very useful probe for studying this behaviour.

$[CdL^{2}Cl_{2}]$ and $[HgL^{2}Cl_{2}]$ act in a very similar fashion in $CD_{2}Cl_{2}$, with the *ortho* proton signal going from a well defined doublet at room temperature to two broad singlets at the low temperature limit of the solvent. Both systems were capable of lineshape analysis to yield thermodynamic data. The $^{31}P\{^{1}H\}$ VT NMR revealed a doublet-triplet system at all temperatures measured and the NMR spectra are consistent with coordination exchange of pyridine arms to the metal centre.

The single crystal X-ray structure for $[CdL^{2}Cl_{2}]\cdot 4CH_{2}Cl_{2}$ contained three molecules of the complex in five and six-coordinate modes, including one disordered molecule showing an intermediate structure exhibiting coordinative exchange of a 2-oxypyridine moeity. However the $^{31}P\{1H\}$ VT NMR spectra can only be interpreted as an $A_{2}X$ system with two equivalent phosphorus sites leading to the conclusion that the five-

coordinate structure is dominant in solution. No evidence can be seen for an intermediate or six-coordinate structure suggesting that they are either not present at the temperatures available or that they have a lifetime that is not detectable on the NMR timescale.

^{1}H and $^{31}P\{^{1}H\}$ VT and COSY NMR spectra for the $[ZnL^{2}Cl_2]$ complex revealed more complex behaviour that can be interpreted as a rapidly exchanging tetrahedral form at room temperature. Below T_c an ABX spectrum in the $^{31}P\{^{1}H\}$ VT NMR spectra with three non-equivalent phosphorus atoms that may be of tetrahedral or octahedral geometry is observed. At the low temperature limit in the $^{31}P\{^{1}H\}$ VT NMR spectra, a minor species A_2X system is evident that is postulated to be the five-coordinate structure as found in the X-ray structure.

Lineshape analysis for the $[ZnL^{2}Cl_2]$ complex was not successful due to the variation in intensity and broadness of the signals, possibly due to an underlying component of the minor species. Despite two X-ray structures indicating different modes of crystallisation, it is postulated that the overriding factors involved are packing forces and solvent dispersal in the crystalline state and that in solution, both structures tbp-$[ZnL^{2}Cl_2]\cdot CH_2Cl_2$ and tet-$[ZnL^{2}Cl_2]$ behave identically as a tetrahedral species at ambient temperature which resolves to the TBP form at the low temperature limit.

4.6 References

1. Canovese, L.; Lucchini, V.; Santo, C.; Visentin, F.; Zambon, A., *J. Organomet. Chem.* **2002,** 642, 58.

2. Di Vaira, M.; Mani, F.; Costantini, S. S.; Stoppioni, P.; Vacca, A., *Eur. J. Inorg. Chem.* **2003,** 17, 3185.

3. Song, D.; Jia, J. L.; Wu, G.; Wang, S., *J. Chem. Soc., Dalton Trans.* **2005**, 433.

4. Schlager, O.; Wieghardt, K.; Grondey, H.; Rufinska, A.; Nuber, B., *Inorg. Chem.* **1995,** 34(26), 6440.

5. Byun, Y.; Min, D.; Do, J.; Yun, H.; Do, Y., *Inorg. Chem.* **1996,** 35, 3981.

6. Ainscough, E. W.; Brodie, A. M.; Depree, C. V.; Otter, C. A., *Polyhedron* **2006,** 25, 2341.

7. Ainscough, E. W.; Brodie, A. M.; Depree, C. V., *Private communication*.

8. Justin Thomas, K. R.; Chandrasekhar, V.; Zanello, P.; Laschi, F., *Polyhedron* **1997,** 16(7), 1003.

9. Rivals, F.; Steiner, A., *Eur. J. Inorg. Chem.* **2003,** 18, 3309.

10. Heston, A. J.; Panzner, M. J.; Youngs, W. J.; Tessier, C. A., *Inorg. Chem.* **2005,** 44(19), 6518.

11. Simonutti, R.; Veeman, W. S.; Ruhnau, F. C.; Gallazzi, M. C.; Sozzani, P., *Macromolecules.* **1996,** 29(14), 4958.

12. Taylor, S. A.; White, J. L.; Elbaum, N. C.; Crosby, R. C.; Campbell, G. C.; Haw, J. F., *Macromolecules* **1992,** 25(13), 3369.

13. Allcock, H. R.; Cameron, C. G.; Skloss, T. W.; Taylor-Meyers, S.; Haw, J. F., *Macromolecules* **1996,** 29, 233.

14. Crosby, R. C.; Haw, J. F., *Macromolecules* **1987,** 20(9), 2324.

15. Van Geet, A. L., *Anal. Chem.* **1970,** 42, 679.

16. Marat, K., SpinWorks, www.umanitoba.ca/chemistry/nmr/spinworks/ accessed June 2006.

17. Bunnett, J. F., *Investigation of rates and mechanisms of reactions*. Bernasconi, C. F., John Wiley and Sons: New York, 1986; Vol 6 (1), p. 288-298.

18. Turner, D. M., *Investigation of rates and mechanisms of reactions*. Bernasconi, C. F., John Wiley and Sons: New York, 1986; Vol.1, Pt2, p. 178.

19. Sheldrick, G. M. *SHELXL Suite of Programs for Crystal Structure Analysis*, Institüt für Anorganische Chemie der Universität, Tammanstrasse 4, Göttingen, Germany: 1998.

20. Van der Sluis, P.; Spek, A. L., *Acta Crystallogr. Sect. A 46,* **1990**, 194.

21. Cahn, R. S.; Ingold, C. K.; Prelog, V., *Ang. Chem. Int. Ed.* **1966,** 5, 385.

22. Shannon, R. D., *Acta Crystallogr. A 32.* **1976**, 751.

23. Addison, A. W.; Rao, T. N.; Reedijk, J.; Van Rijn, J.; Verschoor, G. C., *J. Chem. Soc., Dalton Trans.* **1984,** 7, 1349.

24. Ainscough, E. W.; Brodie, A. M.; Derwahl, A.; Kirk, S.; Otter, C. A., *Inorg. Chem.* **2007,** 46(23), 9841.

25. Hoffman, R. E.; Becker, E. D., *J. Magn. Reson.* **2005,** 176, 87.

26. Bain, A. D.; Rex, D. M.; Smith, R. N., *Magn. Reson. Chem.* **2001,** 39, 122.

27. Kajiwara, T.; Yokozawa, S.; Ito, T.; Iki, N.; Morohashi, N.; Miyano, S., *Agnew. Chem. Int. Ed.* **2002,** 41, 2076.

Chapter 5: Synthesis and Reactions of Polyphosphazenes with Selected Transition Metal Dichlorides

5.0 Abbreviations used in Chapter 5

ROP	ring opening polymerisation
TFE	trifluoroethoxy (CF_3CH_2O)
2O-6-MePy	2-pyridyloxy-6-methylpyridine
biph	2,2'-dioxybiphenyl
2O-4-MePy	2-pyridyloxy-4-methylpyridine
2OPy	2-oxypyridine
DSC	differential scanning calorimetry
PDI	polydispersity index (M_w/M_n)
T_g	glass transition temperature
GPC	gel permeation chromatography
ε	molar absorptivity
M_n	number average molecular weight

$$M_n = \frac{\sum N_i M_i}{\sum N_i}$$ where N_i is the number of molecules of M_{weight} M_i

M_w	weight average molecular weight

$$Mw = \frac{\sum N_i M_i^2}{\sum N_i M_i}$$

TBAN	tetra(butyl)ammonium nitrate

5.1 Introduction

The discovery by Allcock *et al.*[1-3] of a successful route for the uncrosslinked polymerisation of cyclotriphosphazene via thermal ring opening polymerisation (ROP) has led to a burgeoning field of research into polyphosphazenes. Since then, a number of polymerisation methods have been reported in the literature with increasing success in terms of lower temperature syntheses and faster rates, and these are summarised below. Only the more important aspects will be discussed later. Radiation techniques have been reported in the literature[4] but are not discussed further herein, being beyond the scope of the present research.

5.1.1 Timeline synopsis for major synthetic routes to $[NPCl_2]_n$

After the initial report by Stokes[5], it took a further 68 years before an improved method for the synthesis of the polymer was published by Allcock *et al.*[6] This and more recent reports are listed below:

- 1965 Thermal ROP — Allcock *et al.*[1]
- 1990 Solution polymerisation of $N_3P_3Cl_6$ — Mujumdar *et al.*[7]
- 1991 Strain induced polymerisation — Allcock *et al.*[8]
- 1992 Polyphosphazenes from $Cl_3P{=}NP(O)Cl_2$ — D'Halluin *et al.*[9]
- 1995 Ambient temperature synthesis of $(NPCl_2)_n$ — Allcock *et al.*[10]
- 2003 One pot synthesis from PCl_5 — Carriedo *et al.*[11]
- 2005 One pot synthesis from PCl_3 — Wang[12]

Polyphosphazenes have yet to be exploited on a wide commercial basis, due largely to the lack of a successful scale-up regimen and, by implication, cost. Without doubt, the synthetic utility of $[NPCl_2]_n$ as a precursor allows for a wide range of micro- and macroscopic properties to be imparted, dependent upon the pendant side groups substituted onto the polymer backbone, and the polymer architecture employed e.g. linear, copolymer, block copolymer, hybrid, cyclo-matrix, star dendrimer and so on. To date, over seven hundred phosphazene high polymers are claimed by Allcock alone,[13] and over three hundred known poly(organo)phosphazenes were reported in a 1998 review by De Jaeger *et al.*[14]

Whilst the thermal ring opening polymerisation route remains the most common method to date for synthesis of the high polymer, recent years have seen much progress in alternative methods. The thermal route, though expensive in terms of energy demand, requiring the maintenance of a 250°C environment for eight or more hours, can produce polymers with molecular weights in the order of 10^6 Daltons with relatively narrow polydispersities. High molecular weight polymers impart greater mechanical properties on a macroscopic level, though it is known that lower molecular weight polymers more readily facilitate polymer blends.[14] As with most materials, the achievable properties are often a compromise between the desired characteristics, available processing technology, and cost.

5.1.1.1 Thermal ring opening polymerisation (ROP)

The thermal ROP route developed in 1965 by Allcock *et al*.,[1-3] successfully achieved an uncrosslinked and usable polymer by application of more rigorous methods than Stokes[5] was able to utilise. This technique, despite being developed over forty years ago, is still not fully understood in terms of the effects of trace elements and catalytic pathways.

The thermal ROP process is largely reliant on observational experience to monitor the progress of the reaction to decide upon the end point by judging the viscosity and colour of the melt. The end point is generally at 50-60% conversion of the cyclophosphazene to the polymeric form since conversion beyond 75%, or further heating, can lead to crosslinking, formation of side chains and subsequent insolubility ultimately resulting in the "inorganic rubber" described by Stokes,[5] or depolymerisation to cyclic species.[13] The general scheme for the thermal ROP process is shown in Figure 1 where thermal polymerisation is closely followed by nucleophilic substitution of chlorine, under strictly anhydrous conditions, to yield stable polymers.

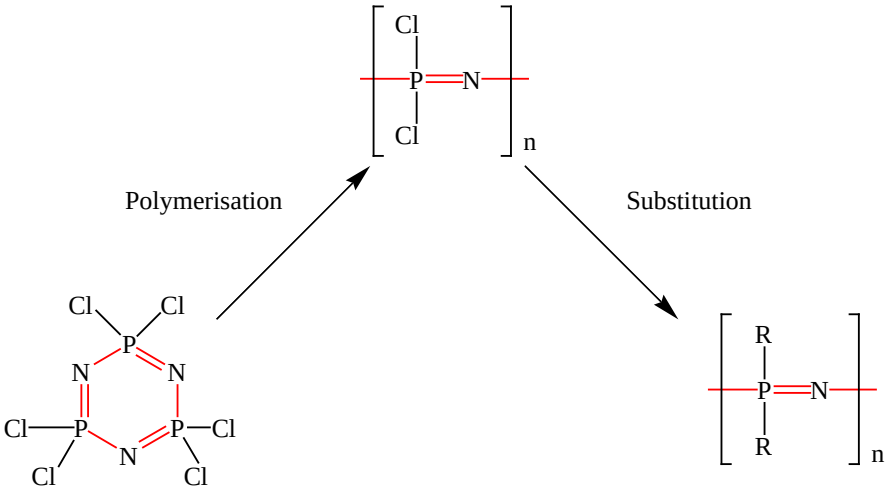

Figure 1 General scheme for thermal ROP

The mechanism of the thermal ROP reaction has been variously discussed in the literature in terms of being radical, anionic or cationic in nature, and it is now generally accepted to be a cationic process.[14] Lee *et al*.[15] concluded a cationic mechanism following in situ light scattering and Raman spectroscopy investigations.
Although still open to debate, a proposed mechanism for initiation, propagation and termination is shown in Figure 2. This scheme also accounts for side branching and crosslinking.[14]

With reference to Figure 2, the steps are:

1) Formation of a phosphazene phosphorus cation by cleavage of a P-Cl bond.
2) Chain propagation by nucleophilic attack on the cation.
3) Termination on decreasing temperature.
4) Formation of side branches.
5) Crosslinking.

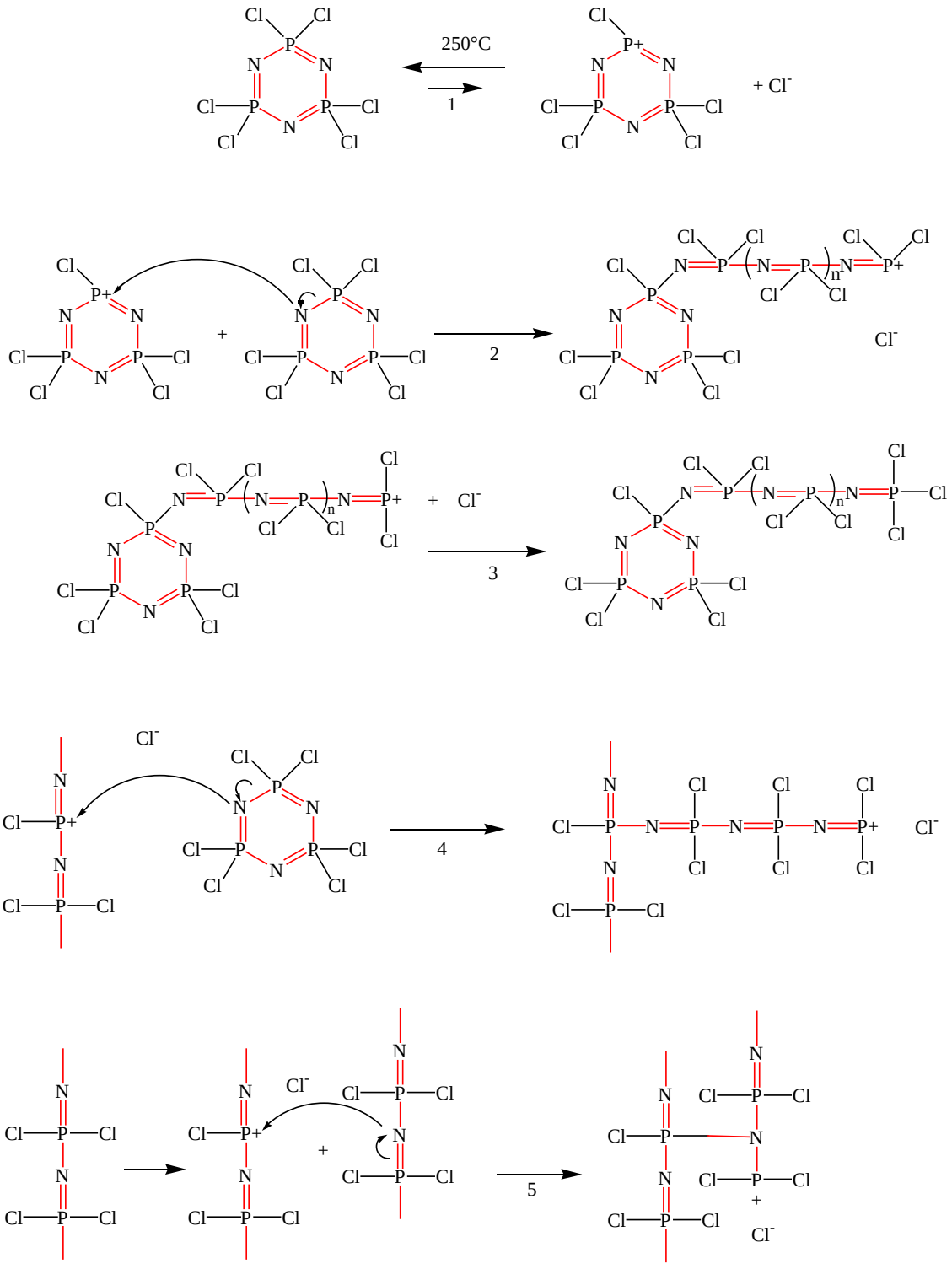

Figure 2 Proposed reaction mechanism for bulk thermal polymerisation of $[N_3P_3Cl_6]$ from De Jaeger *et al.*[14]

5.1.1.2 Effect of water on thermal ROP

Highly purified cyclotriphosphazene may require up to two weeks to polymerise whereas exposure to atmosphere prior to polymerisation can yield 60% polymer in eight hours under the same thermal ROP conditions.[16] It has been shown that traces of water react with the cyclotriphosphazene to form HCl and it is this that is claimed to be responsible for the catalytic effect.[7] The concentration of water is critical, its absence resulting in long reaction times and broad polydispersities. An optimal concentration leads to the formation of HCl and its catalytic effect to give high molecular weight and narrow polydispersity. Too high a concentration leads to side branching and crosslinking through reaction of the P-Cl bonds forming P-O-P bonds between chains.

Early work by MacCallum *et al*.[17] demonstrated the effect of water concentration (Table 1).

Sample	Water conc. %	Polymerisation %	Colour of polymer	Chlorine detected
1	0	38	White	No
2	1×10^{-2}	38	Light brown	No
3	2×10^{-2}	62	Brown	Yes
4	3×10^{-2}	89	Black	Yes

Table 1 Results of water concentration reported by MacCallum *et al*.[17] Samples were heated for 24 hours at 236°C

Gel formation is a secondary feature associated with water in polyphosphazene solutions. Gels are not soluble, and having little synthetic value, are usually discarded. Gabler *et al*.[18] reported gel formation when approximately 7% of the P-Cl groups become hydrolysed and using NMR techniques, suggested that gel formation is the result of hydrogen bonding between Cl-P-OH groups rather than P-O-P crosslinking.

5.1.1.3 Promoters and catalysts for thermal ROP

Various promoters and catalysts have been investigated to improve the synthetic yield. Metals and metal oxides have generally been shown to be poor catalysts for polymerisation of polyphosphazenes.[19, 20]

Ganapathiappan *et al*.[21] reported the use of $CaSO_4 \cdot 2H_2O$ as affording high yield and high molecular weight polyphosphazenes ($M_w \sim 10^6$ Daltons). Cho *et al*.[22] demonstrated that organotin(IV) chlorides could act as inhibitors delaying the rate of polymerisation leading to an improved yield and molecular weight, and that using greater than 2 wt.% of aluminium trichloride as a catalyst gave almost quantitative yield of lower molecular weight (10^4-10^5 Daltons) poly(dichloro)phosphazene. Further work demonstrated that using aluminium trichloride as a catalyst with diethyltin(IV) dichloride gave greater than 90% yield with increased molecular weight (10^6 Daltons).[23] As stated previously, the thermal ROP route has a high energy demand and a number of groups are actively researching alternative methods of inducing polymerisation.

5.1.1.4 Solution polymerisation of $[N_3P_3Cl_6]$

Mujumdar *et al*.[7] continued the work of Ganapathiappan *et al*.[21], studying the solution polymerisation of $N_3P_3Cl_6$ in 1,2,4-trichlorobenzene using sulfamic acid, to give comparable molecular weights to the thermal ROP route ($Mw \sim 10^6$ Daltons). The use of $CaSO_4 \cdot 2H_2O$ as a promoter with sulfamic acid gave reduced reaction times and polydispersities. Varying the catalyst concentration whilst maintaining constant promoter levels led to reduced molecular weight. This solution polymerisation, sometimes referred to as the "Magill method"[11] requires a slightly lower temperature (210°C) than the thermal ROP (250°C).

5.1.1.5 Strain induced polymerisation

Allcock *et al*.[8] reported the first uncatalysed ring opening polymerisation reaction in cyclotriphosphazenes that lacked phosphorus-halogen bonds, therefore proceeding by a different mechanism to that of the bulk chlorotriphosphazene. The traditional route to substituted polyphosphazenes had been to synthesise the chloropolymer $[NPCl_2]_n$ then perform the substitution reactions which leads to a statistical spread of substitution sites and the possibility of side reactions. If ring strain can be used to initiate the polymerisation of a substituted cyclotriphosphazene, then Allcock suggested that

because the substitution patterns for small molecules can be tailored, a possible route to polymers of known architecture might be possible (Figure 3).

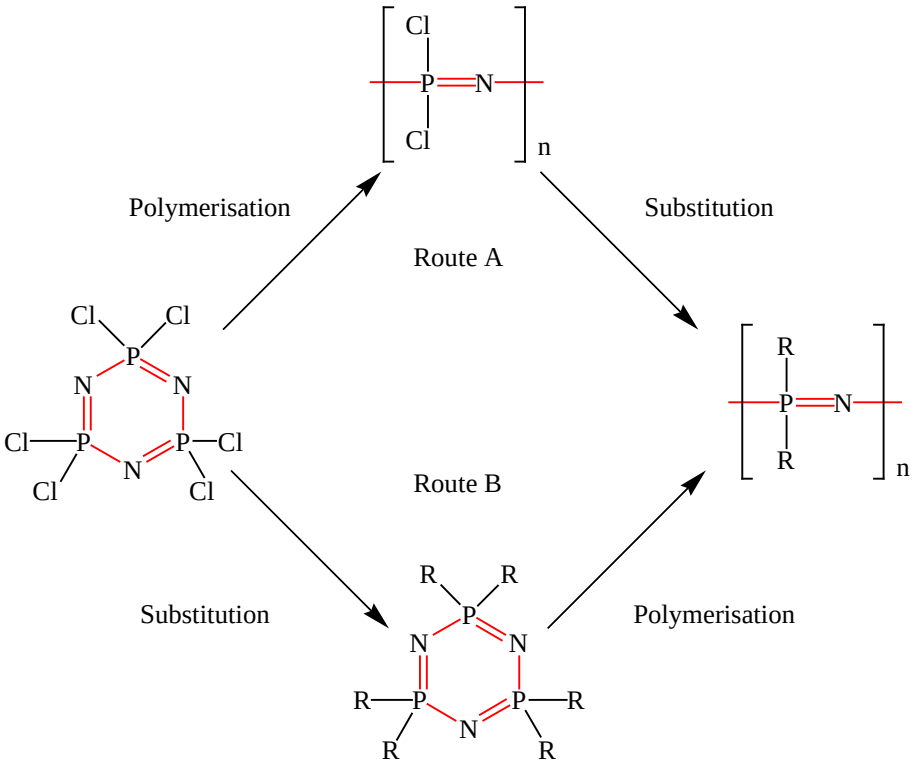

Figure 3 Two possible routes to polymer substitution

Polymerisation of the cyclic $[N_3P_3(OCH_2CF_3)_4(\eta\text{-}C_5H_4)_2Fe]$ occurred when 1 mol % of $N_3P_3Cl_6$ was present in the melt as an initiator (Figure 4). Without $N_3P_3Cl_6$ present, ring expansion to the cyclic hexamer was preferred.[8]

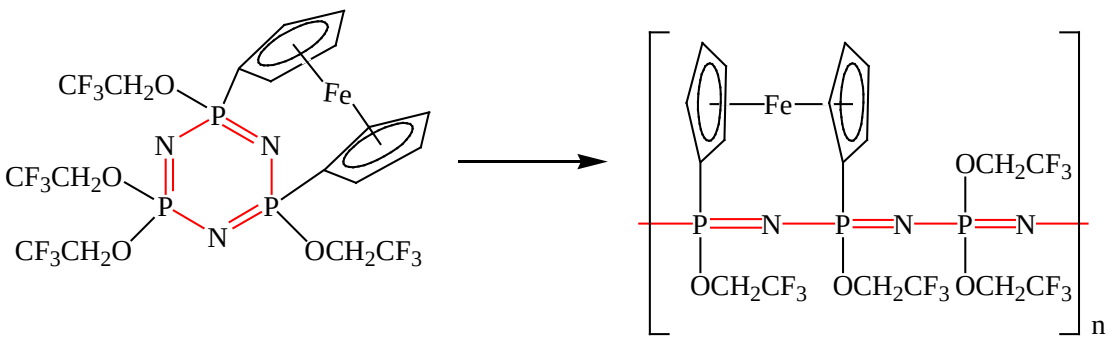

Figure 4 Ring strain induced by transannular ferrocene

Conditions governing the ring opening/ring expansion are:

(i) Steric bulk of the side groups
(ii) Presence or absence of $N_3P_3Cl_6$ as initiator
(iii) Reaction time.

This work was significant for two reasons. Firstly the mechanistic insight that a P-Cl bond was not present, and thus polymerisation occurred by a different route, since it had previously been thought that P-halogen bonds were necessary for initiation and propagation. Secondly, polymers of known architecture could be produced without the statistical distribution formed by nucleophilic substitution of the pendant chlorine on $[NPCl_2]_n$.

5.1.1.6 Polyphosphazenes from $Cl_3P=NP(O)Cl_2$

Polymers with molecular weights in the range $3 \times 10^4 - 1 \times 10^6$ Daltons were reported by D'Halluin *et al*.[9] for the solution polycondensation of P-trichloro-N-(dichlorophosphoryl)monophosphazene as shown in Equation 1.

$$n Cl_3P=N\text{-}P(O)Cl_2 \longrightarrow Cl_3P=N(PCl_2=N)_{n-1}P(O)Cl_2+(n\text{-}1)P(O)Cl_3 \quad \text{Eq 1}$$

The reaction is a two stage process requiring induction at 245°C followed by polymerisation at 276°C. Viscosity of the solution increases with reaction time indicating degree of polymerisation, thus allowing control of molecular weight and high conversion to polymer (~ 98%). As with the thermal ROP, this polycondensation reaction has a high energy demand but despite this, the French manufacturer Atochem saw sufficient promise to warrant pilot scale development.[14]

Allen *et al*.[24] filed a patent on a similar, solvent free synthesis in the melt phase, in which the yield of P-trichloro-N-(dichlorophosphoryl)monophosphazene was essentially quantitative. However, conversion to the poly(dichlorophosphazene) was still a thermal process requiring 225°C and precautions were required to avoid cross linking.[12]

5.1.1.7 Ambient temperature synthesis of $[NPCl_2]_n$

A major breakthrough came with the discovery by Allcock *et al.*[10] of an ambient temperature synthetic route to $[NPCl_2]_n$. Polymerisation of trichloro(trimethylsilyl)-phosphoranimine ($Cl_3P{=}NSiMe_3$) in CH_2Cl_2, initiated by PCl_5 was found to give near quantitative conversion to $[NPCl_2]_n$ with molecular weights up to 10^5 Daltons and narrow polydispersities (M_w/M_n = 1.04). Furthermore, the reaction was determined to be a "living" cationic polymerisation (Figure 5), as defined by Allcock *et al.*[25] which met the following criteria:

- Following first order kinetics with respect to monomer concentration,
- Number average degree of polymerisation is proportional to the monomer conversion. That is, the polymer continues to propagate in the presence of available monomer, ceases to grow when the monomer is consumed and commences growth in the presence of additional monomer,
- Molecular weight distribution corresponds to the Poisson distribution, and
- That the active polymer has a long shelf time.

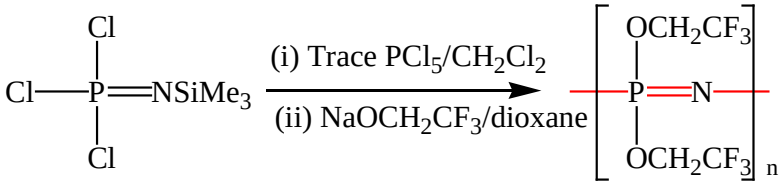

Figure 5 Schematic route for the living cationic polymerisation reported by Allcock *et al.*[25]

Synthesis of the phosphoranimine had been reported earlier by Niecke *et al.*[26] but with only 20% yield. This was increased to 60% by Honeyman *et al.*[27] by lowering the reaction temperature from +10°C to -78°C. However, synthesis of the monomer precursor was challenging due to inseparable side products which inhibited polymerisation.

Allcock *et al.*[28] discovered that reaction of $N(SiMe_3)_3$ with PCl_5 provided a route to either $[N_3P_3Cl_6]$ or pure $Cl_3P{=}NSiMe_3$ dependent on reaction conditions, however the yield of $Cl_3P{=}NSiMe_3$ by this method was still low at 40%.

Wang *et al*.[29] reported a new high yield synthesis of $Cl_3P{=}NSiMe_3$ in 2002 by oxidation of the chlorophosphine $Cl_2PN(SiMe_3)_2$ with sulfuryl chloride (SO_2Cl_2). Not only did this have an 80% yield, but more importantly utilised PCl_3 instead of PCl_5 which meant the concomitant side products were not formed. The temperature range for this reaction was 0°C to 25°C. The reaction is shown in Equations 2 and 3.

$$PCl_3 + LiN(SiMe_3)_2 \xrightarrow[0°C]{Et_2O} Cl_2P\text{-}N(SiMe_3)_2 + LiCl \qquad \text{Eq 2}$$

$$Cl_2P\text{-}N(SiMe_3)_2 + SO_2Cl_2 \xrightarrow[-ClSiMe_3]{Et_2O,\ 0°C} Cl_3P{=}N\text{-}SiMe_3 + SO_2 \qquad \text{Eq3}$$

5.1.1.8 One pot syntheses of $[NPCl_2]_n$

The syntheses discussed thus far are, by their very nature, small laboratory scale processes involving several steps. The key to a commercially exploitable synthetic route would require development of a one pot synthesis with the potential for continuous rather than batch processing. Peterson *et al*.[30] reported that the patent filed by Allen *et al*.[24] was the first reported one pot synthetic route to poly(dichlorophosphazene) but gave a bimodal GPC trace, indicating two discrete weight distributions. The yield was also lower (35%) compared to polymerisation of the purified $Cl_3{=}PNP(O)Cl_2$ which gave higher yield (55%) and a monomodal GPC trace.

Carriedo *et al*.[11] proposed that a one pot synthesis should be possible by elaboration of the scheme reported by Mujumdar *et al*.[7] since $[N_3P_3Cl_6]$ is a formation product from the reaction of PCl_5 and NH_4Cl with $CaSO_4.2H_2O$ as promoter and $HSO_3(NH_2)$ (sulfamic acid) as catalyst. Subsequent addition of trifluoroethanol or 2,2-dioxybiphenyl moieties with Cs_2CO_3 or K_2CO_3 as proton abstractors gave fully substituted polymers with a M_w and PDI similar to that obtained by the thermal ROP route. Although successful in achieving a one pot synthetic route, safety hazards on scale up above 100 g (e.g. small explosions due to sublimation of PCl_5 causing obstructions within the reactor) and the need for refluxing 1,2,4-trichlorobenzene (b.p. 214°C) would require a number of engineering and technical solutions before this process could be considered as

practical. In addition, the use of chlorinated solvents carries with it additional environmental concerns for large scale use.[12]

Wang[12] developed an ambient temperature synthesis for $[NPCl_2]_n$ based on the improved method for synthesising the $Cl_3P{=}NSiMe_3$ monomer [29] and the "living" cationic process developed by Allcock *et al*.[10] This was achieved with a reported 40-50% yield but with broader PDI's than the "living" cationic approach.

5.1.2 Polyphosphazenes with pyridine side groups

Few reports appear in the scientific literature regarding phosphazenes with pyridine pendant groups and the majority of these are based on cyclophosphazenes. Early work in 1943 by Audreith *et al*.[31] and in 1966 by Migachev *et al*.[32] reported that pyridine derivatives formed decomposition products. It was not until 1994 that Diefenbach *et al*.[33] began a systematic study of phosphazenes with pyridine side groups as potential nitrogen donors for coordination to transition metals, since similar nitrogen donors such as imidazolyl and pyrazolyl were known to interact with metals.

Using the rationale that electron withdrawing and sterically bulky phenoxy groups apparently protected the cyclotriphosphazene from degrading, Diefenbach *et al*.[33] synthesised the known pentaphenoxymonochlorocyclotriphosphazene, replacing the remaining chlorine by nucleophilic substitution with, for example, an aminopyridine or a 2-aminoethylpyridine moiety (Figure 6).

Using a similar approach, pyridine side groups were introduced to the polyphosphazene $[NPCl_2]_n$ after substituting to various degrees with trifluoroethoxy side groups. Attempts to fully substitute the polymer with pyridine side groups led, as expected, to polymer degradation and a significantly lower molecular weight polymer.[34] Polymers substituted with phenoxy and pyridylmethylamino side groups in various ratios were later shown to demonstrate selective ion uptake.[35, 36]

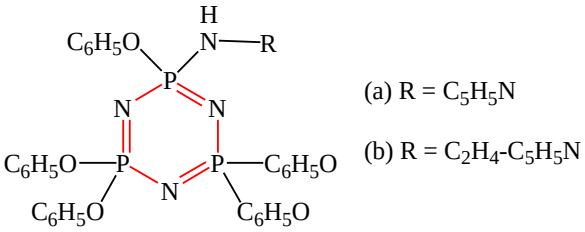

Figure 6 Products from the reaction of pentaphenoxymonochlorocyclotriphosphazene with (a) aminopyridine and (b) 2-aminoethylpyridine.

Carriedo *et al.*[37] have published extensively on 2,2'-dioxybiphenyl (biph) substituted cyclotriphosphazenes and translated this work to polyphosphazenes with 30% substituted 4-oxypyridine side groups. It is interesting to note that even at this low ratio, and with the pyridyl nitrogen *para* to the oxygen spacer, it was suggested that some degree of decomposition of the polymer still occurred during substitution of the pyridyl moiety as evidenced by a reduction in the molecular weight. The efficacy of this polymer as a ligand was demonstrated by subsequent synthesis of a tungsten carbonyl complex.[38]

Carriedo *et al.*[39] developed this work to produce an achiral biph ruthenium complex (Figure 7), and a chiral binapthal ruthenium complex, stating that the latter may have some use in enantiomeric synthesis.

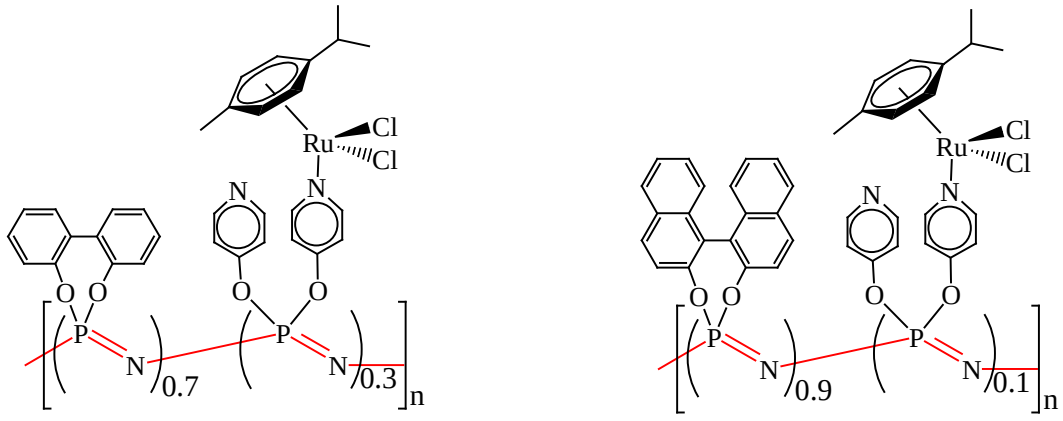

Figure 7 Left: achiral $\{[NP(O_2C_{12}H_8)]_{0.7}[NP(OC_5H_4\text{-}Ru(\eta^6\text{-p-cymene})Cl_2)_2]_{0.3}\}_n$ and Right: chiral $\{[NP(O_2C_{20}H_{12})]_{0.9}[NP(OC_5H_4N)(OC_5H_4N\text{-}Ru(\eta^6\text{-p-cymene})Cl_2]_{0.1}\}_n$ complexes reported by Carriedo *et al.*[39]

More recent work has also seen the development by Carriedo *et al*.[38] of random copolymers of polyspirophosphazene with nitrile, pyridine and phosphine ligands coordinated to tungsten carbonyl (Figure 8), and by Díaz *et al*.,[40] to form solid state metallic nanostructured materials from pyrolysis of organometallic polyphosphazenes with oxypyridine side groups. Most notable, and relevant to the present work, is that the use of biph is reported to give uncrosslinked linear polymer in good yield and high purity,[37] although polyphosphazenes coordinating to transition metals are known to crosslink.[41]

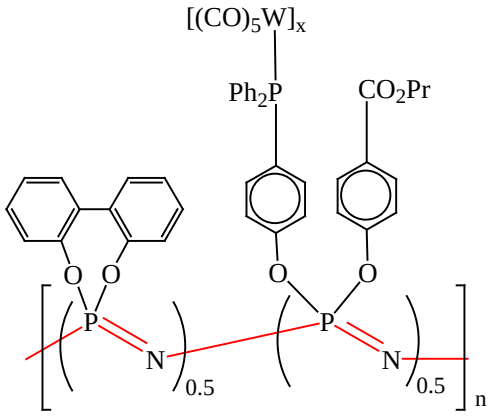

Figure 8 Tungsten carbonyl complex reported by Carriedo *et al*.[38]

5.2 Protocol for polymer syntheses

In the present study, the aim was to prepare homopolymers containing 2-oxypyridine moieties as well as copolymers with biph, where a stabilisation of the polymer is expected. The protocol followed was:

(i) Synthesise the polymer $[NPCl_2]_n$ in accordance with Allcock's thermal ring opening polymerisation strategy.[1]

(ii) Synthesise $[NP(biph)_x(2\text{-pyridyloxy})_y]_n$ polymers where the 2-oxypyridine moiety is either 2-oxypyridine, 2-oxy-4-methylpyridine or 2-oxy-6-methylpyridine.

(iii) Synthesise fully substituted 2-oxypyridine polymers.

(iv) Synthesise the corresponding transition metal halide polymers.

(v) Characterise the polymers.

5.3 Polymer selection

Characterisation of polymeric materials is inherently difficult due to the lack of long range order, especially in solution. The establishment of a datum point was provided by preparation of the fully substituted trifluoroethoxy (TFE) derivative $[NP(TFE)_2]_n$ from $[NPCl_2]_n$. This polymer is extremely stable and hydrophobic, and its characteristics are well documented in the literature.[42] Figure 9 shows the $^{31}P\{^1H\}$ NMR spectrum, demonstrating essentially complete conversion with CHN microanalytical figures being in agreement with calculated and published data, attesting to the integrity of the parent $[NPCl_2]_n$ (see section 5.4.1.1).

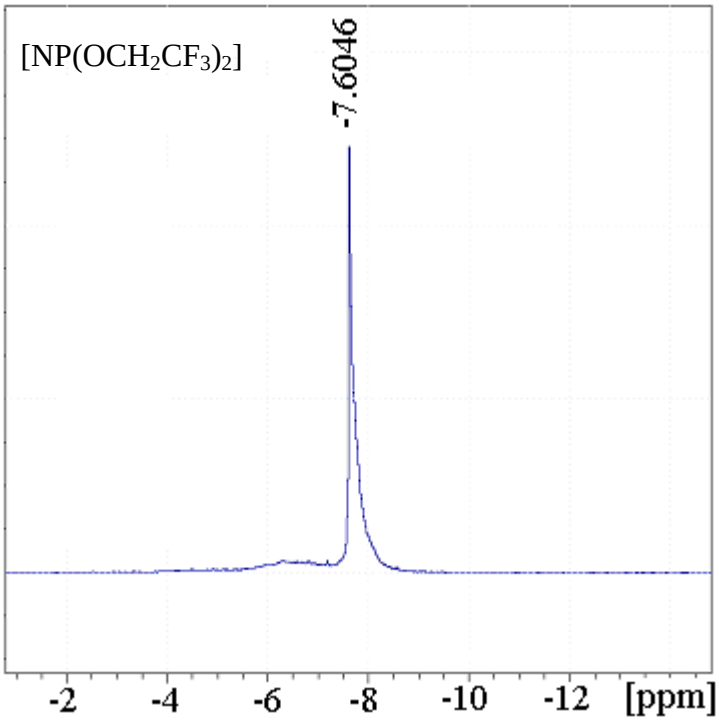

Figure 9 $^{31}P\{^1H\}$ NMR spectrum for $[NP(TFE)_2]_n$

The small molecule syntheses discussed in Chapters 2 and 3 utilised one biph moiety and four 2-oxypyridine groups on the cyclic trimer, as a model template for the polymers. Different solubilities were noted for the cyclotriphosphazene molecules depending on the nature of the 2-oxypyridine moiety and the coordinating transition metal. Substitution of biph and 2-oxypyridine moieties onto the $[NPCl_2]_n$ backbone cannot be controlled or determined in the same manner as for the trimeric compounds and will, at best, be a statistical distribution of the predicted ratios.

For the cyclotriphosphazene model, the architectural possibilities are zero, mono-, bis- and tris-substitution with the 2,2'-dioxybiphenyl moiety, with concomitant substitution of hexakis, tetrakis, bis and zero with the 2-oxypyridine moiety. Tris-substitution with the 2,2'-dioxybiphenyl moiety allows only the phosphazene ring nitrogen for transition metal coordination and this in itself could be negated on steric grounds.

Since the cyclotriphosphazene models indicated that the preferred coordination mode to transition metals involves an N_3Cl_2 (one nitrogen from the phosphazene ring) donor set, then logic dictated that permutations should be made in step changes of two 2-oxypyridine moieties. Thus moiety ratios for polymer substitution were dictated as:

(i) Full substitution with 2-oxypyridine side groups.
(ii) 33% substitution with biph: 66% substitution with 2-oxypyridine side groups.
(iii) 66% substitution with biph: 33% substitution with 2-oxypyridine side groups.

5.4 Experimental section

All manipulations were carried out under argon using standard Schlenk techniques. THF was freshly distilled from benzophenone prior to use. Other analytical grade solvents were purchased from standard chemical suppliers and used without further purification. The cyclotriphosphazene, $N_3P_3Cl_6$ (Otsuka Chemical Co.) was recrystallised from hot heptane, 2-hydroxypyridine, 2-hydroxy-4-methylpyridine and 2-hydroxy-6-methylpyridine (Aldrich) were used as received. $CoCl_2 \cdot 6H_2O$, $CuCl_2 \cdot 2H_2O$ and $ZnCl_2$ (M&B) were dried at 140°C and 2,2'-biphenol was purified by vacuum sublimation.

Microanalyses were performed by Campbell Microanalytical Laboratory, University of Otago. NMR spectra were recorded on a Bruker Avance 400 MHz spectrometer. Electrospray mass spectra were collected from CH_3CN solutions on a Micromass ZMD spectrometer run in positive ion mode. ESR spectra were recorded at 113 K on an X-band Varian E-104A spectrometer. UV-visible spectra were recorded on Shimadzu UV-160A (200-1100 nm) and Shimadzu UV-310PC (200-1500 + nm) instruments. IR spectra were run as KBr discs on Perkin-Elmer Paragon 1000 and Nicolet 5700 spectrophotometers.

DSC measurements were performed by Lee Steely on a Perkin-Elmer DSC-7 unit controlled by a PE7500 computer at the research group of Prof. H.R. Allcock at the Pennsylvania State University, USA. Each sample was annealed twice, 22°C to 80°C and -100°C to 100°C then run -100°C to 225°C.

Molecular weights were performed by: 1) Dr. Stephen Moratti, Otago University, in THF (+ 0.1% tetrabutylammonium nitrate salt) at 1 ml/minute on a PL-GLC50 using a combined UV/refractive index detector at 280 nm with 1 Biorad mixed C column.
2) Lee Steely of the research group of Prof. H.R. Allcock at the Pennsylvania State University, USA, on a Hewlett-Packard HP 1090 GPC with an HP-1047A refractive index detector with AM gel 10 μm and AM gel 10 μm 10^4 Å column.

5.4.1 Polymer substitution reactions

Reported here are the experimental conditions for all the polymer syntheses attempted. Reactions were monitored using $^{31}P\{^1H\}$ NMR. Not all syntheses were successful and these are discussed in subsequent sections.

5.4.1.1 $[NP(TFE)_2]_n$

Under strictly anhydrous conditions, the polymer $[NPCl_2]_n$ (0.70 g, 6.09 mmol) was dissolved in THF (50 ml) and the reaction mixture was stirred until the polymer had fully dissolved. Trifluoroethanol (0.95 ml, 13.30 mmol) was added dropwise to a stirred suspension of NaH (0.32 g, 13.30 mmol) in THF (50 ml) at 0°C. The resulting sodium trifluoroethoxide salt (NaTFE) was added dropwise to the polymer and the solution was stirred at reflux overnight. The reaction mixture was reduced under vacuum using a rotary evaporator until viscous and precipitated from acidified water (5 ml L^{-1}HCL). The polymer was further purified by precipitating twice into hexane from THF, before drying at 50°C overnight under high vacuum. Yield 1.6 g (81%).
Elemental analysis: Calculated for $(C_{12}H_{12}F_{18}N_3O_6P_3)_n$: C, 19.77; H, 1.66; N, 5.76
Found: C, 19.53; H, 1.76; N, 6.02.

5.4.1.2 $[NP(2O\text{-}6\text{-}MePy)_2]_n$

Under strictly anhydrous condition, the polymer $[NP(Cl)_2]_n$ (0.70 g, 6.09 mmol) was dissolved in THF (50 ml) and the reaction mixture was stirred until the polymer had fully dissolved. 2-hydroxy-6-methylpyridine (2.82 g, 25.80 mmol) (2HO-6-MePy) was

added dropwise to a stirred suspension of NaH (0.62 g, 25.80 mmol) in THF (50 ml) at 0°C. The resulting salt, Na(2O-6-MePy) was added dropwise to the polymer and the solution was stirred at reflux for three days. The reaction mixture was reduced under vacuum using a rotary evaporator until viscous and precipitated from water. The polymer was further purified by precipitating into hexane from an equal mixture of THF/CH_2Cl_2 then from an equal mixture of CH_2Cl_2/diglyme, before drying at 50°C overnight under high vacuum. Yield 1.4 g (33%).
Elemental analysis: Calculated for $(C_{36}H_{36}N_9O_6P_3)_n$: C, 55.18; H, 4.63; N, 16.09; Cl, 0.00. Found: C, 54.22; H, 4.75; N, 15.83; Cl, 1.01.

5.4.1.3 $[NP(biph)_{0.66}(2O\text{-}4\text{-}MePy)_{0.33}]_n$

Under strictly anhydrous conditions, the polymer $[NPCl_2]_n$ (0.70 g, 6.09 mmol) was dissolved in THF (50 ml) and the reaction mixture was stirred until the polymer had fully dissolved. 2,2'-biphenol (1.59 g, 8.50 mmol) was added dropwise to a stirred suspension of NaH (0.41 g, 17.00 mmol) in THF (50 ml) at 0°C. The resulting sodium(2,2'-biphenolate) salt (Na_2biph) was added dropwise to the polymer and the solution was stirred overnight. 2-hydroxy-4-methylpyridine (0.93 g, 8.50 mmol) (2-Ho-4-MePy) was added dropwise to a stirred suspension of NaH (0.26 g, 11.08 mmol) in THF (50 ml) at 0°C. The resulting salt, Na(2O-4-MePy) was added dropwise to the solution and stirred overnight. The reaction mixture was reduced under vacuum until viscous and precipitated from water. The polymer was further purified by precipitating into hexane from THF/CH_2Cl_2 and from CH_2Cl_2/diglyme, before drying at 50°C overnight under high vacuum. Yield 1.3 g (32%).
Elemental analysis: Calculated for $(C_{36}H_{28}N_5O_6P_3)_n$: C, 60.09; H, 3.92; N, 9.73; Cl, 0.00. Found: C, 58.02; H, 4.91; N, 9.07; Cl, 1.34.

5.4.1.4 $[NP(biph)_{0.66}(2O\text{-}6\text{-}MePy)_{0.33}]_n$

Under strictly anhydrous conditions, the polymer $[NPCl_2]_n$ (1.50 g, 12.90 mmol) was dissolved in THF (50 ml) and the reaction mixture was stirred until the polymer had fully dissolved. 2,2'-biphenol (1.59 g, 8.50 mmol) was added dropwise to a stirred suspension of NaH (0.41 g, 17.00 mmol) in THF (50 ml) at 0°C. The resulting disodium(2,2'-biphenolate) salt (Na_2biph) was added dropwise to the polymer and the solution was stirred overnight. 2-hydroxy-6-methylpyridine (0.93 g, 11.00 mmol) (2HO-6-MePy) was added dropwise to a stirred suspension of NaH (0.20 g, 11.00 mmol)

in THF (50 ml) at 0°C. The resulting salt Na(2O-6-MePy) was added dropwise to the solution and stirred overnight. The reaction mixture was reduced under vacuum until viscous and precipitated from water. The polymer was further purified by multiple precipitations into hexane from THF/CH_2Cl_2 and from CH_2Cl_2/diglyme, before drying at 50°C overnight under high vacuum. Yield 0.3 g (8.4%).
Elemental analysis: Calculated for $(C_{36}H_{28}N_5O_6P_3)_n$: C, 60.09; H, 3.92; N, 9.73; Cl, 0.00. Found: C, 56.63; H, 4.06; N, 9.54; Cl, 0.85.

5.4.1.5 $[NP(biph)_{0.33}(2O\text{-}6\text{-}MePy)_{0.66}]_n$

Under strictly anhydrous conditions, the polymer $[NPCl_2]_n$ (1.5 g, 12.9 mmol) was dissolved in THF (50 ml) and the reaction mixture was stirred until the polymer had fully dissolved. 2,2'-biphenol (0.79 g, 4.24 mmol) was added dropwise to a stirred suspension of NaH (0.20 g, 8.54 mmol) in THF (50 ml) at 0°C. The resulting disodium(2,2'-biphenolate) salt (Na_2biph) was added dropwise to the polymer and the solution was stirred overnight. 2-hydroxy-6-methylpyridine (1.86 g, 17.00 mmol) (2HO-6-MePy) was added dropwise to a stirred suspension of NaH (0.41 g, 17.00 mmol) in THF (50 ml) at 0°C. The resulting salt Na(2O-6-MePy) was added dropwise to the solution and stirred overnight. The reaction mixture was reduced under vacuum until viscous and precipitated from water. The polymer was further purified by precipitating into hexane from THF/CH_2Cl_2 and from CH_2Cl_2/diglyme, before drying at 50°C overnight under high vacuum. Yield 0.1 g (2.9%).
Elemental analysis: Calculated for $(C_{36}H_{32}N_7O_6P_3)_n$: C, 57.53; H, 4.29; N, 13.05; Cl, 0.00. Found: C, 59.39; H, 5.58; N, 9.83; Cl, 0.67.

5.4.2 Reactions of $[NP(biph)_{0.66}(2O\text{-}4\text{-}MePy)_{0.33}]_n$ and $[NP(2O\text{-}6\text{-}MePy)_2]_n$ with selected transition metal dichlorides

In all of the reactions, anhydrous solid metal halides were added to a solution of the polymer in CH_2Cl_2 (20 ml) and stirred overnight. Where the polymer complexes remained soluble, these were reduced under vacuum until the solid precipitated from solution and the mother liquor was decanted off. The solid was redissolved in CH_2Cl_2 and precipitated into hexane, the solid was then filtered and washed with hexane before drying under vacuum at 50° C overnight. Where the polymer complexes were insoluble and precipitated from solution, these were filtered and washed with CH_2Cl_2, then with hexane, before drying under vacuum at 50° C overnight.

Of the polymers made, only two were stable and pure enough to carry on to studies with transition metal halides. The 2-oxypyridine : metal ratios used are given below:

$[NP(biph)_{0.66}(2O\text{-}4\text{-}MePy)_{0.33}]_n + CoCl_2$ (6:1)

$[NP(biph)_{0.66}(2O\text{-}4\text{-}MePy)_{0.33}]_n + CoCl_2$ (2:1)

$[NP(biph)_{0.66}(2O\text{-}4\text{-}MePy)_{0.33}]_n + CuCl_2$ (6:1)

$[NP(biph)_{0.66}(2O\text{-}4\text{-}MePy)_{0.33}]_n + CuCl_2$ (2:1)

$[NP(biph)_{0.66}(2O\text{-}4\text{-}MePy)_{0.33}]_n + ZnCl_2$ (6:1)

$[NP(biph)_{0.66}(2O\text{-}4\text{-}MePy)_{0.33}]_n + ZnCl_2$ (2:1)

$[NP(2O\text{-}6\text{-}MePy)_2]_n + CoCl_2$ (6:1)

$[NP(2O\text{-}6\text{-}MePy)_2]_n + CoCl_2$ (2:1)

$[NP(2O\text{-}6\text{-}MePy)_2]_n + CuCl_2$ (6:1)

$[NP(2O\text{-}6\text{-}MePy)_2]_n + CuCl_2$ (2:1)

$[NP(2O\text{-}6\text{-}MePy)_2]_n + ZnCl_2$ (6:1)

$[NP(2O\text{-}6\text{-}MePy)_2]_n + ZnCl_2$ (2:1)

Points to note:

(i) Quantities are listed in Tables 2 and 3.

(ii) The ratios given with each complex refer to the following:

6:1 = One metal for every six 2-oxypyridine moieties (Figures 10a and 11a)

2:1 = One metal for every two 2-oxypyridine moieties (Figures 10b)

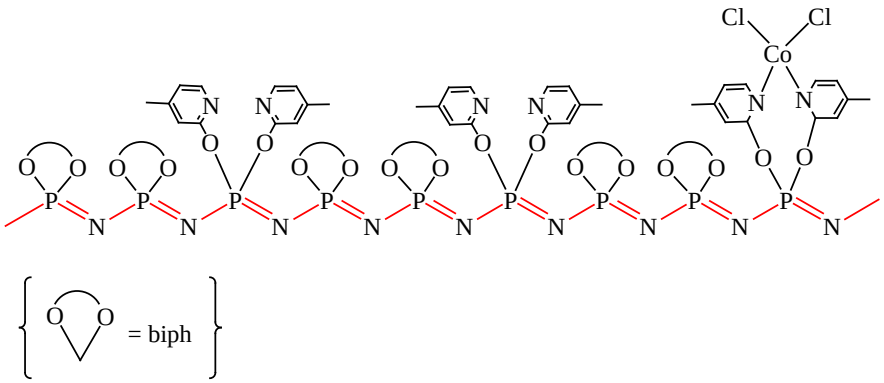

Figure 10a $[NP(biph)_{0.66}(2O\text{-}4\text{-}MePy)_{0.33}]_n + CoCl_2$ (6:1)

6:1 polymer : metal ratio i.e. one metal to every six pyridine groups

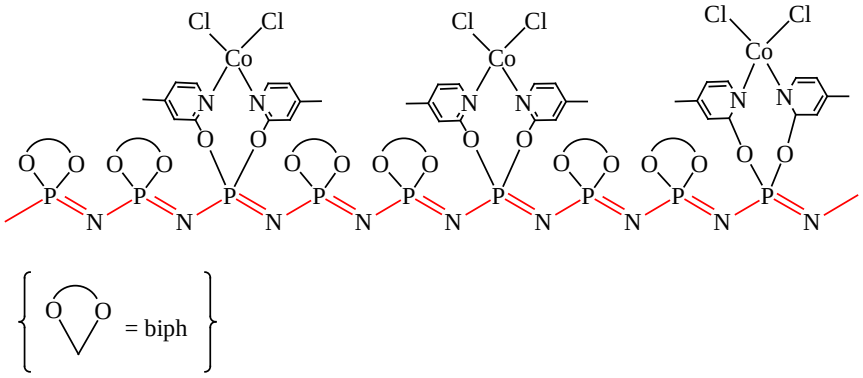

Figure 10b $[NP(biph)_{0.66}(2O\text{-}4\text{-}MePy)_{0.33}]_n + CoCl_2$ (2:1)

2:1 polymer : metal ratio has one metal for every two pyridine groups

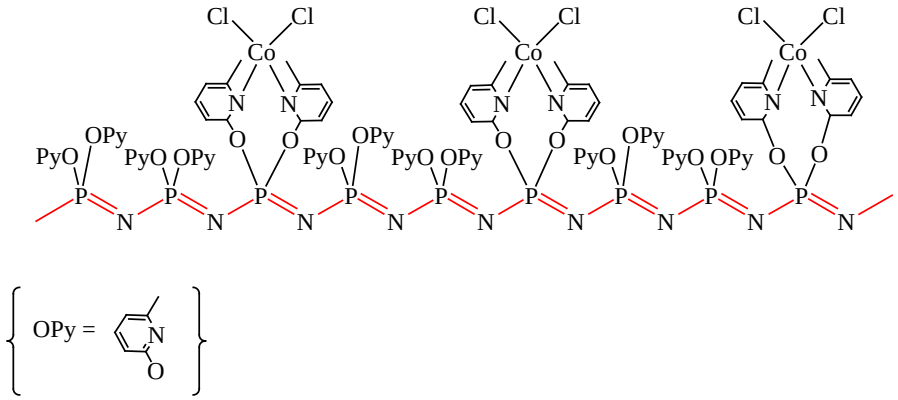

Figure 11 $[NP(2O\text{-}6\text{-}MePy)_2]_n + CoCl_2$ (6:1)

6:1 polymer : metal ratio i.e. one metal to every six pyridine groups (shown)

2:1 polymer : metal ratio has one metal for every two pyridine groups (not shown)

The microanalytical figures given in Tables 2 and 3, demonstrate a broader range of results than those for the cyclotriphosphazene model compounds. A random sample of just fifteen publications on polyphosphazenes gave a spread of up to 4% (measured) for reported carbon figures. The statistical variability of side group distribution, coupled with end group density can affect the accuracy of results, and poor combustion of samples has also been cited.[40, 43]

Complex and CHN figures	Polymer	MCl_2	Yield
$[NP(biph)_{0.66}(2O\text{-}4\text{-}MePy)_{0.33}]_n$ + $CoCl_2$ (6:1)	0.104 g	0.006 g	0.056 g
$C_{108}H_{84}Cl_2CoN_{15}O_{18}P_9$	0.144 mmol	0.048 mmol	50.8%
Calcd: C, 56.68; H, 3.70; N, 9.18; Cl, 3.10 Found: C, 52.37; H, 4.15; N, 9.05; Cl, 3.93			
$[NP(biph)_{0.66}(2O\text{-}4\text{-}MePy)_{0.33}]_n$ + $CoCl_2$ (2:1)	0.099 g	0.017 g	0.109 g
$C_{36}H_{28}Cl_2CoN_5O_6P_3$	0.137 mmol	0.137 mmol	93.3%
Calcd: C, 50.90; H, 3.32; N, 8.25; Cl, 8.35 Found: C, 48.64; H, 3.46; N, 8.37; Cl, 8.05			
$[NP(biph)_{0.66}(2O\text{-}4\text{-}MePy)_{0.33}]_n$ + $CuCl_2$ (6:1)	0.0982 g	0.006 g	0.089 g
$C_{108}H_{84}Cl_2CuN_{15}O_{18}P_9$	0.136 mmol	0.045 mmol	85.3%
Calcd: C, 56.57; H, 3.69; N, 9.16; Cl, 3.09 Found: C, 52.34; H, 3.68; N, 9.18; Cl, 4.54			
$[NP(biph)_{0.66}(2O\text{-}4\text{-}MePy)_{0.33}]_n$ + $CuCl_2$ (2:1)	0.102 g	0.019 g	0.119 g
$C_{36}H_{28}Cl_2CuN_5O_6P_3$	0.141 mmol	0.141 mmol	98.3%
Calcd: C, 50.63; H, 3.30; N, 8.20; Cl, 8.30 Found: C, 46.30; H, 3.35; N, 8.04; Cl, 9.73			
$[NP(biph)_{0.66}(2O\text{-}4\text{-}MePy)_{0.33}]_n$ + $ZnCl_2$ (6:1)	0.108 g	0.006 g	0.093 g
$C_{108}H_{84}Cl_2N_{15}O_{18}P_9Zn$	0.150 mmol	0.049 mmol	81.0%
Calcd: C, 56.52; H, 3.69; N, 9.15; Cl, 3.09 Found: C, 52.62; H, 4.14; N, 9.17; Cl, 4.32			
$[NP(biph)_{0.66}(2O\text{-}4\text{-}MePy)_{0.33}]_n$ + $ZnCl_2$ (2:1)	0.101 g	0.019 g	0.117 g
$C_{36}H_{28}Cl_2N_5O_6P_3Zn$	0.140 mmol	0.140 mmol	98.0%
Calcd: C, 50.52; H, 3.30; N, 8.18; Cl, 8.28 Found: C, 48.74; H, 3.94; N, 8.58; Cl, 7.85			

Table 2 Data for reactions of $[NP(biph)_{0.66}(2O\text{-}4\text{-}MePy)_{0.33}]_n$ with MCl_2 in CH_2Cl_2

NB: Calculated values assume the effect of polymer end groups can be ignored. Major anomalies are discussed in later sections

Complex and CHN figures	Polymer	MCl_2	Yield
$[NP(2O\text{-}6\text{-}MePy)_2]_n$ + $CoCl_2$ (6:1)	0.119 g	0.006 g	0.061 g
$C_{36}H_{36}Cl_2CoN_9O_6P_3$	0.151 mmol	0.050 mmol	51.0%
Calcd: C, 47.33; H, 3.97; N, 13.80; Cl, 7.76 Found: C, 45.00; H, 4.68; N, 12.59; Cl, 9.62			
$[NP(2O\text{-}6\text{-}MePy)_2]_n$ + $CoCl_2$ (2:1)	0.121 g	0.020 g	0.035 g
$C_{36}H_{36}Cl_6Co_3N_9O_6P_3$	0.154 mmol	0.154 mmol	34.0%
Calcd: C, 36.86; H, 3.09; N, 10.75; Cl, 18.13 Found: C, 35.99; H, 4.33; N, 10.78; Cl, 11.11			
$[NP(2O\text{-}6\text{-}MePy)_2]_n$ + $CuCl_2$ (6:1)	0.117 g	0.006 g	0.059 g
$C_{36}H_{36}Cl_2CuN_9O_6P_3$	0.149 mmol	0.049 mmol	53.6%
Calcd: C, 47.10; H, 3.95; N, 13.73; Cl, 7.72 Found: C, 42.82; H, 5.41; N, 11.70; Cl, 4.88			
$[NP(2O\text{-}6\text{-}MePy)_2]_n$ + $CuCl_2$ (2:1)	0.116 g	0.019 g	0.034 g
$C_{36}H_{36}Cl_6Cu_3N_9O_6P_3$	0.148 mmol	0.148 mmol	29.8%
Calcd: C, 36.43; H, 3.06; N, 10.62; Cl, 17.92 Found: C, 39.19; H, 4.10; N, 11.18; Cl, 10.74			
$[NP(2O\text{-}6\text{-}MePy)_2]_n$ + $ZnCl_2$ (6:1)	0.106 g	0.006 g	0.042 g
$C_{36}H_{36}Cl_2N_9O_6P_3Zn$	0.134 mmol	0.049 mmol	37.4%
Calcd: C, 47.00; H, 3.94; N, 13.70; Cl, 7.71 Found: C, 45.67; H, 5.51; N, 12.26; Cl, 5.05			
$[NP(2O\text{-}6\text{-}MePy)_2]_n$ + $ZnCl_2$ (2:1)	0.095 g	0.016 g	0.029 g
$C_{36}H_{36}Cl_6N_9O_6P_3Zn_3$	0.121 mmol	0.121 mmol	24.5%
Calcd: C, 36.26; H, 3.04; N, 10.57; Cl, 17.84 Found: C, 35.33; H, 4.32; N, 10.15; Cl, 12.36			

Table 3 Data for reactions of $[NP(2O\text{-}6\text{-}MePy)_2]_n$ with MCl_2 in CH_2Cl_2

NB: Calculated values assume the effect of polymer end groups can be ignored. Major anomalies are discussed in later sections

5.5 Observations from polymer syntheses

It should be noted that during the course of this work several batches of polymer were synthesised via the thermal ROP route. Each batch demonstrated variances in behaviour e.g. time to dissolve and time for reaction with the biph and 2-oxypyridine moieties. Differences in appearance and macroscopic behaviour were also noted. It was postulated that the appearance of varying degrees of a brown colouration in the cooled reaction vessel could indicate contamination with water as reported by MacCallum *et al.*[17] and that differences in viscosity of the purified polymer could indicate changes in chain length and molecular weight. Due to these variances, and in order to ensure

consistency of interpretation of results, all of the polymer reactions reported herein, were carried out using polymer from a single batch only. The batch in question lacked the rubber-like "balling" when collected from the sublimator, instead demonstrating viscoelastic properties, flowing to form an even layer on the base of the storage vessel. It also displayed rapid solubility, indicating that low molecular weight was possibly the cause of this behaviour.

Comparing the polymers to the cyclotriphosphazene models from Chapter 2, it is noticeable that the yields for the polymers with 2-oxypyridine groups attached are generally much lower. The yields of polymers range from 2.9% to 33%, whereas the cyclotriphosphazenes range from 50% to 98.5%. The $[NP(TFE)_2]_n$ polymer gave 81% yield and this is possibly an early indication that the polymers with 2-oxypyridine groups are less stable and degrading either in the reaction vessel or during workup.

5.5.1 Polymers with 2-oxypyridine side groups

Attempts to synthesise stable polymers with 2-oxypyridine side groups that are not methyl substituted proved unsuccessful. Diefenbach *et al*.[33] have reported that phosphazenes with pyridine side groups are susceptible to polymer degradation.

5.5.1.1 Analysis of the polymers

Where possible, all the polymers have been characterised by $^{31}P\{^1H\}$ NMR spectroscopy, Differential Scanning Calorimetry (DSC), molecular weight determination and for the metal containing species, UV-visible spectroscopy. Metal-free polymers are discussed first.

5.5.1.2 Attempted synthesis of $[NP(2OPy)_2]_n$

Fully substituted $[NP(2OPy)_2]_n$ degrades as the reaction proceeds, as monitored by $^{31}P\{^1H\}$ NMR in CH_2Cl_2 (Figure 12).

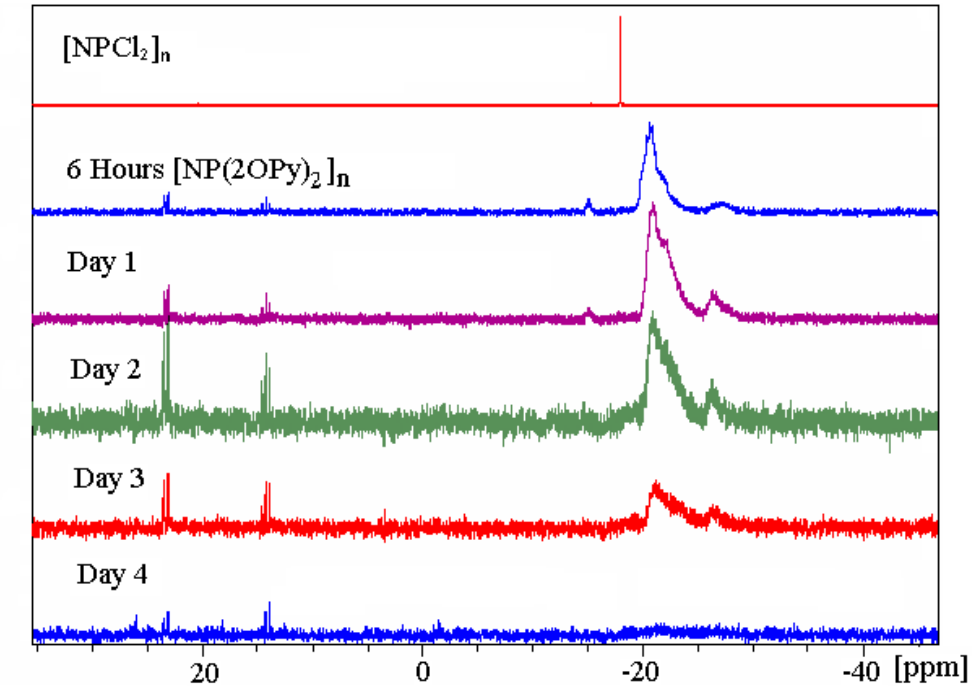

Figure 12 $^{31}P\{^{1}H\}$ NMR in CH_2Cl_2 for $[NP(2OPy)_2]_n$ showing degradation during reaction

Figure 12 above clearly demonstrates polymer degradation with reaction time. Disappearance of the starting polymer $[NPCl_2]_n$ (-17.9 ppm) is complete after six hours with the appearance of a major broad peak at -20.7 ppm.

Continued reaction in solution leads to the disappearance of this signal and the concomitant formation of minor concentrations of small oligomers. Complete disappearance of the major ^{31}P signal is indicative of precipitation or crosslinking, and this was observed to be the case. Attempts were made to isolate the fully substituted polymer between six hours and two days, i.e. before substantial degradation occurs. These attempts led to the recovery of solid material that was insoluble in common solvents. It is not certain whether the work-up procedure of depositing the polymer into water exacerbates the degradation. It is postulated that the lack of any sterically bulky groups in proximity to the pyridyl nitrogen may allow attack of the polyphosphazene backbone with subsequent crosslinking or degradation to smaller linear or cyclic oligomers. A possible initiation step for base-promoted degradation is shown in Figure 13.

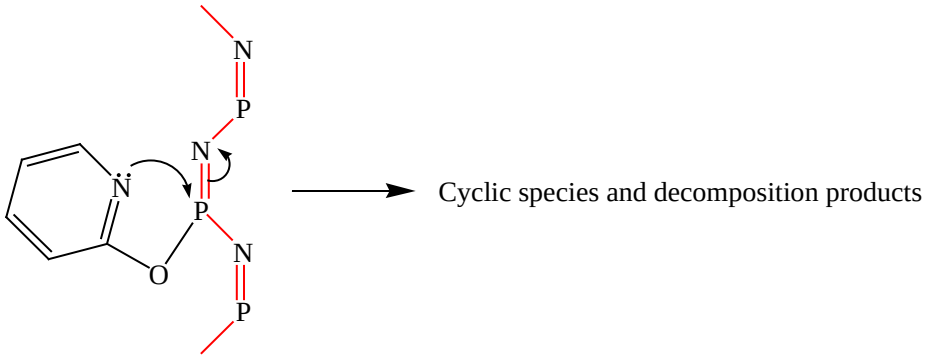

Figure 13 Possible initiation step for base-promoted degradation

5.5.1.3 Attempted synthesis of $[NP(biph)_{0.33}(2OPy)_{0.66}]_n$

Addition of biph to the polymer $[NPCl_2]_n$ was undertaken in a 1:3 ratio, i.e. statistically, one phosphorus site in every three was substituted with biph. Integration of the $^{31}P\{^1H\}$NMR spectrum showed that the substitution ratio of biph:2-oxypyridine was approximately 1:2. As seen in Figure 14, degradation of the polymer with time is evident.

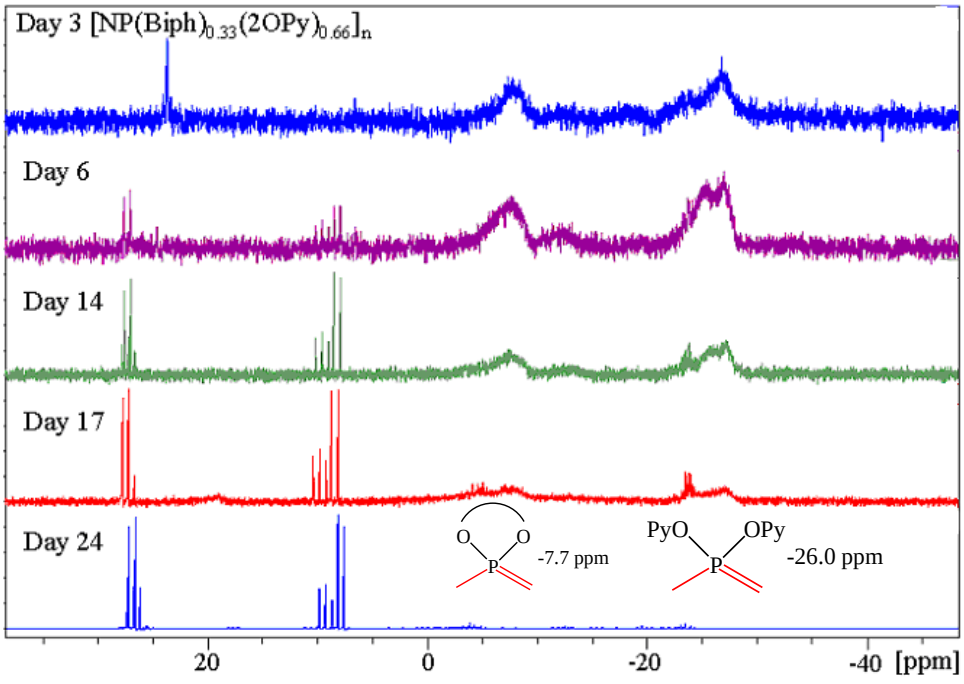

Figure 14 $^{31}P\{^1H\}$NMR spectra showing degradation with time of $[NP(biph)_{0.33}(2OPy)_{0.66}]_n$

5.5.1.4 Attempted synthesis of $[NP(biph)_{0.66}(2OPy)_{0.33}]_n$

Synthesis of the polymer $[NP(biph)_{0.66}(2OPy)_{0.33}]_n$ resulted in some intriguing conclusions. Firstly, during workup, it was observed that the majority of the polymer solidified onto the wall of the reaction vessel. However, some remained in solution and its $^{31}P\{^1H\}$NMR spectrum showed formation of the expected product (Figure 15 (a)). The solid fraction recovered from the glass surface was only partially soluble in CH_2Cl_2, and its $^{31}P\{^1H\}$NMR spectrum indicated a low concentration of the product (Figure 15 (b)).

Secondly, by using a mixture of CH_2Cl_2, diglyme and water, a synthetic regimen was established for successful purification of the polymeric species and elimination of the cyclic or oligomeric contaminants as seen in Figure 15 (c). However, subsequent degradation of the polymer with time, led to complete crosslinking and loss of utility.

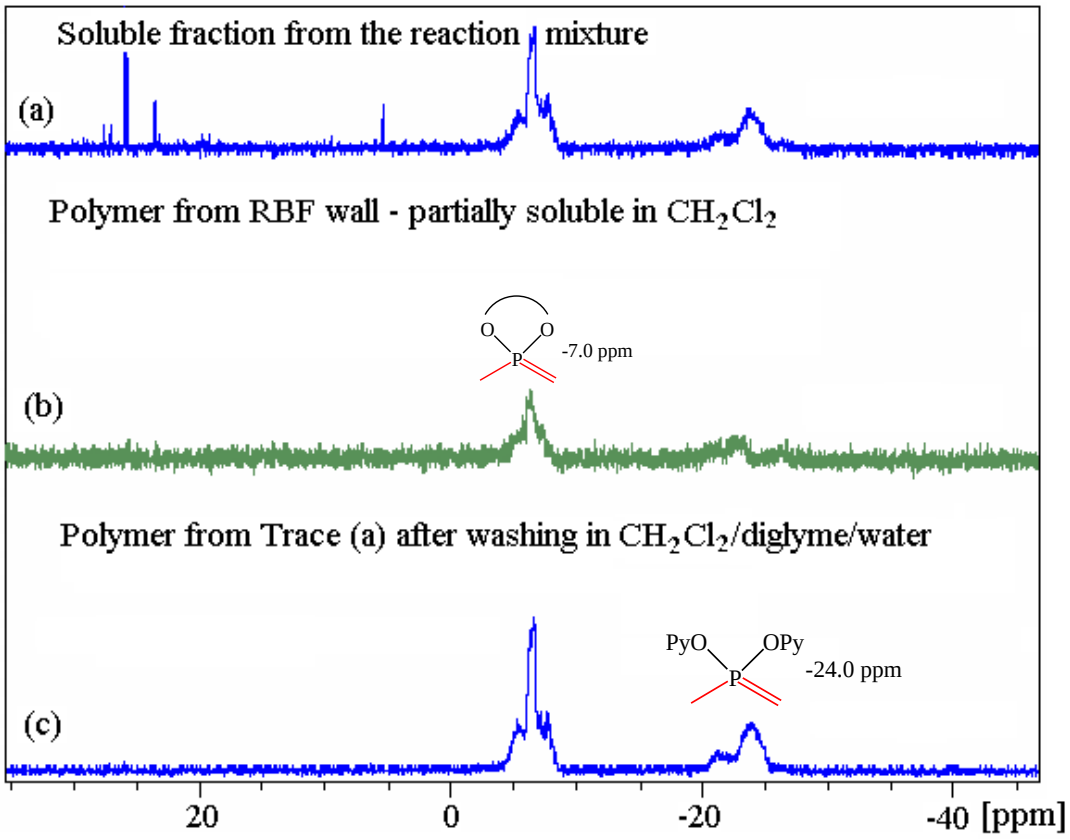

Figure 15 $^{31}P\{^1H\}$NMR spectral study of $[NP(biph)_{0.66}(2OPy)_{0.33}]_n$ in CH_2Cl_2

It is postulated that with respect to the polymer, $[NP(biph)_{0.66}(2OPy)_{0.33}]_n$, intra or inter-molecular reactions are occurring as evidenced by the multimodal nature of the $^{31}P\{^1H\}$NMR spectra. This could be a statistical anomaly and represent partial substitution or different distributions of the biph and 2OPy moieties as follows. The sharp peak at approximately -7.0 ppm is representative of blocks of the biph moiety, whereas the broader shoulders either side are representative of more random distributions.[42] The bimodal peak at approximately -24.0 ppm is assigned to blocks of the 2OPy moiety, with the ratio of biph to 2OPy integrating at approximately 2:1 as expected. As well, the polymer appears to be degrading to oligomeric and/or cyclic species, or the polymer could be forming a high degree of chain branches.

5.5.2 Polymers with 4-methyl-2-oxypyridine side groups

The (2O-4-MePy) moiety has the methyl group *para* to the pyridyl nitrogen, thus as for the (2OPy) moiety, there is little steric bulk preventing approach of the pyridyl nitrogen to the polyphosphazene backbone and this may allow attack and degradation of the polymer backbone. Only when high ratios of biph were used, was a seemingly stable polymer produced and it is postulated that this is either due to the steric bulk of the biph, or that the biph and the 2-oxypyridine methyl group demonstrate some short range interaction to prevent close proximity of the pyridyl nitrogen to the phosphazene backbone, since high ratios of biph with non-methylated 2-oxypyridine groups have been shown to be unstable in the previous section.

5.5.2.1 Attempted synthesis of $[NP(2O\text{-}4\text{-}MePy)_2]_n$

Full substitution of $[NPCl_2]_n$ with the 4-methyl-2-oxypyridine side groups results in polymer degradation. A $^{31}P\{^1H\}$NMR spectrum at Day 3 (Figure 16) shows complete transformation of the starting material (-17.9 ppm) to the substituted polymer (-26.9 ppm), plus cyclic or oligomeric species. The small peak at -15.2 ppm is possibly due to cyclic hexamer $[NPCl_2]_6$.[42] By Day 8, the polymer has completely degraded with no $^{31}P\{^1H\}$NMR signal seen for the polymer.

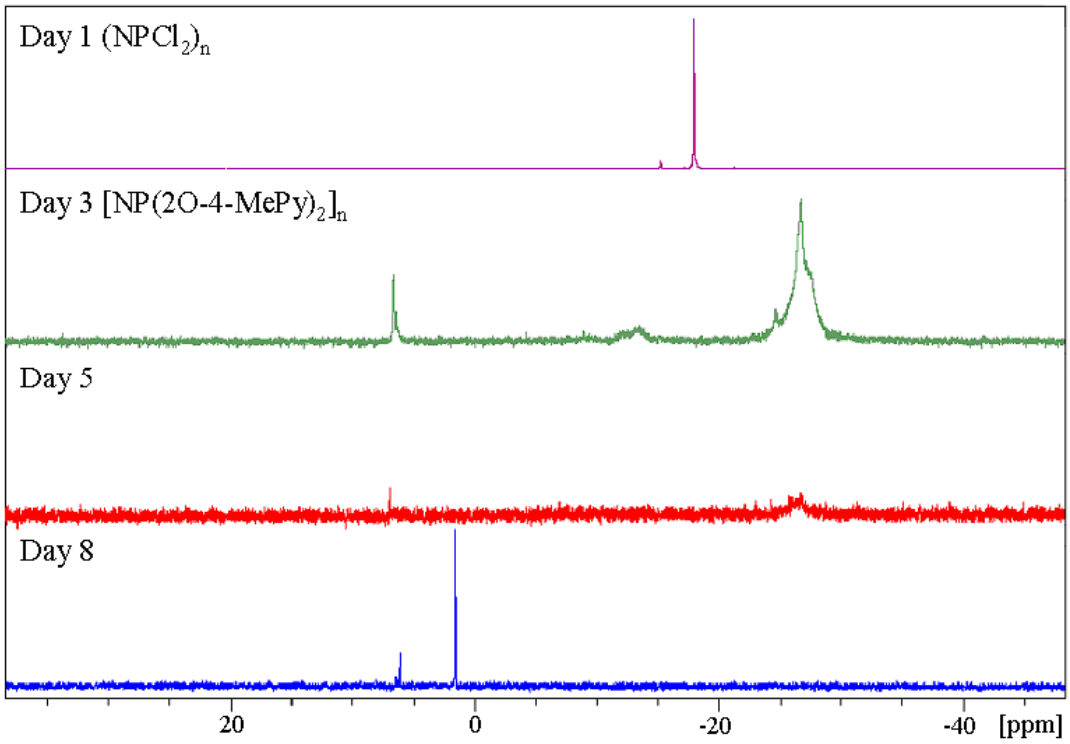

Figure 16 Degradation of $[NP(2O\text{-}4\text{-}MePy)_2]_n$

5.5.2.2 Attempted synthesis of $[NP(biph)_{0.33}(2O\text{-}4\text{-}MePy)_{0.66}]_n$

Following addition of biph to $[NPCl_2]_n$, two polymer peaks are observed in the $^{31}P\{^1H\}$NMR spectrum at -6.7 ppm (P-biph) and -19.7 ppm (P-Cl_2) (Figure 17). On substitution of the remaining chloro groups with the 4-methyl-2-oxypyridine moiety, the associated peak shifts upfield to -26.7 ppm and both peaks broaden. The integrals on Day 6 are in the order of 1:0.17 (biph:4-methyl-2-pyridyloxy) with approximately 3% cyclic species, above 0.0 ppm, that were not present in the starting polymer. Solids were observed in the reaction vessel, and these were collected, dissolved in CH_2Cl_2 and precipitated from hexane to give a white powder after drying. Microanalytical results indicate that degradation had occurred. Calculated for $(C_{36}H_{32}N_7O_6P_3)_n$: C, 57.33; H, 4.29; N, 13.05; Cl, 0.00. Found: C, 35.5; H, 2.9; N, 8.60, Cl, 2.30.

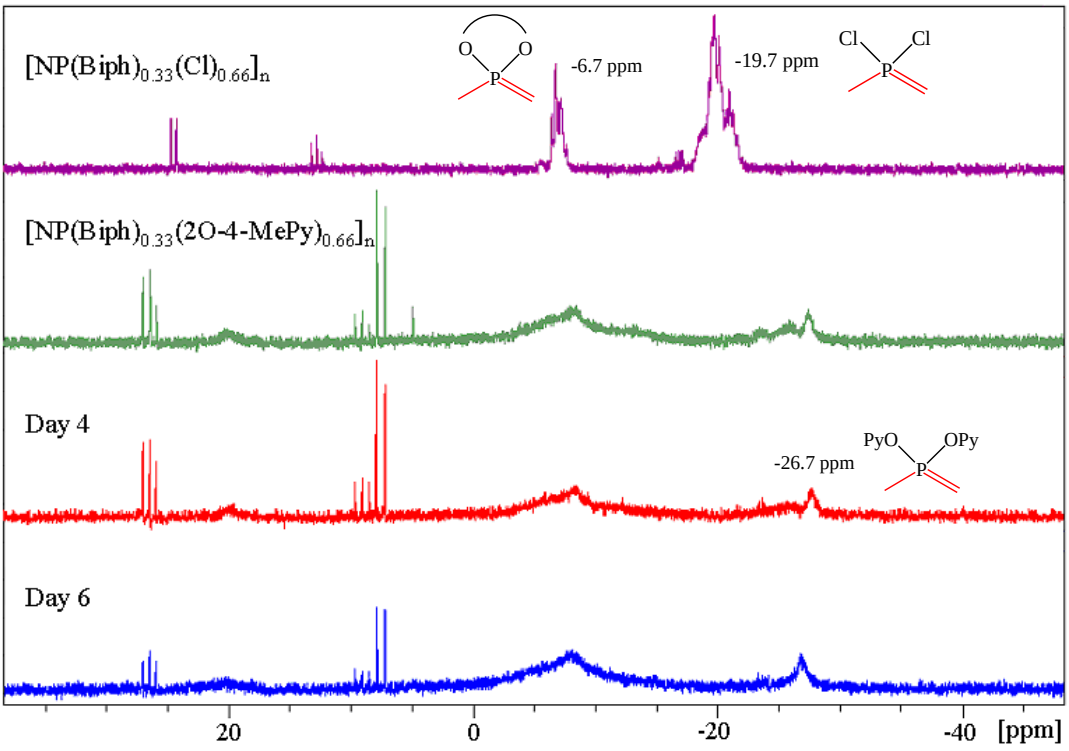

Figure 17 Degradation of $[NP(biph)_{0.33}(2O\text{-}4\text{-}MePy)_{0.66}]_n$

N.B. Peaks above 0.0 ppm are not present in the spectrum of the polymer $[NPCl_2]_n$ and are likely to be cyclic species formed by polymer degradation

5.5.2.3 Synthesis of $[NP(biph)_{0.66}(2O\text{-}4\text{-}MePy)_{0.33}]_n$

A stable polymer was obtained with the higher ratio of biph. The $^{31}P\{^{1}H\}$NMR spectrum shows two well defined peaks at -8.0 ppm and -27.6 ppm (Figure 18 and insets) integrating at approximately 2:1 as expected.

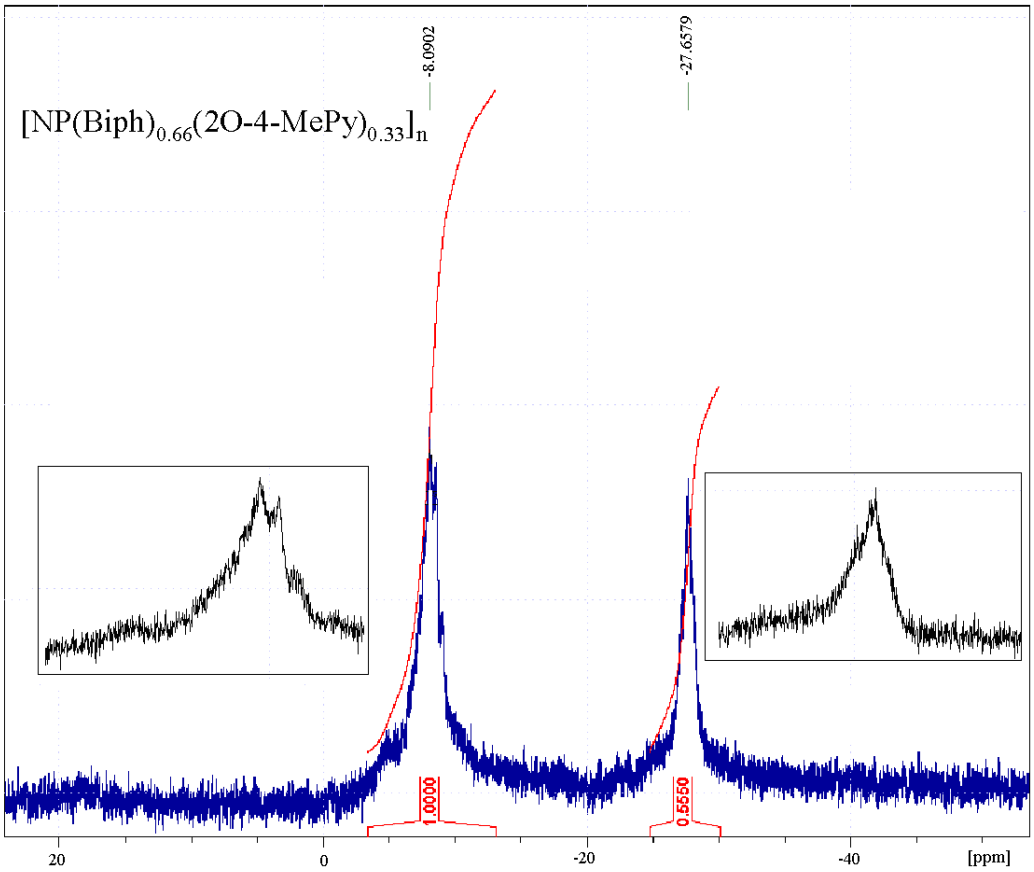

Figure 18 $^{31}P\{^{1}H\}$NMR spectrum for $[NP(biph)_{0.66}(2O\text{-}4\text{-}MePy)_{0.33}]_n$

An interesting observation was made during workup regarding the solubility of the polymer. Following precipitation into water, the hydrated polymer exhibits the bulk property of high elongation (Figure 19). It is soluble in CH_2Cl_2, but is insoluble in THF. Only after drying, which reduced the polymer to a brittle solid, was solubility in THF achieved. It is postulated that the presence of water instigates short range hydrogen bonding that is not disrupted by water miscible solvents such as THF. Similar observations of variable solubility have been made by Allcock *et al*.[43] regarding an osmium complex that apparently crosslinked on precipitation into hexane, having previously been soluble in THF.

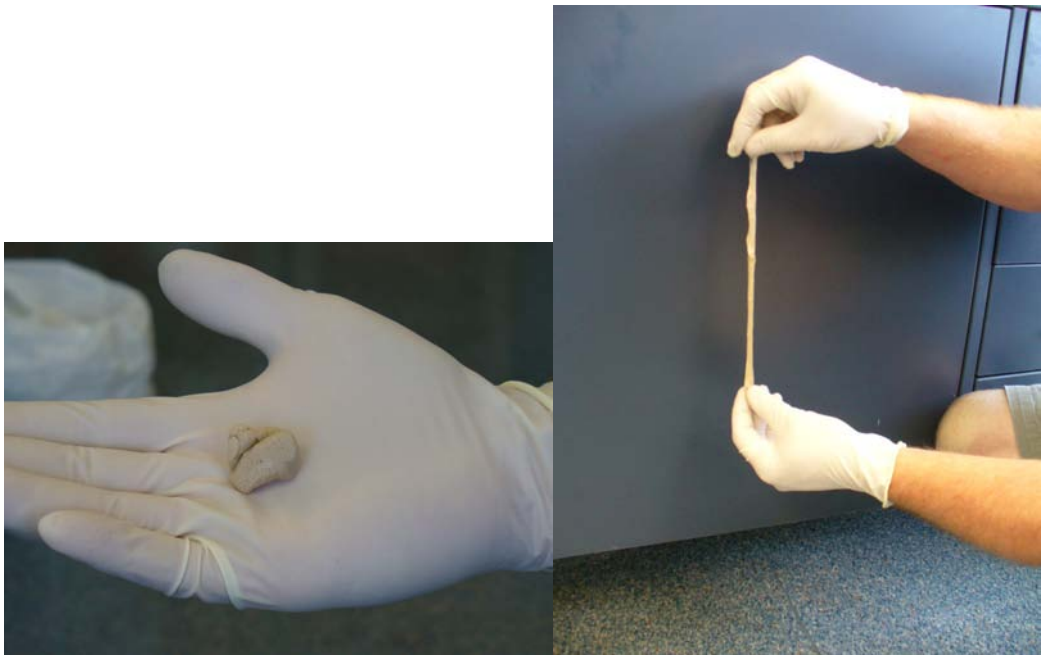

Figure 19 Left: Hydrated polymer precipitated from water. Right: Elongation in the hydrated form

5.5.3 Polymers with 6-methyl-2-oxypyridine side groups

The 6-methyl-2-oxypyridine moiety gave stable polymers in all ratios and it is postulated that having the methyl group *ortho* to the pyridyl nitrogen provides sufficient steric bulk to prevent base promoted degradation of the phosphazene backbone. The X-ray crystal structure of the cyclotriphosphazene model compound N_3P_3(biph)(2O-6-MePy)$_4$ clearly demonstrated that the packing arrangement of the trimeric species is distinct from that of the 2-oxypyridine and 4-methyl-2-oxypyridine compounds. The chloro analogue, N_3P_3(biph)(2O-6-ClPy)$_4$ demonstrated a similar configuration of 2-oxypyridine pendant arms to the 6-methyl derivative as discussed in Chapter 2.

5.5.3.1 Synthesis of [NP(2O-6-MePy)$_2$]$_n$

Full substitution with the 6-methyl-2-oxypyridine moiety gave a stable polymer that exhibited a sharp single peak, indicative of full substitution, at -27.5 ppm in the $^{31}P\{^1H\}$NMR spectrum (Figure 20).

It was observed that the hydrated polymer, following precipitation from water during workup, was soluble in THF. If some short range hydrogen bonding is responsible for

the solubility behaviour, as for the $[NP(biph)_{0.66}(2O\text{-}4\text{-}MePy)_{0.33}]_n$ polymer, then it appears that the biph moiety is a key component.

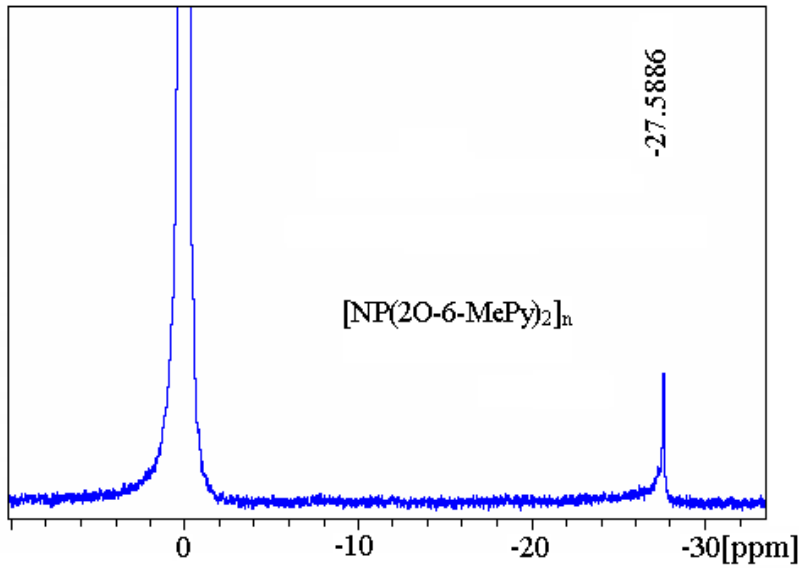

Figure 20 $^{31}P\{^{1}H\}$NMR spectrum for $[NP(2O\text{-}6\text{-}MePy)_2]_n$ relative to phosphoric acid

5.5.3.2 Synthesis of $[NP(biph)_{0.33}(2O\text{-}6\text{-}MePy)_{0.66}]_n$

The moiety ratio in this polymer represents the only stable state mirroring the ratios used in the cyclotriphosphazene model compounds. The $^{31}P\{^{1}H\}$NMR spectrum gives two peaks at -9.8 ppm (biph) and -28.5 ppm (2-pyridyloxy), integrating in a ratio of approximately 1:2 as expected (Figure 21), with no evidence of decomposition with time prior to workup.

The multimodal appearance of the peaks (Figure 21 and insets) is most likely due to the sequence of addition of the biph and 2O-6-MePy moieties. It can be seen from the spectrum for $[NP(biph)_{0.66}(2O\text{-}6\text{-}MePy)_{0.33}]_n$ (Figure 22) that higher loading (66%) of biph results in a slight downfield shift of the -9.9 ppm signal, corresponding to the left hand peak of the bimodal system in the main spectrum of Figure 22. Thus, with the low loading (33%) of the biph being added to the polymer first, it is likely that random accumulations of biph occur, some regions of which will resemble the population density of the higher loaded polymer, and other regions will be less densely populated. Subsequent addition of the 2O-6-MePy moiety displaces the remaining chlorine atoms which must equally have a random distribution, resulting in a multimodal spectrum.

It is also possible that the multimodal spectrum is due to chain branching occurring on a sufficiently high number of chains for the phenomenon to be detected in the $^{31}P\{^{1}H\}$NMR spectrum, however this would lead to insolubility and is thus an unlikely explanation.[42]

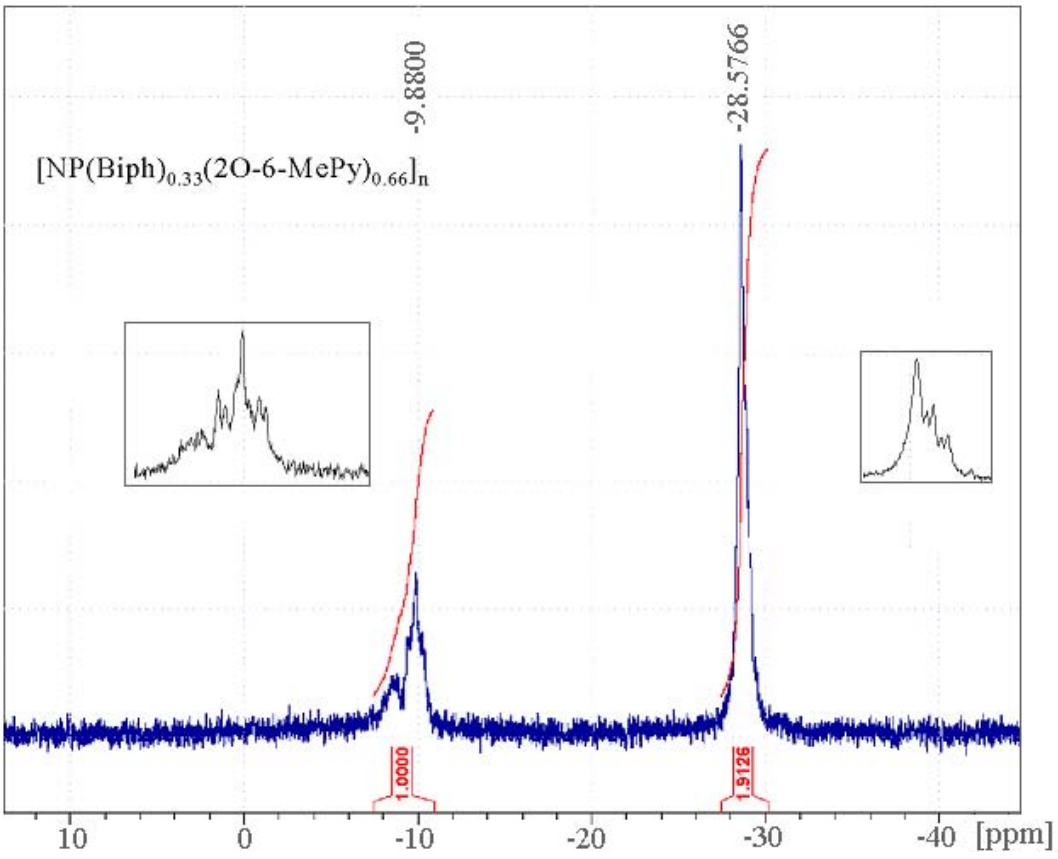

Figure 21 $^{31}P\{^{1}H\}$NMR spectrum for $[NP(biph)_{0.33}(2O\text{-}6\text{-}MePy)_{0.66}]_n$

The polymer exhibited the behaviour of only being completely soluble in THF when thoroughly dehydrated. The yield for this polymer was very low at 2.9% possibly because multiple precipitations from THF/CH_2Cl_2 solution into hexane were required to remove trimeric impurities. Previous attempts to synthesise this polymer had also indicated solubility problems and gel formation during workup.

5.5.3.3 Synthesis of $[NP(biph)_{0.66}(2O\text{-}6\text{-}MePy)_{0.33}]_n$

The $^{31}P\{^{1}H\}$NMR spectrum gives two peaks at -7.9 ppm (biph) and -27.4 ppm (2-pyridyloxy), integrating in a ratio of approximately 2:1 as expected (Figure 22). Bimodal splitting of the biph peak is seen for this polymer but not to the same extent as

for $[NP(biph)_{0.33}(2O\text{-}6\text{-}MePy)_{0.66}]_n$, possibly because the higher loading of biph does not produce the same statistical variation in distribution. No decomposition with time was evident prior to workup. Yield for this polymer was also low at 8.4%, and the same insolubility in THF when hydrated was noted.

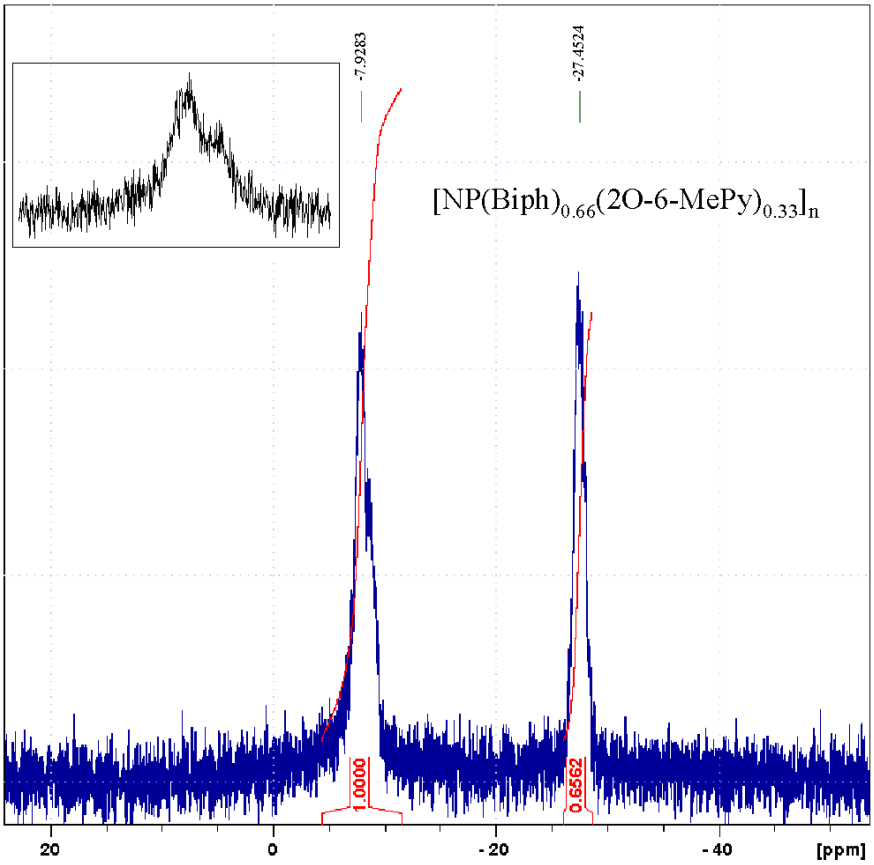

Figure 22 $^{31}P\{^{1}H\}$NMR spectrum for $[NP(biph)_{0.66}(2O\text{-}6\text{-}MePy)_{0.33}]_n$ - Inset shows bimodal splitting in the peak at -7.9 ppm

5.5.4 Analysis by differential scanning calorimetry (DSC)

Thermal analysis by DSC can give some insight into the structure and properties of the polymer by determination of the glass transition temperature (T_g). The T_g represents an approximate measure of conformational rigidity and the transition from a glass, in which the polymer conformation is "frozen" to an amorphous state whereby there is sufficient thermal energy for bond torsion to occur and for the polymer to exhibit elastomeric properties.

A number of factors affect T_g,[43] first, there is the energy barrier to bond torsion which appears to be as low as 0.1 kcal/bond/repeat[44] (approximately 0.4 kJ). There is ongoing debate as to the exact nature of the (-N=P-) bond that permits such ready bond torsion. Second, the distribution of side groups has two effects, one being that the spacing of the side groups is less dense than in organic polymers due to coordination to alternate atoms on the backbone i.e. phosphorus. In addition, for co-substituted polymers, the statistical distribution can inhibit localised aggregations and microcrystalline regions due to random dispersion and lack of symmetry.
Third, the nature of the side groups and interactions between side groups can markedly affect T_g as shown in Table 4.

Polymer	T_g °C (reference)
$[NP(OCH_2CH_3)_2]_n$	-84 [42]
$[NP(OCH_2CF_3)_2]_n$	-66 [42]
$[NP(OC_6H_5)_2]_n$	-8 [45]
$\{[NP(OC_5H_4N)_2]_x[NP(O_2C_{20}H_{12})]_{1-x}\}_n$	296 [46]

Table 4 Effect of side group on T_g

Fourth, crosslink density increases T_g and produces a more rigid and inflexible network by degree, until no transition is observed because individual polymer chains are unable to slide past one another.
Fifth, the architecture of the backbone has an influence depending on whether it is linear, cyclolinear or contains side branches etc.
Lastly, inclusion of solvent molecules is known to occur with polyphosphazenes, even after drying under vacuum at 70 °C and thus careful preheating of the sample is required to avoid ambiguity.

T_g values obtained for the free polymers in the present study show the expected trend of increased T_g relative to the fully substituted trifluoroethoxy derivative $[NP(TFE)_2]_n$, with $[NP(2O\text{-}6\text{-}MePy)_2]_n$ having less of an effect than the presence of the biph moiety (Table 5). The T_g for the polymer $[NP(TFE)_2]_n$ is in fair agreement with published

results (-66°C).[42] The polymers unique to the present study follow the expected trend, the bulky aryloxy groups in $[NP(2O\text{-}6\text{-}MePy)_2]_n$ increase T_g in line with diphenoxyphosphazene homopolymers (-8°C [42]), and the biph moieties increase T_g further still.

Polymer Sample	T_g °C
$[NP(TFE)_2]_n$	-54.52
$[NP(2O\text{-}6\text{-}MePy)_2]_n$	-28.45
$[NP(biph)_{0.66}(2O\text{-}6\text{-}MePy)_{0.33}]_n$	15.97
$[NP(biph)_{0.33}(2O\text{-}6\text{-}MePy)_{0.66}]_n$	23.83
$[NP(biph)_{0.66}(2O\text{-}4\text{-}MePy)_{0.33}]_n$	31.08

Table 5 T_g values for the free polymers

However, Carriedo *et al*.[47] reported T_g for the homopolymer $[NP(biph)]_n$, as 160°C. A 70/30 copolymer with 4-oxypyridine, $\{[NP(biph)]_{0.7}[NP(OC_5H_4N)_2]_{0.3}\}_n$, led to an increase in T_g to 174°C, Carriedo *et al*.[47] thus suggested that the 4-oxypyridine makes a positive contribution to T_g.
Diaz *et al*.[40] reported a T_g of 129°C for the same 70/30 copolymer and a T_g of 156°C for the 80/20 copolymer $\{[NP(biph)]_{0.8}[NP(OC_5H_4N)_2]_{0.2}\}_n$.

Despite the somewhat contradictory reporting given above, the T_g values observed in the present study for the free polymers containing biph, are significantly lower than might be expected based on the conclusions of Carriedo *et al*.,[47] and Diaz *et al*.[40], and since T_g is as representative of a polymer as the melting point is of crystalline materials,[42] it can be postulated that, (a) if the data are correct for the free polymers in the present study, then the pyridyl nitrogen atom position or the presence of methyl groups on the 2-oxypyridine moieties play a significant role in the T_g value, and (b) that the reliability of reported/measured T_g values must be considered in the light of the numerous variables in polymer synthesis and characterisation, especially for co-substituted systems.

5.5.5 Polymer Molecular Weights

Gel permeation chromatography (GPC) is a standard method for determination of molecular weights (M_w) and gives a measure of the number of repeat units present in the polymer chain and the distribution of chain lengths (M_n). Polyphosphazenes have been reported to exhibit anomalous behaviour when analysed using GPC, with non-repeatability of molecular weights (M_w) and adsorption reactions with column fillers resulting in misleading data.[37] In 1987, Nielson *et al*.[48] reported that the use of small quantities (0.1 wt%) of a tetra(butyl)ammonium salt (TBAN) overcame these seemingly intractable problems and nowadays it is common for literature reports to include use of either the bromide[47, 49] or nitrate salt[50], although the reasons for its performance enhancement remain unclear.

Solubility of the polymers was noticeably enhanced with the introduction of the TBAN. A sample of $[NP(biph)_{0.66}(2O\text{-}4\text{-}MePy)_{0.33}]_n$ which was initially only partially soluble in THF, fully dissolved in THF + (0.1 wt% TBAN). However, results from two independent sources indicated that with time, the polymers appeared to be decomposing or branching. Table 6 lists the results of fresh samples analysed by the Allcock group in July 2007 and the same batch analysed by Moratti in December 2007. Assuming that the results are correct then the polymers can at best be described as pseudo-stable and may be subject to hydrolytic ageing.

Results for the $[NP(TFE)_2]_n$ polymer used as the datum indicate that the batch of $[NPCl_2]_n$ is of lower M_w (10^5 Daltons) than would be expected (10^6 Daltons) by the thermal ROP process, confirming in part the observations made regarding the physical characteristics of this batch. The high PDI for the $[NP(TFE)_2]_n$ polymer (Moratti) is unexpected and contrary to published data regarding the stability of this system.

However, since the number of side groups will be in the order of tens of thousands, detection of unreacted P-Cl bonds becomes exceedingly difficult and almost certainly lost within the background of an NMR spectrum. Following the arguments of Visscher *et al*.,[51] it is not unreasonable to surmise that the presence of only a few P-Cl sites could sensitise the polymer to eventual hydrolytic breakdown on reaction with atmospheric water, causing replacement of chlorine by hydroxyl groups. The very high PDI for the

$[NP(biph)_{0.66}(2O\text{-}6\text{-}MePy)_{0.33}]_n$ polymer could also be indicative of long-term hydrolysis and thus the need to optimise reaction conditions to ensure full substitution of chlorine atoms on the backbone is highlighted.

Sample	Penn State Uni. (Allcock)			Otago Uni. (Moratti)		
	$M_n/10^3$	$M_w/10^3$	PDI	$M_n/10^3$	$M_w/10^3$	PDI
$[NP(TFE)_2]_n$	61	106	1.73	5.3	104	19.7
$[NP(2O\text{-}6\text{-}MePy)_2]_n$				160	670	4.1
$[NP(biph)_{0.66}(2O\text{-}4\text{-}MePy)_{0.33}]_n$				6.7	17	2.6
$[NP(biph)_{0.66}(2O\text{-}6\text{-}MePy)_{0.33}]_n$	130	339	2.62	11.8	711	60.0

Table 6 GPC results for the free polymers

5.6 Reaction of the polymers with selected transition metals

Successful synthesis of four, apparently stable polymers containing 2-oxypyridine moieties would indicate that the steric bulk provided by high ratios of the biph, and/or by methyl groups *ortho* to the pyridyl nitrogen are necessary to prevent degradation of the polyphosphazene backbone, and is in agreement with similar steric arguments espoused by Diefenbach *et al*.[33]

The very low yields for the polymers containing 6-methyl-2-oxypyridine and biph moieties, and the fact that previous attempts to synthesise these polymers gave solubility problems and gel formation during workup, resulted in a decision not to proceed with reactions of these polymers with transition metals. It is evident that more work is required to optimise the synthesis for these polymer ratios, especially given the variance in polymer synthesis and the concomitant desire to synthesise comparative polymeric compounds from a single batch.

$[NP(biph)_{0.66}(2O\text{-}4\text{-}MePy)_{0.33}]_n$ and $[NP(2O\text{-}6\text{-}MePy)_2]_n$ were thus chosen for reaction with transition metals.

5.6.1 $[NP(biph)_{0.66}(2O\text{-}4\text{-}MePy)_{0.33}]_n$ with $CoCl_2$, $CuCl_2$ and $ZnCl_2$

Reactions of $[NP(biph)_{0.66}(2O\text{-}4\text{-}MePy)_{0.33}]_n$ with varying ratios of $CoCl_2$, $CuCl_2$ and $ZnCl_2$ resulted in polymers that were soluble in CH_2Cl_2, thereby allowing measurement of electronic spectra for $CoCl_2$ and $CuCl_2$, and NMR studies in the case of $ZnCl_2$. Colours and intensities of the cobalt and copper polymer samples in solution are shown in Figure 23.

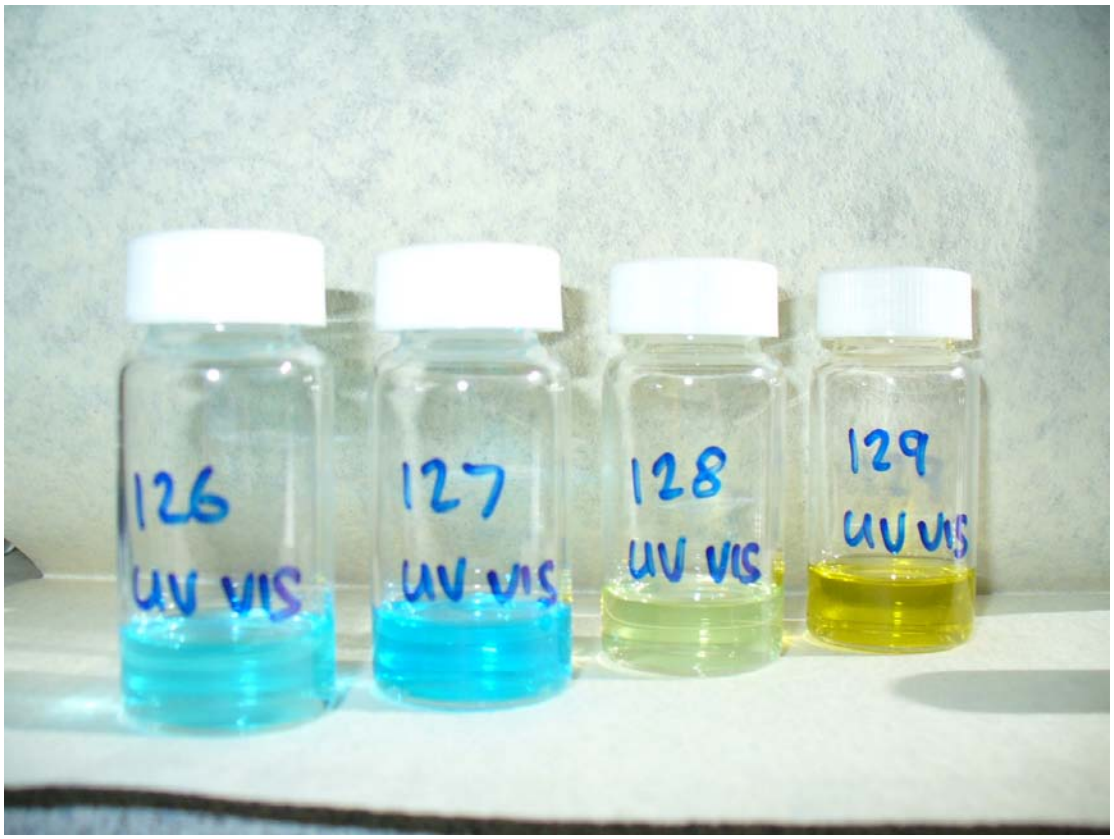

Figure 23 Samples in CH_2Cl_2 of $[NP(biph)_{0.66}(2O\text{-}4\text{-}MePy)_{0.33}]_n$ with, from left: $CoCl_2$ 6:1. $CoCl_2$ 2:1, $CuCl_2$ 6:1, $CuCl_2$ 2:1

5.6.2 $[NP(2O\text{-}6\text{-}MePy)]_n$ with $CoCl_2$, $CuCl_2$ and $ZnCl_2$

The $^{31}P\{^1H\}$ NMR spectrum of the fully substituted $[NP(2O\text{-}6\text{-}MePy)]_n$ polymer exhibited a sharp single peak at -27.6 ppm (Figure 20), indicating full substitution and no evidence for degradation, however, reaction with $CoCl_2$ and $CuCl_2$ rendered insoluble powders at the metal dichloride ratios used, thus only solid state reflectance spectra could be obtained for the ratios 6:1 and 2:1 and doping experiments were

performed on lower ratios. Reactions with $ZnCl_2$ gave soluble polymer complexes that could be studied using NMR techniques.

5.6.2.1 $[NP(biph)_{0.66}(2O\text{-}4\text{-}MePy)_{0.33}]_n$ with $CoCl_2$

IR spectroscopy has been reported by Carriedo *et al.*[47] to provide a fingerprint for coordination of metals to 4-oxypyridine groups. For the free polymer $[NP(biph)_{0.66}(2O\text{-}4\text{-}MePy)_{0.33}]_n$, a strong signal at 1166 cm^{-1} disappeared on coordination to Co(II) though no new signals were seen in the IR spectra for the cobalt polymer complex. Comparison with the cyclotriphosphazene complexes in Chapter 3 would indicate that the signal at 1166 cm^{-1} is assignable to a ν(P-N) stretching mode.

UV-visible spectroscopy studies of the cyclotriphosphazene complexes indicated that the cobalt halide complexes, where soluble, underwent a rearrangement from TBP in the solid state to pseudo-tetrahedral in solution, irrespective of the ligand. For the polymeric complex, only pseudo-tetrahedral geometry was found for solid and solution phases,[52] which could be indicative of decreased basicity of the polyphosphazene backbone nitrogen atoms (Figure 24 and Table 7). Increasing the $CoCl_2$ to polymer ratio resulted in an increase in absorbance as expected. The molar absorptivity of the order of 200 l mol^{-1} cm^{-1} indicates d-d transitions rather than charge transfer.

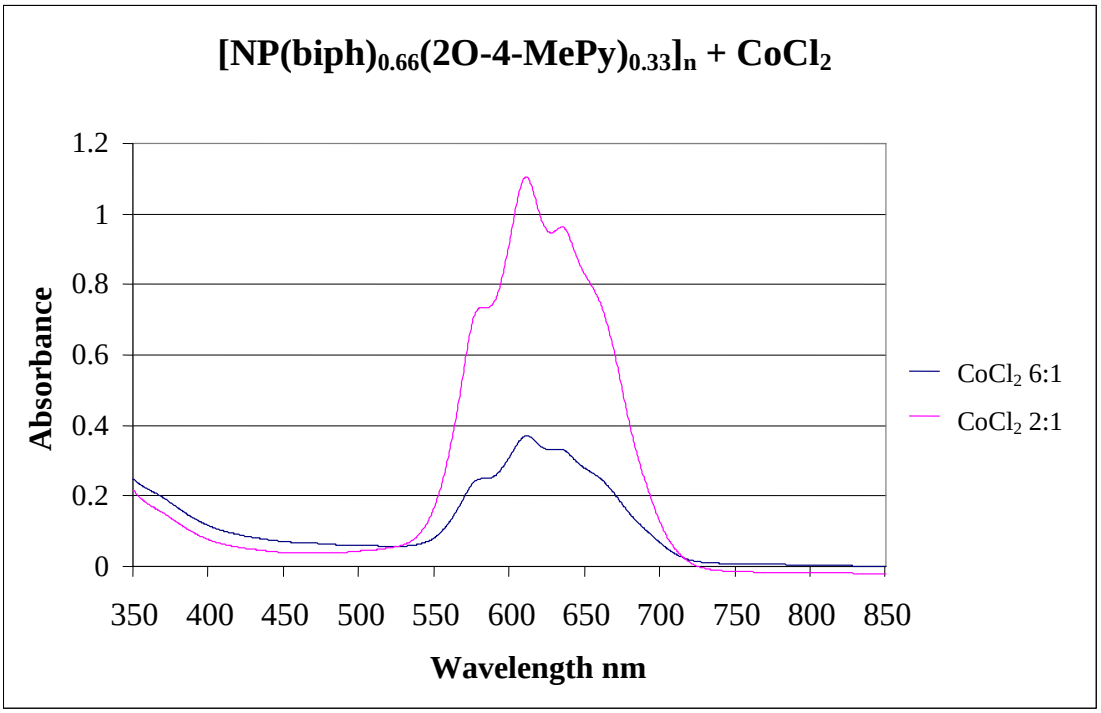

Figure 24 UV-visible spectra for the polymer/$CoCl_2$ complexes in CH_2Cl_2 solution

Polymer Complex	Solution CH_2Cl_2	Solid Nujol mull
	λ_{max}/nm (ε/dm^3 mol^{-1} cm^{-1} per Co)	λ_{max}/nm
$[NP(biph)_{0.66}(2O\text{-}4\text{-}MePy)_{0.33}]_n$ with $CoCl_2$ (2:1)	580 (215), 612 (323), 635 (282), 660 (sh) (222)	580, 610, 635, 660(sh)
$[NP(biph)_{0.66}(2O\text{-}4\text{-}MePy)_{0.33}]_n$ with $CoCl_2$ (6:1)	580 (190), 612 (283), 635 (254), 660 (sh) (190)	580, 610, 635, 660 (sh)
$[CoCl_2(4\text{-}MePy)_2]$	575, 610, 636, 664	

Table 7 Electronic Spectral Data for the polymer/$CoCl_2$ complexes and with tetrahedral $[CoCl_2(4\text{-}MePy)_2]$ for comparision

UV-visible electronic spectra are summarised in Table 7 and it is observed that the solid and solution spectra are in very close agreement indicating no change in stereochemistry between the two phases. Comparison with the complex $[CoCl_2(4\text{-}MePy)_2]$ shows that the spectra are in close agreement and hence it could be inferred that the known tetrahedral $[CoCl_2(4\text{-}MePy)_2]$ is a useful model and consistent with the geometry around the polymeric Co(II) metal centres.[53]

5.6.2.2 Possible coordination modes of $[NP(biph)_{0.66}(2O\text{-}4\text{-}MePy)_{0.33}]_n$ to $CoCl_2$

In the absence of X-ray structures for the polymer complexes, interpretation of the data is, of necessity, somewhat speculative. This does however reinforce the need to synthesize the analogous cyclotriphosphazene complexes to provide a point of comparison and discussion of the possible stereochemistry of the polymeric complexes. For the complex $[NP(biph)_{0.66}(2O\text{-}4\text{-}MePy)_{0.33}]_n$ with $CoCl_2$, only pseudo-tetrahedral geometry was seen in the UV-visible spectra for both solution and solid phases. If one considers a perfect statistical distribution then the potential donor set should consist of just two 2-oxypyridine nitrogen atoms and one of two available polymer backbone nitrogens.

Unlike the cyclic trimer model compounds, coordination to the polymer bound 2-oxypyridine moieties would be from a geminal, not a non-geminal arrangement (unless bond torsion permits the necessary proximity of groups to occur). This arrangement is known for the tet-$[ZnL^2Cl_2]\cdot 5CH_2Cl_2$ cyclotriphosphazene complex described in Chapter 4 and shown in Figure 25 for reference. It can be seen that the zinc centre is held away from the phosphazene ring nitrogen (N10). If this arrangement is the case for the solid state cobalt bearing polymer, then some other factor must come to bear to prevent binding to the polyphosphazene backbone nitrogen, which could be the innate flexibility of the backbone or lower basicity of the backbone nitrogen atoms.

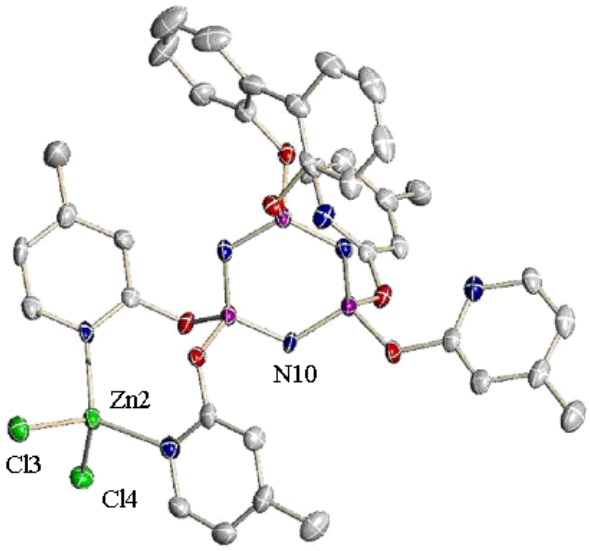

Figure 25 Tetrahedral arrangement around tet-$[ZnL^2Cl_2]\cdot 5CH_2Cl_2$
Thermal ellipsoids are drawn at 50% probability (hydrogen atoms and occluded solvent removed for clarity)

The polymer backbone is inherently more flexible than the cyclic trimer and it is possible that other donor sets can be available through heterocyclic ring formation that would provide the necessary coordination cross section. Alternatively a random distribution would provide blocks of 2-oxypyridine moieties for coordination. At short

range, with the bulky aryloxy groups used, a favoured skeletal conformation for the polyphosphazene backbone would be a planar *cis-trans* arrangement (Figure 26),[42] whereby the lowest energy conformation is achieved by least steric hindrance between the bulky side groups.

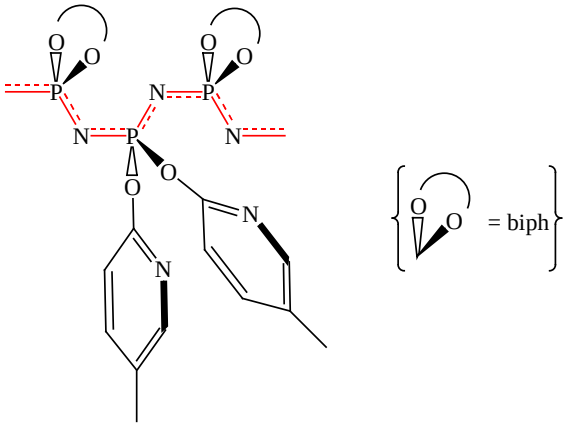

Figure 26 *Cis-trans* planar skeletal conformation of polyphosphazene

Tetrahedral coordination to Co^{2+} is therefore postulated to be via the two 2-oxypyridine nitrogen atoms (Figure 27) since no rearrangement takes place between solid and solution phases.

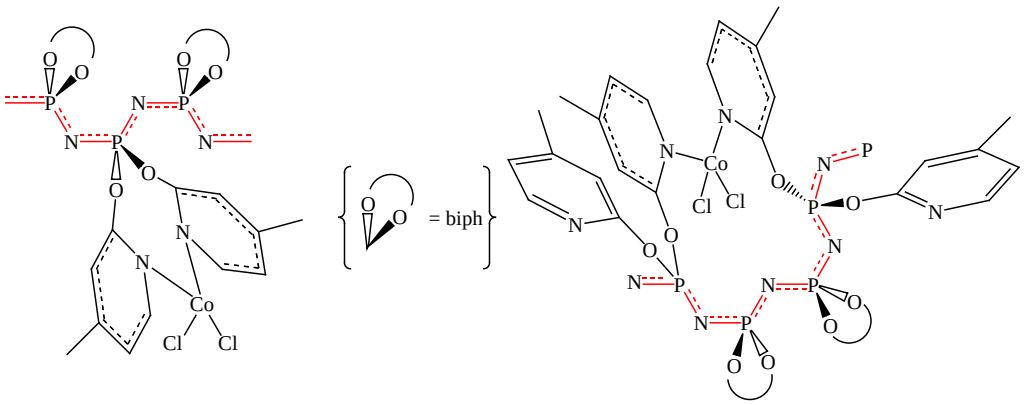

Figure 27 Possible pseudo-tetrahedral geometry around the cobalt centre from geminal or non-geminal 2-oxypyridine groups

In an attempt to gain ^{1}H NMR data that might elucidate additional structural information, the $[NP(Biph)_{0.66}(2O\text{-}4\text{-}MePy)_{0.33}]_n$ polymer was doped with sub molar ratios of $CoCl_2$, even though the paramagnetic nature of the Co^{2+} ion had been shown to obliviate the ^{1}H NMR signal, due to excessive line broadening, for the cyclotriphosphazene complexes. Since $CoCl_2$ is not particularly soluble in CH_2Cl_2, an initial study was made by adding $CoCl_2$ dissolved in methanol to a solution of the polymer dissolved in CH_2Cl_2. The results shown in Figure 4 would seem to indicate that increasing the concentration of $CoCl_2$ produces an upfield shift, and broadening of the signal as shown in the inset of Figure 28.

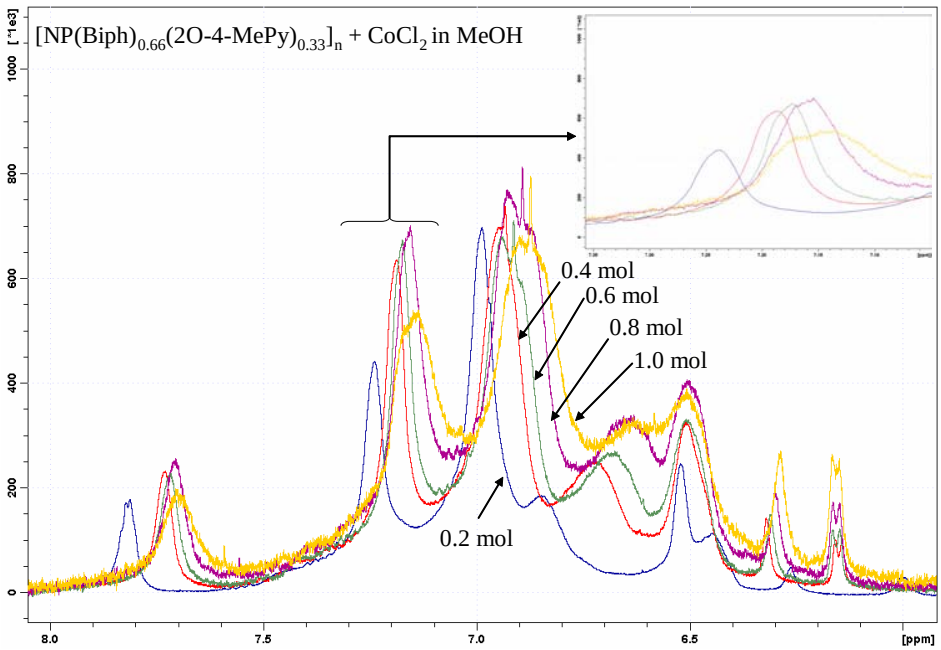

Figure 28 Polymer doping with $CoCl_2$ in methanol

A control experiment was conducted by adding methanol to a solution of the $[NP(Biph)_{0.66}(2O\text{-}4\text{-}MePy)_{0.33}]_n$ polymer. As seen in Figure 29, it can be reasoned that the upfield shift in the ^{1}H NMR spectrum is actually due to an interaction of the polymer with methanol, whilst line broadening is due to the paramagnetic nature of Co(II).

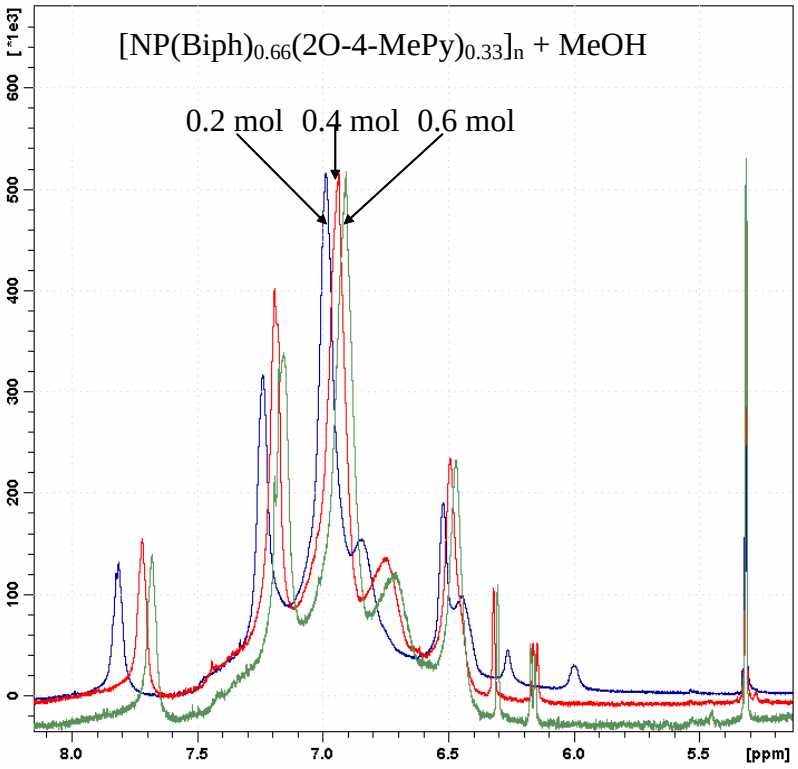

Figure 29 ^{1}H NMR spectrum of $[NP(Biph)_{0.66}(2O\text{-}4\text{-}MePy)_{0.33}]_n$ polymer with successive sub-molar additions of methanol

To confirm the result of the ^{1}H NMR experiment with the addition of $CoCl_2$ to the $[NP(Biph)_{0.66}(2O\text{-}4\text{-}MePy)_{0.33}]_n$ polymer, a sample of the polymer was dissolved in CH_2Cl_2 and anhydrous $CoCl_2$ was added in solid form to the solution and stirred overnight, replicating the actual experimental conditions for synthesis of the polymer complexes. Figure 30 shows that on addition of the anhydrous $CoCl_2$ to the polymer, no chemical shift is evident, but broadening of the signal is quite apparent at relatively low concentrations of $CoCl_2$. Greater broadening of the signal at lower mole ratios is perhaps indicative that the methanol regimen did not allow sufficient time for full coordination of $CoCl_2$ to the polymer. Thus it would seem that the use of ^{1}H NMR is of little utility in further elucidating the structure.

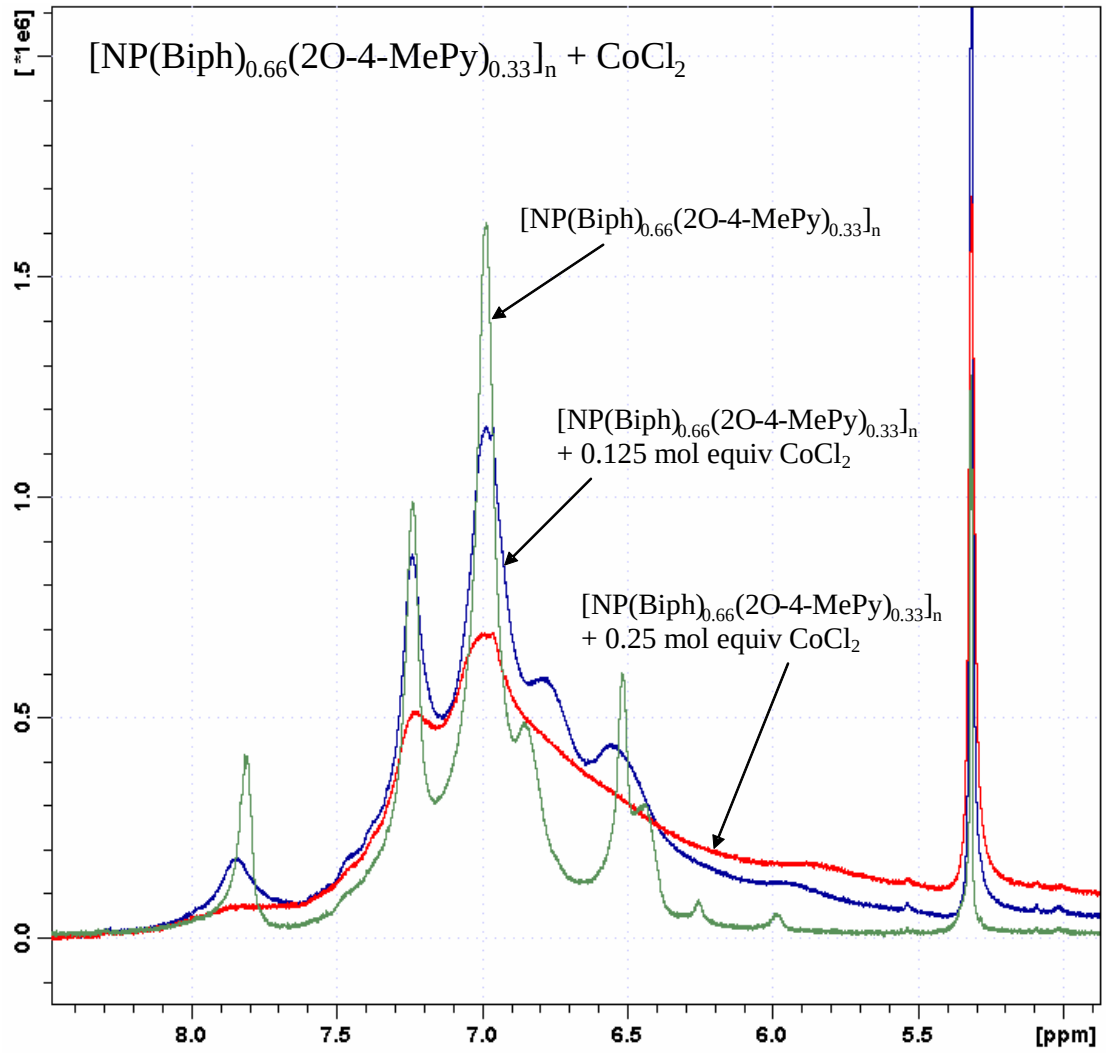

Figure 30 ^{1}H NMR of $[NP(Biph)_{0.66}(2O\text{-}4\text{-}MePy)_{0.33}]_n$ polymer showing line broadening with low concentrations of $CoCl_2$ (the peak at 5.3 ppm is due to the solvent)

$^{31}P\{^{1}H\}$NMR demonstrated a change in the J coupling (Table 8) on addition of $CoCl_2$, although line broadening means an element of error in determination of the exact centre of the peaks, there is a sufficient increase in the J values to be significant at the 0.1 and 0.4 mol. equiv. stages.

Mol. equiv. of $CoCl_2$ added	J Coupling Hz
0.4	3250
0.3	3206
0.2	3208
0.1	3213
0.0	3129

Table 8 Change in J coupling with addition of $CoCl_2$

5.6.2.3 $[NP(2O\text{-}6\text{-}MePy)]_n$ with $CoCl_2$

The IR spectrum for the free polymer demonstrated the loss of two bands at 1630 and 1448 cm^{-1} on coordination to the metal centre, with no evidence for the formation of new bands.

The disappearance of these ν(P-N) stretching bands could be due to loss of backbone torsion caused by the observed crosslinking.

A controlled doping experiment was performed, adding 0.05 - 0.20 mol ratios of $CoCl_2$ to a solution of the polymer (Figure 31) and it was observed that precipitation occurred at the 0.20 mole equivalent stage which is below the ratio of one metal per six 2-oxypyridine moieties (i.e. the (6:1) ratio) and which represents 0.33 mole equivalence. Precipitation is probably indicative of crosslinking through the metal ions, though few studies exist regarding this phenomenon.[42]

At 0.20 mole equivalent, the solution electronic spectra point towards a tetrahedral environment around Co(II) with no shift in wavelength. However the spectra are shifted to higher energy from that of the solid state reflectance spectra (Table 8), which are identical for both ratios of $CoCl_2$, and is indicative of a distorted tetrahedral environment. Comparison of the solid and solution spectra for the polymeric complexes with those of the cyclotriphosphazene complex $[CoL^3Cl_2]$ discussed in Chapter 3 indicates that a similar tetrahedral geometry exists in solution for the cyclic and polymeric forms. However, in the solid state, there is a marked difference in geometry with $[CoL^3Cl_2]$ having a characteristic TBP form, with broad bands at 660 (br) and 850

(vb) nm. The polymeric complexes demonstrate a similar distorted tetrahedral geometry to the solution spectra with bands at 690 (sh), 665, 630 and 615 nm.

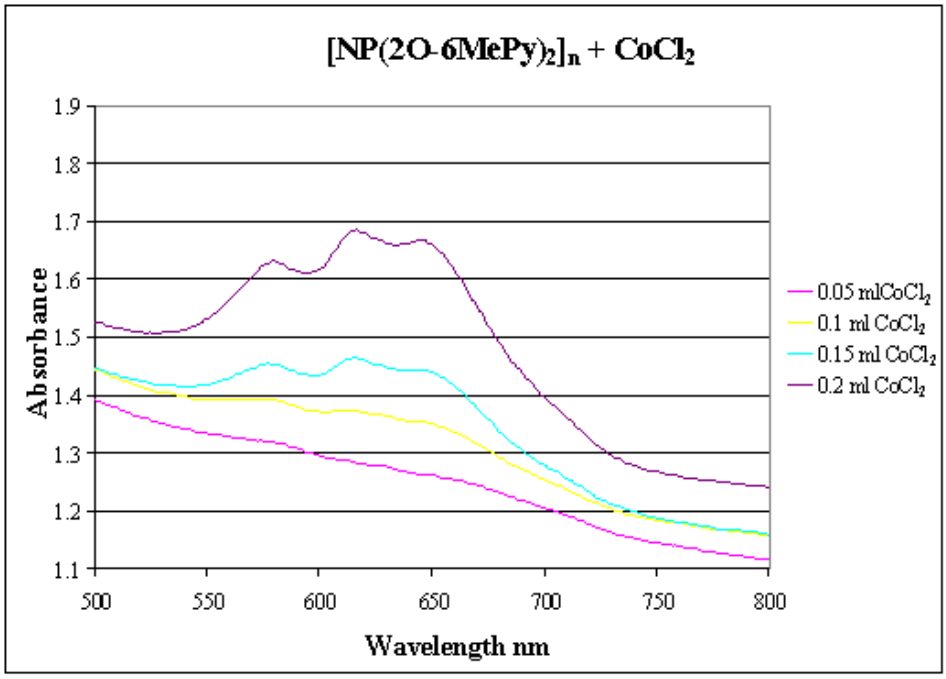

Figure 31 Controlled doping experiment to assess the point of precipitation

Polymer Complex	Solution CH_2Cl_2	Solid Nujol mull
	λ_{max}/nm (ε/dm^3 mol^{-1} cm^{-1})	λ_{max}/nm
[NP(2O-6-MePy)]$_n$ with $CoCl_2$ (2:1)	Insoluble {Doped: 675, 647, 617, 580}	690 (sh), 665, 630, 615 (sh)
[NP(2O-6-MePy)]$_n$ with $CoCl_2$ (6:1)	Insoluble {Doped: 675, 647, 617, 580}	690 (sh), 665, 630, 615 (sh)

Table 9 UV-visible data for [NP(2O-6-MePy)]$_n$ coordinated to $CoCl_2$

5.6.2.4 Possible coordination modes of [NP(2O-6-MePy)]$_n$ to $CoCl_2$

It is postulated that with full substitution, regardless of the backbone orientation, there exists a high propensity for cross linking of polymer chains via the metal centres to give a tetrahedral geometry as illustrated for the Co(II) polymeric complex in Figure 32.

Since only a small number of such crosslinks are necessary to cause insolubility, it is not unexpected that the polymeric complex exhibits such behaviour. Allcock[43] has shown that coordination crosslinking can also occur directly between the metal centre and the polyphosphazene backbone nitrogen, which would also lead to tetrahedral geometry and should not be dismissed as a possibility, although no data exists on the basicity of the polyphosphazene backbone nitrogens with 2-oxypyridine side groups.

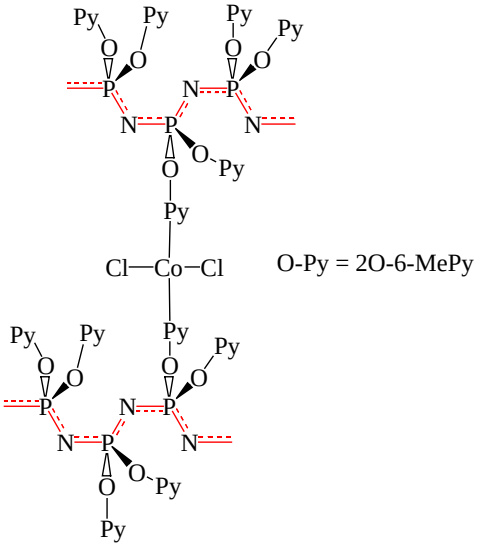

Figure 32 Possible crosslinking through Co(II) centres

5.6.2.5 $[NP(biph)_{0.66}(2O\text{-}4\text{-}MePy)_{0.33}]_n$ with $CuCl_2$

On coordination of $CuCl_2$ to the polymer, the IR band at 1166 cm^{-1} for the free polymer disappeared, as also found for the $CoCl_2$ complex. It appears probable that this signal is a reliable indicator for metal coordination on this particular polymer as suggested by Carriedo *et al*.[47]

Comparison of the solution and solid reflectance spectra (Table 10) indicate that a geometric rearrangement occurs on going from solid to the solution phase with a shift to longer wavelengths.

Polymer Complex	Solution CH_2Cl_2	Solid Nujol mull
	λ_{max}/nm (ε/dm^3 mol^{-1} cm^{-1})	λ_{max}/nm
$[NP(biph)_{0.66}(2O\text{-}4\text{-}MePy)_{0.33}]_n$ with $CuCl_2$ (2:1)	475 (258), 825 (114)	365, 720(vb)
$[NP(biph)_{0.66}(2O\text{-}4\text{-}MePy)_{0.33}]_n$ with $CuCl_2$ (6:1)	470 (71), 770 (78)	385, 720(vb)

Table 10 Summary of Electronic Spectral Data for $[NP(biph)_{0.66}(2O\text{-}4\text{-}MePy)_{0.33}]_n$ with $CuCl_2$

Coordination to $CuCl_2$ at the 6:1 ratio produced two peaks in the UV-visible spectrum, a broad d-d transition centred at 770 nm and a charge transfer band at 470 nm which is assigned to the $[Cu_2Cl_6]^{2-}$ ion.[54-56] This may represent a partial rearrangement in solution, possibly in accordance with Figure 33, where an intramolecular process is outlined:

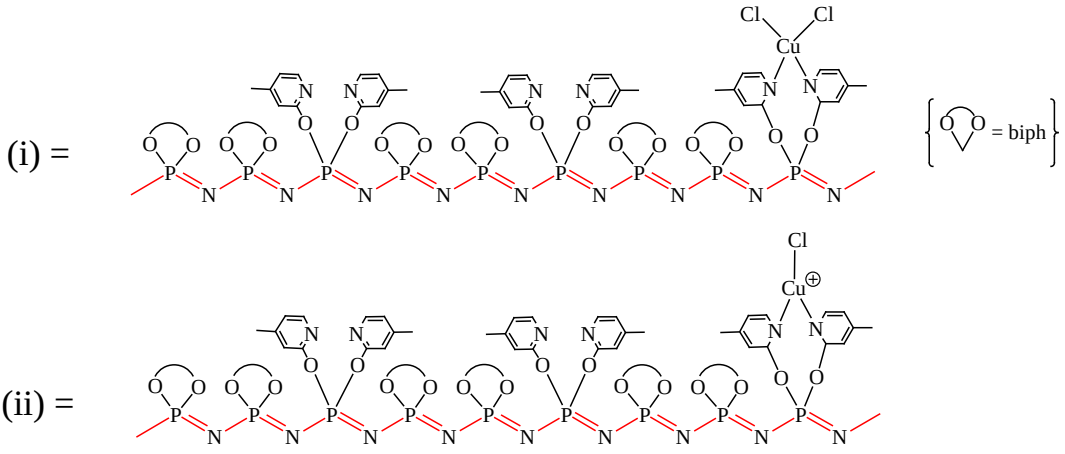

Figure 33 Proposed intramolecular rearrangement for the $CuCl_2$ (6:1) complex

In solution, the d-d transition for $[NP(biph)_{0.66}(2O\text{-}4\text{-}MePy)_{0.33}]_n$ with $CuCl_2$ shifts to longer wavelength with increasing $CuCl_2$ concentration, going from 770 nm to 825 nm. The shift to longer wavelength of the d-d transition warranted further investigation by a control experiment with incremental increases in $CuCl_2$ concentration. As can be seen in Figure 31, the shift is concentration dependent, and reaches a maximum, at approximately 0.8 mole equivalence, of 825 nm, whereas the absorbance continues to increase with increased concentration of $CuCl_2$. In Figure 34, severe signal degradation occurs at the 1 mol equivalence concentration, such that at the detector changeover point the peak around 830 nm is very nearly obscured.

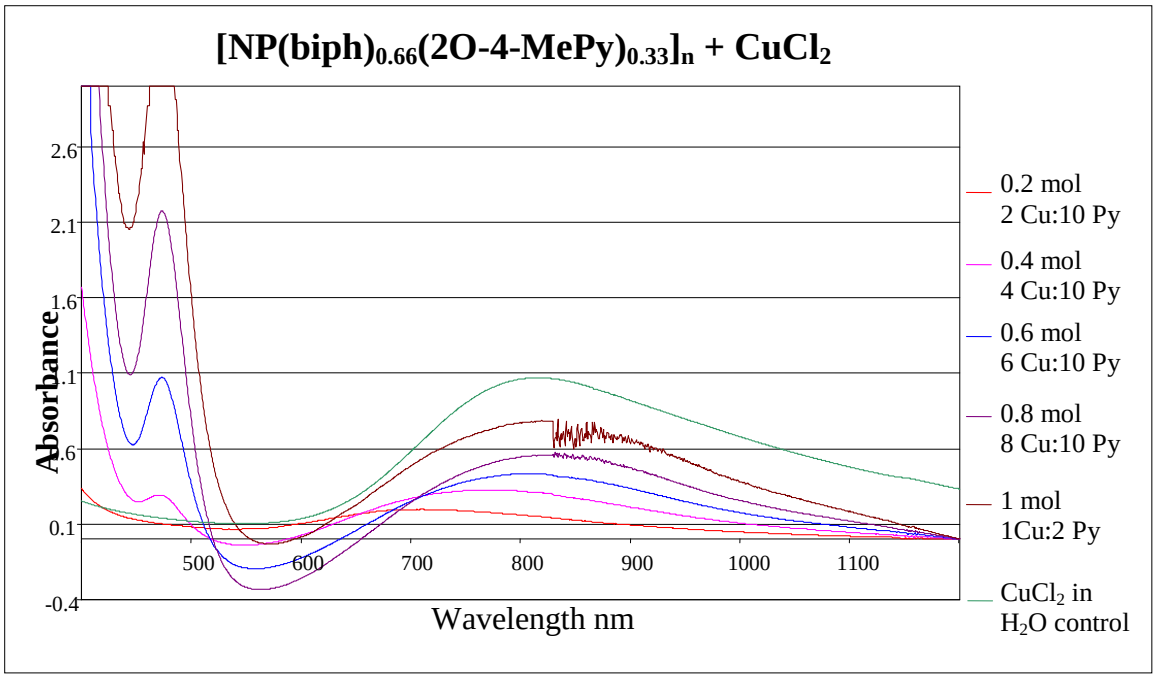

Figure 34 Concentration dependence of $CuCl_2$ spectral shifts in CH_2Cl_2

Analysis of the raw data used for Figure 34 gave the following peak values for the various mole ratios and control conditions (Table 11). It should be noted that no charge transfer band is evident for the control substance which is $CuCl_2$ in H_2O.

Mole ratio	λ_{max}/nm
0.2	710
0.4	775
0.6	805
0.8	825
1.0	825
$CuCl_2$ in H_2O (control)	815

Table 11 UV-visible peak data for varying mole ratios of $CuCl_2$

The shift to longer wavelength with increasing concentration of $CuCl_2$ will also be influenced by (i) the degree of rearrangement in solution which produces two other Cu(II) species and associated d-d spectra and (ii) whilst square planar geometry cannot be ruled out, the concentration dependence of the shift in wavelength is reasoned to be more indicative of distortion between square pyramidal and trigonal bipyramidal via distorted intermediates that shift the d-d transition to lower energy.[57] Possible coordination modes are now discussed.

5.6.2.6 Possible coordination modes of $[NP(biph)_{0.66}(2O\text{-}4\text{-}MePy)_{0.33}]_n$ to $CuCl_2$

For the complex of $[NP(biph)_{0.66}(2O\text{-}4\text{-}MePy)_{0.33}]_n$ with $CuCl_2$, the shift to longer wavelength in the UV-visible spectra follows a similar pattern to that demonstrated for successive replacement of ligating water with NH_3 groups in the complex $[Cu(H_2O)_6]^{2+}$, which is indicative of increased ligand coordination with increasing ligand field strength.[52] It is unlikely that this is the case with the polymeric complex since the high loading of the biph moiety should obstruct the concentration of 2-oxypyridine moieties and prevent higher coordination via steric hindrance.

5.6.2.7 Two-centred rigid mode model of Cu(II) coordination based on a perfect distribution of the biph and 2-oxypyridine groups

Considering the case of a perfect statistical distribution of biph and 2-oxypyridine moieties, coordination of $CuCl_2$ can be speculated to produce a five-coordinate complex

as depicted in Figure 35, assuming that the polyphosphazene backbone nitrogen is sufficiently basic to coordinate to Cu(II) in this way (and since the evidence from the cyclotriphosphazene compounds indicated that Cu(II) is five-coordinate in both the solid and solution phases). Such an arrangement could hypothetically inhibit bond torsion about the P-N bond involved in complexation creating a localised rigid node, since, according to Allcock,[43] the backbone flexibility determines the extent of either random coiling or "rigid rod" character in solution. It is postulated that without the rigidity of the cyclotriphosphazene ring as a scaffold, such a five-coordinate structure would be prone to greater distortion through thermal motion of the adjacent nodes. As the ratio of $CuCl_2$ increases, more localised nodes are created and the backbone increases in rigidity with less distortion occurring thus leading to a lower energy spectral shift. Since there is a low energy barrier to interconversion between the square-pyramidal and trigonal-bipyramidal conformations via a Berry-type pseudorotation,[58] it is not unreasonable to surmise that these two conformations are responsible for the spectral shift. Although square-based distorted trigonal-bipyramidal Cu(II) complexes with the hexakis(4-methyl-2-pyridyloxy) cyclotriphosphazene have been reported in the literature.[55] Perhaps of more relevance is a report by Murphy *et al*.[59] that discusses the interconversion between square-based pyramidal and trigonal bipyramidal geometries for copper complexes and makes the observation that peaks move to higher energy from the trigonal-bipyramidal state as the extent of square-pyramidal distortion increases.

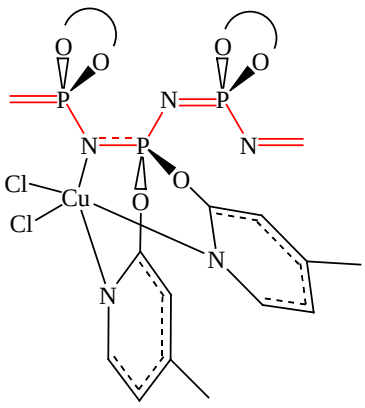

Figure 35 Possible formation of a five coordinate polymeric copper complex

However, whilst the argument espoused above for increasing backbone stiffness by the formation of localised nodes may go some way to explaining the shift to longer wavelength, it does not account for the partial rearrangement and existence of the $[Cu_2Cl_6]^{2-}$ species (see section 5.6.2.5)

5.6.2.8 Three-centred rigid mode model of Cu(II) coordination based on a random distribution of biph and 2-oxypyridine groups

This is a model in which the distribution of side groups along the backbone is more random as may be evidenced by the multimodal and relatively broad $^{31}P\{^1H\}$ NMR spectra for the $[NP(biph)_{0.66}(2O\text{-}4\text{-}MePy)_{0.33}]_n$ base polymer. Here, blocks of the 2-oxypyridine moiety provide a coordination site capable of forming a five-coordinate structure (Figure 36) which may still provide localised nodes of higher bond torsion, but in this model, spread over two bonds, preventing free rotation of the backbone. This arrangement also allows for the interconversion between square-pyramidal and trigonal-bipyramidal conformations, and in addition provides a mechanism for the partial rearrangement and formation of the $[Cu_2Cl_6]^{2-}$ ion, thus explaining the charge transfer band.

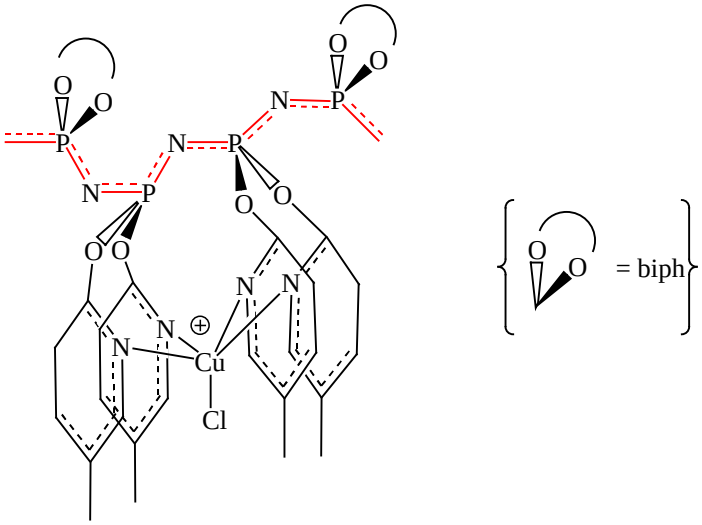

Figure 36 A plausible geometric arrangement to explain the UV-visible spectra

5.6.2.9 UV-visible and ESR spectra

Interpretation of the UV-visible spectra for Cu(II) complexes is often difficult due to the lack of accurate assignments in the literature,[60] the range of overlapping possibilities

shown in Figure 37, and the often broad featureless appearance of the spectra. Solution spectra for Cu(II) fit the interpretation postulated, though other possibilities may exist.

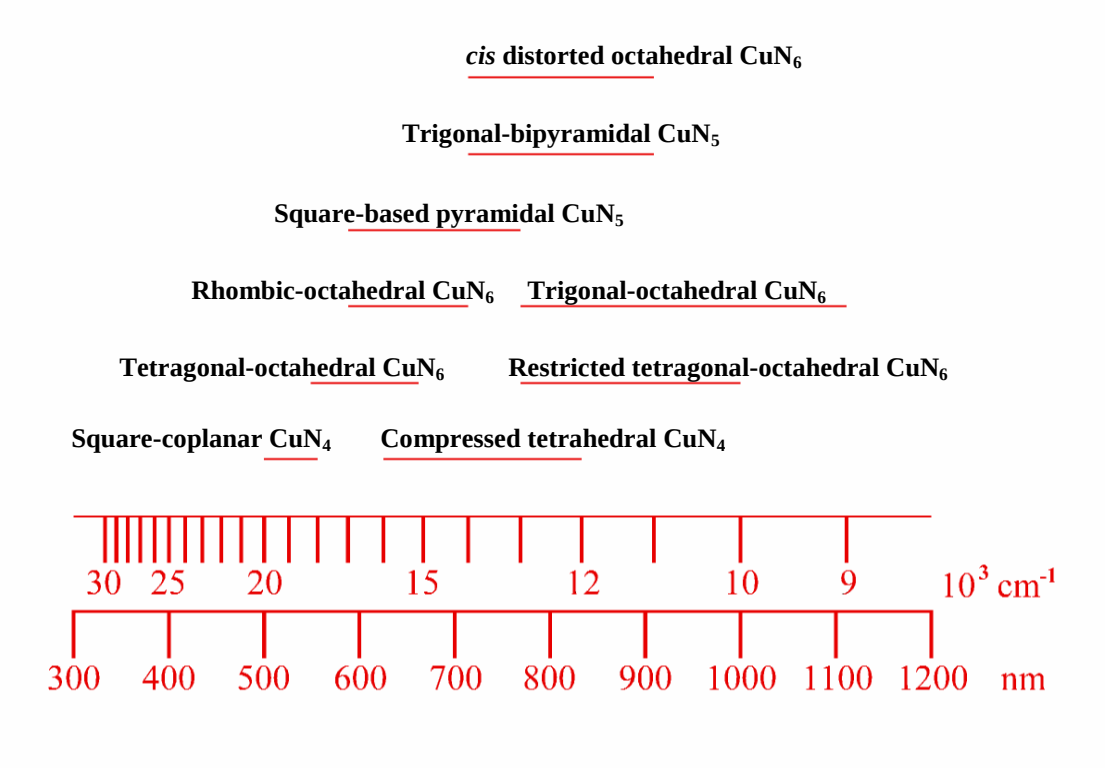

Figure 37 Summary of energy ranges for closely related CuN_x chromophores with different stereochemistries - (Modified from Lever [60])

Electron spin resonance (ESR) spectroscopy is often used as a complimentary technique with the UV-visible data. However, ESR spectra for the polymer complexes demonstrated that at -160°C the ESR spectra were essentially identical except for a slight broadening in the g_ζ region with increased Cu(II) concentration, which may reinforce the supposition that a low energy interconversion process is taking place rather than a structural rearrangement.

5.6.2.10 $[NP(2O\text{-}6\text{-}MePy)]_n$ with $CuCl_2$

Comparison of the IR spectra for the free polymer and copper polymer complex demonstrated loss of a signal at 1662 cm^{-1} and the appearance of new signals at 1678, 1672 and 1396 cm^{-1}. This behaviour is different to that exhibited by the $[NP(biph)_{0.66}(2O\text{-}4\text{-}MePy)_{0.33}]_n$ polymer on coordination to Co(II) and Cu(II), and may

be indicative of different coordination geometries for Co(II) and Cu(II) with the fully substituted polymer, which is understandable given the number of available coordination sites.

As with the cobalt derivative, a controlled doping experiment was performed in an attempt to elucidate any possible geometric information prior to precipitation. At both mole ratios used partial precipitation occurred, which is possibly responsible for the irregular appearance of the spectra in Figure 38. The very small increases in mole ratio, coupled to the noise of the spectra negate the detection of any shift in wavelength. Higher mole ratios resulted in precipitation such that no clear signal was evident. No charge transfer bands were noted at either mole ratio in solution.
The peak is estimated to be at a maximum at approximately 840 nm, in contrast to the control $CuCl_2$ in H_2O at 815 nm.

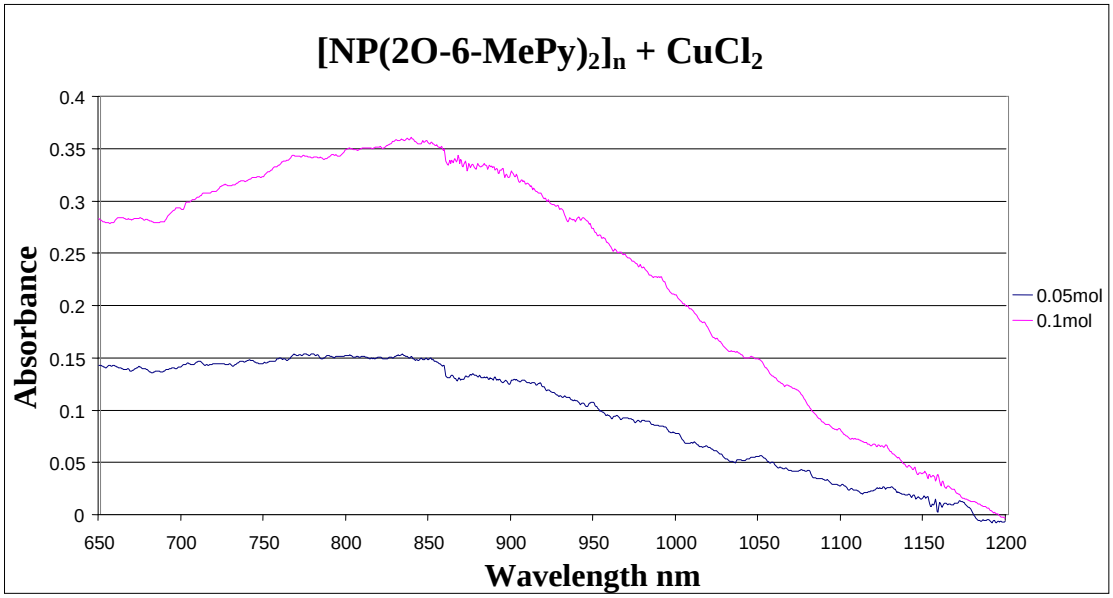

Figure 38 Doping of $[NP(2O\text{-}6\text{-}MePy)_2]_n$ with $CuCl_2$ in CH_2Cl_2

The UV-visible data are given in Table 12 and it can be seen that there is a shift to higher energy in the solid phase relative to the doping experiment, and a shift to higher energy with increased Cu(II) content possibly indicative of a structural rearrangement. A ligand to metal charge transfer band is present in both cases at 360 nm.

Polymer Complex	Solution CH_2Cl_2	Solid Nujol mull
	λ_{max}/nm	λ_{max}/nm
$[NP(2O\text{-}6\text{-}MePy)]_n$ with $CuCl_2$ (2:1)	Insoluble {840 in doping experiment}	360, 610 (sh), 775(vb)
$[NP(2O\text{-}6\text{-}MePy)]_n$ with $CuCl_2$ (6:1)	Insoluble {840 in doping experiment}	360, 820(vb)

Table 12 UV-visible data for $[NP(2O\text{-}6\text{-}MePy)_2]_n$ with $CuCl_2$

5.6.2.11 Possible coordination modes of $[NP(2O\text{-}6\text{-}MePy)]_n$ to $CuCl_2$

Reflectance data for the $CuCl_2$ 2:1 ratio are characteristic of trigonal bipyramidal geometry around the Cu(II) centre, having a very broad signal centred at 775 nm with a shoulder to higher energy.[61, 62] The shift to shorter wavelength with increased Cu(II) concentration in the UV-visible reflectance spectrum is possibly indicative of a distorted environment or even a change in geometry due to degradation as evidenced by the microanalytical figures. The insolubility of the polymer complex can again be reasoned to be due to crosslinking through the metal centres, as for the cobalt polymer complex, however the stereochemical assignment is more difficult but there is no reason not to assume a distorted trigonal bipyramidal arrangement with nitrogen donors from two separate polymer chains due to the high population density of 2-oxypyridine moieties as illustrated in Figure 39.

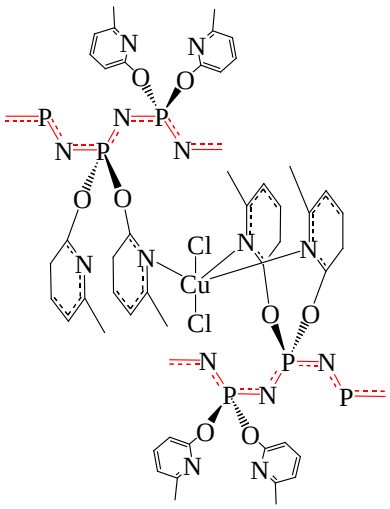

Figure 39 Possible crosslinking via the Cu(II) centre

5.6.2.12 $[NP(biph)_{0.66}(2O\text{-}4\text{-}MePy)_{0.33}]_n$ with $ZnCl_2$

Coordination of the $[NP(biph)_{0.66}(2O\text{-}4\text{-}MePy)_{0.33}]_n$ polymer to $ZnCl_2$ allowed $^{31}P\{^1H\}$ NMR analysis (Figure 40). The integrals for each ratio of $ZnCl_2$ are approximately correct, given the degree of background noise in the spectra. However, the appearance of a third signal at approximately 18 ppm is disconcerting and may represent partial degradation of the polymer to a high cyclic species.

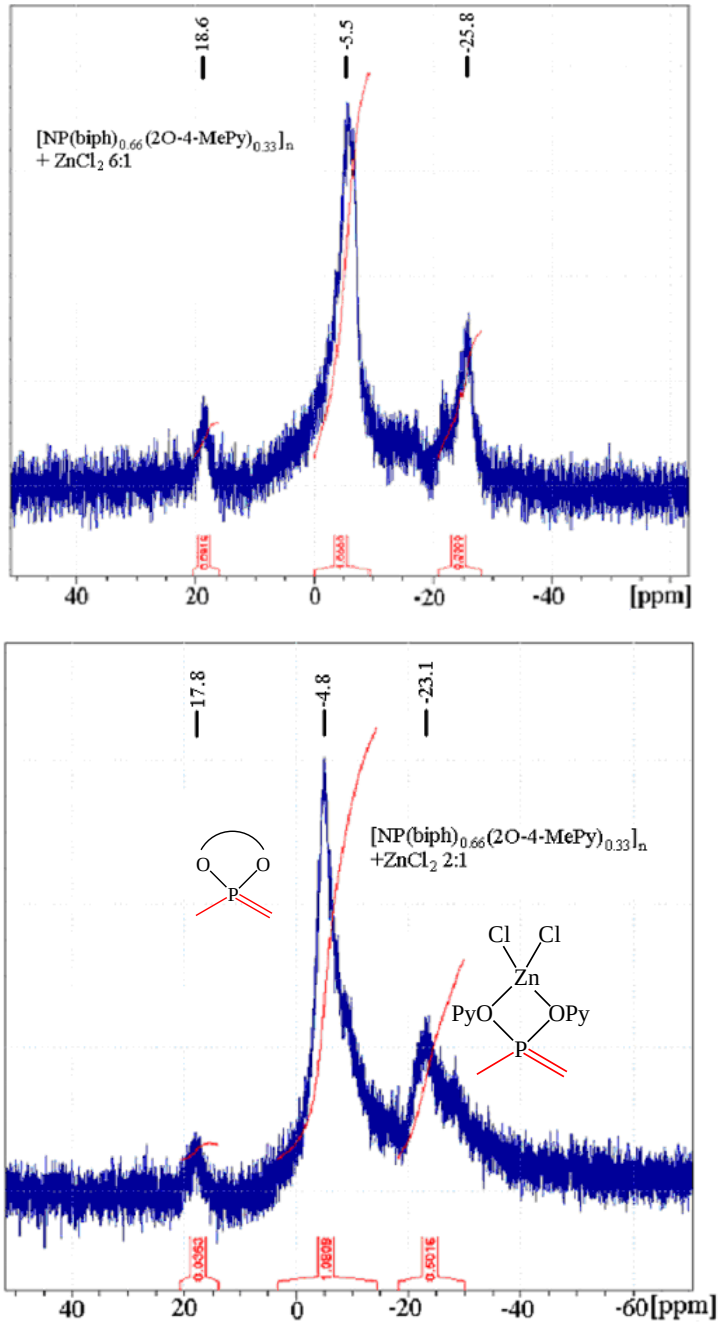

Figure 40 $^{31}P\{^1H\}$ NMR spectra at 298 K for $ZnCl_2$ polymer complexes

For $[NP(biph)_{0.66}(2O\text{-}4\text{-}MePy)_{0.33}]_n$ + $ZnCl_2$ (6:1), there is a minor peak present at approximately -23.1 ppm that, by comparison with the spectra for $[NP(biph)_{0.66}(2O\text{-}4\text{-}MePy)_{0.33}]_n$ + $ZnCl_2$ (2:1) could be indicative of coordination to $ZnCl_2$ while the peak at -25.8 ppm is assigned to uncoordinated 2O-4-MePy moieties.

Independent $^{31}P\{^1H\}$ NMR spectra relative to phosphoric acid confirm that there is a slight downfield shift in the spectra on coordination to zinc. ^1H NMR spectra proved to be of no utility due to excessive line broadening, unlike the cyclotriphosphazene model compound described in Chapter 4 which gave very well defined spectra. The $^{31}P\{^1H\}$ NMR spectra are summarised in Table 13.

	P-biph ppm	P-Py_2 ppm	P-Py_2-$ZnCl_2$ ppm
$[NP(biph)_{0.66}(2O\text{-}4\text{-}MePy)_{0.33}]_n$	-7.6	-27.0	
$[NP(biph)_{0.66}(2O\text{-}4\text{-}MePy)_{0.33}]_n$ + $ZnCl_2$ (6:1)	-5.5	-25.8	-23.1
$[NP(biph)_{0.66}(2O\text{-}4\text{-}MePy)_{0.33}]_n$ + $ZnCl_2$ (2:1)	-4.8		-23.1

Table 13 Summary of $^{31}P\{^1H\}$ NMR data for the Zn(II) polymer complexes

5.6.2.13 Possible coordination modes of $[NP(biph)_{0.66}(2O\text{-}4\text{-}MePy)_{0.33}]_n$ to $ZnCl_2$

The Zn(II) complexes do not absorb in the UV-visible region, so electronic spectra are of no utility in elucidating structural information. The $^{31}P\{^1H\}$ NMR spectrum (Figure 40) demonstrates a bimodal peak for the 2-oxypyridine moiety at the 6:1 ratio (-25.8 and -23.1 ppm) which may be indicative of phosphorus atoms in different environments. Since broad NMR spectra are indicative of random distributions of moieties along the backbone[42] and given the high biph content it is plausible to imagine that the Zn(II) is confined to localised "islands" of 2-oxypyridine containing regions that are separated by the biph moieties from regions of 2-oxypyridine with no Zn(II) coordinated. At the 2:1 ratio, the 2-oxypyridine peak is centred at approximately -23.1 ppm which may indicate that this assumption is correct. The areas containing Zn(II) would appear equivalent due to the known fluxional behaviour.

5.6.2.14 $[NP(2O\text{-}6\text{-}MePy)]_n$ with $ZnCl_2$

Reaction with $ZnCl_2$ at 6:1 and 2:1 ratios yielded soluble polymers allowing variable temperature $^{31}P\{^1H\}$ NMR studies. ^1H NMR gave a broad featureless peak of no utility as for the $[NP(biph)_{0.66}(2O\text{-}4\text{-}MePy)_{0.33}]_n$ polymer.

At a ratio of 2:1, the $^{31}P\{^1H\}$ NMR signal disappears at 263 K with little evidence of line broadening (Figure 41). The polymer sample precipitated from solution at low temperature and was observed to redissolve as the temperature increased with a re-establishment of the ^{31}P NMR signal.

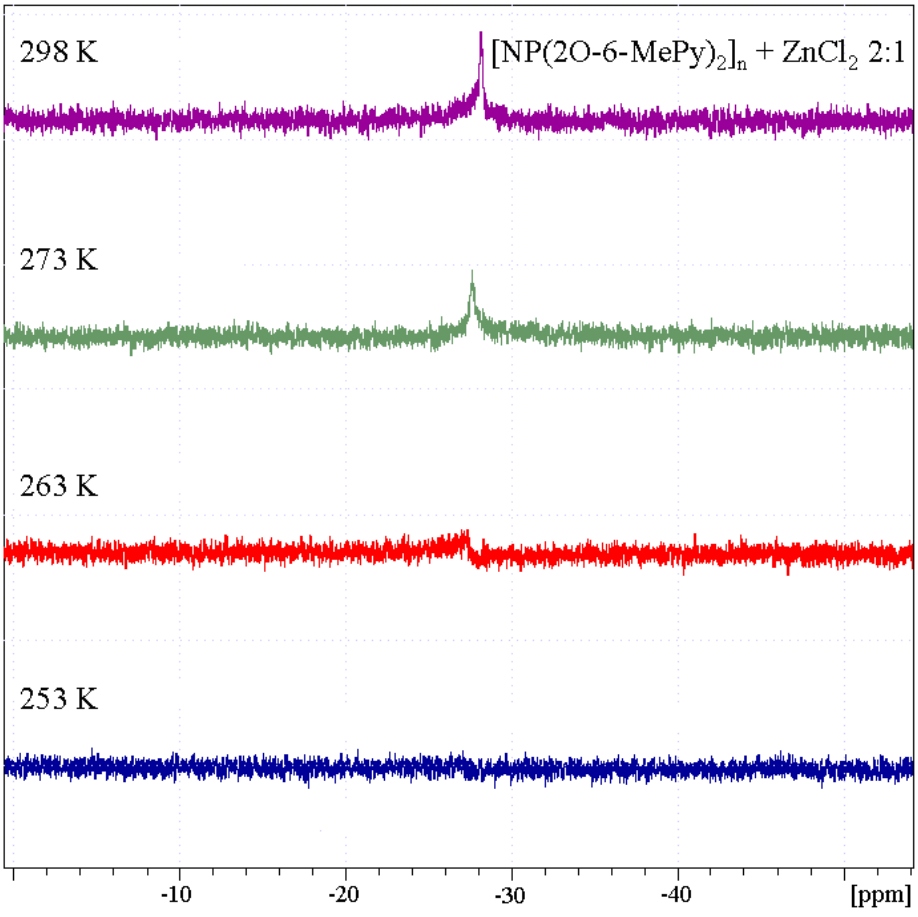

Figure 41 $^{31}P\{^1H\}$ NMR studies of $[NP(2O\text{-}6\text{-}MePy)_2]_n$ with $ZnCl_2$ in CH_2Cl_2.

At a ratio of 6:1 a clear signal is obtained down to the solvent temperature limit (Figure 42). The slight downfield shift of the signal with decreasing temperature, as for the cyclotriphosphazene model compound discussed in Chapter 4, may be a real phenomenon, but since no internal reference could be used due to the low temperature, this cannot be confirmed. However a room temperature shift relative to phosphoric acid was noted on formation of the polymer complexes as shown in Table 14.

Polymer complex	$^{31}P\{^{1}H\}$ NMR at 298 K
$[NP(2O\text{-}6\text{-}MePy)]_n$	-27.6
$[NP(2O\text{-}6\text{-}MePy)]_n + ZnCl_2$ (6:1)	-26.9
$[NP(2O\text{-}6\text{-}MePy)]_n + ZnCl_2$ (2:1)	-24.9

Table 14 NMR shifts (ppm) relative to phosphoric acid on formation of polymer complexes

The most striking feature in Figure 42 is that at all temperatures there is only a single peak in the spectrum indicating that fast exchange is occurring between the phosphorus atoms such that only a time averaged signal is observed. The signal broadens with decreasing temperature, but a sufficiently low temperature was unable to be obtained to observe any splitting of the signal to reveal different phosphorus environments. It is postulated that if it were possible to continue cooling then at least two signals should be observed in the slow exchange region, differentiating between coordinated and uncoordinated phosphorus atoms.

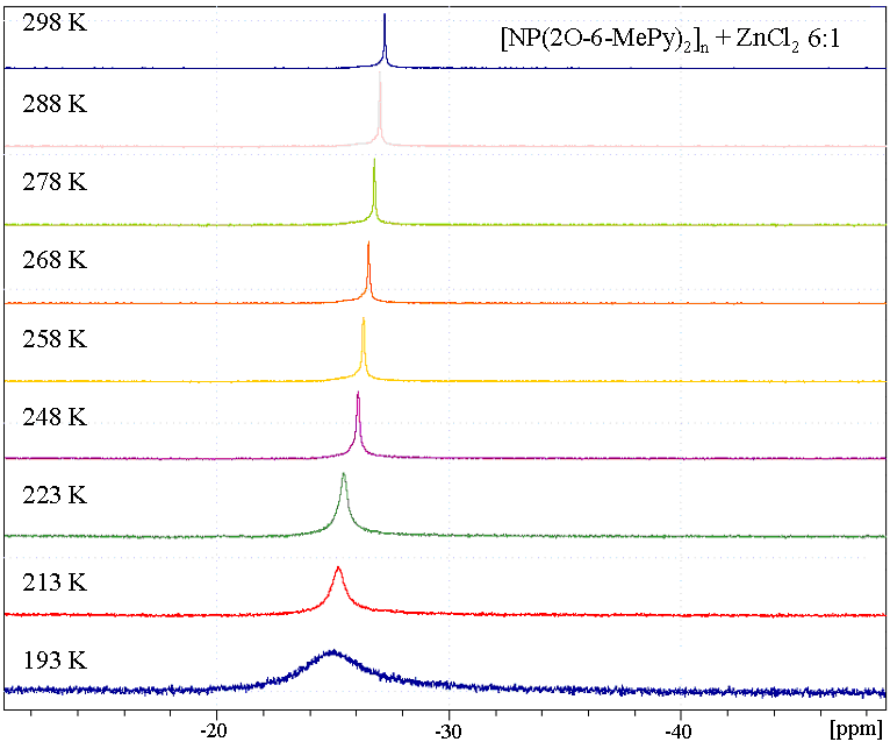

Figure 42 $^{31}P\{^{1}H\}$ NMR studies of $[NP(2O\text{-}6\text{-}Mepy)_2]_n$ with $ZnCl_2$ (6:1) in CH_2Cl_2.

5.6.2.15 Possible coordination modes of $[NP(2O\text{-}6\text{-}MePy)]_n$ to $ZnCl_2$

The Zn(II) polymer with the 6:1 ratio displays fluxional behaviour. Unlike the small molecule complex discussed in Chapter 4 ($[ZnL^2Cl_2]$ for which five-coordinate TBP and four-coordinate tetrahedral X-ray structures were obtained), there is no additional evidence to assist with determining a plausible structure. It is very interesting to note that the Zn(II) polymer is soluble at both ratios used and that whatever crosslinking mechanism is at work with the Co(II) and Cu(II) derivatives does not seem applicable to Zn(II). It is possible that the lability of the Zn(II) centre is such that crosslinking bonds are formed and broken as other donors come into play and no permanent crosslink endures. This may be a thermal phenomenon as illustrated by the $^{31}P\{^{1}H\}$ NMR spectra for the 2:1 $ZnCl_2$ polymer complex. The collision cross section of nitrogen donors may consist solely of adjacent 2-oxypyridine groups i.e. from the same polymer chain.

From the microanalytical figures (*c.f.* Tables 2 and 3) it can be seen that for the fully substituted $[NP(2O\text{-}6\text{-}MePy)_2]_n$ polymer some degree of degradation is occurring as shown by the low Cl percentages, especially for those complexes fully loaded with metal dichlorides. Whilst there is no evidence in the $^{31}P\{^{1}H\}$ NMR for unreacted

chlorine atoms on the backbone, this is not the only route to degradation. Hydrolysis of a phosphorus atom can lead to the formation of P-O-P crosslinks with loss of HCl and 2-oxypyridine side groups. Indeed, hydrolysis of the cyclotriphosphazene compounds in Chapter 3, has demonstrated that a number of hydrolysis products may be obtained.

5.7 Conclusions and final comments

Following the approach suggested by Allcock,[63] regarding the crucial role of small molecule synthesis in trying to understand the underlying and fundamental chemistry of high polymers, the relative stability of cyclotriphosphazenes bearing biph moieties and 2-oxypyridine co-substituents, has prompted investigation into the synthesis of polymers with mixed ratios of both side groups and their subsequent reactions with transition metal dichlorides.

The choice of the cyclotriphosphazene as a basis for modelling the polymeric reactions is somewhat moot. The low bond torsion of the polyphosphazene backbone must lend itself to variations in coordination geometry without the restriction of formalised cyclic rigidity, yet the possibilities of inter and intra molecular bonding must also be restricted by the electronic forces inherent in the structure of the backbone and the attendant side groups. The complete, or incomplete, substitution of P-Cl bonds, and hence the stability of the ensuing polymer is only alluded to in this work. Identification of time dependant hydrolysis as a result of the synthesis or storage conditions requires further work.

However, the evidence presented herein, would seem to indicate that the requirements for the stability of polyphosphazenes bearing 2-oxypyridine side groups are steric in nature, and require bulky groups adjacent to the pyridyl nitrogen, or high loadings of sterically bulky groups on the polymer backbone. It would also appear that optimisation of the synthetic protocols requires refinement and further investigation to ensure complete P-Cl substitution on the polymer backbone, and determination of the rate of hydrolysis for the various moiety ratios.

The characterisation of polymeric materials is currently fraught with problems, due to the lack of accurate techniques and the statistical ambiguity of the distribution of side groups. Attempts to characterise the polymer complexes following reaction with transition metals, leads to speculation regarding geometry, and is further aggravated by

the apparent hydrolysis of the species involved. Notwithstanding that, it is apparent that pseudo-stable polymers containing methylated 2-oxypyridine side groups can be synthesised although since this is the first known report of multidentate polyphosphazenes coordinated to metals via methylated 2-oxypyridine side groups, or a proportion thereof with ratios of biph, there are no data for comparison. The reasoning regarding stereochemistry is therefore, of necessity, somewhat speculative.

5.8 References

1. Allcock, H. R.; Kugel, R. L., *J. Am. Chem. Soc.* **1965,** 87, 4216.

2. Allcock, H. R.; Kugel, R. L., *Inorg. Chem.* **1966,** 5, 1716.

3. Allcock, H. R.; Kugel, R. L.; Valan, K. J., *Inorg. Chem.* **1966,** 5, 1709.

4. Allcock, H. R., *Chemistry and Applications of Polyphosphazenes*. John Wiley and Sons Inc: New York, 2003; p. 300-311.

5. Stokes, H. N., *Am. Chem. J.* **1897,** 19, 782.

6. Allcock, H. R.; Best, R. J., *Can. J. Chem.* **1964,** 42, 447.

7. Mujumdar, A. N.; Young, S. G.; Merker, R. L.; Magill, J. H., *Macromolecules* **1990,** 23(1), 14.

8. Allcock, H. R.; Dodge, J. A.; Manners, I.; Riding, G. H., *J. Am. Chem. Soc.* **1991,** 113(25), 9596.

9. D'Halluin, G.; De Jaeger, R.; Chambrette, J. P.; Potin, P., *Macromolecules* **1992,** 25(4), 1254.

10. Allcock, H. R.; Honeyman, C. H.; Manners, I.; Morrissey, C. T., *J. Am. Chem. Soc.* **1995,** 117, 7035.

11. Carriedo, G. A.; García-Alonso, F. J.; Gómez-Elipe, P.; Fidalgo, J. I.; García-Álvarez, J. L.; Presa-Soto, A., *Chem. Eur. J.* **2003,** 9, 3833.

12. Wang, B., *Macromolecules* **2005,** 38(2), 643.

13. Allcock, H. R., *J. Inorg. Organomet. Polym. Mater.* **2006,** 16, 277.

14. De Jaeger, R.; Gleria, M., *Prog. Polym. Sci.* **1998,** 23, 179.

15. Lee, D. C.; Ford, J. R.; Fytas, G.; Chu, B.; Hagnauer, G. L., *Macromolecules* **1986,** 19, 1586.

16. Allcock, H. R.; Gardner, J. E.; Smeltz, K. M., *Macromolecules* **1975,** 8(1), 36.

17. MacCallum, J. R.; Werninck, A., *J. Polym. Sci., Pt A-1: Polym. Chem.,* **1967,** 5, 3061.

18. Gabler, D. G.; Haw, J. F., *Macromolecules* **1991,** 24(14), 4218.

19. Devadoss, E.; Nair, C. P. R., *Ind. Eng. Chem. Prod. Res. Dev.* **1984,** 23, 272.

20. Konecny, J. O.; Douglas, C. M., *J. Polym. Sci.* **1959,** 36, 195.

21. Ganapathiappan, S.; Dhathathreyan, K. S.; Krishnamurthy, S. S., *Macromolecules* **1987,** 20(7), 1501.

22. Cho, Y.; Sohn, Y. S.; Jun, M., *J. Polym. Sci.* **1993,** 31, 3397.

23. Cho, Y.; Baek, H.; Jung, O.; Jun, M.; Sohn, Y. S., *Bull. Korean. Chem. Soc.* **1996,** 17, 85.

24. Allen, C. W.; Hneihen, A. S.; Peterson, E. S., *Solid State Synthesis of Poly(dichlorophosphazene).* **2001**. (6,309,619). U.S.A.

25. Allcock, H. R.; Crane, C. A.; Morrissey, C. T.; Nelson, J. M.; Reeves, S. D.; Honeyman, C. H.; Manners, I., *Macromolecules* **1996,** 29(24), 7740.

26. Niecke, E.; Bitter, W., *Inorg. Nucl. Chem. Lett.* **1973,** 9, 127.

27. Honeyman, C. H.; Lough, A. J.; Manners, I., *Inorg. Chem.* **1994,** 33, 2988.

28. Allcock, H. R.; Crane, C. A.; Morrissey, C. T.; Olshavsky, M. A., *Inorg. Chem.* **1999,** 38(2), 280.

29. Wang, B.; Rivard, E.; Manners, I., *Inorg. Chem.* **2002,** 41(7), 1690.

30. Peterson, E. S.; Luther, T. A.; Harrup, M. K.; Klaehn, J. R.; Stone, M. L.; Orme, C. J.; Stewart, F. F., *J. Inorg. Organomet. Polym. Mater.* **2007,** 17(2), 361.

31. Audrieth, L. F.; Steinman, R.; Toy, A. D. F., *Chem. Rev.* **1943,** 32, 109.

32. Migachev, G. I.; Stepanov, B. I., *Russ. J. Inorg. Chem.* **1966,** 11(7), 929.

33. Diefenbach, U.; Allcock, H. R., *Inorg. Chem.* **1994,** 33(20), 4562.

34. Diefenbach, U.; Kretschmann, M.; Çavdarci, Ö. *Phosphorus, Sulfur Silicon Relat. Elem.* **1994,** 93-94, 415.

35. Diefenbach, U., Phosphazenes with pyridine side groups. In *Applicative Aspects of Cyclophosphazenes*, ed.; Gleria, M.; De Jaeger, R., Nova Science Publishers Inc: New York, 2004; p. 185-213.

36. Diefenbach, U.; Kretschmann, M.; Stromburg, B. E., *Phosphorus, Sulfur Silicon Relat. Elem.* **1997,** 124-125, 143.

37. Carriedo, G. A., *J. Chil. Chem. Soc.* **2007,** 52(2), 1191 and references therein.

38. Carriedo, G. A.; García-Alonso, F. J.; Díaz Valenzuela, C.; Valenzuela, M. L., *Polyhedron* **2006,** 25, 105.

39. Carriedo, G. A.; García Alonso, F. J.; Presa, A., *J. Inorg. Organomet. Polyms.* **2004,** 14, 29.

40. Díaz, C.; Valenzuela, M. L., *Macromolecules* **2006,** 39(1), 103.

41. Allcock, H. R.; Lavin, K. D.; Tollefson, N. M.; Evans, T. L., *Organometallics* **1983,** 2(2), 267.

42. Allcock, H. R., *Chemistry and Applications of Polyphosphazenes*. John Wiley and Sons Inc: New York, 2003; p. 11.

43. Allcock, H. R., *Chem. Mater.* **1994,** 6(9), 1476.

44. Mark, J. E.; Allcock, H. R.; West, R., *Inorganic Polymers*. 2nd ed, Oxford University Press, Inc.: New York, 2005; p. 144.

45. Allcock, H. R.; Tollefson, N. M.; Arcus, R. A.; Whittle, R. R., *J. Am. Chem. Soc.* **1985,** 107(18), 5166.

46. Carriedo, G. A.; García Alonso, F. J.; Presa-Soto, A., *Eur. J. Inorg. Chem.* **2003,** 24, 4341.

47. Carriedo, G. A.; García-Alonso, F. J.; García-Álvarez, L. J.; Díaz Valenzuela, C.; Sáez, N. Y., *Polyhedron* **2002,** 21, 2587.

48. Neilson, R. H.; Hani, R.; Wisian-Neilson, P.; Meister, J. J.; Roy, A. K.; Hagnauer, G. L., *Macromolecules* **1987,** 20, 910.

49. Bravo, J.; Tarazona, M. P.; Saiz, E., *Macromolecules* **1992,** 25(21), 5625.

50. Diefenbach, U.; Cannon, A. M.; Stromburg, B. E.; Olmeijer, D. L.; Allcock, H. R., *J. Appl. Polym. Sci.* **2000,** 78, 650.

51. Visscher, K. B.; Allcock, H. R., *Chem. Mater.* **1994,** 6, 2042.

52. Cotton, F. A.; Wilkinson, G., *Advanced Inorganic Chemistry, A Comprehensive Text, Pt.2*. 5th ed,; John Wiley and Sons: New York, 1988; 1, p. 770.

53. Kojima, K., *Bull. Chem. Soc. Jpn.* **1988,** 61, 385.

54. Ainscough, E. W.; Brodie, A. M.; Depree, C. V., *J. Chem. Soc., Dalton Trans.* **1999,** 23, 4123.

55. Ainscough, E. W.; Brodie, A. M.; Depree, C. V.; Moubaraki, M.; Murray, K. S.; Otter, C. A., *J. Chem. Soc., Dalton Trans.* **2005,** 20, 3337 and references therein.

56. Cotton, F. A.; Wilkinson, G., *Advanced Inorganic Chemistry, A Comprehensive Text, Pt.2*. 5th ed,; John Wiley & Sons: New York, 1988; 1, p. 730-731.

57. Lever, A. B. P., *Inorganic Electronic Spectroscopy*. 2nd Elsevier: New York, 1984; 33, p. 568.

58. Bennet, S., *S343 Inorganic Chemistry, Block 4*. Nuttall, I.; Tillotson, D., The Open University: Milton Keynes, 1989; p. 39.

59. Murphy, G.; Murphy, C.; Murphy, B.; Hathaway, B., *J. Chem. Soc., Dalton Trans.* **1997**, 2653.

60. Lever, A. B. P., *Inorganic Electronic Spectroscopy*. 2nd Elsevier: New York, 1984; 33, p. 572.

61. Hathaway, B. J., In *Comprehensive Coordination Chemistry*, 1st ed.; Wilkinson, G.; Gillard, R. D.; McLeverty, J. A., Pergamon Press: New York, 1987; 5, p. 533-744.

62. Patra, A. K.; Ray, M.; Mukherjee, R., *J. Chem. Soc., Dalton Trans.* **1999,** 15, 2461.

63. Allcock, H. R., *Phosphorus, Sulfur Silicon Relat. Elem.* **2004,** 179, 661.

Appendix 1: Laboratory Synthesis of Poly(dichloro)phosphazene

In this appendix, synthesis of the poly(dichloro)phosphazene is described in detail. The “as received” cyclophosphazene was dissolved in hot heptane and filtered. The filtrate was cooled to -18°C until white crystals formed which were filtered to remove excess heptane. Approximately 150 grams of the crystals were placed in a purpose made sublimator (Figures 1-4) having an external oil jacket held at 50°C and a cold finger held at 4°C. High vacuum (0.01 mmHg) was applied to the sublimator via a cold trap cooled with liquid nitrogen, and over several hours white crystals of purified cyclophosphazene formed on the cold finger, these were collected for polymerisation.

Figure 1 Purpose made sublimator

Figure 2 Sublimator setup in oil bath with cold trap

Figure 3 Crystals of cyclochlorophosphazene

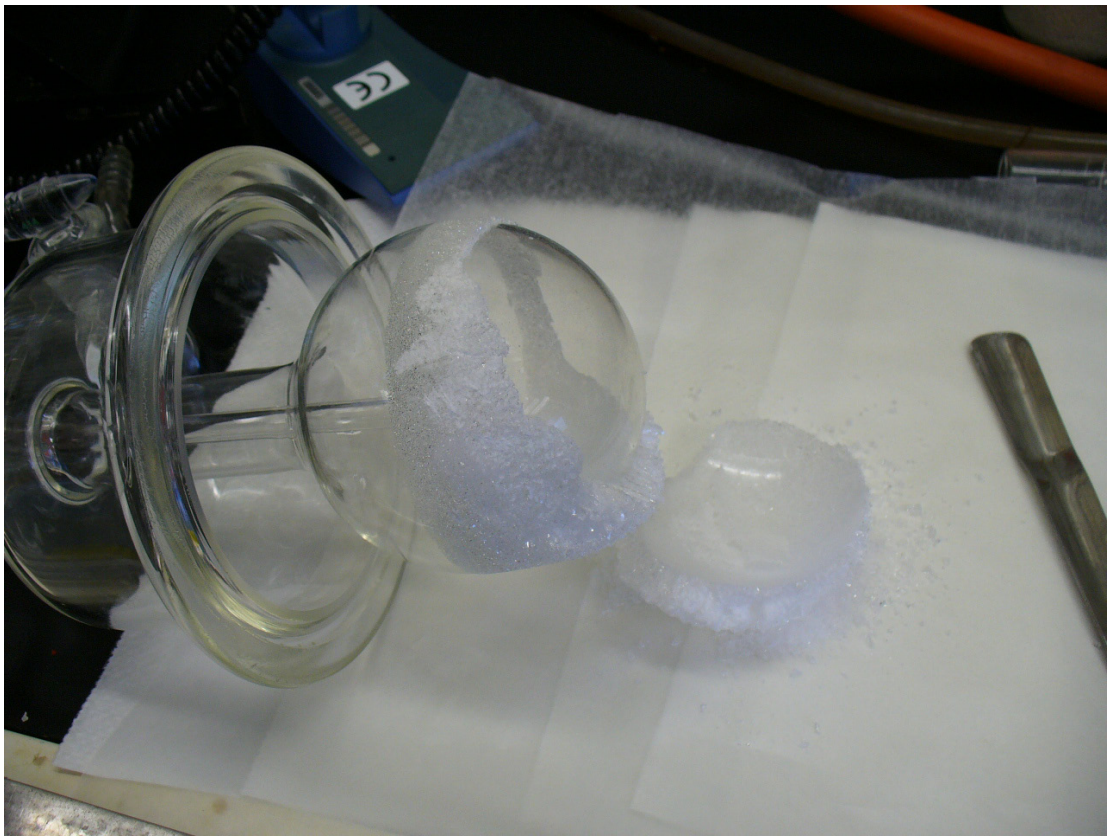

Figure 4 Removing the sublimed cyclochlorophosphazene

Approximately 100 grams of cyclophosphazene were crushed using a pestle and mortar and placed in a purpose made glass tube (Figure 5), ensuring that no cyclophosphazene contaminated the neck area of the tube that would subsequently be flame sealed.

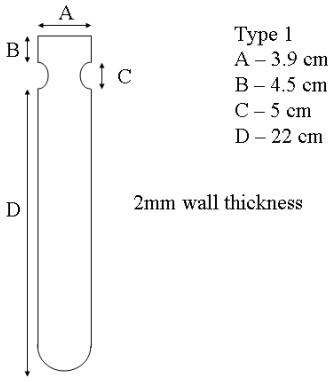

Figure 5 Glass tube dimensions for polymerisation of $N_3P_3Cl_6$

The glass tube had been washed three times with acetone and dried at 140°C for twenty four hours prior to use. High vacuum was applied as before and after a minimum of two hours the glass tube was flame sealed to retain the internal vacuum (Figure 6).

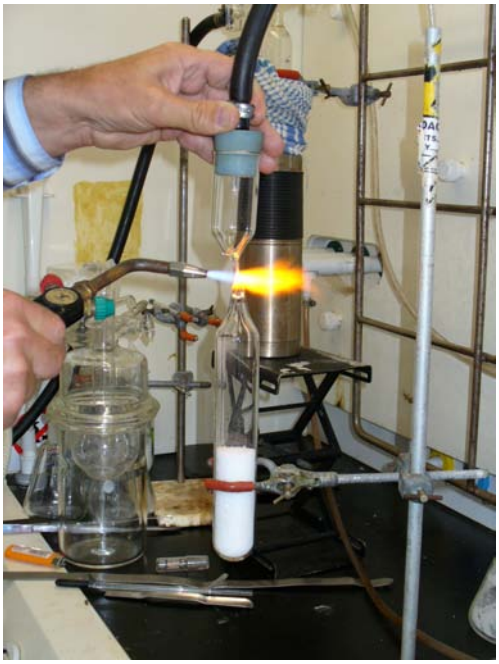

Figure 6 Flame sealing the reaction tube under vacuum

The glass tube was wrapped in aluminium mesh to safeguard against injury in the event of explosion (due to a build up of internal pressure during thermal polymerisation), and placed on a purpose made oscillating plate in an oven that had been preheated to 250°C (Figure 7). The plate was linked to a motor and set to oscillate at 2-3 rpm.

Figure 7 Reaction tube ready for thermal polymerisation

After approximately eight hours, the contents of the glass tube were molten and had the appearance of clear viscous honey, at this point the tube was removed from the oven and left to cool in an upright position. During cooling bubbles appeared as unreacted cyclophosphazene sublimed from the melt. On cooling to room temperature the contents were present as a white solid (Figure 8).

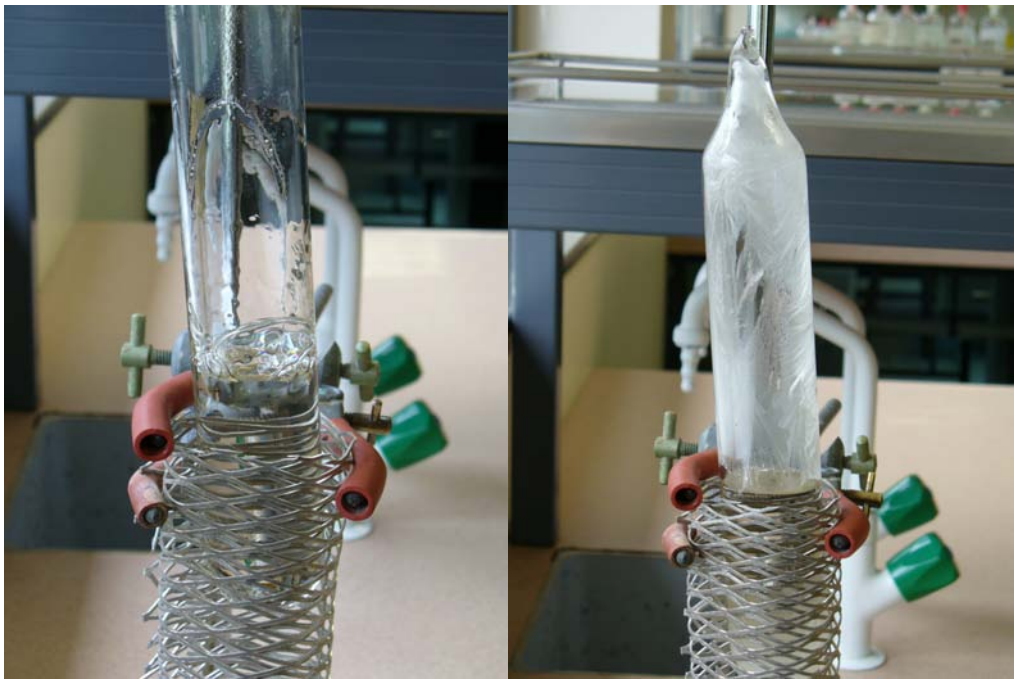

Figure 8 Left: Bubbling of subliming cyclophosphazene Right: Cooled contents

The tube and its contents was subjected to three freeze/thaw cycles with approximately twenty minutes at each stage and with liquid nitrogen being used for the freeze cycle, this process assists with subsequent removal of the polymer from the internal glass surface.

The tube was wrapped in paper towelling and placed in an argon filled glovebag where it was broken open to reveal the polymer and unreacted cyclophosphazenes. The polymer was cut into small pieces and placed into the sublimator under glovebag conditions. Subsequent sublimation removed the cyclophosphazenes to leave the polymer available for use. The polymer was stored in a glovebox under argon until required due to its extreme moisture sensitivity, hydrolysing and cross-linking on exposure to the atmosphere.